Development and application of smart actuation methods for vehicle simulators

Von der Fakultät für Ingenieurwissenschaften,
Abteilung Maschinenbau und Verfahrenstechnik
der Universität Duisburg-Essen

zur Erlangung des akademischen Grades

einer

Doktorin der Ingenieurwissenschaften

genehmigte Dissertation

von

Nona Alina Capustiac
aus
Cluj-Napoca

Gutachter: Prof. Dr.-Ing Dieter Schramm
Prof. Dr.-Ing. Dorel Banabic
Tag der mündlichen Prüfung: 30 September 2011

Acknowledgments

I would first like to express my gratitude to my advisors, **Prof. Dorel Banabic** from the Technical University of Cluj-Napoca, Romania and **Prof. Dieter Schramm** from the University of Duisburg-Essen, Germany for their guidance, support and confidence they offered me.

I would also like to thank the rest of my PhD dissertation committee members for their comments, recommendations and for taking the effort of being part of this commission.

I sincerely thank **Prof. Udo Ossendoth** from the University of Applied Sciences Gelsenkirchen, for his patience and support during the experimental studies conducted during my stay in Germany.

I would like to extend my gratitude to all of my colleagues from the Department of Mechatronics, University of Duisburg-Essen for the pleasant working environment, the helpful advices and their friendship. I appreciate the support and guidance I received during my research stages in Duisburg. I would also like to sincerely thank my colleagues from the Certeta Research Center from the Technical University of Cluj-Napoca, for making me part of the team.

Finally, I would like to thank Romina Sopoian for her help and patience during the preparation of this thesis in English.

This research was financially supported and developed in the frame of the ”PRODOC” POSDRU/6/1.5/S/5 ID7676 project.

I express my deepest thanks to my family and friends, without their support, this achievement would not have been possible.

Abstract

Driving simulators are complex virtual reality systems that integrate visual displays, sound rendering systems, motion platforms, and human-machine-interface devices. They are used in different research areas and consequently, different studies are conducted using these systems, in conditions that would not be safe to be carried out in the real world. However, driving simulators are very expensive research tools. When building such a system, a compromise usually has to be made.

Although a driving simulator cannot reproduce 1:1 real life situations or sensations because of its limitations, researchers still need to use such a device for training and research purposes, due to the realistic driving experience it has to offer to its driver.

This work focuses on developing a three-degrees of freedom Essential Function Driving Simulator that integrates cost and design constraints, the human perception of motion and real vehicle motion achieved through simulated vehicle models, and the classical motion cueing strategy. The goal is, on the first hand, to immerse the driver to a certain extend into the simulation environment by using this virtual reality device and, on the second hand, to investigate the degree of realism of such a solution.

Different actuation solutions are modelled and discussed in this research, with respect to the available workspace, singularity configurations, the system's behaviour and the maximum forces needed in the frame of the overall cost constraints. A solution was chosen following kinematical and dynamical analyses, as a trade off solution among the above mentioned constraints.

The human body finds itself in continuous movement and interaction with the environment. Motion is sensed by the human being through the vestibular system and the skin. The human motion perception mechanisms are mathematically modelled and studied, in order to apply their characteristics in the three-degrees of freedom driving simulator.

Due to the limited workspace and degrees of freedom of the discussed simulator, the motion of the simulated vehicle cannot be identically reproduced by the motion system. Thus, special algorithms are designed to transform the motion of the vehicle model in achievable positions for the three actuators, and additionally, to render correct motion cues.

The influence of the three variable parameters on the overall subjective degree of freedom is investigated using an optimisation method. The studied parameters are: motion, optical flow and haptic response, introduced by using a lane departure warning assistance system. It is shown in this research that the influence of motion cues on the subjective degree of realism rated by the drivers is of 84%. The vibrations in the steering wheel improve the realism of the simulation and have a 15% impact. The participants of these experiments could easily adapt to the provided assistance system and their immersion in the simulated environment was significantly influenced by the activation of the lane departure warning option. It has also been shown that drivers rated the motion and the accelerations felt in the simulator with 70.41%, compared to the experience of driving a real vehicle. These results are interpreted in this research by putting the emphasis on the fact that irrespective of the DOF of the actuation mechanism, a motion driving simulator should provide correct motion cues. The development of the vehicle models and of the motion cueing algorithms should be approached, so that the system provides motion as similar as possible to the real vehicle, as it is further discussed here.

Table of Content

List of Figures

List of Tables

Nomenclature

α	rad/s^2	The input angular acceleration along the canal axis
α_h	-	The area ratio
δ	rad	The angular deviation of the cupula with respect to the skull
$\dot{\delta}$	rad/s	The angular velocity of the cupula with respect to the skull
$\ddot{\delta}$	rad/s^2	The angular acceleration of the cupula with respect to the skull
ζ_f	-	The damping ratio, motion cueing
ζ_h	-	The viscous damping ratio, hydraulic model
ϕ, θ, ψ	rad	The Euler angles: starting from the fixed frame, they are achieved by rotating first around the z axis with ψ, then rotating the new x axis with θ and finally by rotating the new z axis with □
$\rho_{R_i}, i = 1,..,4$	rad	Rotation of the wheel about its roll axis
$\varphi_v, \theta_v, \psi_v$	rad	Cardan shaft angle of the vehicle
ω_{nh}	Hz	The natural frequency, hydraulic model
ω_r	$s-1$	The pulsation of the disturbance factor
$\boldsymbol{\omega_v}$	rad/s	The vehicle's angular velocity
ω_{vf}	Hz	The servo valve natural frequency
$\Gamma_{roll,pitch}$	rad	The tilt angles of the platform
$\boldsymbol{\Theta}$	m	The chain joint coordinates in vector form
$\dot{\boldsymbol{\Theta}}_{\boldsymbol{a}}$	m/s	The actuated joint velocities of the robot in vector form
a_i	-	The Bulk modulus paramaters, hydraulic model
a_0	m/s^2	The amplitude of the vibration acceleration
a_t	m/s^2	The acceleration human threshold
a_y	m/s^2	The piston's acceleration
c_A	Ns/m	The damping coefficient, the vehicle model
d_{c_i}	m	The tyre deflection
d_{s_i}	m	The steady spring deflection
f	Hz	The time frequency
f_{hs}	-	The valve hysteresis
$\boldsymbol{g}$	m/s^2	The gravitational acceleration
h	-	The road surface's profile
h_0	mm	The height of the irregularities of the road
k_A	N/m	The suspension stiffness coefficient
k_i	-	The integral parameter - PID Controller

k_d	-	The derivative parameter - PID Controller
k_f	-	The proportional parameter, motion cueing
k_p	-	The proportional parameter - PID Controller
k_R	*N/m*	The tyre stiffness coefficient
k_v	-	The proportional factor, hydraulic model
l	*m*	The fixed distance between 2 joints of the parallel manipulator
l_h	*m*	The distance from the rear axes to CG, vehicle model
l_r	*m*	The length of the irregularities
l_v	*m*	The distance from the front axes to CG, vehicle model
m	-	The number of rigid bodies within a chain
m_R	*kg*	The un-sprung mass of the quarter car model
m_A	*kg*	The sprung mass of the quarter car model
m_t	*kg*	The total mass of the hydraulic system
m_v	*kg*	The vehicle body mass
n	*cycle/m*	The spatial frequency
n_r	-	The number of common restriction for the elements of a parallel mechanism
n_0	*cycle/m*	The reference spatial frequency
q_i	-	General coordinates of the actuated joints
u_h	*V*	The saturated controlled output, hydraulic model
$\boldsymbol{u_v}$	*m/s*	The velocity of the vehicle
u_v^*	*V*	The valve input voltage
$\boldsymbol{r}\left[r_x, r_y, r_z\right]^T$	*m*	Coordinates of the position vector connecting the mobile coordinate system and the fixed coordinate system of the parallel manipulator.
s	-	Laplace operator
t	*s*	Time
v_t	*rad/s*	The velocity human threshold
$\boldsymbol{v}_k$	-	The measurement noise vector
$w(t)$	-	The white noise signal
w	-	The waviness coefficient
$\boldsymbol{w_k}$	-	The process noise vector
x_0	*m*	The amplitude of the vibration
$\hat{\boldsymbol{x}}_{\boldsymbol{k}}$	-	The estimated state
x_v^*	*m*	The normalized servo valve position
$\dot{x}_v^*$	*m/s*	The normalized servo valve velocity
$\ddot{x}_v^*$	m/s^2	The normalized servo valve acceleration
z	cm^2/s^3	The intensity of vibration

z_{q_i}	m	The actuator strokes, inverse vehicle model
z_{A_i}	m	Displacement of the sprung mass, quarter car model
$z_r(t)$	m	The road roughness
$z_{R_i}, i = 1,..,4$	m	Vertical movement of the wheel
$\boldsymbol{A}$	-	Matrix function of the pose parameters and joints variables
$\boldsymbol{A_i}\left[x_{A_i}, y_{A_i}, z_{A_i}\right]^T$	m	The coordinates of the points belonging to the fixed platform of the parallel manipulator
$\boldsymbol{A_k}$	-	The matrix relating the state at the previous step to the state at the current step
A_p	m^2	The piston area
A_r	m^2	The rod area
ACC	-	Adaptive Cruise Control
ADAS	-	Advanced Driver Assistance Systems
$\boldsymbol{B}$	-	Matrix function of the pose parameters and joints variables
$\boldsymbol{B_i}\left[x_{B_i}, y_{B_i}, z_{B_i}\right]^T$	m	The coordinates of the points belonging to the mobile platform of the parallel manipulator
B_d	*Ns/m*	The damping coefficient of the cupulo-endolymph system
$\boldsymbol{B_k}$	-	The matrix relating the optimal control input to the state $\boldsymbol{x}$
C_i	-	The number of joints with i DOF of a mechanism, i=1..6
$\boldsymbol{C_k}$	-	The matrix relating the state $\boldsymbol{x}$ to the measurement $\boldsymbol{z_k}$
CF	-	The correction factor
$\boldsymbol{CG}\left[x_v, y_v, z_v\right]^T$	m	Coordinates of the vehicle's centre of gravity
$D(\dot{p})$	-	The power dissipation
D_v	-	The servo valve damping factor
DMP	-	Differential motion parallax
DOF	-	Degrees of Freedom
E()	-	The expected value
E_{max}	-	The maximum bulk modulus
EFDS	-	Essential Function Driving Simulator
$\boldsymbol{F_v}$	N	The vehicle body forces in all three axes (x, y, z)
F_e	N	The external load considered in the hydraulic actuators modelling
F_f	N	The friction force
F_w^d	N	The dynamic wheel load
FFT	-	Fast Fourier Transformation
FOV	-	Field of View
$G_q(n)$	*dBm/Hz*	The road power spectral density
$G_q(\Omega_0)$	$m^2/(cycle/m)$	The road roughness coefficient
$\boldsymbol{H}$	-	The transformation matrix between the mobile coordinate system and

		the fixed coordinate system of the parallel manipulator
HMI	-	Human-machine-interface
I	kgm^2	The moment of inertia of the endolymph
$\boldsymbol{I_v}$	kgm^2	The vehicle moment of inertia
ISO	-	The International Standard Organization
$\boldsymbol{J}$	-	Jacobian matrix of the robot
K	N/m	The stiffness coefficient of the cupulo-endolymph system
K_{vib}	-	The vibration perception coefficient
$\boldsymbol{K_k}$	-	The Kalman gain matrix
LDW	-	Lane Departure Warning
$\boldsymbol{M_v}$	Nm	The vehicle body moments in all three axes (x,y,z)
M_d	-	The number of degrees of freedom of the system
M_p	-	The number of identical degrees of freedom of one mechanism
$\boldsymbol{M_s}$	-	The acceleration sensor's orientation matrix
MCA	-	Motion cueing algorithm
$O_{m_{x_0}z_0y_0}$	M	The mobile coordinate system of the parallel manipulator
$O_{0_{x_m}z_my_m}$	M	The fixed coordinate system of the parallel manipulator
P	-	Prismatic joint
PSD	-	The Power Spectral Density
P_a	bar	The pressure in chamber A_h
P_b	bar	The pressure in chamber B_h
P_h	-	The factor percentage contribution
$\boldsymbol{P_k}$	-	The prediction error covariance
P_0	bar	The supply pressure, hydraulic model
P_T	bar	The tank pressure, hydraulic model
Q_{L_i}	m^3/s	The flow leakage
$\boldsymbol{Q_k}$	-	The process noise covariance
$\boldsymbol{R_k}$	-	The measurement noise covariance
S	-	Spherical joint
S_h	-	The sum of squares – Taguchi method
S_k	-	The innovation covariance
S_{pal}	pal	The intensity of the vibration
S_{vibrar}	vibrar	The intensity of the vibration
$T(p, \dot{p})$	J	The kinetic energy
T_B	J	The kinetic energy of the vehicle body

T_d	s	The time delay
T_U	J	The kinetic energy of the un-sprung masses
T_w	s	The resonance time constant
U	-	Universal joint
$U(p)$	J	The potential energy
U_S	J	The potential energy stored in the suspension
U_T	J	The potential energy stored in the tyres
$\boldsymbol{VE}$	-	Acceleration sensor vector expressed in the earth fixed coordinate system
$\boldsymbol{V_L}$	-	Acceleration sensor vector expressed in the 3DMG's local coordinate system
V_{LA}	cm^3	The volume of pipe in chamber A_h
V_{LB}	cm^3	The volume of pipe in chamber B_h
$\boldsymbol{W_m}$	-	The full twist of the end effector corresponding to the velocities of the m degrees of freedom of the parallel manipulator
W_{max}	m	The maximum displacement allowed by the motion platform
$\boldsymbol{X}$	-	The generalized coordinates of the mobile platform

1 Introduction

From research until automotive industry, driving simulators are used in a wide range of different applications: testing and implementing new systems [Tsimhoni and Liu, 2003; Kamada et al., 2008], evaluation of driver's behaviour [Peli et al., 2005], training the drivers [Wang et al., 2005], vehicle dynamics studies [Griffiths and Gillespie, 2005], traffic safety studies [Hirata, 2005], etc. The driving task, the decisions to be made and its implications for the driver are still challenging tasks to be modelled from a mathematical point of view. In order to use a driving simulator for training and research purposes, this virtual reality tool has to offer a naturalistic driving experience to its driver. It is well known that a driving simulator cannot reproduce 100% real life situations or sensations, due to workspace and actuators limitations [Nehaoua et al., 2006]. Although there is much research available dealing with the development and optimization of driving simulators [Chapron and Colinot, 2007; Slob, 2008; Berger et al., 2010], it is very difficult to find an extensive work dealing with the driving simulators limitations and failures, while trying to render realistic cues. This motivates the present research.

This doctoral work is part of a joint cooperation between the Department of Manufacturing Engineering from the Technical University of Cluj-Napoca and the Chair of Mechatronics from the University of Duisburg-Essen and is focusing on developing an Essential Function Driving Simulator (EFDS) that integrates cost and design constraints, the human perception of motion and real vehicle motion achieved through simulated vehicle models and the classical motion cueing algorithms (MCA). The goal is to immerse the driver to a certain extend into the simulation environment using a cost effective driving simulator and to investigate the degree of realism of such a solution.

A complete understanding of the human motion perception process is crucial in order to provide a realistic simulation environment and it is discussed in the second chapter of this work. The driving task was often described in the literature as a purely visual task, due to the significant amount of information the driver is collecting through the visual channels, while driving [Sivak, 1996]. However, the information that the human driver uses other channels too for spatial-temporary information is available in literature [Kemeny and Penerai, 2003].

Chapter 3 presents the mathematical modelling of the considered actuation solutions for the EFDS and the human sensitivity to motion and vibrations of the simulated vehicle is studied. All the control strategies studied in this thesis are implemented with respect to the human perception of motion. The fourth chapter presents the hardware implementation of the MCA, and discusses the methodology and results of the experimental testing.

Chapter 5 deals with the validation of the models and results. The approach used in this work regarding the validation consists in estimating transfer functions between signals obtained from the model of the simulated vehicle and signals recorded and measured on the simulator's headrest. By means of these transfer functions, any other researcher could refer to the capabilities and limitations of the system, both from a human perception and from a dynamical point of view. The velocities and accelerations of the driver's head can be obtained while knowing the velocities and accelerations of the simulated vehicle. The velocities and accelerations perceived by the driver can be obtained from the vestibular human models presented in Chapter 3. The conclusions of this work and future research directions are discussed in Chapter 6.

2 State of the Art of Driving Simulators

Driving simulators render the dynamics of the vehicle and its interactions with the world (road, traffic signs, buildings, other vehicles, etc.) as already defined by Eskandarian et al. in [Eskandarian et al., 2008]. These research tools are integrating visual displays, sound rendering systems, actuated mechanisms and human-machine-interface (HMI) devices (steering wheel, pedals, gear shift lever, etc.) with the goal of immersing the driver in the simulated virtual environment. In this research, a virtual reality environment stands for a real-time graphical environment, as defined in [Lewis and Griffin, 1997]. This provides the driver with visual cues. A computer generates these cues, dependent on the dynamical model of the simulated vehicle; while driving in a simulated scenario, the image will move with respect to the angles of the vehicle body. Lewis and Griffin define partial immersive virtual reality as a virtual environment projected on a wide field of view (FOV) display [Lewis and Griffin, 1997]. The authors also claim that a fully immersive virtual reality refers to visual cues provided by a head movement display. This work is dealing with partial immersive virtual reality.

Driving simulators are usually categorized in literature as *low level, mid level and high level simulators*, according to the authenticity degree of the simulation offered to its driver [Straus, 2005]. *Low-level simulators* usually do not provide any motion, and the driver interacts with the simulated world through pedals, steering wheels, and visual displays [Slob, 2008]. These systems provide force feedback and reproduce audio cues through speakers. *Mid-level simulators* usually include a mock-up of the vehicle and visual displays with a larger FOV than the low-level driving simulators; they provide force and audio feedback and are usually actuated along one mechanical degree of freedom (DOF) [Slob, 2008]. *High-level simulators* include a motion base, which provides the driver with accelerations and therefore a more realistic driving experience [Peli et al., 2005]. They offer a large FOV of usually 220º [Slob, 2008].

Figure 2.1: A low level driving simulator (MiniSim) [NADS, 2011], a mid level driving simulator (Volkswagen) [Slob, 2008], and a high level driving simulator (NADS) [NADS, 2011]

Motion simulation was first used in flight simulators, starting with the 1950s [Durkee, 2010]. Applying this concept in the automotive industry, soon generated a lot of interest, and so, Volkswagen built the first driving simulator in 1970 [Slob, 2008]. Over the last 40 years, driving simulators became trustable tools used in different research applications [Harms, 1993; Griffiths and Gillespie, 2005; Colombet et al, 2008]. Different systems are being tested with respect to their performance and limitations prior to implementing them in an expensive prototype vehicle. Of high interest for the automotive industry remains the interaction human-vehicle-environment; in a driving simulator, the driver is integrated in the virtual environment and its behaviour is closely observed.

Consequently, different studies are conducted using a driving simulator, in conditions that would not be safe to be carried out in the real world [Blana, 1996]. Understanding human

driving behaviour is very important in order to improve the traffic safety [Horst and Hogema, 2011]. Studies concerning the influence of alcohol or drug use, of bad weather conditions, of different diseases on the driving task, all lead to a better understanding of the decisions the driver makes while driving. Another topic of high interest in the automotive industry represents the development and implementation of advanced driver assistance systems (ADAS). Testing these system limitations together with the acceptance of the driver is crucial before any implementation in mass production [Bruenger-Koch, 2005].

Highway simulators have been available since the 1960s [Blana, 1996]. It was not until 1985 that Daimler-Benz (now Daimler AG) built the first driving simulator integrating a Stewart platform [Slob, 2008]. Daimler upgraded the simulator in 1993 and once more in 2010. The simulator is now used in the Sindelfingen production and development plant [DAI, 2011]. It still uses a Stewart platform which can slide on a 12 m rail and it is used for testing new systems and auto models, in accident and safety researches, etc. [DAI, 2011].

Since 1985, other automobile manufacturers have built this kind of tool as well: Mazda and General Motors in 1985, Ford in 1988, Nissan in 1999, etc. [Slob, 2008].

Mazda introduces their first 4 DOF driving simulator in 1985, conducting studies concerning mainly the driver's behaviour, human perception mechanism, breaking reaction time, comfort, safety and validation [Blana, 1996; MAZ 2011].

Ford Company builds its first driving simulator in 1988, bringing forth the first studies about driver's performances [Blana, 1996]. Ford was the first in North America to develop a full motion based driving simulator, Virtual Test Track Experiment Simulator (VIRTTEX), in order to continue the already advanced research focused on safety, driver reaction, and behaviour, according to [FORD, 2011].

Renault uses its driving simulators in testing new systems, safety studies, implementation and evaluation of ADAS, driver behaviour, physical and perceptual validation, etc. [Blana, 1996; Kemeny, 2009]. At Renault's Technocentre several simulators with different topologies have been used in research since 1989 [Blana, 1996]. Very interesting theses were written based on the studies developed in this centre, especially using a Renault mock-up motion simulator actuated by a Stewart platform, focusing on development and implementation of new systems, safety and HMI studies [Reymond and Kemeny, 2000; Kemeny and Penerai, 2003; Kemeny, 2009].

BMW designed its first driving simulator mainly for HMI studies [Reich et al., 1996]. The automobile manufacturer upgraded the simulator in 2003, providing a dome and entrance made through a tunnel, in order to give the driver the impression he enters a car and not a driving simulator [Slob, 2008; BMW, 2011].

The Swedish National Road and Transport Research Institute, VTI, introduced their first driving simulator in 1984 [Blana, 1996]. This was able to simulate large lateral motion and comprised a real car mock-up and colour TV projectors, as stated in [Olstam, 2007]. In the early 1990s, the second VTI driving simulator was developed and it incorporated a truck cabin that was used for professional driver training [VTI, 2011]. In the late 1990s, a third driving simulator with a larger workspace was designed, being able to rotate the mobile platform around 90º. The current research focuses on the driver's behaviour in the transportation system, heavy vehicles behaviour, road users' requirements on road surface conditions, implementation of different ADAS, etc. [VTI, 2011].

The traffic safety issue started to be approached in Japan in the 1960s, concerning the increasing number of fatalities [Kamada et al., 2008; Yoshimoto and Suetomi, 2008]. Starting with the late 1980s, the Japanese automotive companies have been developing their own

simulators, according to [Yoshimoto and Suetomi, 2008]. The Japan Automotive Research Institute started using their 6 DOF driving simulator in 1996 [Slob, 2008].

The KITDS simulator was developed in 2001 as a cooperation between the Kitami Institute of Technology, Japan and the Japan Road Research Department [Maeda et al., 2005]. The driving simulator integrates a 6 DOF actuation mechanism and it provides two main functions: to generate different road response using measured profile data and to reproduce movements using measured vehicle motion data [Maeda et al., 2005].

A 6 DOF simulator was also designed at the Kookmin University, South Korea in 1998 and the main focus of the studies conducted is: human-vehicle interaction, efficiency of using driving simulators in HMI studies, studies on traffic light location and concerning implementation of Adaptive Cruise Control (ACC) in vehicles and behavioural adaptation to ACC, tunnel design, etc., according to [Lee et al., 1998]. In 2007, the research department replaced the motion platform with four actuators, which simulate the suspension travel as well as the roll, pitch, and heave motion [Lee et al., 2007]. The driving simulator provides a horizontal FOV of 140º and a head-eye tracking system for measuring the required data [Lee et al., 2007].

The University of Grönigen, Netherlands first gave in use the TRC Simulator in 1991; the research focuses on the evaluation of information systems and road design, driver decision making and performance, as noted by Blana in [Blana, 1996].

The Human Factor Research Institute, Netherlands designed the TNO Simulator, focusing on safety and comfort through the establishment of the important human factors. The initial version had 4 DOF and was used in experiments investigating the behavioural evaluation of different design characteristics for tunnels, the human decisions while braking, consequences of using ACC in the vehicle, etc. [Blana, 1996]. Nowadays, TNO covers a wide range of simulators, from motion based ones until high level simulators like Desdemona or the BMW 318i mock-up motion simulator actuated by a Stewart platform and the research focuses mainly on implementation of ADAS and tunnel design characteristics [Horst and Hogema, 2011]. The fixed base driving simulator incorporates a Volkswagen 4 mock-up and it provides force feedback in the steering wheel and a horizontal FOV of 180º [Horst and Hogema, 2011].

The SIMUSYS Simulator was designed as a cooperation between institutions from Spain, Italy and France, being functional starting from 2003 [SIM, 2003]. It is a motion simulator with 4 DOF and it was build to be used in entertainment, training and research. Different studies were conducted and the physical condition of participants was analyzed, the authors recommending people with high blood pressure not to use this kind of virtual reality devices [SIM, 2003].

The George Washington University, US designed a motion based driving simulator, using a real vehicle in the structure, and developing tests focused on safety studies, concerning the avoidance of collisions and crashes [GWU, 2011].

The national advanced driving simulator (NADS-1) was developed in 2003 [NADS, 2011]. It is a driving simulator with 13 DOF consisting of a Stewart platform which travels on a XY table [Slob, 2008]. The ongoing research focuses on traffic safety studies, human factor investigations, the development and implementation of new systems (ADAS, new simulation technologies), etc. Different vehicles were modelled and are now available for use in this simulator: a Ford Taurus, Chevrolet Malibu, Jeep Cherokee, a tractor-semitrailer, etc. [Heydinger et al., 2002]. The simulator provides a 360º horizontal FOV, achieved with the help of 15 projectors and it is very flexible with respect to the scenarios that can be simulated, according to [NADS, 2011]. The vehicle model includes the power train, cruise control, tyres,

brakes, steering and aerodynamics in order to provide the driver with a realistic driving experience [Heydinger et al., 2002; NADS, 2011].

In 2007, the NADS simulator was exceeded in size by the Toyota driving simulator, as stated in [Slob, 2008]. The simulator has 13 DOF and it includes a real vehicle, inside of a dome, actuated by a 6 DOF Stewart platform, mounted on a linear robot system, which is connected to a XY turntable; the road response is transmitted to the car with the help of a vibration simulator with a maximum displacement of 0.05 m [TOY, 2011].

2.1 Applicability

The question of how efficient driving simulators are in human behavioural studies remains open because of the restrictions of these systems [Kemeny, 2009]. However, many articles were published illustrating successful results using a driver simulator, and enabling the better understanding of different vehicle systems or the driver's behaviour. The following subchapter discusses the efficiency of these tools and reviews some of the results obtained in experiments conducted with such virtual reality devices.

Snowden, Stimpson and Ruddle proved in [Snowden et al., 1998], after performing experiments in a driving simulator able to simulate different weather conditions scenarios, that the velocity of the vehicle increased as the density of the fog increased too. The drivers involved in the experiments were not able to correctly estimate the speed of the vehicle [Snowden et al., 1998].

Evans showed that humans cannot perceive well the velocities of the vehicle approaching from opposite direction, recommending that the drivers should consult their speedometer before approaching an overtaking manoeuvre [Evans, 1991]. The studies published in [Milosevic and Milic, 1990] showed that around 90% of the drivers do not consult their speedometer before such a manoeuvre and perceive the speed of the vehicle based on the information collected from the environment through the visual channels.

Planque et al. stated that under drowsiness, the driver makes larger and more imprecise movements with the steering wheel, compared with when he or she is in an alert state; resulting in changes of the trajectories when one is tired [Planque et al., 1991]. Harms conducted a study in 1993 where he observed that velocities recorded in the simulator were higher than the velocities recorded in real life scenarios [Harms, 1993]. Peli et al. performed experiments in which they evaluated the driving performance of subjects with vision impairments, in order to better understand the impact of the visual or other physical disabilities on the driving task performances [Peli et al., 2005].

Koutsopoulos et al. presented the development and validation of a PC driving simulator, used for collection of data on driver route choice behaviour in the presence of information in [Koutsopoulos et al., 1994]. The data obtained from the experiments conducted was used to study different behaviours such as: route choice, day-by-day patterns, etc. [Koutsopoulos et al., 1994].

Lee et al. used the Kookmin Simulator to evaluate the influence of ACC on the driver; it was found that the use of ACC draws consistency in the head-away time, but it does induce distractions to the driver, resulting in reduced lane keeping ability [Lee et al., 2007].

Jones et al. conducted a study using a fixed base driving simulator with the goal of investigating whether the use of galvanic vestibular stimulation can reduce the symptoms of simulator adaptation syndrome [Jones et al., 2007]. The galvanic vestibular stimulation refers to the process of using electrical stimulation for vestibular nerves; the authors proved that the incidence of simulator adaptation syndrome can be reduced by using this method [Jones et al.,

2007]. However, the authors stated that there is limited empirical evidence to prove this theory and the current research is being conducted concerning this theme.

Kamada et al. designed and implemented a forward collision warning system in a driving simulator, in which the warning output timing can be changed by the foot position of the driver. The effectiveness of this algorithm was experimentally confirmed [Kamada et al., 2008].

In [Kondoth et al., 2008] the results from experiments conducted with the help of a fixed base driving simulator from the Nissan Research Centre concerning safety and risk perception are discussed. The results show that the driver's perception of risk is strongly affected by the time head-away and the time to collision. With the help of these results, the authors could formulate an equation that estimates the driver's perception of risk with respect to these two parameters [Kondoth et al., 2008].

2.2 DRIVASSIST

Due to the work being conducted on ADAS at the Chair of Mechatronics, University of Duisburg-Essen, a tool was developed to test ADAS in combination with a real driver in the loop [DRV, 2011]. The static driving simulator DRIVASSIST provides good results for high-way traffic scenarios, as already stated in [Hesse et al., 2009]. The DRIVASSIST simulators have different topologies and combine visual, acoustical and haptic cues submerging the driver into a sufficient degree of realism, with the help of visualization of driving situations and scenarios through screens, engine sounds simulated with loudspeakers, a force-feedback steering wheel, force-feedback pedals and steering torque [DRV, 2011].

The static mock-up simulator represents a flexible solution (please see Fig. 2.2). Its applications are diverse, ranging from new system implementation to presentations at fairs and events; the full functionality of DRIVASSIST can be used. In what concerns the design, special attention was paid to the ergonomics of the driver's workplace. As a HMI device, the simulator interacts with the driver through a fully functional force feedback steering wheel and gas/brake pedals [DRV, 2011]. The visualization of the simulated environment is done on a 52 inch LCD TV; the extension to rear views can be added, if desired [DRV, 2011].

The second DRIVASSIST static simulator was developed based on a Ford Fiesta JA8 model, while keeping the entire driver's workspace and control. The steering feedback is realised with the help of a high performance actuator; the visualization is done with a total of four 55 inch LCD screens, front and rear view also, and an 8 inch TFT [DRV, 2011].

The Volkswagen static simulator was implemented based on a VW Golf IV model. The conventional steering system was replaced by a force-feedback steering; the visualization is done with two bright HD projectors on a large screen in front of the vehicle and it can be extended to a panoramic view [DRV, 2011].

Figure 2.2: DRIVASSIST Simulators: Mock-up Simulator, Ford Fiesta Simulator, and Volkswagen Golf Simulator [DRV, 2011]

The analyzed manoeuvres on these devices were mainly quasi static, and therefore, no vehicle movement was needed for a more realistic impression [Hesse et al., 2009]. However, ADAS are getting more and more complex. Assistance for longitudinal and lateral vehicle guidance is combined. Additionally, they also cover guidance, as well as stabilization tasks [Capustiac et al., 2011a]. Therefore, the manoeuvres to be tested in a simulator gain complexity. This also means that the simulator itself has to fulfil new requirements; a static simulator could not be enough for evaluating the performance of assistance systems for all relevant driving manoeuvres. In order to expand the simulation scenarios to more complex manoeuvres, e.g. driving on country roads and in the city, and to evaluate corresponding ADAS with such manoeuvres, an active driving simulator is required to offer a more realistic driving experience to the driver [Capustiac et al., 2010a]. Thus, this work focuses on the development of such an EFDS, as already being discussed by the author in [Capustiac et al., 2010a].

2.3 Limitations

Independent of the available workspace and number of DOF, driving simulators cannot reproduce identically the accelerations of the simulated vehicle [Nehaoua et al., 2006]. Denne stated in [Denne, 2004] that some sustained accelerations cannot be reproduced in motion driving simulators.

Different strategies are therefore used in order to immerse the driver in the virtual environment and to increase the degree of authenticity of the simulation [Capustiac et al., 2011b]: e.g. MCA [Telban and Cardullo, 2005], a complete enclosed environment [Denne, 1996], a large FOV [Baron et al., 1980], visual and audio cues [Hesse et al., 2009]. The motion cueing strategy, the term used in literature for the strategy concerning the transformation of the vehicles accelerations, and velocities in achievable motion by the simulators [Arioui et al., 2009] was first used for aircraft simulators [Jamson, 2000]. There has been done significant research in this field. The classical MCA have a simple architecture and consist of low and high pass filters [Nehaoua et al., 2006]. The disadvantage of these algorithms is that their parameters are kept constant during the simulation [Chapron and Colinot, 2007]. The adaptive algorithms were developed in order to overcome this disadvantage by introducing time varying gains in their structure [Augusto and Loureiro, 2009]. The optimal algorithms solve a transfer function that relates the vehicle's motion to the achievable motion by the platform, so that the difference between the signals is minimized [Nehaoua et al., 2006].

However, the use of driving simulators has its disadvantages: *motion sickness*, *false cues* that can occur, *validity*, *limited workspace*, etc. [Blana, 1996] and they will be discussed in this subchapter.

Motion sickness is defined as a condition that appears when there are discrepancies between the information perceived through the visual channels and the vestibular system [Eskandarian et al., 2007]. It can cause e.g. nausea, dizziness, headache, fatigue, vomiting, blurred vision, eyestrain, postural instability, and drowsiness, as described in [Lewis and Griffin, 1997]. *Simulation sickness* is a type of motion sickness, causing the same symptoms and appearing when false cues are applied to the person driving the simulator [Mollenhauer, 2004]. *False cues* are usually incorrect motion, visual or audio cues introduced in the virtual environment, causing a conflict between what the drivers are used and expecting to perceive through their vestibular system and what they are actually perceiving in the driving simulator. This can occur from errors introduced in the provided cues or from time delay between the commands given to the simulator and its response. This is a very important aspect concerning motion simulation, being well known that no motion is preferred to false movement [Denne, 1996].

Three main theories are discussed in the literature concerning motion sickness: *cue conflict theory*, *poison theory* and *postural instability* [Mollenhauer, 2004].

The *cue conflict theory* is based on the assumption that sickness is caused by a conflict between what the vestibular system is expecting to perceive and what information it actually perceives [Treisman, 1977].

The *poison theory* is an evolutionary theory and assumes that while experiencing symptoms like dizziness, headache, and blur vision, the brain reacts like in the case of poisoning, and while trying to drain the contents of the stomach, it will cause vomiting, nausea, etc. [Treisman, 1977].

The *postural instability theory* is based on the idea that the body is constantly trying to keep a postural stability. Sickness appears when the body is trying to maintain this stability in an unknown environment [Riccio and Stoffgregen, 1991]. Lewis and Griffin stated that there are two main types of sensory conflicts to cause motion sickness:

- The conflict between the eyes and the vestibular sense organs, referring to *inter-modality rearrangement*;
- The conflict between the semicircular canals and the vestibule, referring to *intra-modality rearrangement* [Lewis and Griffin, 1997].

Validation of a driving simulator is an important factor that has to be approached while designing a driving simulator [Eskandarian et al., 2008]. There are two methods described for validation of such devices in literature.

The dynamics of the simulator is compared to the dynamics of the simulated vehicle; this is referred to in literature as *tuning* [Durkee, 2010] and it can be made by measuring experimental real data and by comparing it with recorded data during simulations: accelerations and velocities of the vehicle, steering angle, road noise, etc. [Eskandarian et al., 2008]. The fidelity of a driving simulator increases with the number of real life situations that can be simulated; thus, it is assumed in literature that a high-level simulator will provide more realistic driving experiences than a low-level driving simulator [Godley et al., 2002], but the discussions concerning which DOF a driving simulator should reproduce or how does motion cueing affect the driver's behaviour are still open [Colombet et al., 2008].

Although dynamical validation is necessary, it is useless in the research concerning the driver's interaction with the vehicle, without the *behavioural validation*, as stated in [Godley et al., 2002]. This sort of validation can be made if there is a parallelism between human behaviour in the real vehicle and in the driving simulator. There are four methods described in literature for behavioural validation: *comparing different data* (lane position, steering angle, gas and brake pedal position, velocity of the vehicle, etc.) recorded in a real vehicle with the one recorded in a driving simulator, analyzing the *psychological loading* in real world and simulation environment, using *subjective criteria* or *education and informational transfer* [Blaauw, 1982]. This research deals with subjective criteria in order to determine the realism degree of the driving simulator.

Low level driving simulator may be worth from 5,000 € - 100,000 €, a mid level driving simulator can be purchased starting from 100,000 €, and a high-level driving simulator can be worth from hundreds of thousands of Euros up to more than 1,000,000 €, depending on their configuration and equipment [InM, 2011]. Many factors have to be considered when designing a driving simulator: cost, application area, test to be carried, etc. In Fig. 2.3 the dependence between the number of DOF and the cost of a driving simulator can be observed. Usually a compromise has to be made when building such a system. The goal of this thesis

was to develop a cost effective driving simulator with 3 DOF (EFDS) and to investigate its degree of realism, as already described by the author in [Capustiac et al., 2011b].

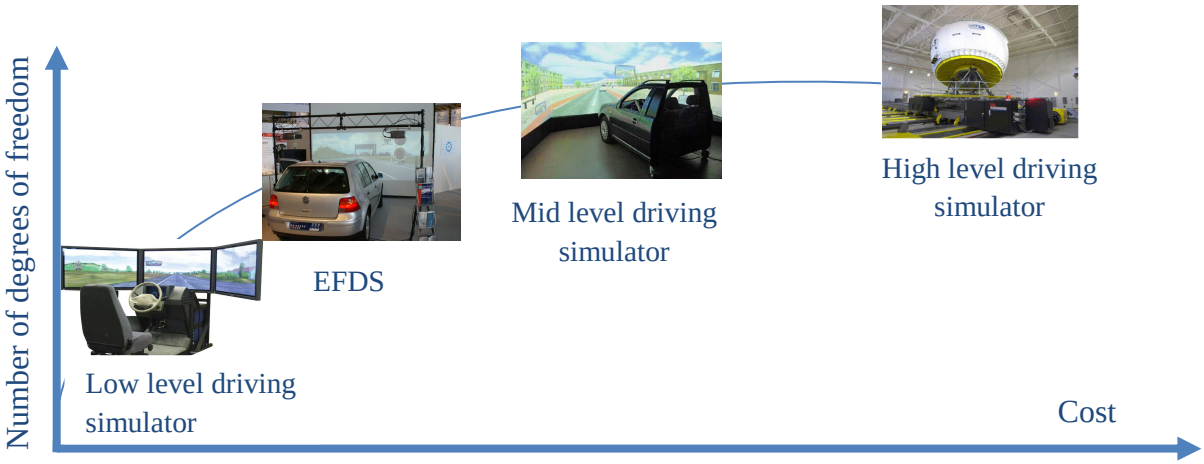

Figure 2.3: A representation of different driving simulators with respect to cost and DOF [Slob, 2008; NADS, 2011]

Liang, Show and Green defined the *temporal* and *spatial realism* as very important characteristics to be considered while designing a virtual reality environment [Harrison et al., 2010]. The *temporal realism* is defined with respect to the time lags in the system, which has to be minimized, and the simulation to run in real time [Harrison et al., 2010]. The *spatial realism* refers to the fact that the driver has to be able to move around in the simulated environment and he or she has to be able to observe different objects from more perspectives [Harrison et al., 2010]. The time delay in the system and the update rate were found to affect the performance task in a virtual reality environment [Lewis and Griffin, 1997]. Nilsson also argued that the simulations must run in real time in a virtual reality environment [Nilsson, 1993]. This doctoral work is dealing with real time simulation.

2.4 Actuation

There are various solutions used for actuating driving simulators; they are being discussed in literature and some of the most often proposed are being presented in this subchapter. Driving simulators usually integrate *serial* or *parallel mechanisms*. Although parallel mechanisms remain the preferred solution by researchers, plenty of driving simulators use open loop mechanisms. Mazda introduced their simulator with 4 DOF in 1985 and the mechanism proposed allows rotations around all axes and linear displacement along y axis, as presented in the following figure, using a gimbals – rail system [MAZ, 2011].

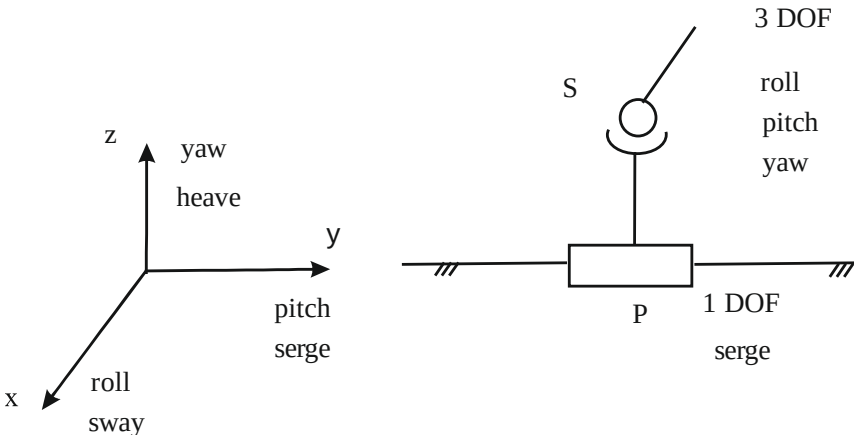

Figure 2.4: Kinematic scheme for the Mazda driving simulator [MAZ, 2011]

Table 2.1: The Mazda driving simulator parameters [MAZ, 2011]

Simulator	**Characteristics**						
Mazda Driving Simulator	Type	Number of DOF				Actuation	Number of actuators
	4 DOF gimbals Rail system	4 DOF				Electrical	4
		Yaw	Pitch	Roll	Serge		
		±160°	±40°	±40°	±3.6 m		

The Desdemona Simulator uses a 6 DOF mechanism, as shown in Fig. 2.5 and it was build together with the Austrian company AMST [Horst and Hogema, 2011].The mobile platform is mounted on a gimballed system with 3 DOF, which can perform vertical motion along Z and Y axis, and rotation around a central axis to perform centrifugal motion. Its designers claim that this topology offers a wider dynamic range with respect to the conventional hexapod topology [Roza et al., 2007]. The available workspace and characteristics are given in Table 2.2. A vehicle mock-up can be mounted on the platform. The Desdemona simulator is used in experiments focusing on flight and driving simulation, HMI and disorientation research [Roza et al., 2007].

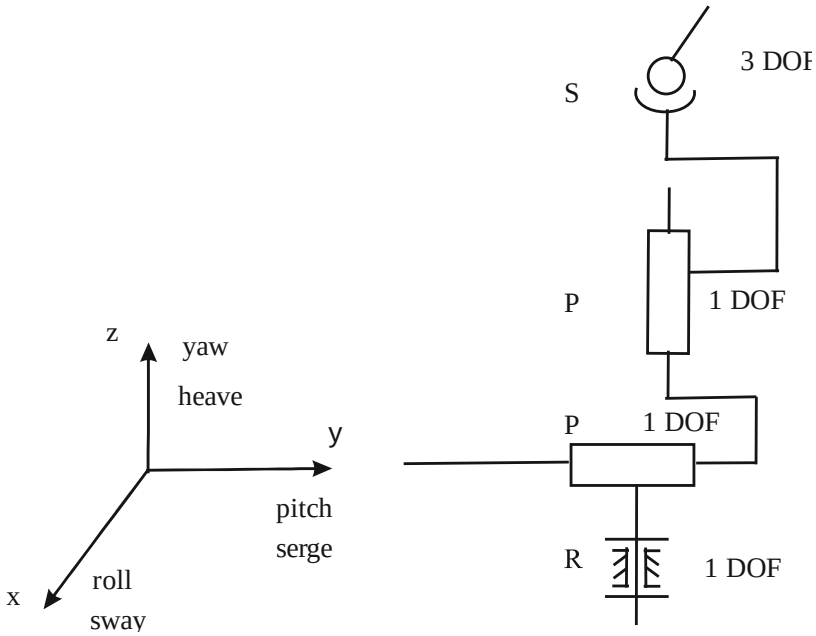

Figure 2.5: Kinematic scheme for Desdemona driving simulator [Roza et al., 2007]

Table 2.2: The Desdemona driving simulator parameters [Slob, 2008]

Simulator	**Characteristics**							
Desdemona	Type	Number of DOF					Actuation	Number of actuators
	Hexapod	6 DOF					Hydraulic	6
		Yaw	Pitch/ Roll	Heave	Sway/ Serge	Acceleration		
		±45°	±45°	±1 m	±4 m	Centrifugation around yaw axis		

A large number of driving simulators integrate the Stewart Platform. This is a kind of parallel mechanism with closed kinematic chains. This kind of mechanisms was first introduced by Gough [Gough, 1957]. It consists of a fixed and a mobile platform connected to each other by six variable length links (please see Fig. 2.6). By controlling these links, the positioning of the platform in 6 DOF is allowed. All the six accelerations of the vehicle can be simulated with this structure in a relatively big workspace.

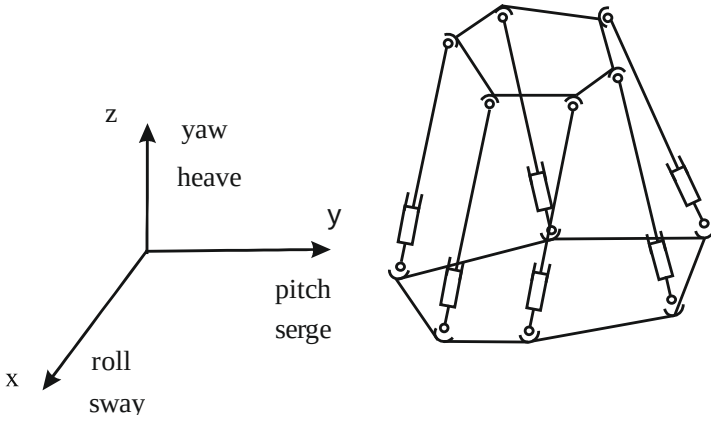

Figure 2.6: Kinematic scheme for a 6 DOF Stewart Platform [Karimi and Nategh, 2011]

A parallel mechanism, proposed by Merlet in [Merlet, 2006] is shown in Fig. 2.7. As it can be observed, the mechanism integrates a passive kinematic chain with 3 DOF which allows two rotations and only vertical translation for the mobile platform. This kind of architecture for parallel mechanisms, where the passive link is connected to the platform through a universal joint, enabling the rotation around its own axis was first introduced by Reboulet [Merlet, 2006]. The InMotion Company integrates such a solution in one of their simulators [InM, 2011]. This simulator does not use linear actuators as motor joints, but a combination of a lever and a rotary motor, as described by Merlet in [Merlet, 2006]. Table 2.3 gives the available workspace of the 3 DOF simulator developed by Inmotion [InM, 2011].

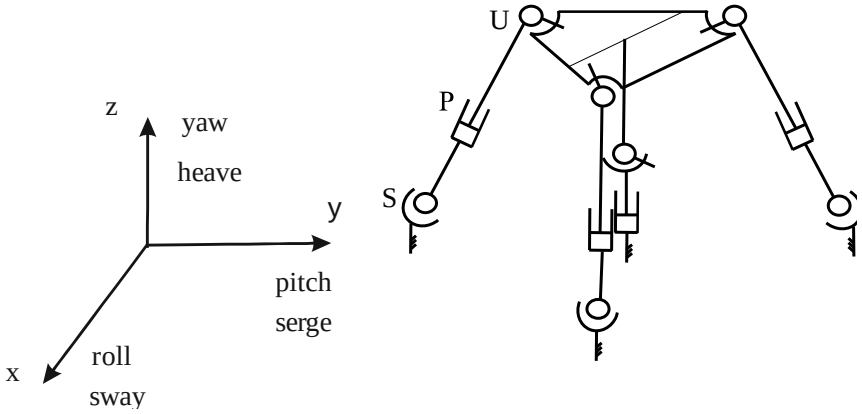

Figure 2.7: Kinematic scheme for the 3DOF parallel manipulator [Merlet, 2006]

Table 2.3: The InMotion driving simulator parameters [InM, 2011]

Simulator	**Characteristics**						
InMotion Simulation	Type	Number of DOF				Actuation	Number of actuators
	3 DOF structure	3 DOF				Rotary motors; Electrical	3
		Pitch	Roll	Max. Heave	Max. Acceleration		
		±25°	±25°	0.12 m	0.5g		

There are numerous flight simulators that integrate parallel mechanisms in their structure. Merlet noted that truck driving simulators are the sector where the Stewart platform is the most successful [Merlet, 2006]. However these mechanisms are used for flight, ships, trains or vehicle simulators. The University of Iowa introduced in 2003 their 13 DOF driving simulator, which integrates such a platform [NADS, 2011]. The Us Army Centre for Tanks Research uses such a type of simulator; this machine is capable of rendering 4 to 6 g vertical acceleration and it is mainly used in studies concerning the interior's tank ergonomics and arm stabilization systems [Merlet, 2006]. The Air France Airbus A340 simulator or the Czech Airlines Airbus A320 simulator, both integrates such a mechanism in their flight simulator [CzA, 2011].

Ford Motor introduced their 6 DOF driving simulator in 1988, and it was used in different research studies [Blana 1996; Slob, 2008; and FORD, 2011]. It offers a large workspace as it can be observed in Table 2.4. The parallel platform is actuated by six hydraulic cylinders powered by a 440 hp power system [Slob, 2008].

Table 2.4: The Ford Motor driving simulator parameters [Slob, 2008]

Simulator	**Characteristics**					
	Type	Number of DOF			Actuation	Number of actuators
Ford Motor Driving Simulator	Hexapod	6 DOF			Hydraulic	6
		Yaw	Pitch/Roll	Heave	Sway/ Surge	
		±20°	±10°	±1 m	±1.6 m	

Renault also developed a 6 DOF driving simulator incorporating a Stewart Platform [Kemeny, 1993]. The parameters describing this simulator are provided in Table 2.5. The control of the Rexroth-Hydraudyne 6-axes electric mobile platform is made at 100 Hz for rendering linear and angular accelerations up to 0.5 g [Dagdelen et al., 2002]. The visual cues are presented on a forward FOV of 150º, together with rear view mirrors. This virtual reality device uses a Clio II cockpit with fully operational commands [Reymond et al., 2000]. The steering wheel provides a force feedback with a maximum torque of 8 Nm; the simulated environment is displayed with the help of six projectors, three for the front- and three for the rear-view mirrors [Dagdelen et al., 2002].

Table 2.5: The Renault driving simulator parameters [Dagdelen et al., 2002]

Simulator	**Characteristics**					
	Type	Number of DOF			Actuation	Number of actuators
Renault Driving Simulator	Hexapod	6 DOF			Electrical	6
		Yaw	Pitch/ Roll	Heave	Sway/ Surge	
		±15°	±15°	±0.22 m	±0.22 m	

The Kitami Institute of Technology from Japan developed in 2001 the 6 DOF driving simulator, KITDS [Shiraishi, 2001]. Table 2.6 shows the simulator's characteristics. The available workspace is relative small compared to Renault and Ford solutions, as it can observed while consulting the parameters. The configuration is low-height and compact and

the driving simulator's main purposes are training and research in safety driving, according to [Shiraishi, 2001].

Table 2.6: The KITDS parameters [Slob, 2008]

Simulator	**Characteristics**							
KIDTS	Type	Number of DOF					Actuation	Number of actuators
	Hexapod	6 DOF					Electrical	6
		Yaw	Pitch/ Roll	Heave	Sway/ Surge	Maximum acceleration		
		±8°	±10°	±0.1m	±0.1m	0.5 g		

The University of Iowa introduced their simulator the National Advanced Driving Simulator (NADS-1) in 2003, setting new standards for driving simulators [NADS, 2011]. It consists of a 6 DOF platform which travels on a XY table, as can be observed in Fig. 2.8. A dome, with a real vehicle inside can perform rotation around Z-axis, and the vehicle inside the dome is actuated by 4 hydraulic cylinders, in order to reproduce the road irregularities [Slob, 2008].

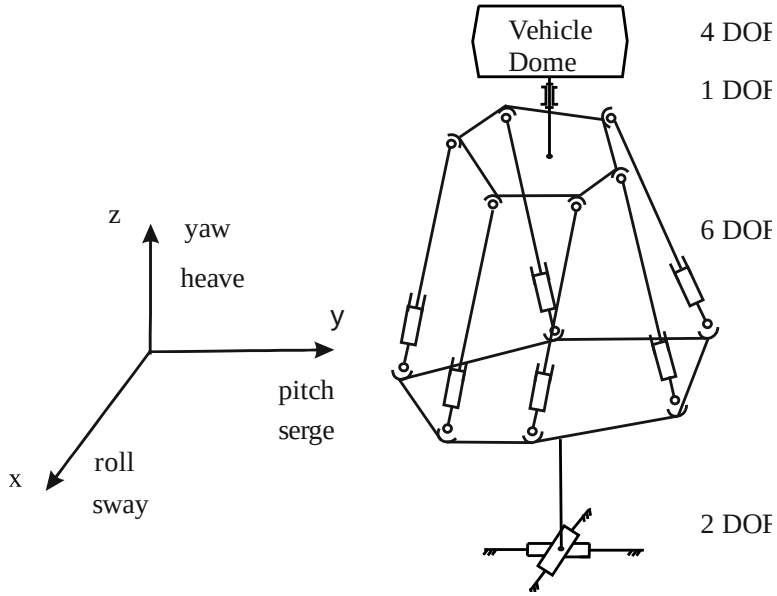

Figure 2.8: Kinematic scheme for NADS-1 [NADS, 2011]

Table 2.7: The NADS-1 parameters [Slob, 2008]

Simulator	**Characteristics**							
NADS	Type	Number of DOF					Actuation	Number of actuators
The National Advanced Driving Simulator	A XY-table on which a hexapod travels.	13 DOF					Hydraulic Servo motor driven steel belts	13 (10 hydraulic + 3 electric)
		Yaw	Pitch/ Roll	Heave	Serge/ Sway	Vibration displacement		
		330°	±25°	±0.6 m	±9.7 m	±5.08 mm up to 40Hz		

The control system uses a complex MCA that transforms the accelerations of the vehicle model in achievable motion by each DOF of the system; this simulator can reproduce very

complex manoeuvres and real life situations. Continuous improvement is realized concerning this system; transfer functions for each DOF are frequently generated, to ensure the flattest response possible for each bandwidth [NADS, 2011]. The horizontal FOV is of 360º and the hearing cues are rendered through multiple speakers placed in and around the vehicle.

Toyota introduced in 2007 their 13 DOF driving simulator, exceeding in size the NADS-1 simulator; the simulator slides on a XY table allowing motion 25 m laterally and 35 m longitudinally. It provides accelerations up to 0.5 g; the vibrations introduced in the vehicle have maximum amplitudes of 0.01 m [TOY, 2011]. The design of the Toyota simulator is very similar to NADS-1 one, with the difference that the Toyota simulator is bigger, and the yaw turning mechanism actuates the car inside the dome and the case of the NADS-1 simulator it actuates the whole dome; Toyota engineers described it as the most realistic virtual driving environment currently in existence [TOY, 2011].

Another type of simulators are the so called *'road simulators'*; these are mechanisms directly connected to a vehicle. They are usually used in durability tests and can provide from 3 to 6 DOF [MTS, 2011]. The advantage of these systems is the observation that the actuator displacements are similar to the road profile and its roughness. When integrated in a driving simulator, these mechanisms introduce the road characteristics, which are defined as one of the main inputs for vehicle dynamics [Guglielmino et al., 2008]. This can have positive impact on the realism degree of the driving simulator, since the human body is sensitive to vibrations, especially to high frequency vibration which are easily transmitted trough tissues [Capustiac et al., 2011b].

2.5 The Human Perception of Motion

Gregory defined perception as a process that includes 'making inferences' from what we see and trying to make the best guess out of this information [Gregory, 1974]. He also estimated that the amount of information lost from the moment it is perceived by the eye until it is processed by the brain is around 90%. This is the reason why the brain has to guess what the eye is seeing, based on past experiences. This shows that people are actively building their perception of reality, as stated in [Gregory, 1974].

The *perception of motion* is defined as the interpretation of the sensory information by the humans, while *ego motion* represents the motion of the body in space, according to [Kemeny and Penerai, 2003]. The motion is sensed by the human through the balance organs in the ear and the skin by judging the acceleration through skin pressure [Denne, 2004]. The human body finds itself in continuous movement and interaction with the environment and the space-temporal information is gathered with the help of the perceptual system. The illusion one may have of linear or rotational self motion while driving a motion simulator is known in literature as *vection* [Lewis and Griffin, 1997]. This subchapter provides basic information concerning human motion perception. Once the human perception of movement and the driver's implication in its decisions are understood, the importance of introducing motion cues in a driving simulator is emphasized [Capustiac et al., 2011b].

The perceptual process includes the human ear as well. The ear has two parts: the *cochlea*, the auditory part of the ear and the *vestibular system*, the non-auditory part of the ear [Mollenhauer, 2004].

The vestibular system is responsible of controlling the equilibrium and motion senses in the human body; its role is to transfer information about the accelerations and rotations applied on the body to the brain [Tsimhoni and Liu, 2003]. The vestibular system has two parts: the *semicircular canals* and the *vestibule*, composed by the *utricle* and the *saccule*, as it can be observed in Fig. 2.9 [Meiry, 1958]. The semicircular canals are three tubes, which control the

human body's sense of balance; these canals have almost the same structure and dimensions and are positioned perpendicularly to each other, permitting them to perceive the motion in all directions, as described in [Meiry, 1958]. The fluid inside the canals moves as the body moves, bending the hairs inside the canal and enabling the brain to determine the movement of the body through space, depending on the excitation level of the sensorial cells, according to [Kemeny and Penerai, 2003]. These canals are heavily damped, angular accelerometers [Van Egmond et al., 1949]. Each canal starts at the utricle, dilates at the ampulla, contracts again and terminates at the other end of the utricle, as defined by Meiry. The utricle is the largest component of the vestibule and a multidimensional linear accelerometer and the otolith is the moving mass of this accelerometer and it is a gelatinous substance allowing a limited sliding travel of about 0.1 mm [Meiry, 1958].

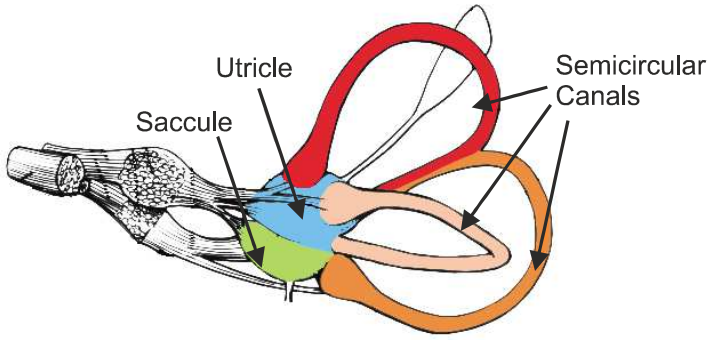

Figure 2.9: The human vestibular system as presented in [Kemeny and Penerai, 2003]

The vestibular system is very sensitive to accelerations, especially to acceleration variation and less to vibration frequencies. However, the frequency strongly influences the human body's reactions, as stated in [Buzdugan, 1980].

Steinhausen was the first to model the semicircular canals using the concept of a heavy damped pendulum [Van Egmond et al., 1949]. The modelling is made based on the assumption that the moment of inertia of the pendulum corresponds to the fluid from the semicircular canals and the spring corresponds to the elasticity given by the cupula. The name of the fluid located in the canals is *endolymph* and the *cupula* is a structure of the vestibular system, located in each of the three canals. Using this model, the *cupulo-endolymph* system was described with the help of a second order linear differential equation [Van Egmond et al., 1949]:

$$I\ddot{\delta} + B_d\dot{\delta} + K\delta = I\alpha \tag{2.1}$$

Where I is the moment of inertia of the endolymph, B_d is the damping coefficient, K is the stiffness, $\ddot{\delta}, \dot{\delta}, \delta$ are the angular deviation, velocity, respective acceleration of the cupula with respect to the skull and α is the input angular acceleration along the canal [Van Egmond et al., 1949]. The mathematical model of this human organ can be used as a basic tool for evaluating the expected, subjective orientation of the driver. As defined by Young and Ormsby, the outputs of this system should be the orientation of the driver's head with respect to the gravitational acceleration, the rate of the rotation and the translational acceleration of the head [Ormsby and Young, 1977]. Meiry found that the information is transmitted to the brain by frequency modulation and that when it is not being stimulated, the sensors show nerve action potentials of about 8-10 pulses per second [Meiry, 1958].

Fig. 2.10 shows the driver head planes used in motion simulation. The frontal and the sagittal plane are perpendicular on each other and the intersection form the vertical axis, which is collinear to the gravity vector. As described by Meiry, the input to the vestibular system is a vector with magnitude and direction. However, the output is not a vector [Meiry, 1958].

The information from the vestibular system's components is sent to the central nervous system, though an awareness of the sensation of motion is perceived by the human [Meiry, 1958]. The indication of orientation is kept in a vector, but the sense of magnitude is applicable only on a comparative basis. However, the sensed orientation is the essential cue that the human feels while experiencing accelerations applied on his or her body; this sensed or perceived sensation is considered the vestibular system´s output in literature [Meiry, 1958] and is investigated here.

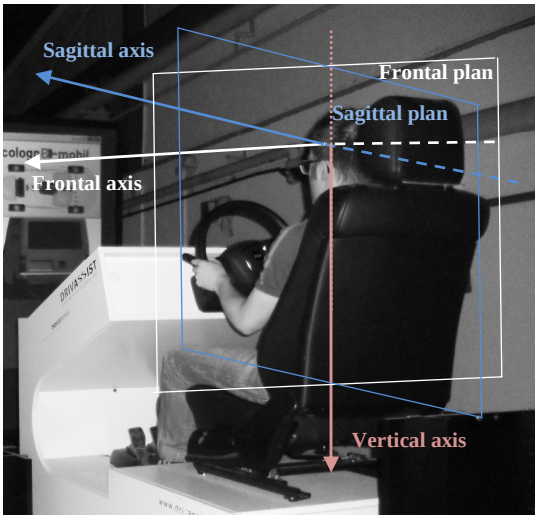

Figure 2.10: The head planes and axis used in motion perception

The existence of human motion thresholds was investigated and proved by scientists [Telban and Cardullo, 2005]. Below to such a threshold, the body does not perceive a constant acceleration and physically this threshold represents the minimum deflection of the cupula [Meiry, 1958; Telban and Cardullo, 2005]. Meiry was one of the first researchers to show in his doctoral work that the threshold for perception of angular acceleration around a vertical axis will vary subjectively between 0.1 and 0.2 $^{o}/s^{2}$, with a mean value of 0.14 $^{o}/s^{2}$ [Meiry, 1958]. The same author stated that if a threshold is associated with the minimum displacement of the otolith, the latency time to detect input acceleration of a certain magnitude will correspond to the duration of travel of the otolith from rest position to the threshold deflection [Meiry, 1958]. If the human body experiences constant accelerations from 10 to 20 s, this will be perceived by the brain as the acceleration ceases because the hair follicles of the vestibular system will return to their neutral position, as stated in [Meiry, 1958]. It is very important to understand how the vestibular system functions, in order to apply it characteristics in a dynamic driving simulator [Capustiac et al., 2011b].

Different motion cues can be reproduced in a driving simulator with respect to human motion perception [Capustiac et al., 2011a]. For example, a turn to the left will be felt by the driver as an inertial force to the right [Denne, 2004]. The sideways acceleration can be simulated by roll movement [Denne, 1996]. In a motion simulator, only lateral accelerations can be presented to the driver as long duration cues, according to Denne. Long duration cues are defined as cues that last many seconds, and all other acceleration cues are extremely short, being limited by the cylinder strokes [Denne, 2004].

Each cue, taken separately is also important in simulating a real driving situation, but it is important to correctly combine them [Capustiac et al., 2011a]. For example, for reproducing convincingly the forward acceleration of the vehicle, the platform will be tilted backwards and the visuals will move forward, the appropriate sound effects for this manoeuvre being thus provided [Capustiac et al.,2011a]. This strategy is known in literature as *tilt coordination*

[Kemeny and Penerai, 2003]. The illusory tilt effect is described as the linear acceleration being interpreted as the tilt of the body, as described in [Kemeny and Penerai, 2003].

The *Müller Effect* appears when the human body is leaned in the dark, to the left or right; a vertical or horizontal line will appear to lean in the same direction as the human body, as defined in [Borah et al., 1988]. The tilt has to be made in the range between 20º and 60º. The Aubert effect appears when the vertical or horizontal line leans in the opposite direction of the body's tilt. For such an effect to appear, the degree of motion ranges from 70º to 90º, as stated in [Borah et al., 1988].

The *Coriolis Effect* appears when the head is tipped forward as the body is rotating around the vertical axis; a sensation that one is falling sideways can appear [Borah et al., 1988]. The oculogyral illusion is explained by the sensation that objects are moving relative to the human's head [Borah et al., 1988].

The humans use the visual channels while driving a car in order to collect different information about the surrounding environment [Sivak, 1996]. In a driving simulator, the visual cues are introduced by a graphic system [Kemeny and Panerai, 2003]. The *optical flow* (OF) is one of the most investigated visual cue in a driving simulator. It is defined as the motion experience, which takes place while running, driving, and walking [Mollenhauer, 2004]. It occurs while heading towards a certain point. While fixing this point, this does not show movement. However, when looking around, the FOV appears to be extending, as noted in [Dursteler, 2004]. This effect is accurately perceived by the human brain, helping to control locomotion and continuous movement towards the destination. Jamson proved in [Jamson, 2000] that for correct speed perception in a driving simulator, a horizontal view of at least 120° is required. It was proven that the OF is used in certain situations for distance estimation [Lappe et al., 1999]. In a driving simulator, the OF can be changed in what concerns the visual complexity of the environment [Durkee, 2010]. Beusmans proved that OF is used to compare spatial intervals along the sagittal and frontal direction [Beusmans, 1998]. Jamson also stated that, while dealing with image characteristics when designing a driving simulator, the image resolution should be compromised to the widening of the simulator's FOV, emphasizing the importance of this parameter [Jamson, 2001].

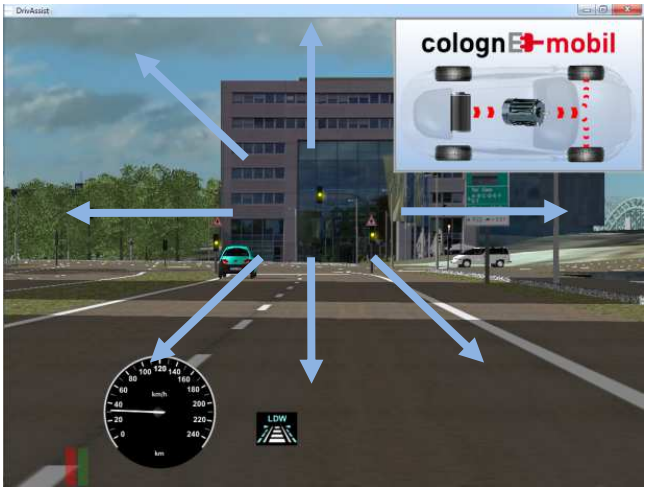

Figure 2.11: The OF in the DRIVASSIST driving simulator

Differential motion parallax (DMP) is defined as the perceived difference in velocity of close objects compared to distant ones [Kemeny and Panerai, 2003]. The DMP is easily perceived when looking through the window of a moving vehicle; the velocity of nearby objects appears to be greater than that of far away objects. This cue is usually missing in driving simulators, as noticed in [Evans, 1991]. According to [Jamson, 2000], the ability of perceiving the

velocity in a driving simulator minimizes while the FOV decreases. In order to estimate the speed, the driver uses space-temporal information taken from the environment [Milosevic and Milic, 1990]. A large FOV will offer more information to the driver, enabling a better estimation of the velocity [Durkee, 2010]. Gibson stated that processing the information is not necessary; the information has enough details from human-environment interaction and he formulated this theory based on the occurrence of DMP [Gibson et al., 1959].

It is stated in [Evans, 1991] that the *peripheral vision* has been thought to be responsible of motion perception: the spatial location, orientation, and large stimulus pattern. The same author stated that the *optokinetic reflex* is active in the range of 1 to 7 Hz, compensating for head movement in this range and is not accurate in the range of 0.1 to 1 Hz [Evans, 1991, Mollenhauer, 2004]. This reflex starts to develop at the age of sex months and allows the eye to follow a moving object while the head remains still.

The human eye is defined as an orientation sensor of prime importance for the body and it perceives body orientation with respect to the environment. There are two kinds of defined motion: the *tracking motion* and the *compensatory motion*. Three movement sensors control the eye motion: *the eye, the semicircular canals* and *the receptors* in the neck [Meiry, 1958]. Ellis and Chalmers stated that rotational motion is likely to have a greater impact on the human visual system, compared to the translational motion [Ellis and Chalmers, 2006]. The same authors conducted an experiment with twenty-six participants, where they proved that no decreasing of visual cues quality was noticed, when rendering motion cues in the driving simulator [Ellis and Chalmers, 2006]. The visualization of the environment in the DRIVASSIST is done with the help of a commercial game engine [TRQ, 2011]. This ensures a high level of realism and an easy adaption of scenarios [Hesse et al., 2009].

Rendering of the hearing cues in a driving simulator can increase its degree of realism considerably [Eskandarian et al., 2008]. Different sounds can be simulated in a driving simulator: engine sounds based on current engine states, vehicle type, velocity, load, wind sounds, horns, sirens, road noise [Capustiac et al., 2011a]. These sounds can be subjective to road roughness, vehicle velocity, etc. The engine and road sounds can increase the fatigue of the driver, together with the vibrations introduced in the simulator. Thus, they represent one important piece of information about the state of the vehicle. Perceiving audio cues is not limited to the hearing sensation and it is linked also to vibration and visual cue perception. Having in mind that most drivers experience low frequency chassis resonances while driving, it is important to introduce these frequencies in a driving simulator, or as stated in [Sottek et al., 2005], at least some amount of tactile vibration in the seat and steering wheel. It is further shown in this research how vibrations in the steering wheel affect the human in a driving simulator.

It is believed that the steering task is mainly controlled by visual cues information [Reymond et al., 2001]. However, since humans respond first to tactile and then to visual cues, the steering characteristics have been especially addressed during the development of DRIVASSIST [Capustiac et al., 2011a]. A multi-body model is used to derive the steering wheel torque in real-time and a DC motor is then used to generate exactly that torque at the steering wheel; this force-feedback steering wheel has already been used during the design of lane-keeping assistance systems and other studies and its realism has been shown during these studies, as shown in [Hesse et al., 2009]. In the DRIVASSIST vehicle simulators the correct usage feeling of the pedal is achieved by using the original vehicle pedals and the original brake booster support. The acoustic set up in DRIVASSIST meet the needs of a modern game. The used game engine enables a 3D sound of vehicles, the environment or triggered sound-emitters. This is not only used to create a realistic vehicle sound, but it can also be used as a HMI device [DRV, 2011].

2.6 The Driving Task

Driving a vehicle is a complex task, in which the driver is interacting with the traffic, has to obey the traffic rules, to control and drive safely the vehicle and also to pay attention to other traffic participants. It was found that not paying attention to the forward road is one of the major factors for incidents and accidents [Rydstrom, 2009].

While driving a vehicle, the human body experiences a complex sum of accelerations. There are two kinds of accelerations felt: *gravitational* and *inertial* (speed up, slow down, cornering, etc). Denne stated in [Denne, 1989] that in an enclosed environment it is impossible to distinguish between gravitational and inertial forces, due to the vestibular system's functionality. Exposure to centrifugal or linear accelerations, as well as coriolis forces is interpreted by the human as reorientation with respect to the gravity vector, as stated by [Meiry, 1958].

Denne defined the following parameters as very important in a simulator: *complete isolation* and *small amplitude motion* [Denne, 1989]. A *complete enclosed environment* will disable the driver to sense his orientation with respect to the gravitational vector and the *small amplitude motion* will induce the feeling of not being connected to an actuation mechanism [Denne, 1989]. The same author discussed about the 'threshold of credibility' that enables the driver to realise he or she is driving a simulator and not a real vehicle until the point where the focus will be turned exclusively on the task to be performed and on the simulator's picture. He also stated that 'a sense of real fear in an absolute safe environment' is necessary in order to provide the driver with a realistic driving experience [Denne, 1989].

Rasmusen proposed three levels of information processing: *skill, rule* and *knowledge based* [Reymond et al., 2001]. Driving is usually addressed in the literature as a skill based task. But it was noticed that, for example, driving in curves combines the control of both steering and speed [Reymond et al., 2001]. The same authors stated that performing such a manoeuvre requires vehicle velocity anticipation and control.

There are two sources of excitations while driving a vehicle: the *control actions of the driver* (cornering, accelerating and braking are all actions of the driver, which result in predictable forces, depending on the dynamics of the vehicle) and the *interaction vehicle-environment* (e.g. road response, potholes) [Denne, 2004]. There are two types of tasks that describe driving [Lee, 1976]:

- Velocity or following distance estimation by the drivers;
- Adjustment of these variables by usage of braking and acceleration pedals.

Lee proved in [Lee, 1976] that while braking, the driver is using the time to collision and not parameters as the distance, velocity or acceleration/deceleration of the vehicle. In the experiments conducted it was shown that the braking response time is in the range of 1 to 2 s [Lee, 1976]. The braking of a vehicle for a stationary obstacle can be described by the following parameters: steady velocity, the time to collision, the margin value and the time the driver needs to achieve an appropriate deceleration [Lee, 1976].

This chapter presented the state of the art of driving simulators, different actuation solutions used for acceleration rendering purposes, the capabilities and limitations of these systems and basic information about the human perception. This information represents the ground base of this doctoral work. The kinematical and dynamical analysis of the mechanisms, the design of the control algorithms, all relate to the literature review presented above.

3 Modelling and Simulation

Denne stated in [Denne, 1996] that simulating roll, pitch and heave motion is normally adequate for leisure simulation. The same author claims that yaw motion is not required to be simulated, due to the fact that the small rotations around z axes have no physiological effect and can be considered equivalent to the human head's rotations. Sway and surge motion, on the other hand can be coupled in the roll and pitch components in a driving simulator [Denne, 1996]. According to Kemeny, low cost motion simulation should take into account real vehicle motion through a simulated vehicle model, human perception of motion and various constraints such as performance and overall cost [Kemeny, 1993]. Based on these two observations, this research is focusing on the development of a 3 DOF EFDS, which will integrate *design and cost constraints, the human perception of motion* and *real vehicle motion*.

3.1 Design and Cost Constraints for the 3 DOF EFDS

This subchapter presents different structures of mechanisms with 3 or 4 DOF to be integrated in the EFDS. The motion of a vehicle where the chassis is considered a rigid body and without constraint of the road has 6 DOF and are classified as follows [Guglielmino et al., 2008]:

- Longitudinal translation – X axes (forward and backward motion);
- Lateral translation – Y axes (side slip);
- Vertical translation – Z axes (bounce or heave);
- Roll – Rotation around the longitudinal axis;
- Pitch – Rotation around the transverse axis;
- Yaw – Rotation around the vertical axis, as noted in [Guglielmino et al., 2008].

The 3 DOF chosen to be simulated with the active driving simulator are roll, pitch, and respectively heave. The DOF were chosen with respect to the simplicity of the design, type of psycho-physic studies to be carried out and the global cost of such a system, as already discussed by the author in [Capustiac et al., 2010a].

Due to the work already conducted on DRIVASSIST static simulators, two main actuation concepts were studied: *actuation of a mock-up driving simulator* and *actuation of a real vehicle*.

- The *mock-up driving simulator* is designed as a 3 DOF motion system, actuated by 3 electrical actuators [Capustiac et al., 2011b];
- The *vehicle driving simulator* is designed as a motion simulator where the wheels of the car are placed on 4 hydraulic actuators. The car itself acts as a mobile platform. The 3 DOF are realized by vertical excitation of the wheels through the hydraulic actuators as it was already discussed by the author in [Capustiac et al., 2011a].

Although the second solution includes a redundant mechanism, its advantages are the modular properties of the simulator and the assumption that for the applications considered, the link between the tyre and the road is not lost and hence it doesn't require modelling [Capustiac et al., 2010a].

Two major motion aspects are to be realized in the EFDS. First the *road excitation* can be introduced to the simulator by means of actuators, so that the actuators' displacements (high frequency) are very similar to the profile of the original road surface [McCann and Nguye, 2007]. The second aspect is to impose a *defined motion* (low frequency) to the vehicle body (inverse model) [Capustiac et al., 2010a]. The dynamic transfer path between the actuators and the vehicle body has to be understood because not only street excitation needs to be controlled, but also the roll, the pitch, and the heave motion of the simulator and it was already discussed by the author in [Capustiac et al., 2010a].

The goal of reproducing the accelerations is to give the driver a feed-back about the manoeuvre he or she is performing. Supposing the vehicle is driving a steady state circular manoeuvre, the driver needs to feel the lateral acceleration on his body, which is realized through a defined roll angle. Although the DOF and the workspace of the simulator are limited it will resituate a sufficient sensation of movement as closely as the one sensed in a real vehicle for the planed driving scenarios, as already stated by the author in [Capustiac et al., 2010b].

In order to understand the behaviour of a vehicle, the IPG Car Maker software was used [IPG, 2011]. This software offers the possibility of obtaining the dynamical parameters of a simulated vehicle, using complex non-linear dynamic models and all simulation solutions of this software are completely integrated into Matlab/Simulink [MAT, 2011]. This enables the data collections through Simulink blocks. The software allows the user to simulate different manoeuvres. The positions, velocities and accelerations of a simulated vehicle driving a wide range of manoeuvres, including high dynamical manoeuvres were registered and analysed.

It was concluded that the vehicle performs roll motion in a range not higher than ±4º and pitch motion not higher than ±2º. The maximum values for both angular motions were obtained while driving the highway exit and while performing the return manoeuvre. The data collected in these simulations were used further in designing the actuation mechanisms of the driving simulator. The Fast Fourier Transformation (FFT) implemented in Matlab was used to study the frequency response of the signals recorded with the help of IPG Car Maker software. The frequency values for the vehicle body were determined, as it can be observed in the following table.

Table 3.1: Values of the vehicle frequencies obtained in simulations [IPG, 2011]

Measuring Point	**Manoeuvre**	**Amplitude acceleration**	**Frequency**
Seat	Slalom 18 m	$0.19 - 0.5 \frac{m}{s^2}$	2.8-4 Hz
Carrier centre point	Slalom 18 m	$\leq 1.13 \frac{m}{s^2}$	1-2 Hz
Vehicle body CG	Slalom 18 m	$0.17 - 0.4 \frac{m}{s^2}$	1.1-2 Hz

The values obtained in the simulations were validated by vehicle frequency values taken from literature [Mitschke, 1995]:

- Seat frequencies 2.5 – 5 Hz;
- Wheel frequencies 8 – 15 Hz;
- Vehicle body frequencies 0.7 – 2 Hz [Mitschke, 1995].

3.1.1 Actuation of the EFDS

As stated before, two approaches were studied in this doctoral work. This subchapter deals with the design and the mathematical modelling of different actuation mechanisms for both the mock-up simulator and the vehicle simulator.

The actuation solutions discussed in this subchapter were chosen following kinematical and dynamical analyses, as trade off solutions with respect to the available workspace, singularity configurations, the system's behaviour and the maximum forces needed in the frame of the overall cost constraints.

The parallel mechanisms considered in this research incorporate *spherical*, *universal*, *rotational* and *prismatic* joints. A *spherical joint* (S) allows rotation around three axes, a *universal joint* (U) allows rotation along two axes, a *rotational joint* (R) allows rotation around one axis and a *prismatic joint* (P) allows displacement along one axis [Schramm et al., 2010].

For all the mechanisms considered, the motor joints are the prismatic ones. Some of the presented parallel mechanisms comprehend passive kinematic chains. These chains do not use motor joints, but they can affect the active joint forces required for positioning, as observed by Merlet in [Merlet, 2006]. Adding passive joints enables the flexibility of the DOF of the mechanism and is used in this research especially for taking the dynamical load.

The PSU Parallel Manipulator with 3 DOF

Fig. 3.1 presents the topology of the prismatic – spherical – universal (PSU) 3 DOF system, the first solution considered for actuating the driver simulator mock-up. The geometrical parameters that describe the manipulator are given in Table 3.2.

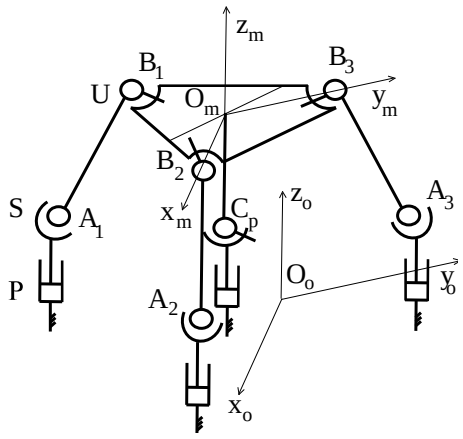

Figure 3.1: The parallel manipulator with 3 DOF, with PSU topology

As it can be observed from Fig. 3.1, the mechanism has a passive kinematic chain with 3 DOF, introduced with the purpose of taking the dynamic load through a spring-damper system. The mechanism incorporates three active kinematic chains with PSU topology.

This topology includes two rotational joints with 2 and respectively 3 DOF and one translational joint. The passive kinematic chain allows the moving of the platform along Z axes and rotation around X, respectively Y axes.

Table 3.2: The geometrical parameters of the PSU manipulator

Geometrical Parameters	**Values**
Distances between the points of the mobile platform	$\overrightarrow{\mathbf{B}_1\mathbf{B}_2} = 0.44$ m, $\overrightarrow{\mathbf{B}_1\mathbf{B}_3} = 0.37$ m, $\overrightarrow{\mathbf{B}_2\mathbf{B}_3} = 0.37$ m
Distances between the connection points of the fix platform	$\overrightarrow{\mathbf{A}_1\mathbf{A}_2} = 0.70$ m, $\overrightarrow{\mathbf{A}_1\mathbf{A}_3} = 0.69$ m, $\overrightarrow{\mathbf{A}_2\mathbf{A}_3} = 0.69$ m
Fixed distance between the joints	l = 0.35 m

Considering the relation of the number of DOF of a parallel mechanism [Merlet, 2006]:

$$M_d = (6 - n_r) \cdot m - \sum_{i=1}^{5} (i - n_r) \cdot C_i - M_p. \tag{3.1}$$

where M_d represents the number of DOF, M_p is the number of identical DOF of one mechanism, m is the number of rigid bodies within a chain, n_r is the number of common restrictions for the kinematic chains and C_i is the number of joints with i DOF of the mechanism.

Considering a parallel mechanism without restrictions, the system's DOF is:

$$M_d = 6 \cdot m - \sum_{i=1}^{5} i \cdot C_i. \tag{3.2}$$

The DOF of the 3 DOF PSU manipulator was calculated as it follows:

$$M_d = 6 \cdot m - 5 \cdot C_5 - 4 \cdot C_4 - 3 \cdot C_3 - 2 \cdot C_2 - C_1, \tag{3.3}$$

$$M_d = 6 \cdot 8 - 5 \cdot 4 - 4 \cdot 4 - 3 \cdot 3 = 3. \tag{3.4}$$

The virtual model for the 3 DOF PSU manipulator was built in Dymola [Dym, 2011]. This software is a complex tool for the modelling and simulating complex systems in different applications. It enables the simulation of dynamic behaviour and interactions between systems [DYM, 2011]. The elements of inertia were introduced in the model and the dynamical behaviour of this mechanism was analysed.

The discussed configuration was chosen in order to avoid singularities with the method proposed in [Kapur et al., 2007]. The similarity of the triangles describing the mobile, respectively the fixed platform was checked. The singular poses are defined by Merlet as particular configurations in which the parallel mechanisms end effector will gain uncontrollable DOF [Merlet, 2006]. These configurations need to be avoided because once the end effector reaches these positions it cannot be controlled [Merlet, 2006]. As presented in [Merlet, 2006] the relation between the actuated joint velocities of the parallel mechanism and the m dimensional twist $\boldsymbol{W}_m$ is:

$$\boldsymbol{A}\dot{\boldsymbol{\Theta}}_a + \boldsymbol{B}\boldsymbol{W}_m = 0. \tag{3.5}$$

With respect to this relation, three types of kinematical singularities can occur [Merlet, 2006]:

- When matrix $\boldsymbol{A}$ is singular and there is a velocity vector non-zero for which the platform doesn't perform any motion;
- When matrix $\boldsymbol{B}$ is singular and there is a non-zero m dimensional twist for which the joint velocities are zero enabling certain DOF to be uncontrollable;
- When both matrices are singular, the platform can be moved with locked actuators and vice versa [Merlet, 2006].

Where $\boldsymbol{A}$ and $\boldsymbol{B}$ are defined to be matrices function of the pose parameters and joints variables and $\dot{\boldsymbol{\Theta}}_a$ represents the vector of the actuated joint velocities [Merlet, 2006].

The proposed mechanism can perform an approximately large angular motion of ±19º around roll axis and ±13º around pitch axis and vertical displacement of ± 0.1 m. While designing such a mechanism, a very important step deals with determining the minimum and maximum values of the joint coordinates [Merlet, 2006]. Merlet stated that hence the limitations of the DOF in a parallel mechanism are usually coupled; the graphical illustration of a parallel mechanism workspace is possible only for a mechanism with no more than 3 DOF [Merlet, 2006]. According to the definition proposed by the same cited author, this research is dealing with maximal workspace. There are three kinds of workspace calculation methods that are known: *the geometrical, the discretizational and the numerical method*. The method implemented in this work is the geometrical one. By varying the lengths of the active segment (prismatic actuator) between their minimal and their maximum values, the reachable positions of the mobile platform describing the points B_i, i=1,..,3 were computed. The set of these coordinates provides the possibility to visualize the robot's workspace. Fig. 3.2 visualizes the 3D robot workspace.

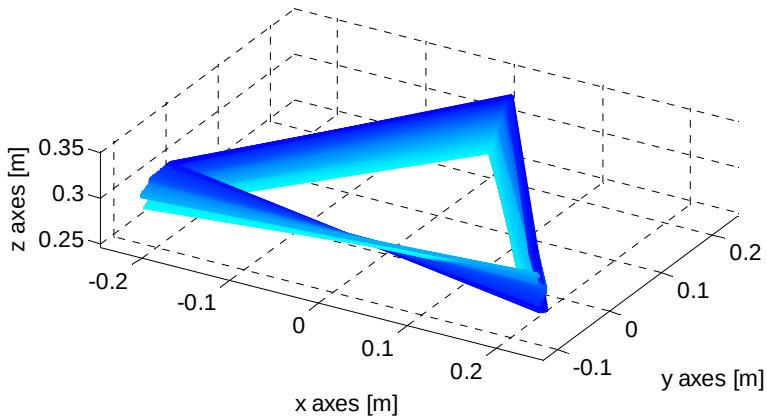

Figure 3.2: Visualization of the 3 DOF PSU parallel manipulator achievable positions

The SPU Parallel Manipulator with 3 DOF

Fig. 3.3 presents the topology of the spherical – prismatic – universal (SPU) 3 DOF system, that is the second solution considered for actuating the driving simulator mock-up. The geometrical parameters that describe the manipulator are presented in Table 3.3. The motor joints remain the prismatic ones. The same passive kinematic chain allows motion along the same 3 DOF as in the first solution. It can be easily observed that such a solution will bring advantages like portability and reduced friction in joints, with respect to the first solution presented [Merlet, 2006]. This manipulator has the same DOF and the same number and type of joints in its structure as the first solution, but it uses another type of kinematic

chain, the SPU type. A similar solution was discussed by Merlet and Inmotion Simulation uses such a 3 DOF mechanism, as it was already discussed in Chapter 2. The difference between the two solutions represents the type of actuators. The solution proposed in this research uses linear actuators and other types of joints in the structure of the mechanism.

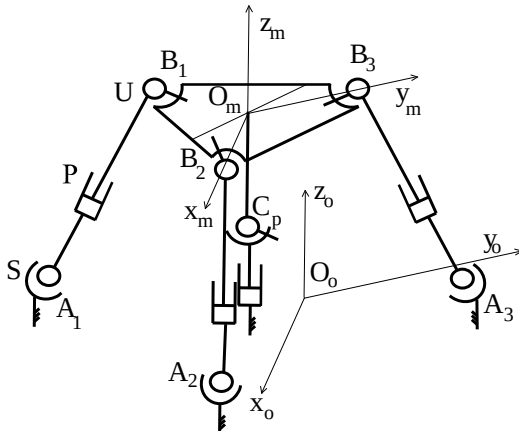

Figure 3.3: The parallel manipulator with 3 DOF, with SPU topology [Merlet, 2006]

Table 3.3: The geometrical parameters of the SPU manipulator

Geometrical Parameters	**Values**
Distances between the points of the mobile platform	$\overrightarrow{\mathbf{B}_1\mathbf{B}_2} = 0.55$ m, $\overrightarrow{\mathbf{B}_1\mathbf{B}_3} = 0.67$ m, $\overrightarrow{\mathbf{B}_2\mathbf{B}_3} = 0.6$ m
Distances between the connection points of the fix platform	$\overrightarrow{\mathbf{A}_1\mathbf{A}_2} = 0.90$ m, $\overrightarrow{\mathbf{A}_1\mathbf{A}_3} = 1.03$ m, $\overrightarrow{\mathbf{A}_2\mathbf{A}_3} = 1.03$ m
Fixed distance between the joints (actuator rest position)	$l = 0.48$ m
The fixed distance from the mobile platform to the universal passive joint	$\overrightarrow{\mathbf{O}_m\mathbf{C}_p} = 0.13$ m

The following figure visualizes the 3D robot workspace, obtained by using the same method as described above.

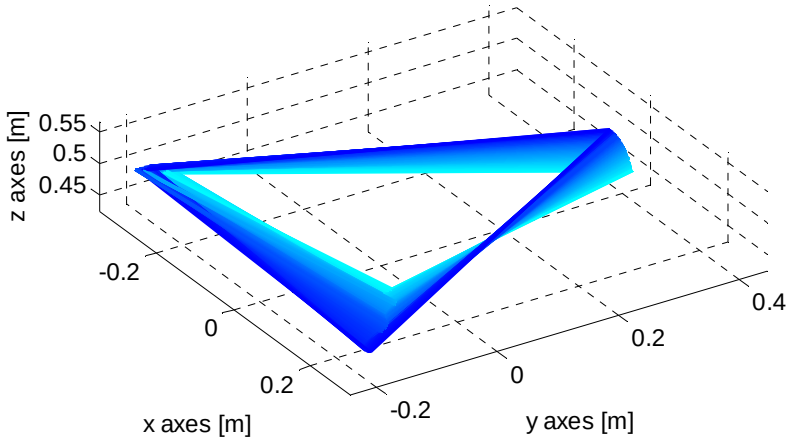

Figure 3.4: Visualization of the 3 DOF SPU parallel manipulator achievable positions

The workspace of the SPU manipulator is smaller than the PSU one and it can perform an angular motion of ±9º around the roll axis, and of ±10º around the pitch axis and the vertical displacement of ± 0.1 m. The virtual model for the 3 DOF driving simulator was built in Dymola and the forces required to reach an acceleration of 1g were calculated with the help of this model and were found to have a maximum value of 2 KN. As stated before, all the solutions presented were designed to be integrated with a mock-up driving simulator. A virtual model was developed for this system with the help of Solid Works as it can be observed in Fig. 3.5 [SW, 2011].

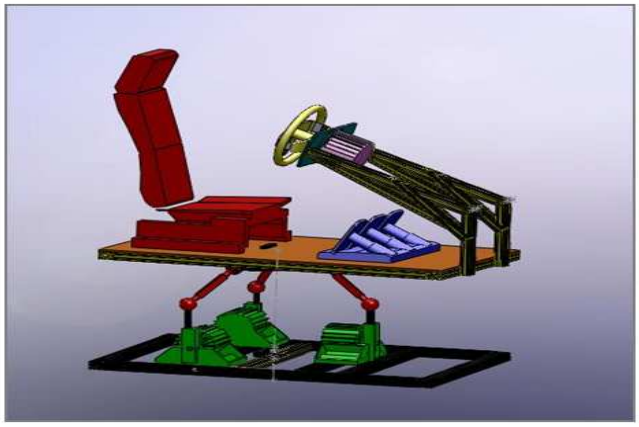

Figure 3.5: Solid Works model of the cockpit

The Parallel Manipulator with 3 DOF actuated by linear actuators

The third solution, proposed for the actuation of the EFDS, integrates three linear actuators connected directly to the motion platform through 3 spherical joints (S) and to the fixed platform through 3 rotational joints (R), as it can be observed in Fig. 3.6 and 3.7. The mechanism can perform an angular motion of ±7º around the roll and pitch axis and a vertical displacement of ± 0.175 m. The simulator is 2.2 m long, 1.35 m wide and 0.77 m high. Three linear motors, type SL2-250S produced by SEW Company are used for this application [Rode, 2007]. The maximum force these actuators can generate is of 4800 N and the maximum velocity is of 1 m/s; the maximum accelerations achieved are given in Table 3.4.

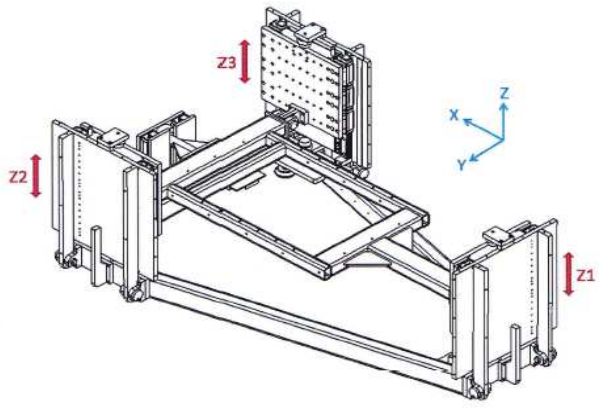

Figure 3.6: The 3 DOF actuating system using 3 linear actuators [Rode, 2007]

The 3 DOF of the system are calculated as follows:

$$M_d = 6 \cdot m - 5 \cdot C_5 - 4 \cdot C_4 - 3 \cdot C_3 - 2 \cdot C_2 - C_1, \tag{3.6}$$

$$M_d = 6 \cdot 7 - 5 \cdot 6 - 3 \cdot 3 = 3. \tag{3.7}$$

Table 3.4: The maximum linear accelerations of the 3 DOF driving simulator [Rode, 2007]

Axes	**Maximum Acceleration**
X	$19.63 \frac{m}{s^2}$
Y	$28.38 \frac{m}{s^2}$
Z	$19.81 \frac{m}{s^2}$

Fig. 3.7 presents the kinematical scheme of the considered mechanism.

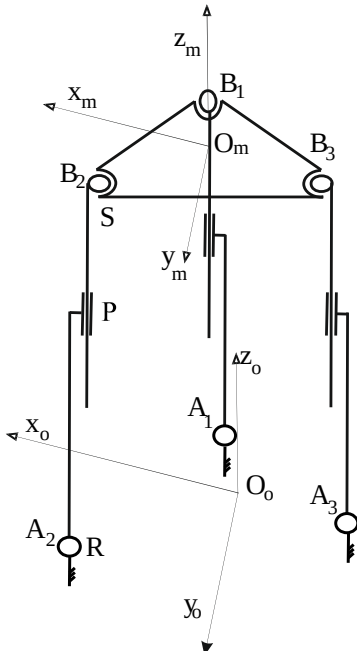

Figure 3.7: The kinematical scheme of the 3 DOF motion system, with RPS topology

The available workspace of the platform was calculated with the help of Matlab/Simulink and the visualization of it is presented in Fig. 3.8. It can be observed that the workspace of this mechanism is smaller than the one of the PSU 3 DOF, but the advantages of this solution are portability and reduced cost.

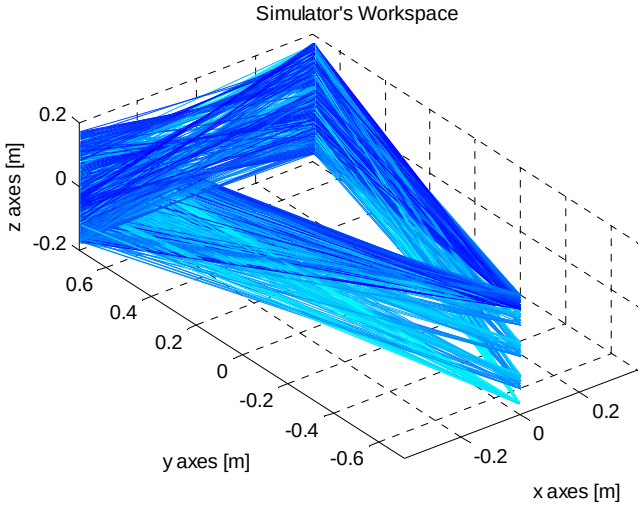

Figure 3.8: Visualization of the 3 DOF RPS parallel manipulator's achievable positions

The 4 DOF Parallel Manipulator

The fourth proposed solution for the active driving simulator was actuating the same platform, but with 4 actuators. Koevermans was the first to introduce a 4 DOF flight simulator [Merlet, 2006]. Merlet proved that it is impossible to design a 4 DOF parallel mechanism with identical legs. Hence, the possibility of designing a 4 DOF parallel robot is to either integrate a passive kinematic chain in its structure, or to use different topologies for the four legs, or a specific mechanical design [Merlet, 2006]. In order to design such a mechanism, this research introduces a passive kinematic chain in the structure of the 4 DOF driving simulator.

The geometrical parameters, which describe the manipulator analysed in this doctoral thesis, are given in Table 3.5. The advantage of this solution is that the simulator can reproduce more manoeuvres, with respect to the 3 DOF simulator. Each wheel of the car should be replaced by an actuator. Fig. 3.9 presents the parallel manipulator with 4 DOF.

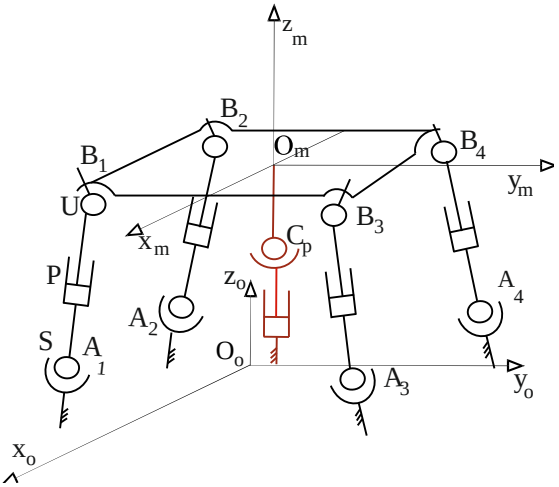

Figure 3.9: The parallel manipulator with 4 DOF, with SPU topology

The topology of the chosen kinematic chains is SPU. The kinematic chain highlighted with red represents the passive chain from the system. The DOF of the system was calculated as follows:

$$M_d = 6 \cdot m - 5 \cdot C_5 - 4 \cdot C_4 - 3 \cdot C_3 - 2 \cdot C_2 - C_1, \tag{3.8}$$

$$M_d = 6 \cdot 10 - 5 \cdot 5 - 4 \cdot 4 - 3 \cdot 5 = 4. \tag{3.9}$$

The 4 DOF are: roll, pitch, yaw and heave. The mechanism can perform an angular motion of ±5º around roll axis, of ±5º around the pitch and yaw axis, and the vertical displacement of ± 0.1 m.

Table 3.5: Geometrical parameters for the 4 DOF manipulator

Geometrical Parameters	**Values**
Distances between the points of the mobile platform	$\overrightarrow{\mathbf{B}_1\mathbf{B}_2} = \overrightarrow{\mathbf{B}_3\mathbf{B}_4} = 0.7$ m, $\overrightarrow{\mathbf{B}_1\mathbf{B}_3} = \overrightarrow{\mathbf{B}_2\mathbf{B}_4} = 1.48$ m
Distances between the points of the fix platform	$\overrightarrow{\mathbf{A}_1\mathbf{A}_2} = \overrightarrow{\mathbf{A}_3\mathbf{A}_4} = 0.72$ m, $\overrightarrow{\mathbf{A}_1\mathbf{A}_3} = \overrightarrow{\mathbf{A}_2\mathbf{A}_4} = 1.57$ m
The initial length of the actuator (rest position)	l = 0.5 m
The fixed distance from the mobile platform to the universal passive joint	$\overrightarrow{O_m C_p} = 0.13$ m

In order to develop the equations of motion of a vehicle chassis, considered as a rigid body without constraint of the road, the Newton-Euler equations are used, as already discussed by the author in [Capustiac et al., 2010c].

The motion equations in the body coordinate frame are [Schramm et al., 2010]:

$$\begin{aligned} F_x &= m_v \cdot (\dot{u}_x + u_z \cdot \omega_y - u_y \cdot \omega_z), \\ F_y &= m_v \cdot (\dot{u}_y + u_x \cdot \omega_z - u_z \cdot \omega_x), \\ F_z &= m_v \cdot (\dot{u}_z + u_y \cdot \omega_x - u_x \cdot \omega_y), \\ M_x &= I_{xx} \cdot \dot{\omega}_x - \omega_y \omega_z \cdot I_{yy} + \omega_y \omega_z \cdot I_{zz}, \\ M_y &= I_{yy} \cdot \dot{\omega}_y + \omega_x \omega_z \cdot I_{xx} + \omega_x \omega_z \cdot I_{zz}, \\ M_z &= I_{zz} \cdot \dot{\omega}_z - \omega_y \omega_x \cdot I_{xx} + \omega_y \omega_x \cdot I_{yy}. \end{aligned} \tag{3.10}$$

The equations of motion for the considered 4 DOF parallel driving simulator are:

$$\begin{aligned} m_v \cdot u_z \cdot \omega_y &= 0, \\ -m_v \cdot u_z \cdot \omega_x &= 0, \\ F_z &= m_v \cdot \dot{u}_z, \\ M_x &= I_{xx} \cdot \dot{\omega}_x - \omega_y \omega_z \cdot I_{yy} + \omega_y \omega_z \cdot I_{zz}, \\ M_y &= I_{yy} \cdot \dot{\omega}_y + \omega_x \omega_z \cdot I_{xx} + \omega_x \omega_z \cdot I_{zz}, \\ M_z &= I_{zz} \cdot \dot{\omega}_z - \omega_y \omega_x \cdot I_{xx} + \omega_y \omega_x \cdot I_{yy}. \end{aligned} \tag{3.11}$$

Such a solution can bring into the same hardware and software architecture both road and dynamics vehicle simulation. From the hardware point of view the concept is based on simulation of the road using the 4 DOF platform.

The virtual model of this system was built in Dymola software and the sample time was considered to be of 1 ms. The maximum forces needed were of 1.6 KN, in order to reach a maximum acceleration of 8.1 m/s^2, with a maximum stroke for the actuators of 200 mm. These simulations showed that the yaw rate can be uncontrollable. Although the inputs of the actuators were given with the purpose of obtaining roll and pitch rate, the platform produced only yaw and heave rate.

For this reason the solution of replacing the spherical joint from the passive link with a universal joint was considered, blocking in this way the yaw angle and obtaining a redundant mechanism as it can be observed in Fig. 3.10. The Solid Works model of this system was developed to be able to investigate and visualise better the mechanism's behaviour.

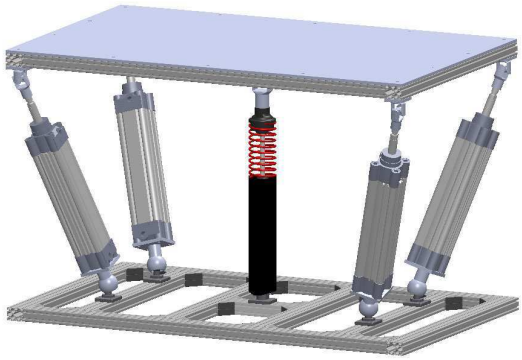

Figure 3.10: Solid Works model of the prototype with 4 DOF

An approximate cost of the actuation system was calculated around 19000 €, using the actuators from GSM-40 family, defined by the following characteristics: maximum force of 4 KN, maximum velocity of 953 mm/s, and stroke between 254 – 457 mm [ADR, 2011]. The overall cost of the system was too high and not justified, due to the low portability of the solution and the reduced available workspace.

Actuation of the entire vehicle

Fig. 3.11 presents the solution considered for the actuation of a real vehicle. The goal is to combine real road response signals together with certain imposed movements of the vehicle to create a realistic impression of driving, as discussed in [Capustiac et al., 2010a].

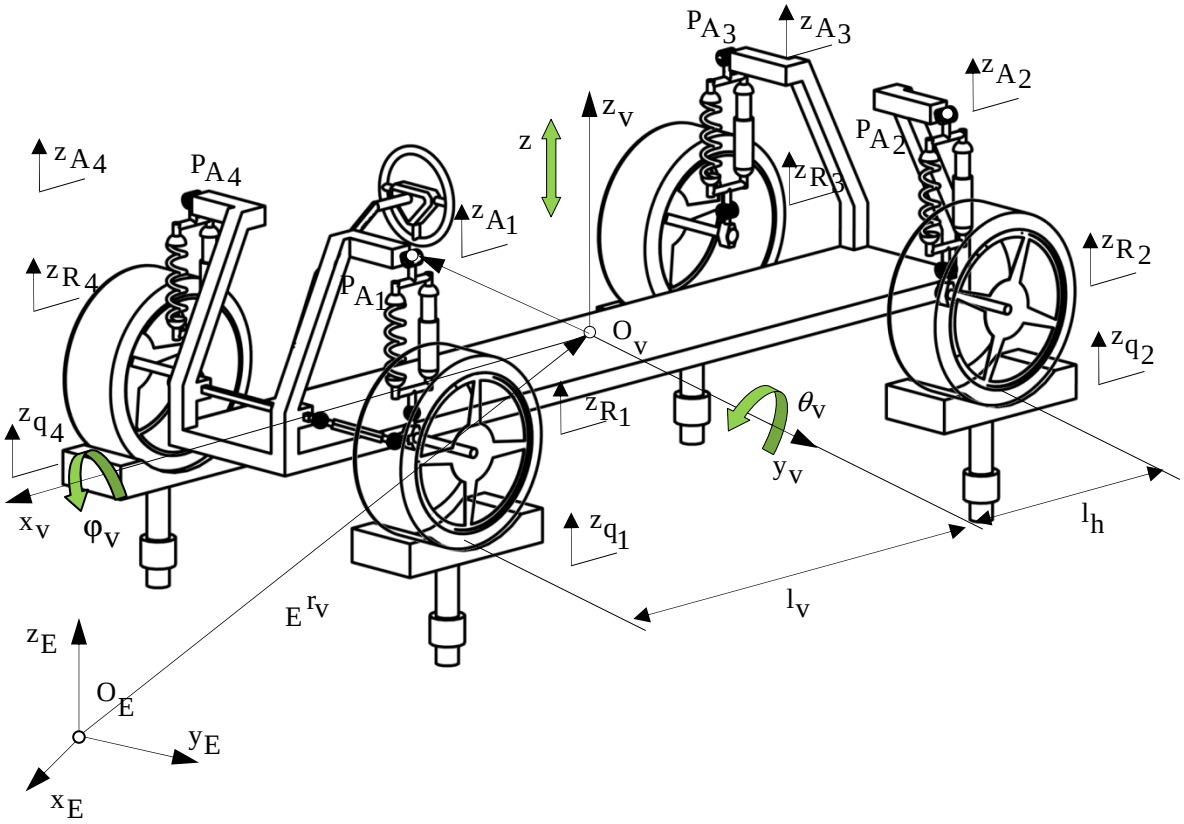

Figure 3.11: Actuation of the entire vehicle [Schramm et al., 2010]

The primary forces by which a high-speed motor vehicle is controlled are developed in the four points where the tyres have contact with the road [Schramm et al., 2010]. Each wheel of the vehicle is actuated by a hydraulic cylinder. The goal is to develop a modular setup that can adapt its functionality to a variety of vehicles, by actuating any car just by using actuators under each tyre [Capustiac et al., 2010a]. The hydraulic actuators to be used are available at the Duisburg-Essen University belonging to a previous project from the Chair of Mechatronics [Heckhoff et al., 2007]. These actuators are developed by Integral Hydraulik [InH, 2011]. While actuating such a driving simulator, the structure of the mechanisms connected to the vehicle's wheels have to be addressed as well; these mechanisms have the function to introduce road characteristics. The DOF of the driving simulator are roll, pitch and heave, as already described. It can be easily observed that such a system is a redundant one. According to Pierrot, there are three cases of redundancy for a parallel manipulator: *kinematical*, *actuation*, and *measurement redundancy* [Merlet, 2006].

The mechanism considered in Fig. 3.11 deals with *actuation redundancy,* since the system has 3 DOF and it is actuated by 4 motor joints (the hydraulic cylinders). Merlet states that this type of redundancy can be used to avoid singularities [Merlet, 2006]. In this research, it is used for the above mentioned purpose and for cost and design constrains.

With respect to the solutions discussed, the following parameters can be expressed as being important in designing such a system: cost, dynamical behaviour, portability and reconfigurability.

As defined by Mellor, the reconfigurability of a system is concerned with its *modularity, integrability, convertability, scaleability* or *diagnosability* [Mellor, 2002]. These characteristics should allow a driving simulator to be upgraded in response to different demands and to actuate any mock-up or vehicle, depending on the application. A reconfigurable system should be able to adapt its functionality and capacity to the actual demands. In this research, the reconfigurability of the system is concerned with its *modularity* and *integrability*.

In this subchapter different actuation systems were discussed with respect to their kinematical parameters. The cost of such systems is high, so understanding the system's kinematical and dynamical behaviour is crucial before building it. It was discussed what kind of mechanism can be proposed while trying to develop an EFDS.

3.1.2 Kinematical Analysis of the Considered Mechanisms for Actuation

The inverse kinematics of a parallel manipulator is described by Merlet in [Merlet, 2006] as the relation between the unknown positions of the actuated joint coordinates with respect to the known position of the manipulator's end-effector. The inverse kinematics for the presented systems was solved and implemented in Matlab/Simulink using the methodology already presented by the author in [Capustiac and Brisan, 2010].

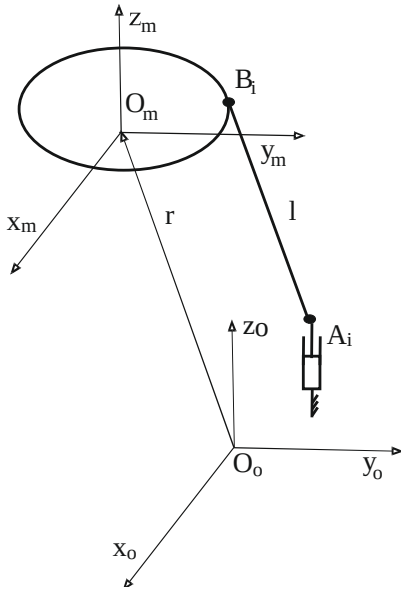

Figure 3.12: A random kinematical chain of a parallel mechanism

While assuming the kinematic chain presented in Fig. 3.12, we can define the fixed platform of the parallel mechanism, described by points A_i and the fixed coordinate system, $O_{o_{x_0y_0z_0}}$ and the mobile platform described by points B_i and the mobile coordinate system $O_{m_{x_my_mz_m}}$.

$r = [r_x, r_y, r_z]^T$ represents the position vector connecting the mobile platform and the fixed platform.

The inverse kinematics can be solved by implementing the following steps:

- Finding the coordinates of the mobile platform by multiplying the initial coordinates of the mobile platform vectors (the known coordinates – the initial position) with the transformation matrix, $\boldsymbol{H}$ from the mobile coordinate system to the fixed coordinate system:

$$\boldsymbol{H} = \begin{pmatrix} cos\theta \cdot cos\psi & -cos\varphi \cdot sin\psi + sin\varphi \cdot sin\theta \cdot cos\psi & sin\varphi \cdot sin\psi + cos\varphi \cdot sin\theta \cdot cos\psi & r_x \\ cos\theta \cdot sin\psi & cos\varphi \cdot cos\psi + sin\varphi \cdot sin\theta \cdot sin\psi & -sin\varphi \cdot cos\psi + cos\varphi \cdot sin\theta \cdot sin\psi & r_y \\ -sin\theta & sin\varphi \cdot cos\theta & cos\varphi \cdot cos\theta & r_z \\ 0 & 0 & 0 & 1 \end{pmatrix}; \tag{3.12}$$

- Finding the generalized coordinates of the actuated joints by applying the sphere equation:

$$q_i = z_{B_i} \pm \sqrt{(l^2 - (x_{B_i} - x_{A_i})^2 - (y_{B_i} - y_{A_i})^2}; \tag{3.13}$$

where x_{A_i}, y_{A_i} are the coordinates of the points A_i, belonging to the fixed platform of the mechanism, and $x_{B_i}, y_{B_i}, z_{B_i}$ are the coordinates of the points B_i with respect to $O_{x_0 y_0 z_0}$ coordinate system (i=1,...,6), and l is the length of the vector $\overrightarrow{\boldsymbol{A_i B_i}}$ [Capustiac and Brisan, 2008].

The general analytical method for solving the inverse kinematics is described by Merlet in [Merlet, 2006]. The vector $\overrightarrow{\boldsymbol{AB}}$ can be determined with the help of the chain joint coordinates vector, $\boldsymbol{\Theta}$ and the generalized coordinates of the mobile platform, $\boldsymbol{X}$ [Merlet, 2006]:

$$\overrightarrow{\boldsymbol{AB}} = \boldsymbol{H}_1(\boldsymbol{X}), \tag{3.14}$$

$$\overrightarrow{\boldsymbol{AB}} = \boldsymbol{H}_2(\boldsymbol{X}, \boldsymbol{\Theta}).$$

Resulting in the equality:

$$\boldsymbol{H}_1(\boldsymbol{X}) = \boldsymbol{H}_2(\boldsymbol{X}, \boldsymbol{\Theta}). \tag{3.15}$$

When using the derivation of equation (3.15), a relation between the angular velocity of the end-effector, $\dot{\boldsymbol{X}}$ and the actuated joint velocities of the robot, $\dot{\boldsymbol{\Theta}}_a$ is obtained [Merlet, 2006]:

$$\begin{gathered} \boldsymbol{A}\dot{\boldsymbol{\Theta}}_a + \boldsymbol{B}\dot{\boldsymbol{X}} = 0, \\ \dot{\boldsymbol{\Theta}}_a = -\boldsymbol{A}^{-1}\boldsymbol{B}\dot{\boldsymbol{X}} = \boldsymbol{J}^{-1}\dot{\boldsymbol{X}}, \\ \boldsymbol{A}\dot{\boldsymbol{\Theta}}_a + \boldsymbol{B}\boldsymbol{W}_{\boldsymbol{m}} = 0. \end{gathered} \tag{3.16}$$

where $\boldsymbol{J}^{-1}$ is the inverse jacobian matrix [Merlet, 2006]. As noted by Merlet, equation (3.16) relates the velocities of the mobile platform and the derivatives of the orientation representations to the velocities of the actuated joint, in this work, assumed to be prismatic joints.

The velocity problem can be solved by implementing equations (3.16). The equations presented above were implemented in Matlab with the purpose of obtaining the positions and velocities of the actuators for the mechanisms discussed and presented above.

The inputs for the model developed in Matlab/Simulink were positions recorded with the help of IPG Car Maker Software. For test purposes, angles and body movements were given as inputs to the system. The desired actuator strokes are calculated.

Fig. 3.13 shows the vehicle body centre of gravity (CG) roll and pitch angles and Fig. 3.14 shows the vertical displacement and velocity of the vehicle body recorded while driving the IPG Car model through a double lane change manoeuvre.

Such a manoeuvre is frequently used for driving dynamics and handling evaluation. It is defined by ISO 3888-1 and it requires driving forward, then changing the lane to the left and then coming back on the initial lane [ISO 3888, 1999].

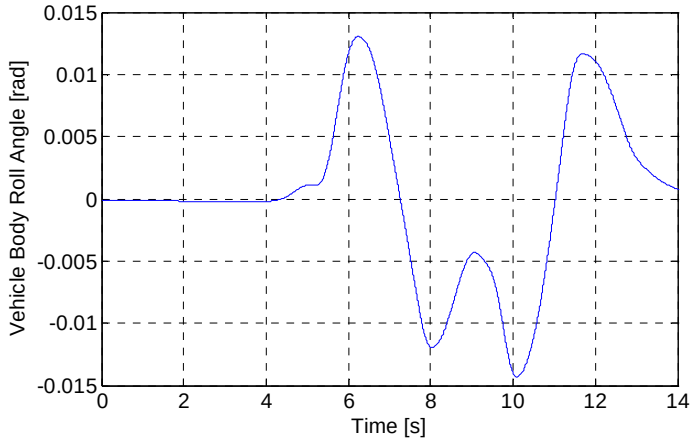

Figure 3.13a: Roll angle of the vehicle body recorded with IPG Car Maker Software

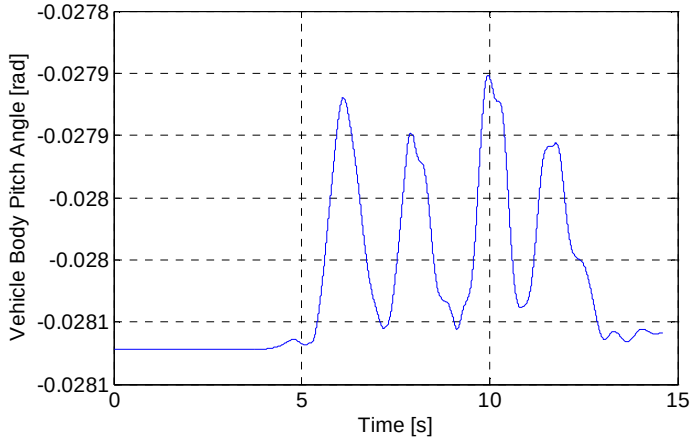

Figure 3.13b: Pitch angle of the vehicle body angles recorded with IPG Car Maker Software

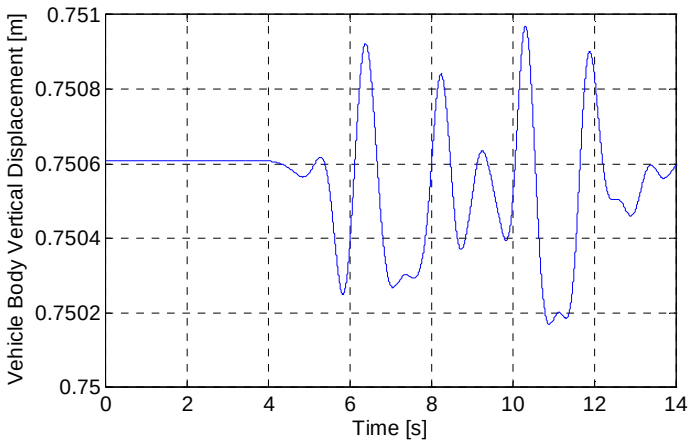

Figure 3.14a: Vehicle body CG vertical displacement recorded with IPG Software

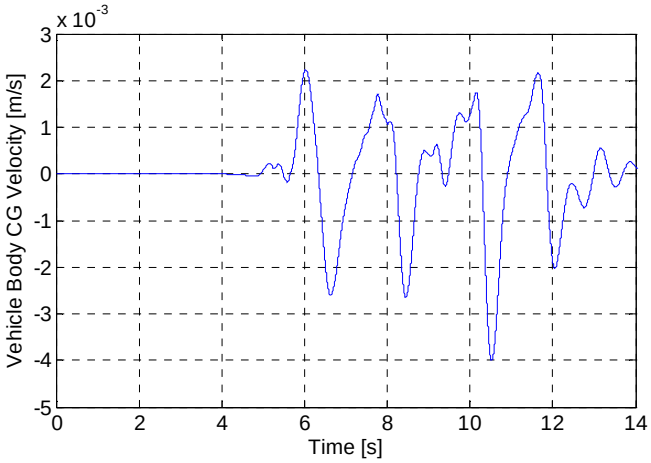

Figure 3.14b: Vehicle body CG vertical velocity recorded with IPG Software

Fig. 3.15 presents the simulation results of the inverse kinematics of the 3 DOF PSU manipulator inputting the data presented in Fig. 3.13 and 3.14. The displacements of the actuators and their velocities while the mobile platform of the PSU manipulator is reproducing the roll, pitch and heave corresponding to a double lane change manoeuvre can be observed.

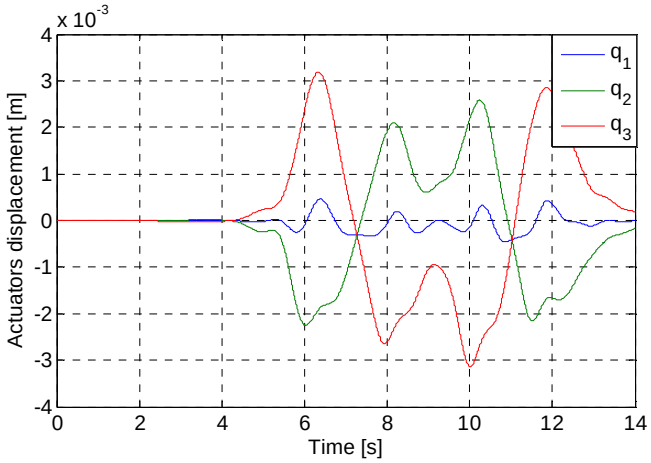

Figure 3.15a: The actuator displacements of the 3 DOF PSU manipulator

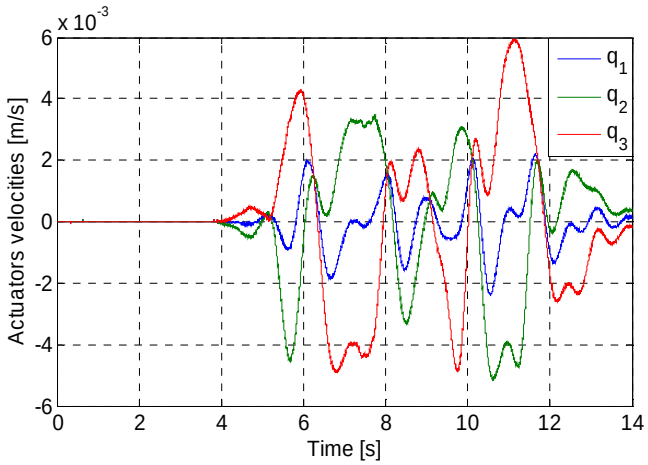

Figure 3.15b: The actuator velocities of the 3 DOF PSU manipulator

Although it requires a larger assembly workspace and it is not the best solution regarding portability, the topology of the PSU 3 DOF manipulator needs the smaller actuator strokes and velocities with respect to the other 2 solutions studied.

Fig. 3.16 presents the simulation results of the inverse kinematics of the 3 DOF SPU manipulator inputting the data presented in Fig. 3.13 and 3.14.

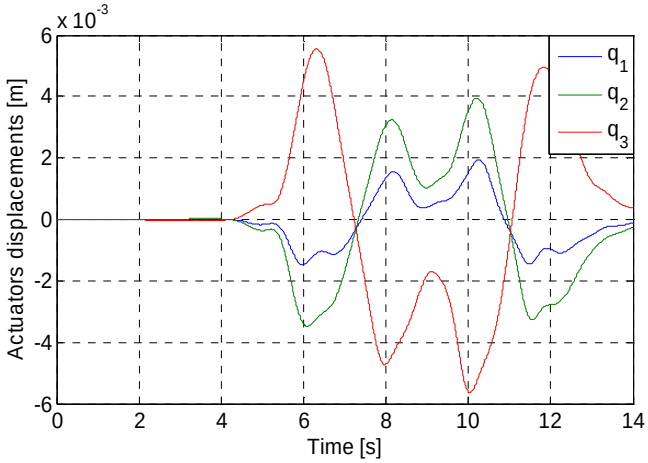

Figure 3.16a: The actuator displacements of the 3 DOF SPU manipulator

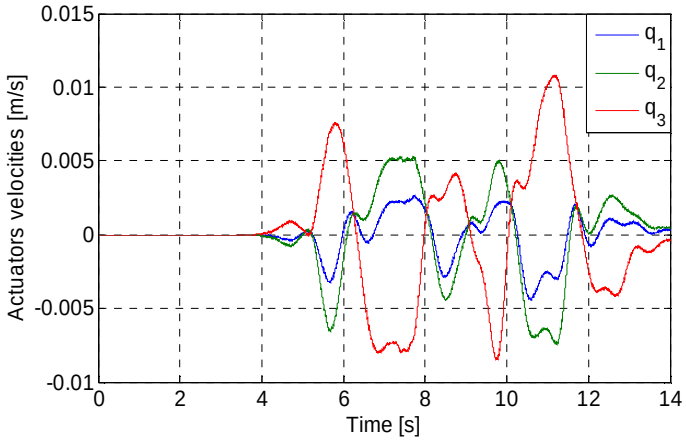

Figure 3.16b: The actuator velocities of the 3 DOF SPU manipulator

Fig. 3.17 presents the simulation results of the inverse kinematics of the 3 DOF actuation mechanism with linear actuators inputting the data presented in Fig. 3.13 and 3.14. It can be observed that it needs the highest amplitudes of the actuator displacements to reproduce a double change manoeuvre. However, it was assumed in this research that this solution presents the advantages needed for the EFDS: portability and a higher vertical motion available (0.35m).

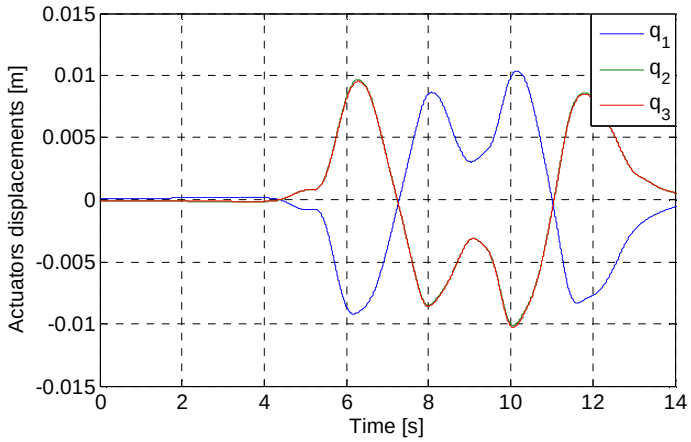

Figure 3.17a: The actuator displacements of the 3 DOF actuating system using linear actuators connected direct to the platform, RPS topology

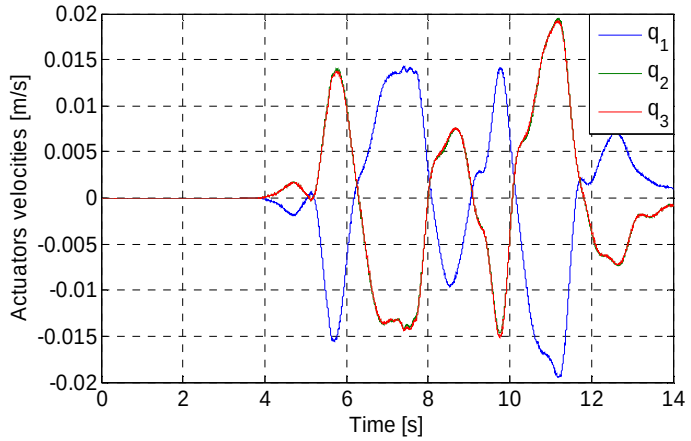

Figure 3.17b: The actuator velocities of the 3 DOF actuating system using linear actuators connected direct to the platform, RPS topology

All 3 sets of kinematical models calculated the actuator displacements and velocities for the same vehicle body vertical displacement and velocity recorded, while driving the IPG Car model through a double lane change manoeuvre.

The last 3 sets of figures show interesting results with respect to the actuation strokes and velocities needed for different topologies of 3 DOF mechanisms given the same input. It is shown that the actuator strokes and velocities vary with respect to the topologies of the mechanisms proposed here.

3.1.3 Road Response of the EFDS

There are two sources of excitations while driving. The first are given by the *control actions of the driver* and result in forces felt by him or her. These forces are predictable results of the driver's actions and are solved by the vehicle dynamics model. The second type of excitations are given by the vehicle-change in *environment interaction*; e.g. potholes, road irregularities [Capustiac et al., 2010].

As stated before, the EFDS should be able to introduce both road and dynamics vehicle simulation. The ride of the vehicles on different road categories is permanently accompanied by vibrations and shocks, which are felt in the sprung and un-sprung vehicle masses as described by Untaru [Untaru, 1981]. They can be caused by road irregularities or by the vehicle's engine, wheel – road system, transmission or direction. While driving a vehicle, the following vibrations can occur: chassis and vehicle body, twisting and bending of the engine parts, directional wheels flutter, vehicle seats, road irregularities, etc. [Untaru, 1981]. The mechanical vibrations can be transmitted to the driver through the skin, while he or she is interacting with the vehicle (hands on the wheels, feet on the pedals, etc).

In the development of the vehicle, road roughness data is used for investigating its effect on the behaviour of the vehicle (braking and steering behaviour, tyre deflection) [Buzdugan, 1980]. ISO defined the comfort of driving a vehicle in terms of root mean square acceleration over a frequency range [ISO 2631, 2003].

The chassis and the vehicle body vibrations caused by road irregularities are high frequency vibrations. Generally, vibrations can be evaluated through *displacements*, *velocities*, *accelerations* and *frequencies* [Buzdugan, 1980].

Buzdugan in [Buzdugan, 1980] defined the intensity of the vibration as:

$$z = \frac{a_o^2}{f} = 16\pi^4 x_o^2 f^3. \tag{3.17}$$

Where a_0 is the amplitude of the vibration acceleration, f is the frequency and x_0 is the amplitude of the vibration. Similar to the noise level of perception, the level of the perception was introduced for vibrations too. The intensity in vibrar was first defined by Zeller in [Zeller, 1932] and can be calculated with the following formula:

$$S_{vibrar} = 10log_{10}(\frac{z}{z_0}). \tag{3.18}$$

Where z is the intensity of the vibration and the reference values is assumed to be $z_0 = 0.1\,cm^2/s^3$ [Buzdugan, 1980]. The intensity in Pal can be calculated [Zeller, 1932]:

$$S_{pal} = 10log_{10}(\frac{z}{z_1}). \tag{3.19}$$

Where the intensity of vibration reference value is assumed to be $z_1 = 0.5\,cm^2/s^3$ [Buzdugan, 1980].

According to the DIN 4150 Standard, vibrations are categorized with respect to the perception level as it follows:

- Hardly perceptible vibrations, until 5 Pal;
- Well discernible vibrations, 5-10 Pal;

- Strongly perceptible vibrations, 10-20 Pal;
- Harmful vibrations, 20-40 Pal [DIN4150, 1999].

The level of perception was used for the first time when the measurement scale for the subjective evaluation of the sound intensity was introduced. The resonance domain for the vehicle body's own frequencies is located between 0.7-2 Hz and for the wheel between 8-16 Hz [Untaru et al., 1981]. Based on experimental testing, a vibration perception coefficient was established, with respect to vibration effects on the human body [VDI 2057, 2002]. According to this standard, Table 3.6 presents the levels of the human vibration perception.

Table 3.6: The human vibration perception levels [VDI 2057, 2002]

Perception coefficient K_{vib}	**Level**	**Perception**
0.1	A	Imperceptible
0.25	B	Perception threshold
0.63	C	Perceptible
1.6	D	Well discernible
4	E	Well perceptible
10	F	Strongly perceptible
25	G	Strongly perceptible
63	H	Strongly perceptible
	I	

The profile of the road surface is described by the length of the irregularities, the height and the frequency of the irregularities. When the irregularities have a linear profile, the profile of the road surface can be considered sinusoidal and described as it follows [Untaru et al., 1981]:

$$h = \frac{h_o \cdot (1_r - \cos \omega_r t)}{2}, \tag{3.20}$$

where h_0 represents the height of the irregularities, l_r represents the length of the irregularities and ω_r is the pulsation of the disturbance factor [Untaru et al., 1981].

The pulsation of the perturbation factor is described as a function of the vehicle's velocity, u and the length of the irregularities, l_r [Untaru et al., 1981]:

$$\omega_r = 2\pi \frac{u}{l_r}. \tag{3.21}$$

Because of their random nature, road profiles are described and modelled using different mathematical techniques. One of the most used methods represents the power spectral density function (PSD) [Hac, 1987; He et al., 2008]. Macaulay described the road surface irregularities with respect to the frequency and amplitude distribution [Macaulay, 1963].

Hac used the PSD function to describe the road irregularities [Hac, 1987]. The spectrum of the regularities is modelled using a transfer function of low order for designing a linear shaping filter with a white noise input. The author proved that the spectrum of irregularities changes with the vehicle speed. Fig. 3.18 shows the road irregularities dependence on vehicle speed as proved in [Hac, 1987].

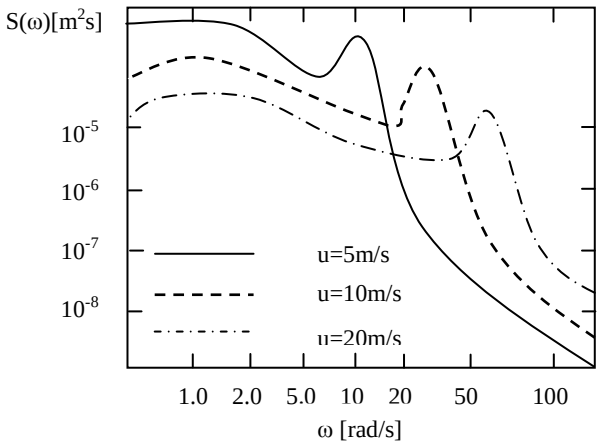

Figure 3.18: Power spectral density function for a paved road and various velocities as described in [Hac, 1987]

The specialized literature offers a wide range of articles where, for research purposes, the road profile is not modelled, but measured. Different approaches were used in order to obtain real road roughness profiles. The first instruments used to achieve this were the high speed profilometers [Spangler, 1966]. These devices were used for inspection of new roads with velocities less than 15 km/h.

When a vehicle is driven over a random road profile, it mainly performs heave, pitch and roll motions [Rill, 2008]. Because of the inclinations of the road, the vehicle will also perform longitudinal, lateral and yaw motion; in order to limit the complexity of the stochastic description, usually less complex road models are used, as stated in [Rill, 2008].

The approach used in this work for modelling different road profiles is the one already described by the author in [Capustiac and Brisan, 2009] and implemented first by He et al. in [He et al., 2008]. It focuses on using a differential equation in order to obtain the road roughness dependent on the road roughness coefficient and the velocity of the vehicle.

Assuming that a vehicle is travelling with a constant velocity on a random road and that the tyre is always in contact with the road, the PSD of the considered road can be expressed [He et al., 2008]:

$$G_q(n) = G_q(n_0)(\frac{n}{n_0})^{-w} \quad (3.22)$$

The relationship between the time frequency, f and the vehicle's velocity, u is [He et al., 2008]:

$$f = u \cdot n \quad (3.23)$$

Derived from equation (3.22), the PSD of the road roughness has the following form, [He et al., 2008]:

$$G_q(f) = \frac{G_q(n_0)n_0^2 u}{f^2} \quad (3.24)$$

The road roughness in the frequency domain is defined as [He et al., 2008]:

$$G_q(\omega) = \frac{G_q(\Omega)}{u} = \frac{G_q(\Omega_0)u}{\omega^2} \quad (3.25)$$

Where $G_q(n)$ is the road PSD, n is the spatial frequency, n_0 is the reference spatial frequency, defined as 0.1 cycle/m, $G_q(\Omega_0)$ is the road roughness coefficient, w is called

waviness and ω is the angular velocity [He et al., 2008]. He et al. use the Laplace transformation to write a transfer function between the white noise signal and the road irregularities, obtaining the following equation [He et al., 2008]:

$$\dot{z}_r(t) + 2\pi u n_0 z_r(t) = \sqrt{G_q(\Omega_0) u}\, w(t). \tag{3.26}$$

Where $z_r(t)$ represents the road roughness, $w(t)$ is a white noise signal. The road roughness can be calculated with the help of equation (3.26).

ISO 8608 characterizes each road class based on its own reference value in 8 classes (class A – class H) [ISO 8608, 1995]. The classification for class A – E is given in Table 3.7.

Due to computing facilities that the band limited white noise signal type offers, this kind of noise is frequently used in road characteristic modelling.

Table 3.7: ISO Classification of the road classes [ISO 8608, 1995]

Road Class	**Degree of roughness $G_q(\Omega_0)$**		
	Lower limit	**Geometric mean**	**Upper limit**
A (very good)	-	16	32
B (good)	32	64	128
C (average)	128	256	512
D (poor)	512	1024	2048
E (very poor)	2048	4096	8192

In order to be able to simulate different road categories, the equation (3.26) was implemented in Matlab/Simulink. For simulations purpose the white noise signal's power spectral density was assumed to be 1 and the waviness coefficient was assumed to be 2, following the approach from [Capustiac and Brisan, 2009].

The aim of modelling the road response is to give the human driver a more realistic driving experience through a haptic feeling, as it was already stated and proved by the author in [Capustiac et al., 2010a].

Random road irregularities are characterized by their stochastic properties and can be approached as of long or infinite duration disturbances, as stated by Gaspar and Nadai [Gaspar and Nadai, 2007].

The chassis and body vibrations caused by road irregularities have a differential action on the human body, depending on the parameters of the vibration [Guglielmino et al., 2008]. The intensity of the vibration is dependent on the displacement, velocity and acceleration of the amplitudes, the exposure length, and the frequency of the vibration, as defined in [ISO 2631, 2003]. It is important to study the characteristics of road and the influence of vibrations on humans, so the driving simulator can offer a realistic driving experience.

The following figures present results obtained in simulations while modelling different road profiles. In Fig. 3.19 can be observed the road irregularities obtained from the Matlab/Simulink model while assuming to drive a vehicle with a 100 km/h velocity over a very good road – category A (Fig. 3.19a) and with 50 km/h over an average road – category C (Fig. 3.19b). The coefficients describing the road were taken from Table 3.7.

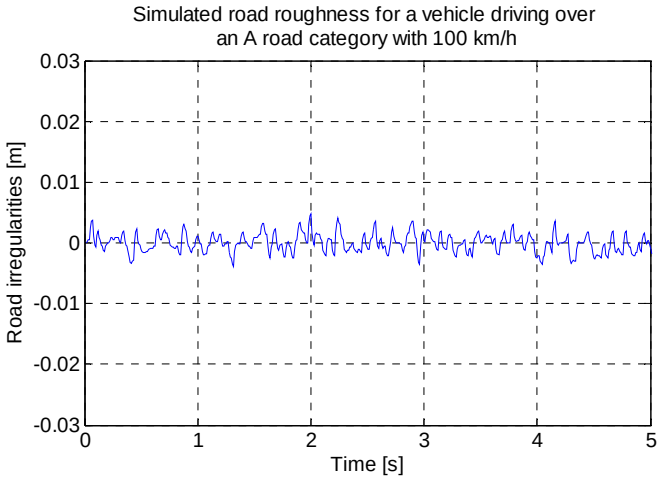

Figure 3.19a: Road roughness modelled for a vehicle driving with 100 km/h constant velocity over an A category road

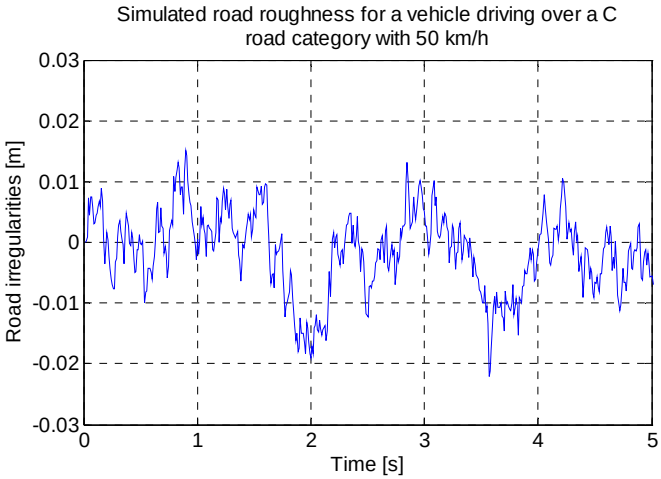

Figure 3.19b: Road roughness modelled for a vehicle driving with 50 km/h constant velocity over a C category road

In order to observe the influence of the vehicle's velocity on the excitation of the vehicle, a set of simulations using the static DRIVASSIST were conducted.

A scenario was driven with the simulator and the velocity of the vehicle was registered and used in the Matlab/Simulink model to evaluate the influence of the velocity variation. Fig. 3.20 shows the vehicle velocity inputted to the model described by the equation (3.26), where the velocity is assumed to be time dependent $u(t)$.

Fig. 3.21a shows the road roughness obtained assuming the vehicle is driving with the given velocity over an A road category and Fig. 3.21b over a C road category.

Different road profiles were modelled with respect to the desired road conditions so as to be introduced in the driving simulator. These models will be used for the frequency response analysis of the vehicle body and hydraulic actuators, and also for experimental testing.

The analysis of the time response is the first step towards understanding the dynamic behaviour of the studied system. Further, the frequency response of the system will be obtained using Laplace transforming of the differential equations of motion. The advantage that Laplace transform method shows is that differential equations are transformed into algebraic equations by introducing a complex variable (the Laplace operator). These

equations can be used to determine transfer functions of the quarter car model. Based on the quarter car model, a model for the entire car will be developed.

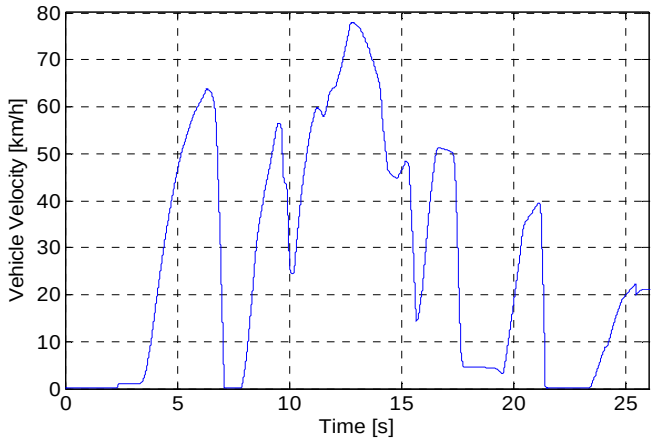

Figure 3.20: DRIVASSIST vehicle model velocity recorded from simulations

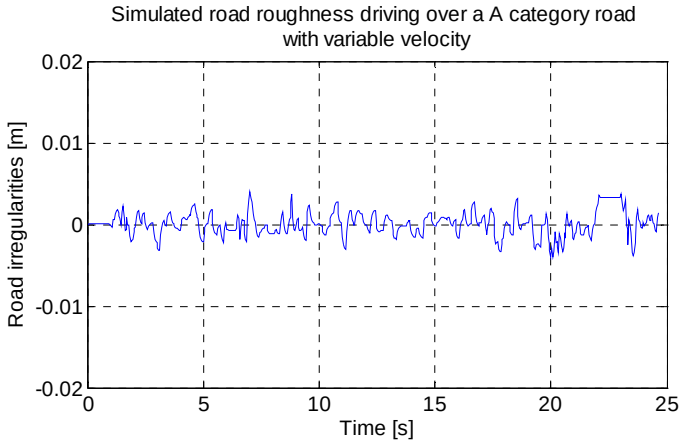

Figure 3.21a: Road roughness modelled for a vehicle driving with the velocity from Fig. 3.20 over an A category road

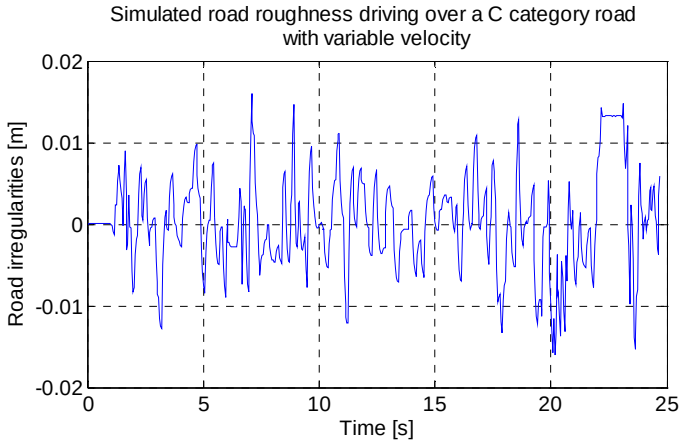

Figure 3.21b: Road roughness modelled for a vehicle driving with the velocity from Fig. 3.20 velocity over a C category road

Once the tyre-road system is introduced in the driving simulator it can be assumed that the actuator displacements are very similar to the profile of the road [Capustiac et al., 2010a]. The actuators transmit forces in the vehicle through its tyres.

The overall performance of the vehicle is subjected to the tyre-suspension mechanism. Three types of suspensions can be designed and are used in the vehicles: passive, semi-active and active [Guglielmino et al., 2008]. The passive ones use spring-damper systems and their advantages are simplicity and low cost. The semi-active suspensions use a variable damping constant. Usually the active suspension demands complex design and higher cost [Liang and Li, 2005]. The simplified quarter car model used for studying the suspension response is presented in Fig. 3.22.

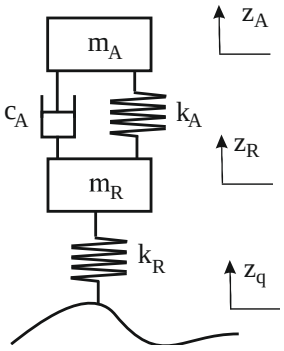

Figure 3.22: Quarter car model with 2 masses

The quarter car model was validated by Kim and Ro in 1998 [Capustiac and Brisan, 2009]. The simplified spring of the tyre and the suspension-spring behave as a two DOF system. It is assumed here that the vehicle components are able to behave in the same way as they would on the road. The limitations of the quarter car are known and discussed in the literature [Liang and Li, 2005]. However, this model can give good results in judging the ride comfort of the drive, as it was already discussed and published by the author in [Capustiac and Brisan, 2009]. By modelling such a mechanism, its response to different road excitations can be investigated. The following analysis focuses on the frequency response of the system.

Considering the quarter model presented in Fig 3.23, the motion equations are:

$$\begin{aligned} m_A\ddot{z}_A &= -c_A(\dot{z}_A - \dot{z}_R) - k_A(z_A - z_R), \\ m_R\ddot{z}_R &= c_A(\dot{z}_A - \dot{z}_R) + k_A(z_A - z_R) - k_R(z_R - z_{q_i}). \end{aligned} \tag{3.27}$$

The dynamic wheel load is described [Rill, 2008]:

$$F_w^d = k_R(z_R - z_q). \tag{3.28}$$

The above equations were implemented in Matlab/Simulink and the coefficients describing the model are given in Table 3.8.

Table 3.8: Quarter car model parameters

Simulation Data	**Value**	**Unit**
Sprung mass – m_A	290	kg
Un-sprung mass – m_R	59	kg
The damping coefficient – c_A	1000	$\frac{Ns}{m}$
Suspension spring stiffness coefficient – k_A	16182	$\frac{N}{m}$
Tyre spring stiffness coefficient – k_R	190000	$\frac{N}{m}$

A full vehicle model considers the links between the sprung masses to be solid rods [Kruczek and Stribrsky, 2007]. Such a model is more complex than a quarter car one, considering the roll, pitch and heave motion for the vehicle's CG and the vertical displacements of the wheels centres [Rill, 2008]. Also the dynamic forces that act directly on the car body are introduced.

The Lagrange general equations for this system with the generalized coordinates system $\boldsymbol{p} = \left[z, \varphi_v, \theta_v, z_{R_i}\right]^T$ are [Rill, 2008]:

$$\frac{d}{dt}\frac{\partial T(p,\dot{p})}{\partial \dot{p}} - \frac{\partial T(p,\dot{p})}{\partial p} + \frac{\partial D(\dot{p})}{\partial \dot{p}} + \frac{\partial u(p)}{\partial p} = 0. \tag{3.29}$$

The kinetic energy for the vehicle body and the un-sprung masses is given by the following equation [Gaspar and Nadai, 2007]:

$$\begin{cases} T_B = \frac{1}{2} m_v \dot{z}^2 + \frac{1}{2}\theta_{xx}\dot{\varphi}_v^2 + \frac{1}{2}\theta_{yy}\dot{\theta}_v^2, \\ T_U = \frac{1}{2} m_R(\dot{z}_{R_1}^2 + \dot{z}_{R_3}^2) + \frac{1}{2} m_R(\dot{z}_{R_2}^2 + \dot{z}_{R_4}^2). \end{cases} \tag{3.30}$$

The sum of this energy will give the total kinetic energy which includes the tyre deflection due to road vibrations as given in [Azad, 2006]. The tyre deflection is calculated [Rill, 2008]:

$$d_{c_i} = z_{R_i} - z_{q_i}, \tag{3.31}$$

and the suspension deflection [Rill, 2008]:

$$d_{s_i} = z_{A_i} - z_{q_i}. \tag{3.32}$$

Assuming z_{R_i} to be the vertical movement of the wheel and z_{q_i}, the road irregularities input to each wheel.

The potential energy stored in the suspension, respectively in the tyres, is given by the following equation [Gaspar and Nadai, 2007]:

$$\begin{cases} U_s = \frac{1}{2} k_{sf}(d_{s1}^2 + d_{s3}^2) + \frac{1}{2} k_{sr}(d_{s2}^2 + d_{s4}^2), \\ U_T = \frac{1}{2} k_{tf}(d_{c1}^2 + d_{c3}^2) + \frac{1}{2} k_{tr}(d_{c2}^2 + d_{c4}^2). \end{cases} \tag{3.33}$$

The calculated dissipation energy for the effect of shock absorbers [Gaspar and Nadai, 2007]:

$$D = \frac{1}{2} c_A(\dot{d}_{s1}^2 + \dot{d}_{s3}^2) + \frac{1}{2} c_A(\dot{d}_{s2}^2 + \dot{d}_{s4}^2). \tag{3.34}$$

It was assumed that k_{s_f} and k_{s_r} stand for the suspension stiffness coefficient, front respectively rear and that k_{t_f} and k_{t_r} stand for the tyre stiffness coefficient, front respectively rear [Gaspar and Nadai, 2007].

The performance of a vehicle is a response to the forces imposed. The predominant forces acting on a vehicle for performance control are the forces developed by the tyre against the road [Gillespie, 1992]. Thus it is important to understand the behaviour of this system.

The road profiles modelled and described above were inputted to the vehicle model in order to investigate the maximal wheel street contact forces. The values obtained in simulation are presented in the following table.

Table 3.9: The maximal vehicle contact forces

Maxim road wheel contact force [kN]	**Road Category**	**Vehicle speed [m/s]**
4.2	Category A	20
4.8		30
4.9		50
4.25	Category C	1
5.5		10
8.2		20
6.2	Category E	1
10		10

The calculation was conducted for all road categories described by the international standard 8608, but for research purposes, only the above presented types were considered [ISO 8608, 1995]. In order to see the parameters describing the 3 types of roads, Table 3.7 can be consulted.

The frequency response of the quarter car model was studied inputting different road profiles to the Matlab/Simulink model. This analysis was made using the FFT. The typical syntax to compute the FFT was written in Matlab and was used to obtain the frequency representation of the sprung mass acceleration, wheel displacement and suspension travel signals.

The distribution of the frequency can be observed in these figures together with the two peaks, first at around 4 Hz and the second at around 11 Hz. Fig. 3.23 presents results from the frequency analysis.

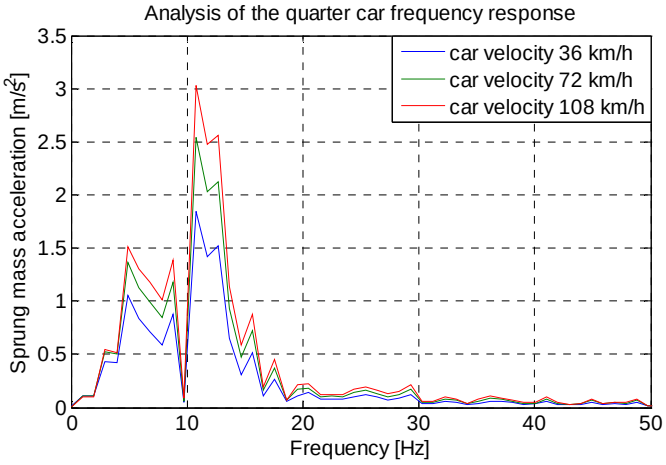

Figure 3.23a: Frequency response of the sprung mass acceleration with respect to different vehicle velocities

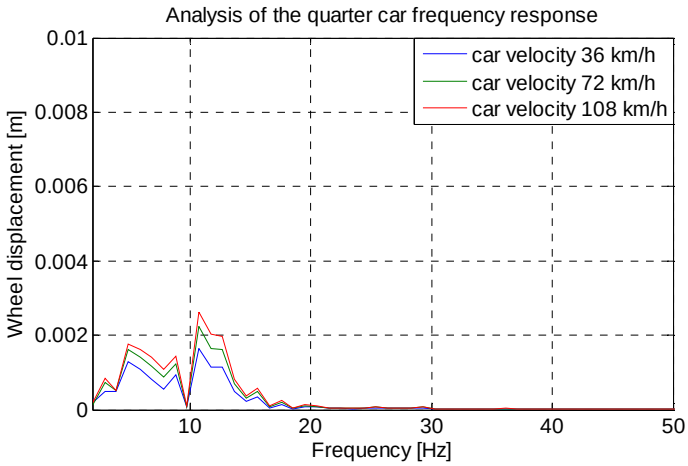

Figure 3.23b: Frequency response of the wheel displacement with respect to different vehicle velocities

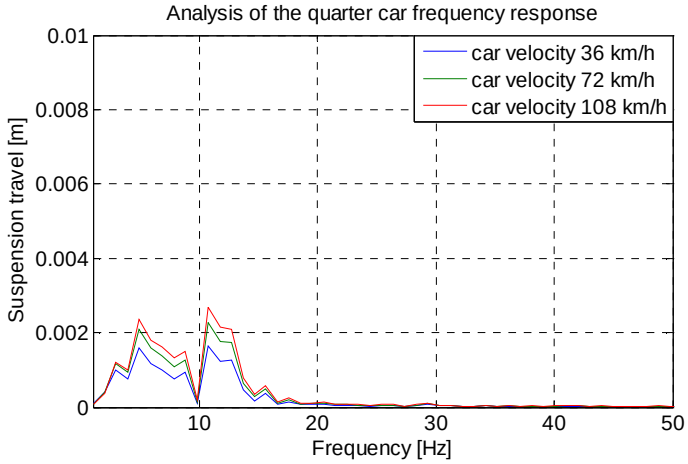

Figure 3.23c: Frequency response of the suspension travel with respect to different vehicle velocities

3.1.4 Mathematical Modelling of the Hydraulic Cylinders

Fig. 3.24 shows the hydraulic cylinders to be tested and used in actuating the vehicle motion simulator and Fig. 3.25 presents the vehicle to be actuated. Table 3.10 presents the technical data of the hydraulic cylinders developed by Integral Hydraulik [InH, 2011].

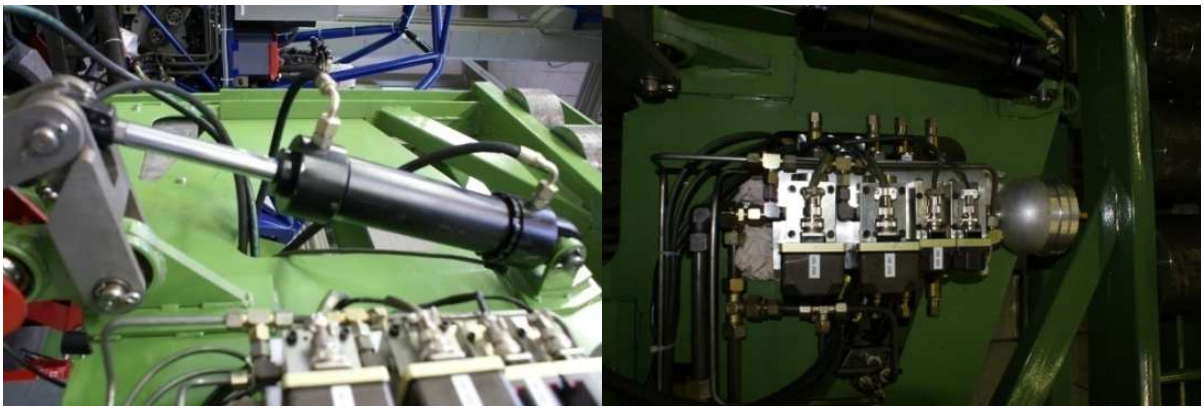

Figure 3.24: Hydraulic components that will be used for actuating the driver simulator

Table 3.10: The parameters of the type ZXH63/28-250 hydraulic cylinders [InH, 2011]

Parameter	**Value**
Pressure [bar]	160
Nominal diameter [mm]	63
Piston rods diameter [mm]	28
Stroke [mm]	250
Max. pressure Force [kN]	40
Max. traction [kN]	40
Nominal resistance of the potentiometer [kΩ]	3.75
Weight [kg]	9.9

In order to be able to simulate the behaviour of the hydraulic cylinders, a model of these actuators was built in Matlab/Simulink. The goal of simulating the dynamical behaviour of this system was to integrate a simple vehicle model together with the hydraulic model, before setting up the hardware.

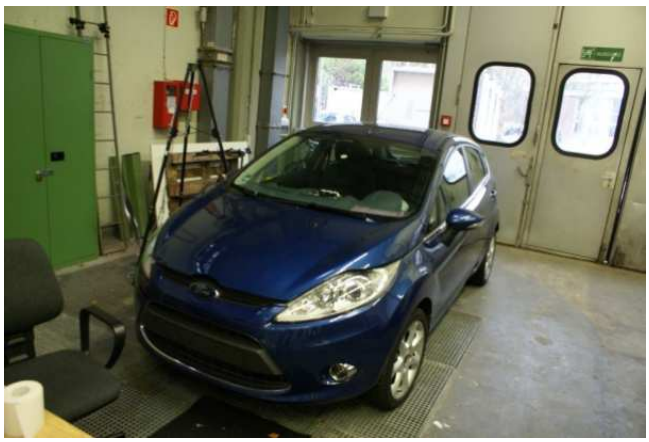

Figure 3.25: The EFDS – the vehicle to be actuated

A hydraulic cylinder transforms the hydraulic energy into mechanical energy (force or position). The following model is based on the equations already presented in [Heckhoff et al., 2007]. The following equation describes the model of the servo valve spool dynamics, written as a second order model of the form:

$$\frac{1}{\omega_{n_h}^2}\ddot{x}_v^* + \frac{2\zeta_h}{\omega_v}\dot{x}_v^* + x_v^* + sign(\dot{x}_v^*) = k_v u_v^*, \tag{3.35}$$

where x_v^* is the normalized servo valve position, $\dot{x}_v^*$ is the velocity, $\ddot{x}_v^*$ is the acceleration, u_v^* is the valve input voltage with respect to the maximum stroke of 250 mm (±125 mm) and maximum valve voltage (1 V), k_v is a proportional factor, f_{hs} is the valve hysteresis, ζ_h is the damping ratio and ω_{nh} is the natural frequency [Heckhoff et al., 2007]. The hydraulic cylinder model was obtained implementing the following equation of motion:

$$a_y = \frac{1}{m_t}(A_r(P_a - P_b) - F_e - F_f), \tag{3.36}$$

where m_t is the total mass of the system, A_r is the piston rod area, P_a and P_b are the pressures in chamber A_h respectively chamber B_h, A_p is the piston area, F_e is the external load, F_f is the friction force and a_y is the piston's acceleration [Heckhoff et al., 2007].

The pump supplies the system with a constant pressure. The system inputs are the valve voltage u_1 and the external force $u_2 = F_e$. The system outputs are the pressures in both chambers P_A respectively, P_B and the position of the piston, x_p [Heckhoff et al., 2007].

Defining the state space vector of the system as $\boldsymbol{x} = [x_i]^T$, with $\boldsymbol{x} = [x_p, \dot{x}_p, P_A, P_B, x_v, \dot{x}_v]^T$ the state space equations of the system are [Heckhoff et al., 2007]:

$$\dot{x}_1 = x_2, \tag{3.37}$$

$$\dot{x}_2 = \frac{1}{m_t(x_1)}\left[(x_3 - \alpha_h x_4)A_p - F_f(x_2) - u_2\right], \tag{3.38}$$

$$\dot{x}_3 = \frac{E_A(x_3)}{v_A(x_1)}\left[Q_A(x_3, x_5) - A_p x_2 + Q_{L_i}(x_3, x_4)\right], \tag{3.39}$$

$$\dot{x}_4 = \frac{E_B(x_4)}{v_B(x_1)}\left[Q_B(x_4, x_5) + \alpha_h A_p x_2 - Q_{L_i}(x_3, x_4)\right], \tag{3.40}$$

$$\dot{x}_5 = x_6, \tag{3.41}$$

$$\dot{x}_6 = \omega_{v_f}^2\left[u_1 - \frac{2D_v}{\omega_{v_f}} x_6 - x_5 - f_{hs}\,sign(x_6)\right]. \tag{3.42}$$

Where Q_{L_i} is the flow leakage, D_v is the servo valve damping factor, α_h is the area ratio, ω_{v_f} is the servo valve natural frequency. As described in [Heckhoff et al., 2007], the fractions of the effective Bulk modulus over the chamber A_h respectively chamber B_h are:

$$E_A(x_3) = a_1 E_{max}\, log\left[a_2 \frac{x_3}{p_{max}} - a_3\right], \tag{3.43}$$

$$E_B(x_4) = a_1 E_{max}\, log\left[a_2 \frac{x_4}{p_{max}} - a_3\right], \tag{3.44}$$

and

$$V_A(x_1) = V_{LA} + (x_{p_0} - x_1)A_p, \tag{3.45}$$

$$V_B(x_1) = V_{LB} + (x_{p_0} - x_1)\alpha_h A_p, \tag{3.46}$$

where $E_{\max}$ is the maximum bulk modulus, x_{p_0} is the initial piston position, V_{LA} is the volume of pipe in chamber A_h and V_{LB} is the volume of pipe in chamber B_h, $a_1 \ldots a_3$ are the Bulk modulus parameters and $c_{v_1} \ldots c_{v_4}$ are the valve flow coefficients [Heckhoff et al., 2007].

The pressure in the chambers can be calculated with:

$$Q_A = c_{v1} sg(x_5) sign(P_0 - x_3) \sqrt{|P_0 - x_3|} - c_{v2} sg(-x_5) sign(x_3 - P_T) \sqrt{|x_3 - P_T|}, \quad (3.47)$$

$$Q_B = c_{v3} sg(-x_5) sign(P_0 - x_4) \sqrt{|P_0 - x_4|} - c_{v4} sg(x_5) sign(x_4 - P_T) \sqrt{|x_4 - P_T|}. \quad (3.48)$$

Where P_0 is the supply pressure and P_T is the tank pressure and the following switching functions as approximated in [Heckhoff et al., 2007]:

$$sg(x) := \begin{cases} x, x \geq 0 \\ 0, x < 0 \end{cases}, \quad (3.49)$$

$$sign(x) \approx \frac{2}{\pi} arctg(x), \quad (3.50)$$

$$|x| \approx \frac{2}{\pi} x arctg(x). \quad (3.51)$$

In order to control the position of the piston, a proportional integral derivative (PID) controller was designed and implemented in Matlab/Simulink.

It contains three constant parameters: a *proportional* gain, an *integrator* and a *differentiator* [Bouma, 2011]. Their summing produces the output of the controller. The transfer function reads:

$$TF_{PID} = \frac{k_D s^2 + k_p s + k_I}{s}. \quad (3.52)$$

Fig. 3.26 shows the output of the model when, as desired position, a sinus function with the amplitude of 0.1 m and frequency of 1 rad / s is given.

The piston follows this inputted function. Fig. 3.27 shows the pressure in chamber A_h, respectively B_h.

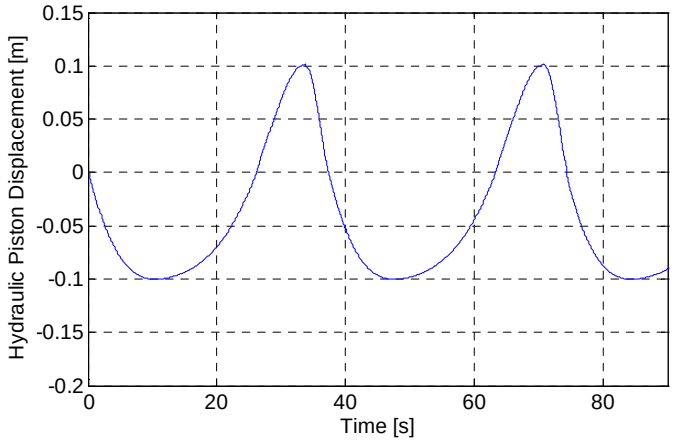

Figure 3.26: The simulated hydraulic piston displacement obtained in simulations

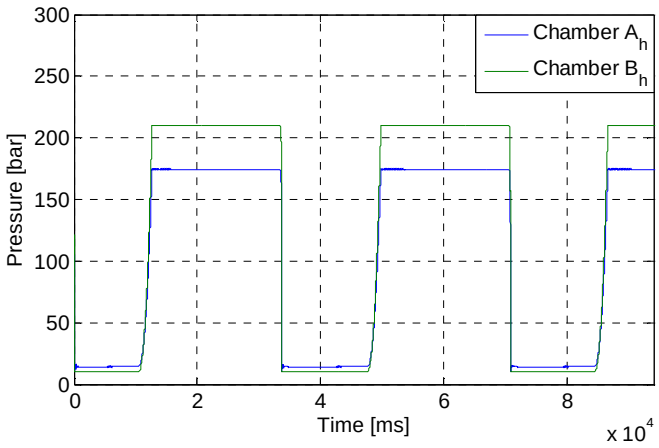

Figure 3.27: The simulated pressure in the chamber A_h respectively chamber B_h

Initially, a PID controller implemented in Matlab/Simulink. The signal e marks the difference between the desired actuator position and the actual actuator position, while u_h is the saturated controlled output. The output represents the voltage applied to the valve. The role of the saturation block is to keep the value of u_h in the $\pm 1V$ range.

To study the behaviour of the modelled system and the effect of the PID controller, data presented in Fig. 3.15 was given as desired actuator position. Values from z_{q_3} were considered. Fig. 3.28 presents the error obtained from the controller.

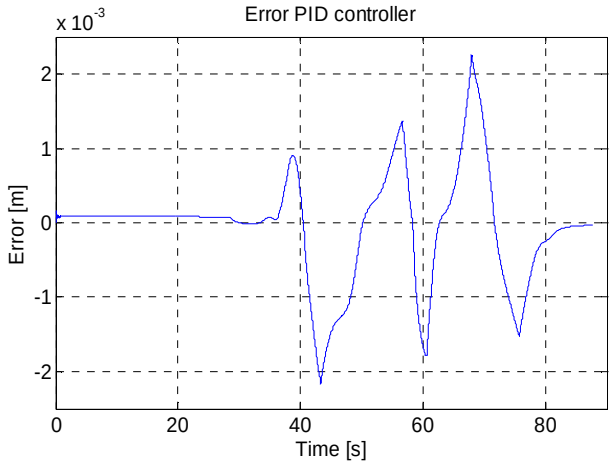

Figure 3.28: The error registered with the PID Controller

Because the errors obtained weren't acceptable, a PI controller replaced the PID. A new set of simulations was conducted and the results are shown in the following two figures.

In the literature PI controllers are more common, since derivative action is very sensitive to measurement noise, and the absence of an integral value may prevent the system from reaching its target value due to the control action, as noticed by Hyder [Hyder, 2010]. The PI controller uses two constant parameters, the proportional and the integral parameter. This controller is minimizing the error between the desired hydraulic actuator displacement and the actual displacement. By setting the integrative and proportional constants, the error could be reduced under 0.1 mm. Fig. 3.29 presents the error and Fig. 3.30 presents the differences between the actual actuator position and desired actuator position when the same values from z_{q_3} were considered for the PI controller.

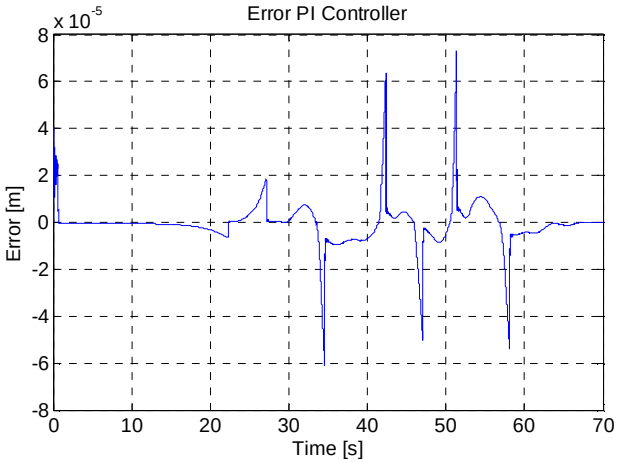

Figure 3.29: The error registered with the PI Controller

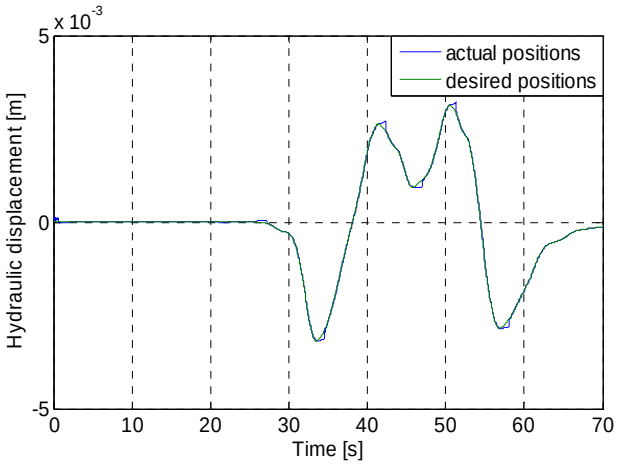

Figure 3.30: The actuators strokes registered in simulations

3.2 The human perception of motion in the EFDS

It is still difficult to define the driving task from a mathematical point of view, because of the many parameters that interact with each other in such a complex process [Capustiac et al., 2011a] (Fig. 3.31).

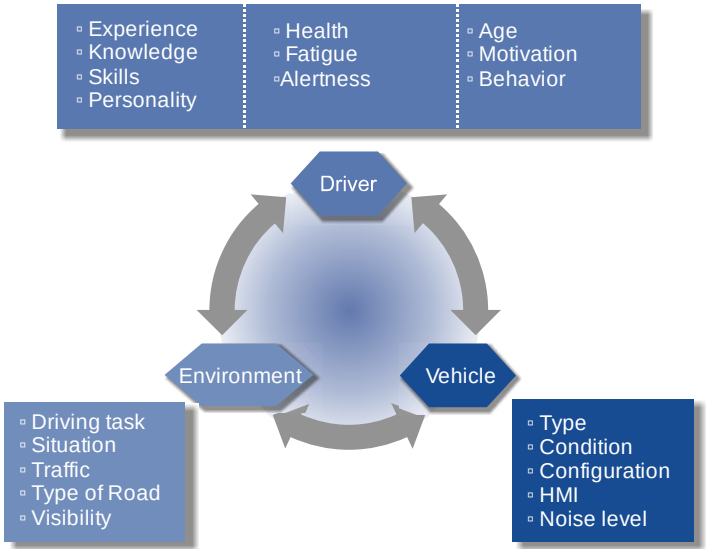

Figure 3.31: The interaction among the driver, vehicle and environment

The second parameter modelled and integrated in the EFDS is concerned with the human perception of motion. As stated before, the motion is sensed by the humans through the skin and the vestibular system [Denne, 2004]. Both of these aspects are studied and modelled here.

3.2.1 The effect of introducing vibrations in the EFDS

Vibrations have a differential action on different human organs, depending on the parameters of the vibration. For low frequencies, the human body can be modelled as an assembly composed of masses, springs and dampers [Untaru et al., 1981]. There are various driver models discussed in literature [Barbu et al., 2007; Stein and Mucka, 2003].

Fig. 3.32 presents two such models. The model proposed by Muksian and Nash takes into consideration the head, torso, diaphragm, spine, abdomen, pelvis and legs (please see Fig. 3.32, left). The authors also included in the motion equations of the model the coulomb friction forces, in attempting to model a human body in sitting position, and subjected to vertical vibrations [Muksian and Nash, 1974].

The model proposed by Goldman and Von Gierke on the other hand, includes the head, upper torso, arms, thorax-abdomen, hips and legs base [Stein and Mucka, 2003]. The model was used to determine the influence of shocks and vibrations on the human body (Fig. 3.32, right). The response of the human body to vibrations and shocks is widely described in literature. Tchermychouk states that the human body is most fatigue sensitive to low frequency vibrations [Tchermychouk, 1999].

The natural frequencies of the human body in standing position were determined to be in the range of 4 to 5 Hz [Alidoost et al., 2010]. Most vital organs have the natural frequency in this range, unlike the spine and the eyeball, whose natural frequency is of 20 – 25 Hz.

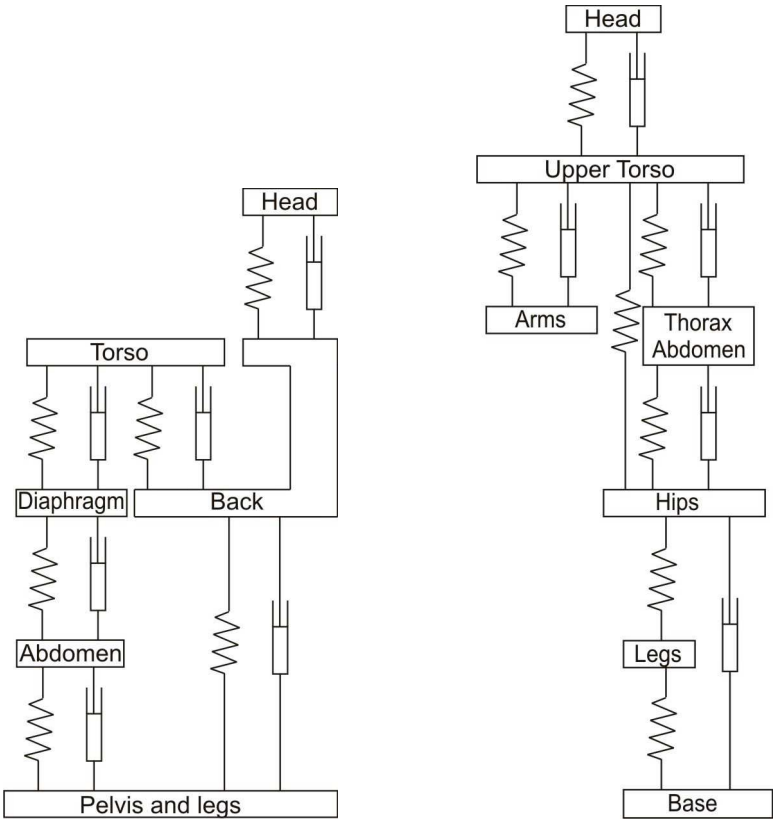

Figure 3.32: Human model proposed by Muksian and Nash (left) and Goldman and Von Gierke (right) [Stein and Mucka, 2003]

The driver model proposed and studied here is a simple 3 DOF model, connected to a vehicle dynamic model through a 1 DOF seat, as presented in Fig. 3.33. The model considers the seated part, the thorax and the head of the human being.

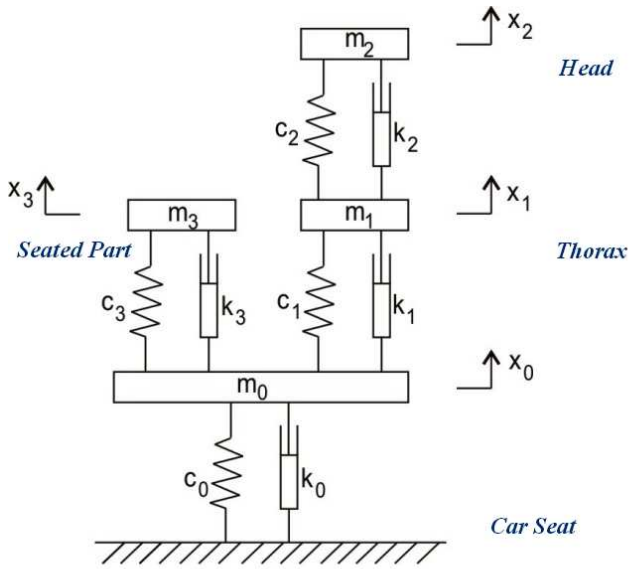

Figure 3.33: The 3 DOF human model [ISO 5982, 2001]

This 3 DOF model is discussed in the International Standard IOS 5982, 2001 concerning the estimation of mechanical impedance, apparent mass and transmissibility for vertical vibration [ISO 5982, 2001].

Since the goal is to study the effect of the vehicle motion on the driver and the frequency response of such a system, this model of the seated human body was considered sufficient and it was discussed and presented by the author in [Capustiac et al., 2011a].

The standard ISO 5982:2001 gives various standard weights for the human body: 55/75/90 kg. In this research it is assumed that the weight of the driver is 90 kg, with the seated part of 56 kg [ISO 5982, 2001]. The seat's parameters correspond to the ones defined in from [VDI 2057, 2002].

The motion equations of this model are:

$$m_0\ddot{x}_0 = c_1(\dot{x}_1 - \dot{x}_0) + c_3(\dot{x}_3 - \dot{x}_0) - c_0(\dot{x}_0 - \dot{u}_v) + k_1(x_1 - x_0) + k_3(x_3 - x_0) - k_0(x_0 - u_v), \quad (3.53)$$

$$m_1\ddot{x}_1 = c_2(\dot{x}_2 - \dot{x}_1) - c_1(\dot{x}_1 - \dot{x}_0) + k_2(x_2 - x_1) - k_1(x_1 - x_0), \quad (3.54)$$

$$m_2\ddot{x}_2 = -c_2(\dot{x}_2 - \dot{x}_1) - k_2(x_2 - x_1), \quad (3.55)$$

$$m_3\ddot{x}_3 = -c_3(\dot{x}_3 - \dot{x}_0) - k_3(x_3 - x_0). \quad (3.56)$$

The motion equations were implemented in Matlab/Simulink, together with the coefficients given in Table 3.11. It is assumed here that u_v corresponds to the vertical displacement of the car seat (Fig. 3.33).

Table 3.11: Human Model Simulation Data [ISO 5982, 2001; VDI 2057, 2002]

Simulation Data	Value	Units
Vehicle seat (stiffness coefficient, damping coefficient, mass)	$k_0 = 54600$	N/m
	$c_0 = 278$	Ns/m
	$m_0 = 2$	kg
Driver's thorax (stiffness coefficient, damping coefficient, mass)	$k_1 = 9990$	N/m
	$c_1 = 387$	Ns/m
	$m_1 = 6$	kg
Driver's head (stiffness coefficient, damping coefficient, mass)	$k_2 = 34400$	N/m
	$c_2 = 234$	Ns/m
	$m_2 = 2$	kg
Driver's seated part (stiffness coefficient, damping coefficient, mass)	$k_3 = 36200$	N/m
	$c_3 = 1390$	Ns/m
	$m_3 = 56$	kg

The dynamics of the human body has been studied to determine to which frequencies the subject is the most sensitive. Human sensitivity can be identified by analysing the frequency response of the human system-seat. Once the acceleration, velocity and displacement of the human body are known, this data can be transformed into the frequency domain.

The output is the frequency response of the system, which gives important information about the human body. While designing a motion simulator, which will also render vibrations, it is crucial to know to which vibrations, the human being is most sensitive.

The Comfort Vehicle Model

The implementation of a vehicle model is necessary in order to predict the behaviour of the simulated vehicle. As stated before, EFDS integrates real vehicle motion as well. The vehicle model is a very important element of a driving simulator and it calculates the positions, velocities and accelerations of the simulated vehicle with respect to the driver's inputs. Two basic vehicle models are discussed in this doctoral work. The one presented below represents the vertical vehicle model. Although it does not consider all vehicle body displacements and rotations or the wheel rotations, it represents the proper tool to investigate the effect of vibrations on the human driver and on the vehicle. In order to analyze the behaviour of the vehicle, a dynamic model was built using Matlab/Simulink.

The dynamics of the vehicle can be investigated in vertical, lateral and longitudinal direction [Schramm et al., 2010]. Vertical dynamics is used for estimation of vibration behaviour with respect to driving safety and comfort. For this analysis, a dynamic vehicle model was used, which will be referred to as a direct vehicle model, since it solves the direct dynamics problem as already discussed by the author in [Capustiac et al., 2010a]. The model consists of 5 bodies, the chassis and the 4 wheels being combined with the wheel carriage. The wheels are allowed to move only vertically. The vehicle chassis is supported through mass-less spring and damper elements. The spring and damper are attached to the wheels and the vehicle

chassis as shown in Fig. 3.11. The vehicle body can move in vertical direction and can perform roll and pitch motion. The steering system is not used in this set up.

The linearized Newton equation for the vehicle model read [Schramm et al., 2010]:

$$m_v \ddot{\boldsymbol{z}}_v = \sum_{i=1}^{4} (k_{A_i} \underbrace{(z_{R_i} - z_{A_i})}_{\Delta z_{RA_i}} + c_A \underbrace{(\dot{z}_{R_i} - \dot{z}_{A_i})}_{\Delta \dot{z}_{RA_i}}) \tag{3.57}$$

$$\theta_{xx} \ddot{\varphi}_v = \frac{S_v}{2}((k_{A_1} \Delta z_{RA_1} + c_A \Delta \dot{z}_{RA_1}) + (k_{A_2} \Delta z_{RA_2} + c_A \Delta \dot{z}_{RA_2}) - (k_{A_3} \Delta z_{RA_3} + c_A \Delta \dot{z}_{RA_3}) - (k_{A_4} \Delta z_{RA_4} + c_A \Delta \dot{z}_{RA_4})) \tag{3.58}$$

$$\theta_{yy} \ddot{\theta}_v = -l_v((k_{A_1} \Delta z_{RA_1} + c_A \Delta \dot{z}_{RA_1}) + (k_{A_3} \Delta z_{RA_3} + c_A \Delta \dot{z}_{RA_3})) + l_h((k_{A_2} \Delta z_{RA_2} + c_A \Delta \dot{z}_{RA_2}) - (k_{A_4} \Delta z_{RA_4} + c_A \Delta \dot{z}_{RA_4})) \tag{3.59}$$

The Newton equations for the vehicle wheels are:

$$m_{R_i} \ddot{z}_{R_i} = k_{R_i}(z_{q_i} - z_{R_i}) + k_{A_i}(z_{A_i} - z_{R_i}) + c_A(\dot{z}_{A_i} - \dot{z}_{R_i}) \quad i = 1,\ldots,4 \tag{3.60}$$

The set of equations (3.57) – (3.60) were implemented in Matlab together with the parameters given in Table 3.12.

Different road profiles simulated and discussed previously were inputted to this vehicle model as already discussed in [Capustiac et al., 2010a]. Two sets of simulations were conducted.

- In the first set, it is assumed that the vehicle is driving on a very good road with 100 km/h speed;
- In the second set of simulations, it is assumed that the vehicle is driving over an average road with 50 km/h.

Table 3.12: Vehicle Model Simulation Data

Data for the Vehicle Model	**Value**	**Units**
k_{A_i} – Wheel suspension spring stiffness	17000	N/m
k_{R_i} – Tire spring stiffness	85000	N/m
c_A – Wheel suspension damping coefficient	5401	Ns/m
m_V – *Vehicle mass*	1300	kg
m_{R_i} – Wheel+ wheel carrier mass	30	kg
$z_{A_{Oi}}$ – Initial vertical position of suspension attachement point P_{A_i} at the chassis	0.54	m
$z_{R_{Oi}}$ – Initial vertical position of suspension attachement point at the wheel centre	0.34	m
$z_{q_{Oi}}$ – Initial vertical position of the actuator	0	m
l_v – Distance front axes to CG	1.11	m
l_h – Distance rear axes to CG	1.23	m
S_v – Track width	0.65	m

Fig. 3.34, 3.35 and 3.36 present results from the simulations conducted with the vehicle model, when the road profiles discussed previously were given as input.

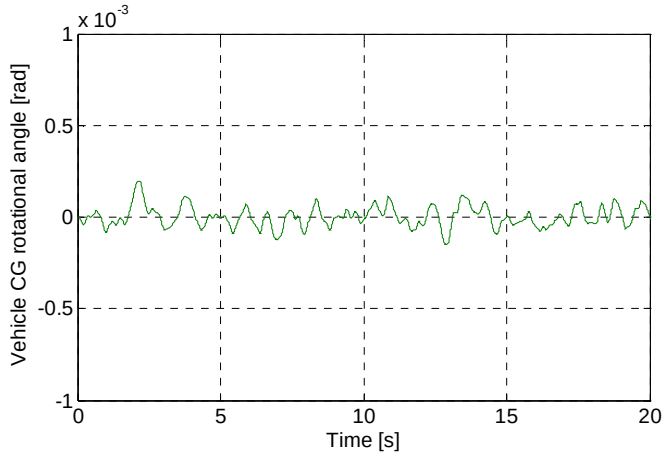

Figure 3.34a: Pitch angle of the vehicle body driving on an A category road with a 100 km/h velocity

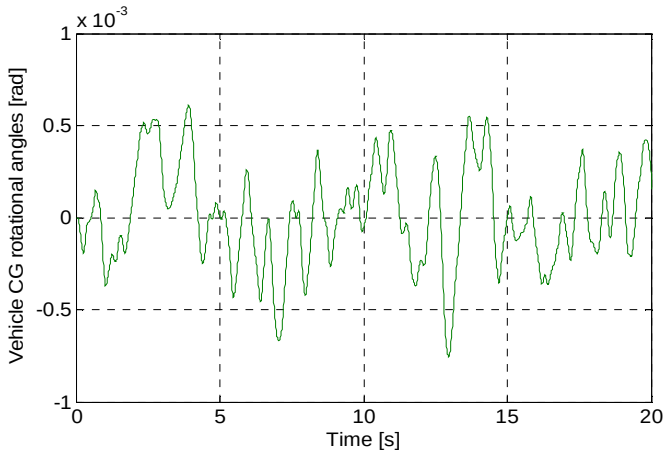

Figure 3.34b: Pitch angle of the vehicle body driving on a C category road with a 50 km/h velocity

The variation of the pitch angle and the angular velocity can be observed in Fig. 3.34, respectively in Fig. 3.35. The yaw angle is not being considered and the roll angle is zero, due to the fact that both, right and left wheels are driving over the same kind of surface.

A time delay Simulink block was used; dependent on the velocity of the vehicle and the distance between the front and rear axis, as it can be observed in Fig. 3.35a and 3.35b, and on the delay between the front wheel centre displacements and rear wheel centre displacements.

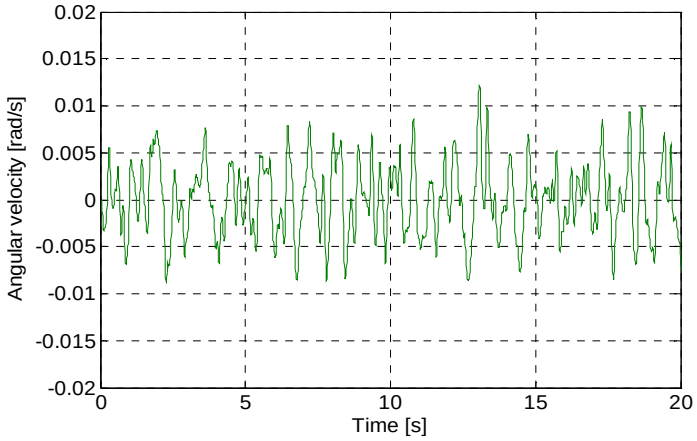

Figure 3.35a. Pitch angular velocity of the vehicle body driving on an A category road with a 100 km/h velocity

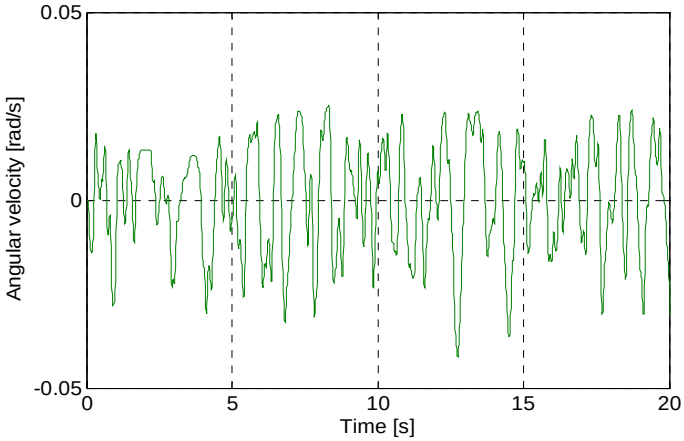

Figure 3.35b: Pitch angular velocity of the vehicle body driving on a C category road with a 50 km/h velocity

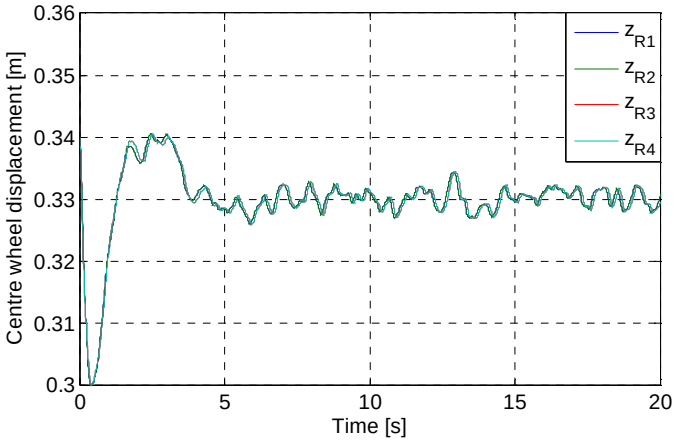

Figure 3.36a: Wheel displacements of the vehicle driving on an A category road with a 100 km/h velocity

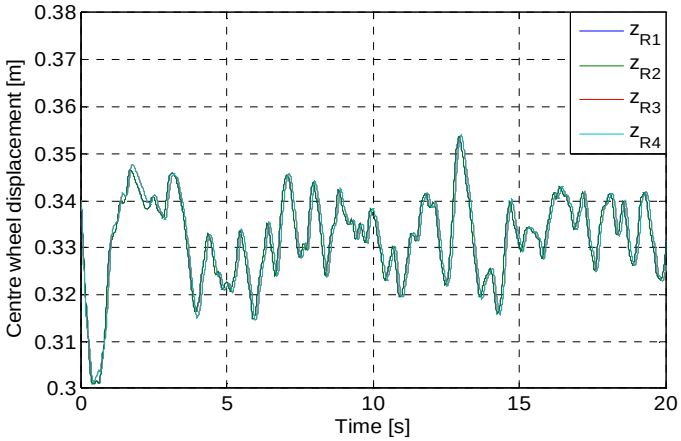

Figure 3.36b: Wheel displacements of the vehicle driving on a C category road with a 50 km/h velocity

The discussed vehicle model is referred to as a 7 DOF vehicle model in literature. It offers information about the vehicle body, the suspension, the un-sprung system and the tyres – road interaction. Since the model considers only 2 rotations and 1 displacement of the vehicle body, and of course all the four vertical displacements of the un-sprung masses, the model has 7 DOF. The human-seat model was connected to the vehicle dynamics model with the goal of analyzing the frequency response of the human model. The displacements of the human body

parts simulated: head, thorax and seated part, were registered in Matlab/Simulink and then investigated with the help of FFT. The results are presented below.

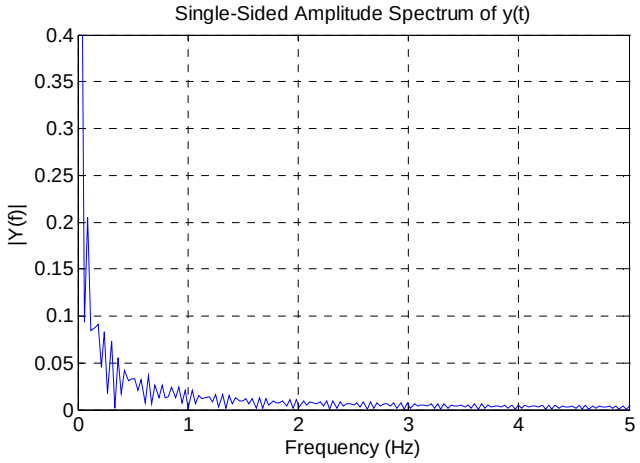

Figure 3.37a: The simulated driver's head response in frequency domain

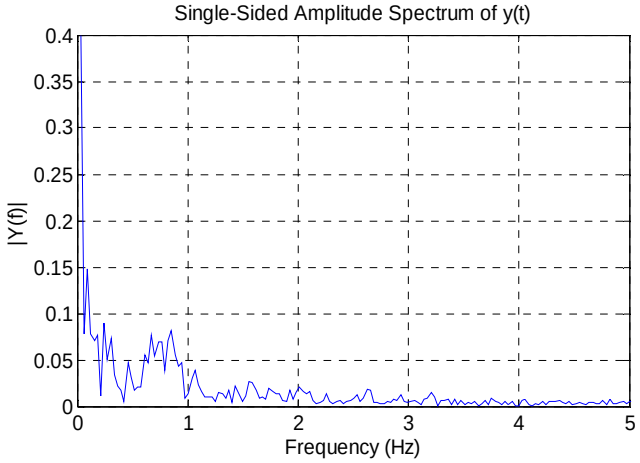

Figure 3.37b: The simulated driver's thorax response in frequency domain

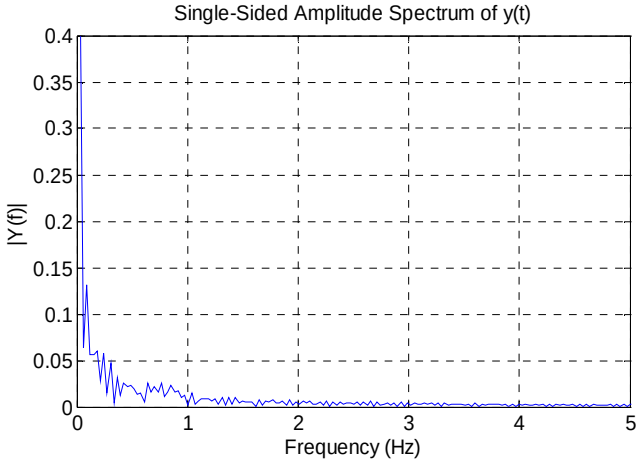

Figure 3.37c: The simulated driver's seated part response in frequency domain

The results obtained in the simulations using the human model showed that the range of frequencies in which the human being is most sensitive is of 0.2 – 5 Hz. The highest values were obtained while simulating the drive of the vehicle model on an E road category. It is assumed in Fig. 3.37 that the vehicle is driving on an A road category. Low frequency

vibrations of the human body, in the range 0.1 – 0.5 Hz can cause motion sickness according to VDI 2057 [VDI 2057, 2002] and should be avoided [Guglielmino et al., 2008].

Kruczek and Stribrsky used a similar approach to determine the driver's reaction. Although the driver model was the same, they used another vehicle model [Kruczek and Stribrsky, 2007]. However the authors stated that the human being is most sensitive in the range 4 to 8 Hz for the vertical motion and 1 to 2 Hz for the horizontal motion. Since the vehicle model considered in the present research does neglect the horizontal motion, only the first range of frequencies were considered for validation purposes.

Tchermychouk performed simulations with different human models (1 – 4 DOF) [Tchermychouk, 1999]. He found the most important frequencies at the 1 – 8 Hz range. Another conclusion was that the human body contributes considerably in reducing the fundamental frequency, peak acceleration transmissibility and the vibration transmission in the isolation frequency range and that the human body dynamics contributes considerably to the overall performance [Tchermychouk, 1999]. Yu and Jun, on the other hand, used a simpler human vehicle model with one DOF together with a vertical vehicle model that integrated four active suspensions. They concluded that the vibrations of the vehicle are strongly affecting the passenger factors [Yu and Jun, 2005].

3.2.2 Mathematical Modelling of the Human Vestibular System

It is important to understand how the human vestibular system functions, in order to apply its characteristics on a motion driving simulator. Its limitations and functions offer very important information, as already discussed by the author in [Capustiac et al., 2011c].

It was already stated that human motion perception thresholds exist. Under these thresholds, the brain does not perceive the variation of velocity [Prothero, 1998]. This characteristic is used in designing the control algorithms of a driving simulator. Bringing the mobile platform to the neutral position should not be sensed by the driver. It is an important command because without it, saturation of the actuators will occur.

Researchers defined perception thresholds for both, velocity and acceleration [Mollenhauer, 2004; Nehaoua et al., 2006]. As highlighted by Telban and Cardullo, the determination of the angular acceleration thresholds was mainly made using angular acceleration step input stimuli [Telban and Cardullo, 2005]. The same authors stated that it was Mulder, who first observed that the product between acceleration magnitude and latency time was approximately constant. Hence, Mulder pointed out the existence of angular velocity thresholds [Telban and Cardullo, 2005]. Meiry used the step response in order to measure the latency time in driving simulator experiences [Meiry, 1958] and to determine the angular velocity thresholds that are also used here.

Von der Heyde and Riecke defined the following as the most used strategies in a driving simulator: *rendering motion below the human motion threshold* for gaining additional simulation space, *tilt coordination* and *usage of vibrations and jitter* to distract the driver [Von der Heyde and Riecke, 2001].

From the above statements it can be observed that the control of a motion driving simulator can be designed with respect to the human motion perception. Hence, the importance of studying the vestibular system is emphasized.

Different transfer functions between the human head's accelerations and the sensed motion can be written similar to Fig. 3.38.

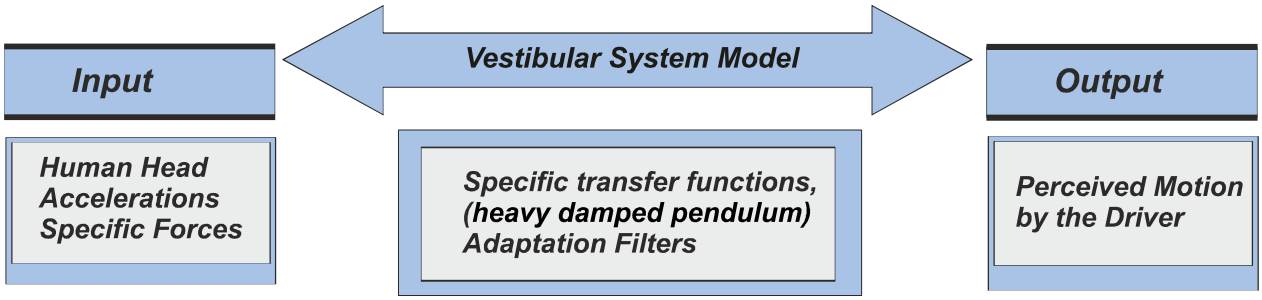

Figure 3.38: Model of the human vestibular system

There are different approaches used in literature for modelling the semicircular canals and the otolith [Meiry and Young, 1968; Dagdelen et al., 2009]. Significant research was made in this field and this chapter deals with the mathematical modelling of the vestibular system.

As stated before, the motion simulator to be developed has 3 DOF. For this reason, the mathematical modelling was considered only for the roll, pitch and heave motion.

With the purpose of studying different motion cueing strategies in the Desdemona driving simulator, the vestibular system was modelled by TNO using the following transfer functions, with the coefficients from Table 3.13 [Wentink et al., 2005]:

$$TF_{pitch,roll} = k_{vs}\frac{1+\tau_L s}{1+\tau_I s}, \qquad TF_{heave} = \frac{1+\tau_L s}{1+\tau_b s}. \tag{3.61}$$

Table 3.13: TNO Human vestibular system coefficients [Wentink et al., 2005]

Parameters	**Values**	**Units**
τ_L	0.11	s
τ_I	5.9	s
τ_b	0.12	s
k_{vs}	5.9	-

Reid and Nahon described the semicircular canals by implementing the following transfer functions with the parameters given in Table 3.14 [Chuang et al., 2008]:

$$TF_{pitch,roll} = \frac{\tau_L \tau_a s^2}{(1+\tau_L s)(1+\tau_s s)(1+\tau_a s)}. \tag{3.62}$$

Table 3.14: Reid&Nahon Human vestibular system coefficients [Chuang et al., 2008]

Parameter	**Values**	**Units**
$\tau_{L_{pitch}}$	6.1	s
$\tau_{L_{roll}}$	5.3	s
τ_a	30	s
τ_s	0.1	s

Zacharias described the otolith by implementing the following transfer function with the parameters given in Table 3.15 [Dagdelen et al., 2009]:

$$TF_{heave} = k_{vs} \frac{1+\tau_a}{(1+\tau_L s)(1+\tau_s s)}. \tag{3.63}$$

Table 3.15: Zacharias vestibular system coefficients [Dagdelen et al., 2009]

Parameter	**Values**	**Units**
τ_L	5.33	s
τ_a	13.2	s
τ_s	0.6	s
k_{vs}	0.4	-

Meiry described the vestibular model using the following transfer functions, with the coefficients from Table 3.16 [Meiry, 1958]:

$$\begin{aligned} TF_{pitch,roll} &= \frac{\tau_L \tau_a s^2}{(\tau_L s+1)(\tau_a s+1)}, \\ TF_{heave} &= k_{vs} \frac{(\tau_1 s+1)}{(\tau_2 s+1)(\tau_s s+1)}. \end{aligned} \tag{3.64}$$

Table 3.16: Meiry Human vestibular system coefficients [Meiry, 1958]

Parameter	**Values**	**Units**
$\tau_{L_{roll}}$	6.1	s
$\tau_{L_{pitch}}$	5.3	s
τ_a	30	s
k	0.4	-
τ_1	13.2	s
τ_2	5.33	s
τ_s	0.66	s

All the parameters described above were tested for subjective perception by the authors. The outputs of the transfer functions are human perceived sensations. The above described transfer functions were implemented in Matlab/Simulink with the goal of understanding the human vestibular system. For simulation purposes, there were used the data recorded from simulations conducted with the IPG Car Maker software. The same manoeuvre, meaning the double lane change was used.

Knowing the vehicle's body motion, with the help of the human model described by equations (3.53) – (3.56), the driver's head vertical velocity and acceleration was obtained in simulation. For the roll and pitch motion a simple kinematical transformation matrix as presented in equation (3.12) was used. Since the goal of this subchapter is to study the system behaviour, introducing these simulated data was sufficient.

The data presented in Fig. 3.39 was inputted to the mathematical models of the vestibular system, as presented in Fig. 3.38.

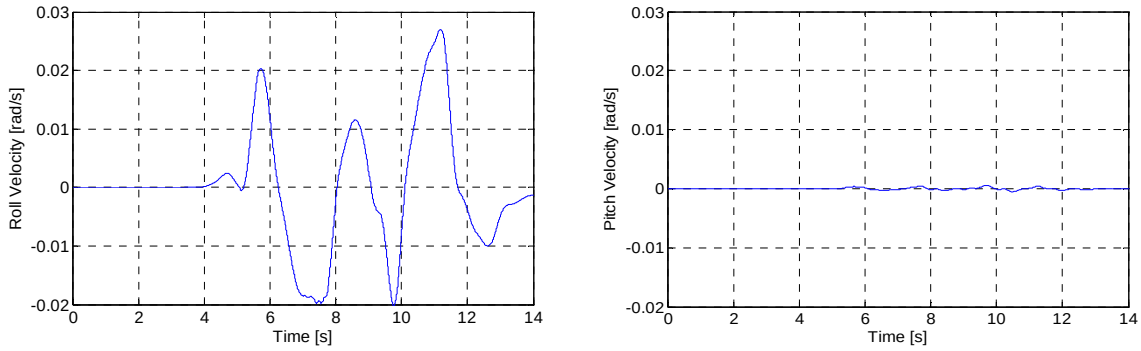

Figure 3.39a: Roll and pitch angular velocity of the driver's head – simulated

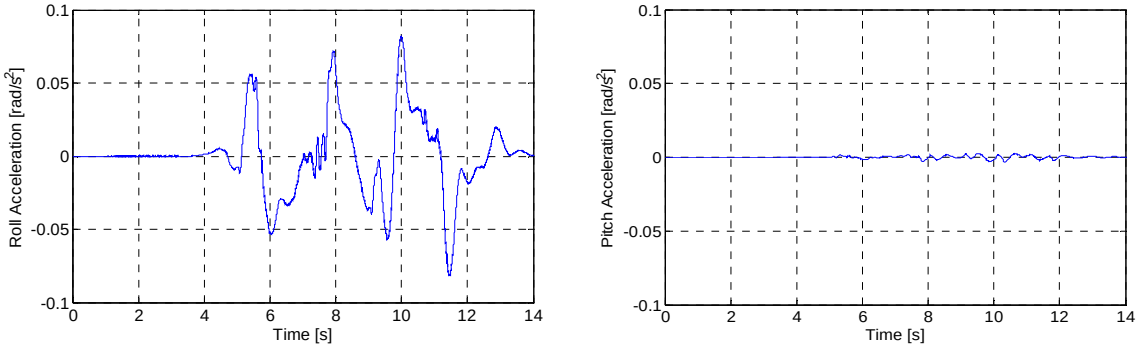

Figure 3.39b: Roll and pitch angular acceleration of the driver's head – simulated

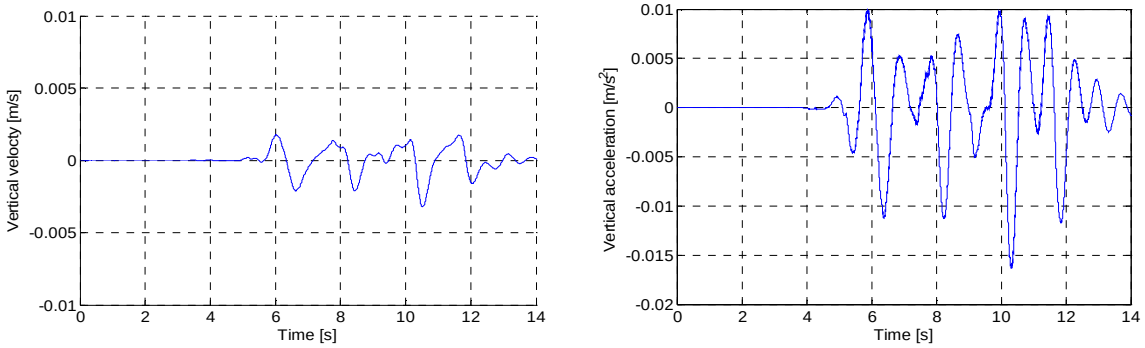

Figure 3.39c: Vertical velocity and acceleration of the driver's head – simulated

The simulation results obtained while implementing the transfer functions (3.61) proposed in [Wentink et al., 2005], in Matlab/Simulink are given in Fig. 3.40.

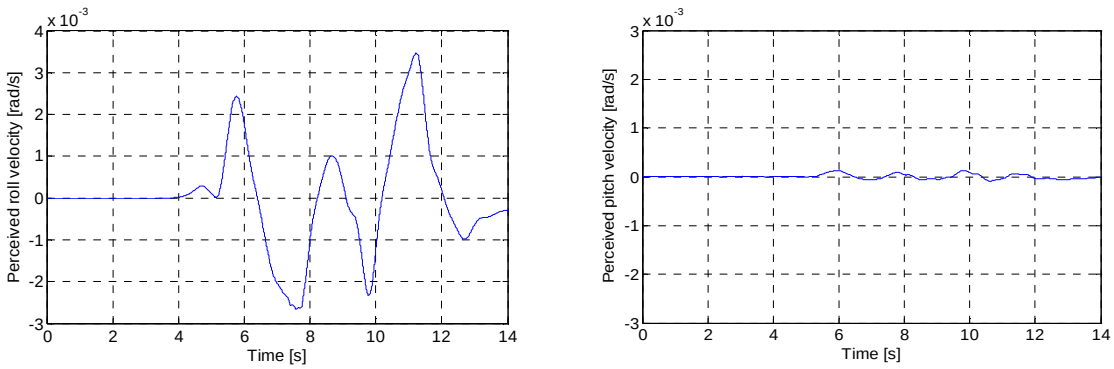

Figure 3.40a: Roll and pitch angular velocity perceived by the driver, TNO algorithm

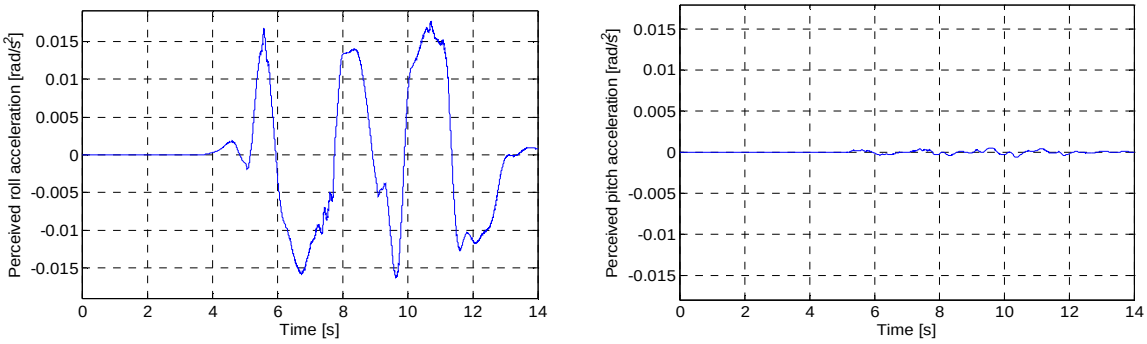

Figure 3.40b: Roll and pitch angular acceleration perceived by the driver, TNO algorithm

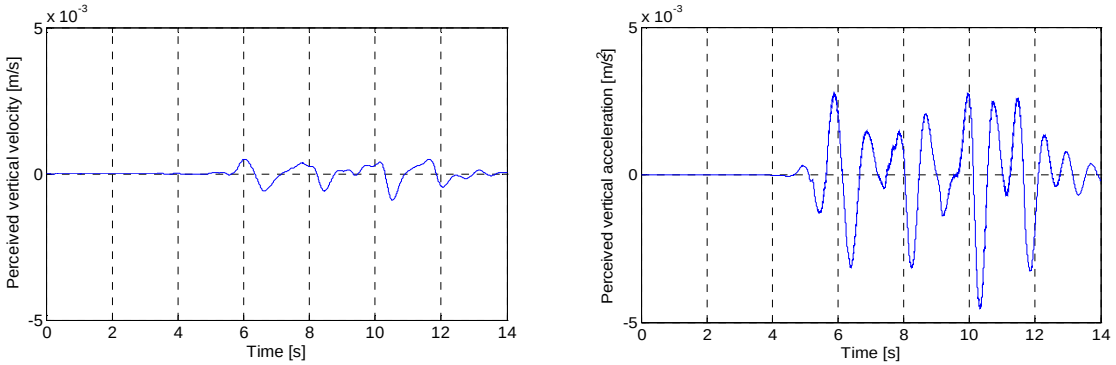

Figure 3.40c: Vertical velocity and acceleration perceived by the driver, TNO algorithm

These sets of figures present the outputs of different mathematical models of the vestibular human system proposed in literature. It can be easily observed the behaviour of this system while introducing the motion of the driver's head.

The outputs of the system are the perceived motion and they contain very important information concerning the perception process. It can be observed that the amplitudes of the outputted signals are smaller. Thus, the frequency response of the system was investigated. The set of Bode diagrams are presented bellow together with the intervals where the subjective sensation is that of the motion applied.

The simulation results obtained while implementing the transfer function (3.62) proposed in [Chuang et al., 2008], in Matlab/Simulink are given in Fig. 3.41.

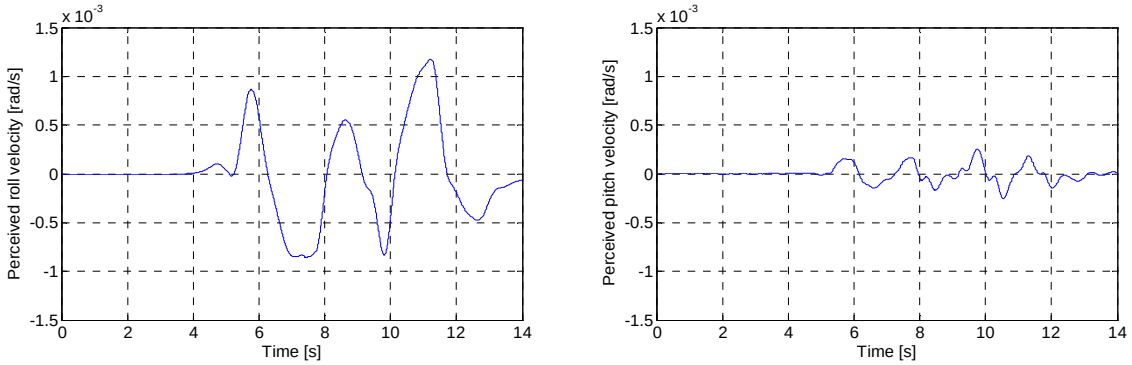

Figure 3.41a: Roll and pitch angular velocity perceived by the driver, Reid and Nahon algorithm

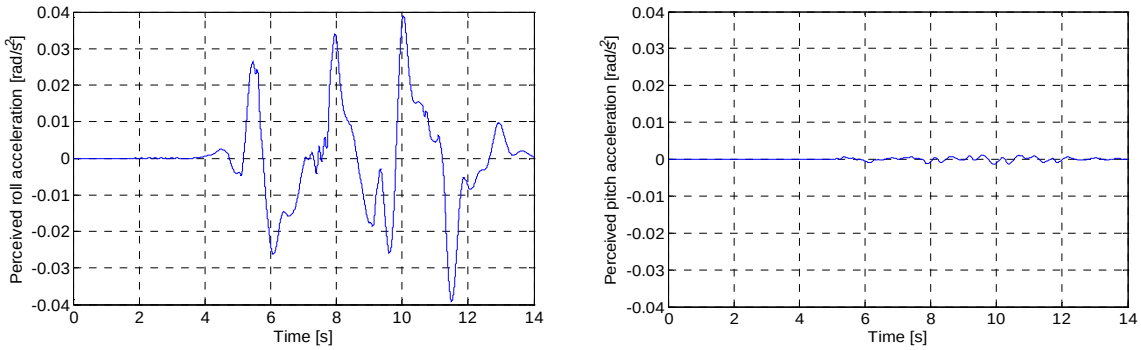

Figure 3.41b: Roll and pitch angular acceleration perceived by the driver, Reid and Nahon algorithm

The simulation results obtained while implementing the transfer function (3.63) proposed in [Dagdelen et al., 2009], in Matlab/Simulink are given in Fig. 3.42.

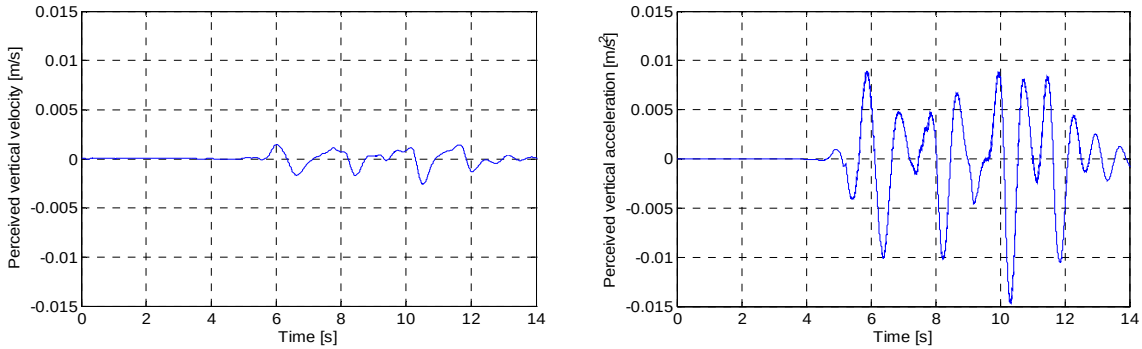

Figure 3.42: Vertical velocity and acceleration perceived by the driver, Zacharias algorithm

The simulation results obtained while implementing the transfer functions (3.64) proposed in [Meiry, 1958], in Matlab/Simulink are given in Fig. 3.43.

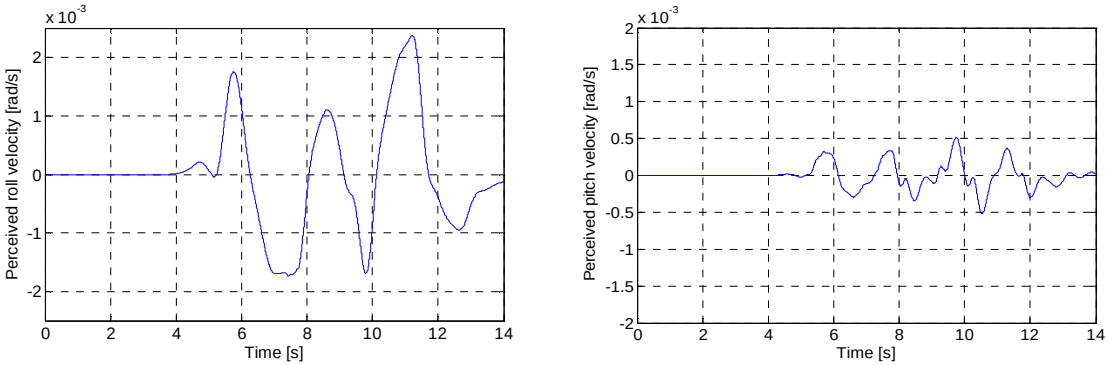

Figure 3.43a: Roll and pitch angular velocity perceived by the driver, Meiry algorithm

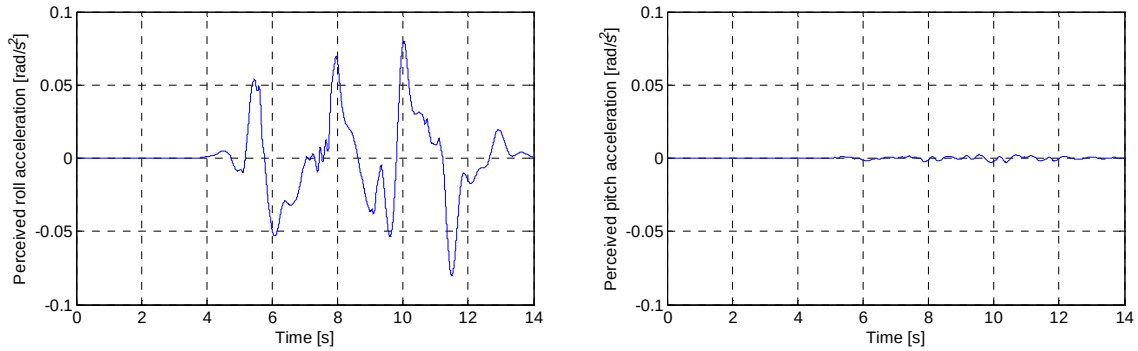

Figure 3.43b: Roll and pitch angular acceleration perceived by the driver, Meiry algorithm

For EFDS's design and for understanding human motion perception, the models developed by Meiry were considered here. Fig. 3.44 shows the bode diagram of the transfer function describing the semicircular canals.

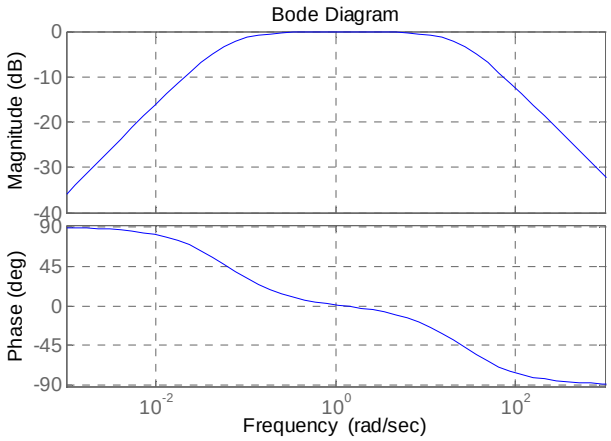

Figure 3.44: The Bode diagram of the Semicircular Canals transfer function (rotation about roll axis)

From this diagram it can be obtained information about the subjective perception of angular displacement. From 0 until 20 rad/s (0 Hz to 3.18 Hz) the subjective sensation is that of the angular velocity of the motion applied. Meiry noted in [Meiry, 1958] that, while a rotation with constant angular velocity is not perceived by the semicircular canals, a constant angular acceleration motion is sensed over time so that the perception coincides with the instantaneous angular velocity of the motion applied on the human being. The otolith was modelled by Meiry as a system where inputting the specific force, the output obtained is the subjective sensation of tilt and linear velocity. The specific forces $\boldsymbol{f}_t$ are defined in literature as a relation between the translational acceleration $\boldsymbol{a}$ and the gravitational vector $\boldsymbol{g}$ [Augusto and Loureiro, 2009]. The specific vertical force is calculated using its definition [Augusto and Loureiro, 2009]:

$$\boldsymbol{f}_t = \boldsymbol{a} - \boldsymbol{g} \,. \tag{3.65}$$

Using the transformation matrix from the inertial coordinate system to the vehicle coordinate system means that the vector of the specific force with its 3 components can be written, with respect to the three components of the acceleration vector. Fig. 3.45 shows the Bode diagram of the otolith transfer function.

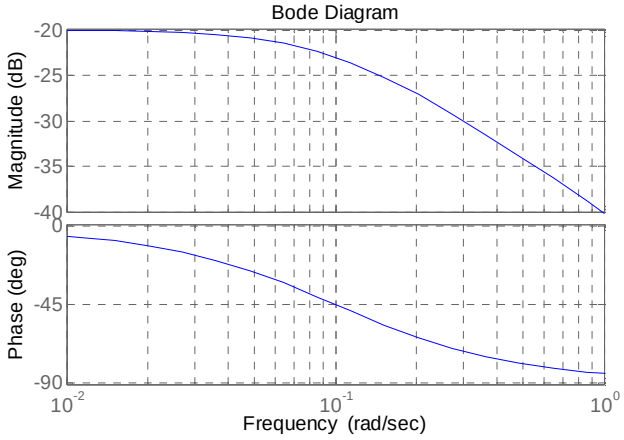

Figure 3.45: The bode diagram of the Otolith transfer function

Young proved that in the range 0.1 to 1 Hz, the otolith functions as a specific force transducer [Young, 1982]. Meiry defined the vestibular organs as the centre of detection and control of the voluntary changes of a posture along with monitoring orientation during passive manoeuvres of the head and the human body [Meiry, 1958]. By using these models, the driver's motion sensed in a car can be analyzed. It is important to know the values of the accelerations sensed by the human being in a vehicle in order to be able to filter these signals and implement them in the MCA. Meiry defined the perceived motion as the most important sensation that the human being experiences in response to an input acceleration. Tchermychouk identified the utricle as a sensor with linear characteristics when in the sagittal plane, the linear accelerations in the range ±0.1 g are applied [Tchermychouk, 1999]. Meiry proved that the otolith functions dynamically in the range 0.016 – 0.25 Hz [Meiry, 1958].

3.3 MCA in the 3 DOF EFDS

Due to the workspace and actuator limitations, driving simulators cannot perfectly reproduce the motion of the vehicle being simulated [Nehaoua et al., 2006]. Although the workspace of the driving simulator considered in this doctoral work is limited, it should be able to provide realistic and correct motion cues [Capustiac et al., 2010a]. This is mostly related to the design of the vehicle models and the control algorithms [Capustiac et al., 2011b].

There are two mainly strategies used in designing MCA:

- The *washout algorithms*, where the platform is moved conform to the inputs given by the vehicle dynamics, and then it is brought back in the neutral position without the driver' having to detect this motion [Nehaoua et al., 2006];
- The second strategy consists in the *tilt coordination* and reproduces accelerations by coupling the gravitational vector. The vestibular system interprets this motion as negative or positive acceleration depending on the inclination's direction. The gravitational vector can be varied with respect to the human body that has to display long sustained accelerations without sensing the rotational movement [Nehaoua et al., 2006].

This subchapter deals with the development and implementation of the vehicle models used in the driving simulator and the MCA that were designed as part of the contribution to this doctoral work.

3.3.1 Mathematical Modelling of the Vehicle

This subchapter is dedicated to discuss the vehicle models used in the EFDS.

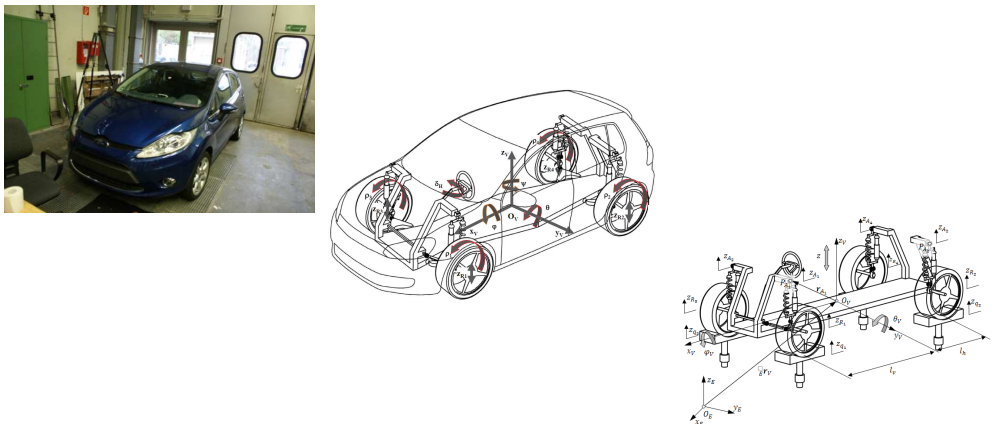

Figure 3.46: Vehicle Models development

The vehicle models are a very important component of a driving simulator. With the help of these models, the EFDS can render the dynamics of a vehicle system.

The inverse dynamics of the full vehicle model

Since not only street excitation, but also the roll, pitch and heave motion of the simulator is to be controlled, the dynamic transfer path between the actuators and the vehicle body has to be understood as well. In order to be able to develop a control strategy for the EFDS concept integrating a real vehicle, the inverse vertical model for a vehicle was developed, as a contribution to this work and was already published in [Capustiac et al., 2010a]. The goal is to determine the strokes of the actuators $z_{q_i}, i = 1,...,4$ for different applied roll, pitch and heave motions φ_V, θ_V, z_v. The system formed by equations (3.66) – (3.70) describes the inverse dynamics of the comfort model:

$$z_{q_i} = \frac{1}{k_{R_i}}(m_{R_i}\ddot{z}_{R_i} - c_A(\dot{z}_{A_i} - \dot{z}_{R_i}) - k_{A_i}(z_{A_i} - z_{R_i}) + k_{R_i} z_{R_i}), \quad i = 1,...,4, \tag{3.66}$$

where the velocity of wheel centre $z_{R_i}, i = 1..4$ is given by:

$$\dot{z}_{R_i} = \frac{1}{c_A}(m_A\ddot{z}_{A_i} + k_{A_i}(z_{A_i} - z_{R_i})) + \dot{z}_{A_i}. \tag{3.67}$$

The vertical position z_{A_i} of the suspension attachment point P_{A_i} at the chassis is defined as:

$$z_{A_i} = z_v + r_{y,A_i}\sin\varphi_V + r_{z0,v}\cos\varphi_V\cos\theta_V - r_{x,A_i}\cos\varphi_V\sin\theta_V. \tag{3.68}$$

The unload spring length of the simplified tyre model is:

$$l_{0,R_i} = (m_{R_i} + m_V)\frac{g}{k_{R_i}} + (z_{R0_i} - z_{q0_i}), \tag{3.69}$$

and respectively the unload spring length of chassis suspension:

$$l_{0,A_i} = \frac{m_A g}{k_{A_i}} + (z_{A0_i} - z_{R0i}). \tag{3.70}$$

All vehicle parameters used in the simulations are given in Table 3.12. The equations were implemented in Matlab/Simulink. For simulation purposes a lane change manoeuvre from IPG Car Maker was used. The vehicle body motion was given as input to the vehicle model and is presented in Fig. 3.47.

The simulated manoeuvre is more dynamically moderate than the one used before, as it can be observed in the above presented figures. The same methodology was applied, and the recorded data was given as input to the simulated inverse vehicle model.

The vehicle roll and pitch angle, respectively angular velocity and vertical displacement, respectively velocity was saved through the Simulink blocks and used further in this research. The aim of imposing a certain movement on the vehicle body is to relate certain driving manoeuvres and to impose forces on the human body while driving [Capustiac et al., 2011a].

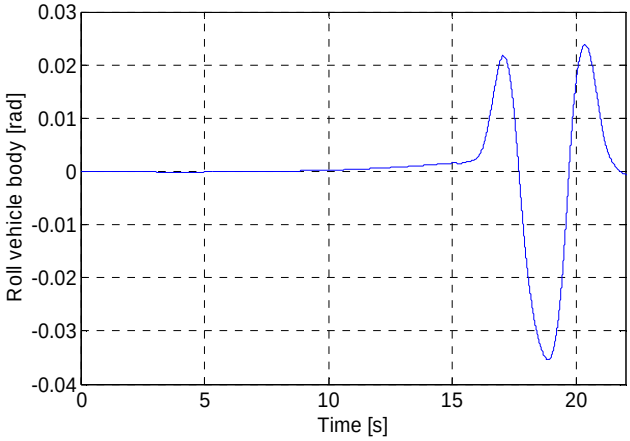

Figure 3.47a: Vehicle roll body angle recorded with IPG Car Maker Software

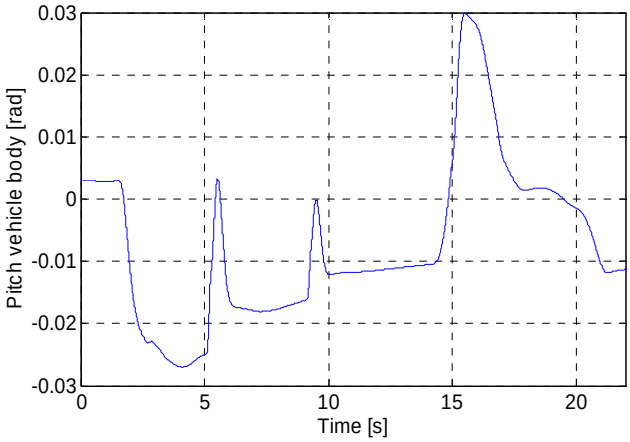

Figure 3.47b: Vehicle pitch body angle recorded with IPG Car Maker Software

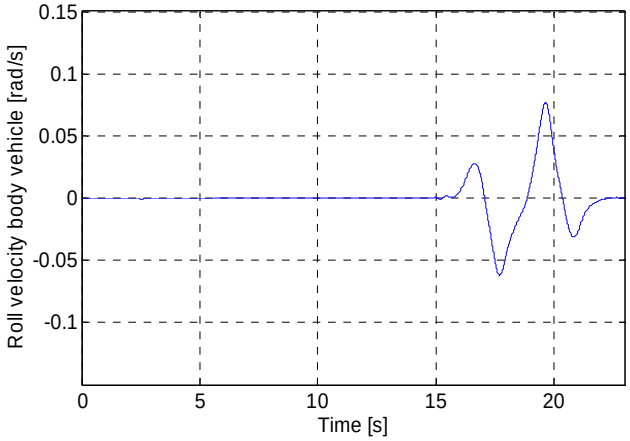

Figure 3.47c: Vehicle body roll angular velocities recorded with IPG Car Maker Software

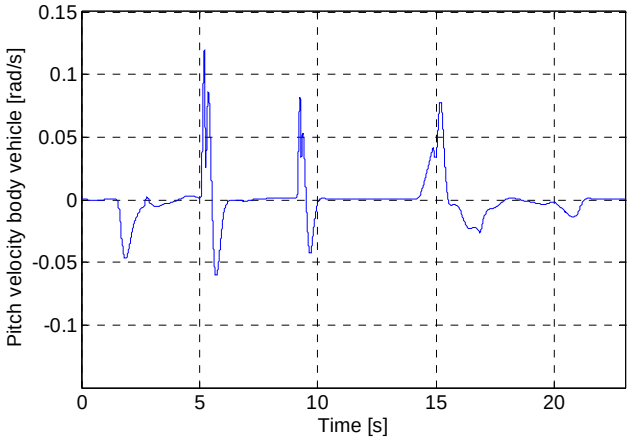

Figure 3.47d: Vehicle body pitch angular velocities recorded with IPG Car Maker Software

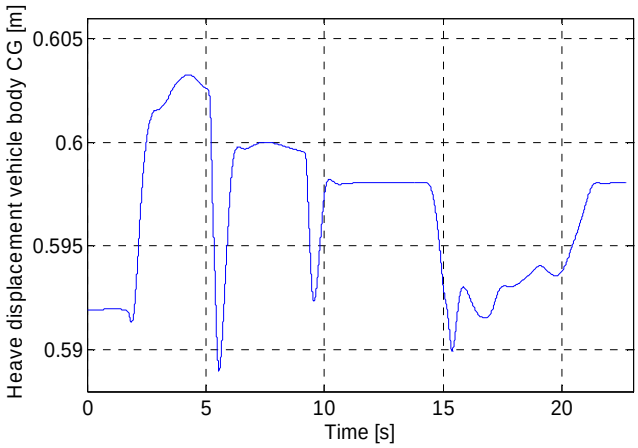

Figure 3.47e: Vehicle body vertical displacement recorded with IPG Car Maker Software

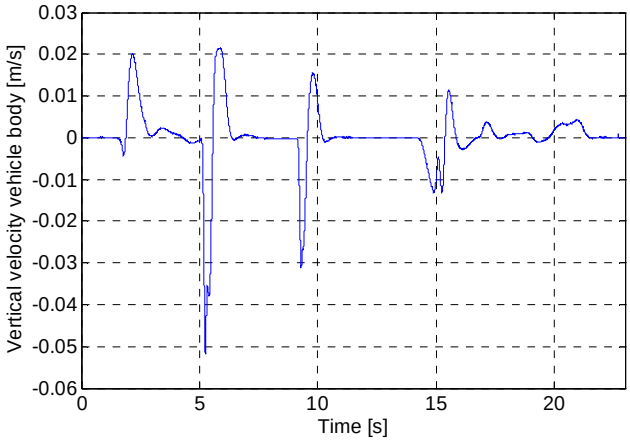

Figure 3.47f: Vehicle body vertical velocity recorded with IPG Car Maker Software

The displacements of the actuators and the forces of the vehicle models were obtained. In this contribution the vehicle body is substituted with a vehicle model. This enables studying the control strategy without setting up the real system.

The resulting movement from the Matlab vehicle model is shown below. The displacements and velocities of the four hydraulic actuators can be observed.

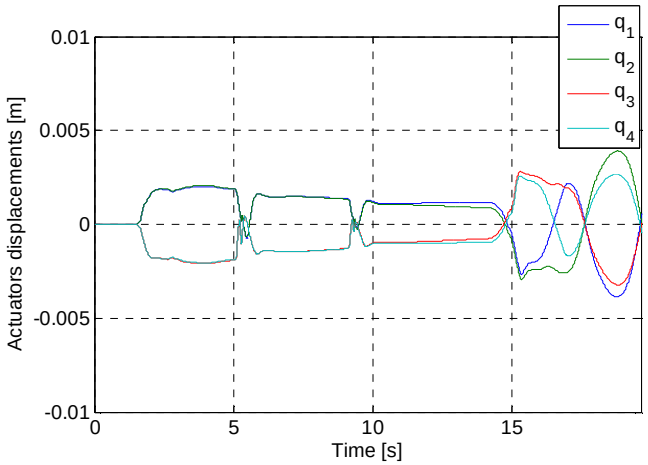

Figure 3.48a: Actuator displacements obtained in simulations

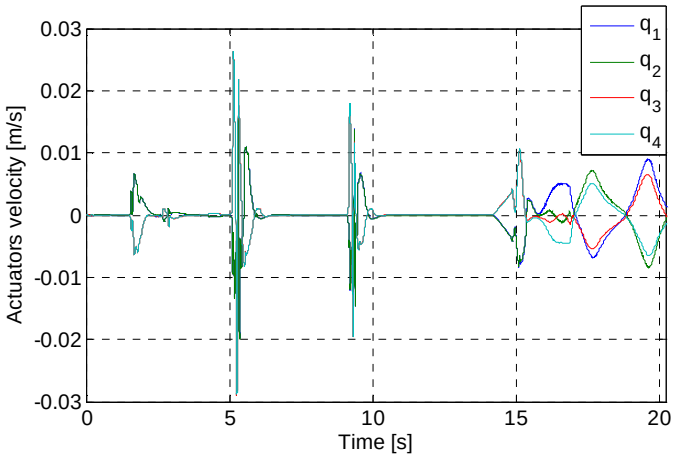

Figure 3.48b: Actuator velocities obtained in simulation

The chassis damping spring and tyre spring forces of the model were also determined and are presented in Fig. 3.49. Concerning with the design of the EFDS, the determination of the tyre – road forces system is very important since this system is an input to its dynamics.

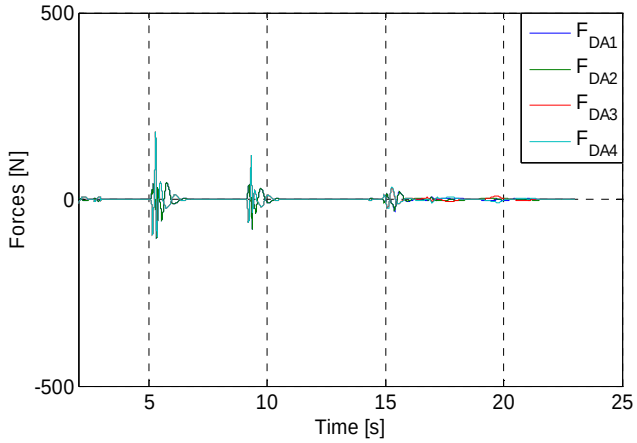

Figure 3.49a: Chassis damping forces obtained in simulation

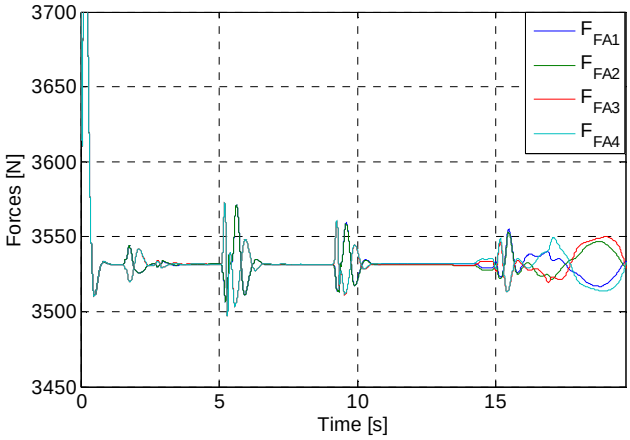

Figure 3.49b: Chassis spring forces obtained in simulation

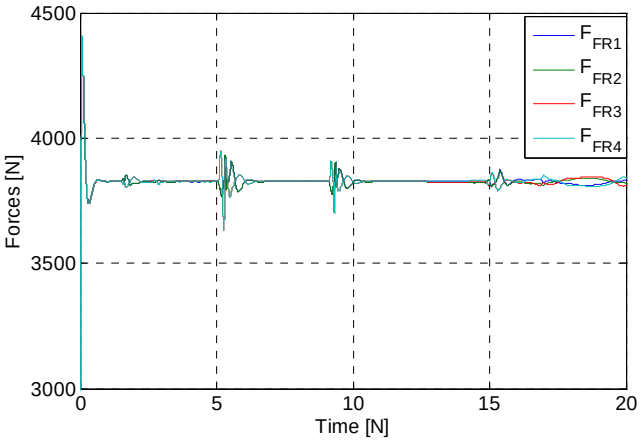

Figure 3.49c: Tyre spring forces obtained in simulation

Since the goal is to obtain a control strategy using the inverse dynamics of the vehicle combined with a PI controller of the hydraulic valve, the inverse dynamics was coupled with the hydraulic model described by equation (3.35) – (3.51). Values from the third actuator obtained and presented previous were considered corresponding to the rear left wheel. The following figure present the error from the PI Controller and the differences between the actual actuator position and the desired actuator position, while running the simulation proposed in Fig. 3.50.

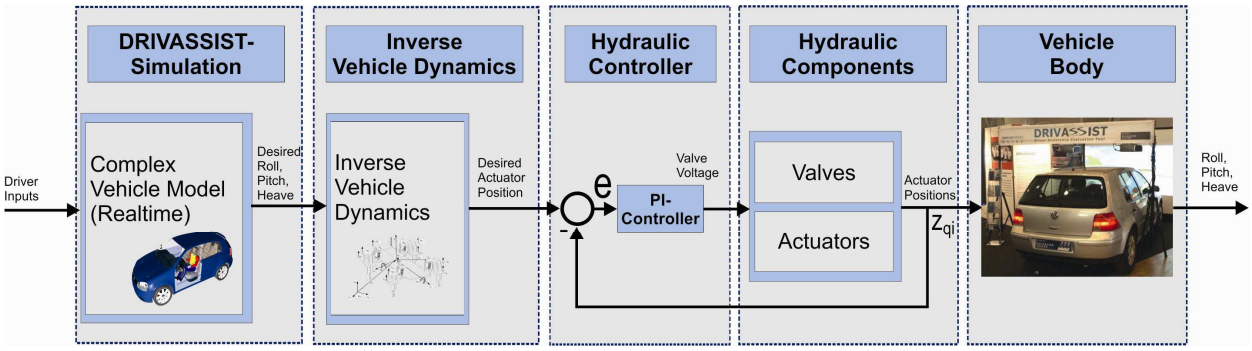

Figure 3.50: The overall proposed control strategy

This strategy was proposed for controlling the EFDS that integrates a real vehicle. Since a complete set of simulations was needed before setting up the real system, recorded data was

used as desired roll, pitch and heave motion. The PI controller is minimizing the error between the desired and the actual position.

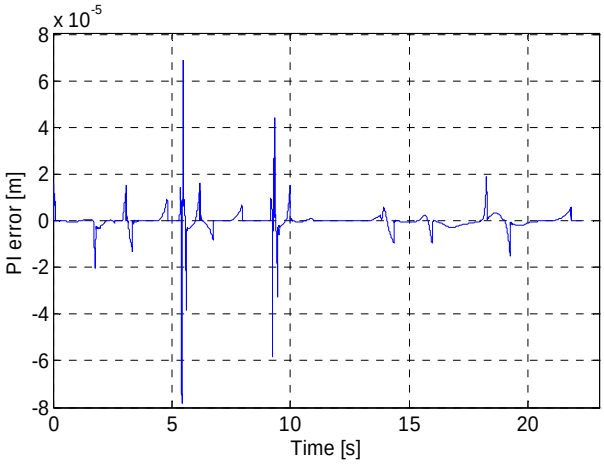

Figure 3.51: The error from the PI Controller

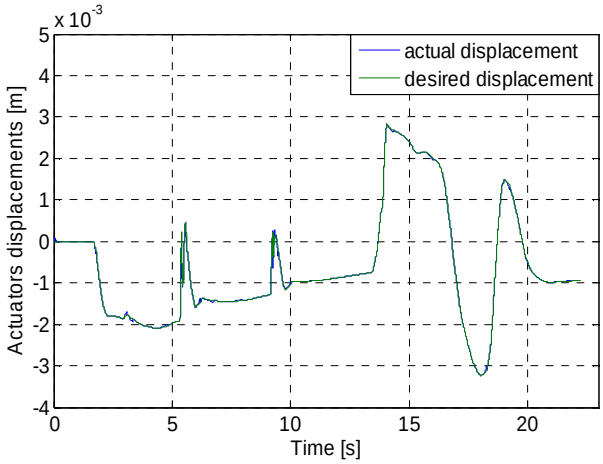

Figure 3.52: The differences between the actual hydraulic actuator displacement and the desired displacement

With the help of Virtual Reality, a Matlab Toolbox, a virtual environment was build. After creating the Simulink model, this environment was developed and its objects were connected with the Virtual Reality Toolbox blocks. This toolbox has a flexible Matlab interface. The positions and the proprieties of the objects were set in Matlab and the virtual environment was visualized with the help of a viewer – VRML viewer [MAT, 2011].

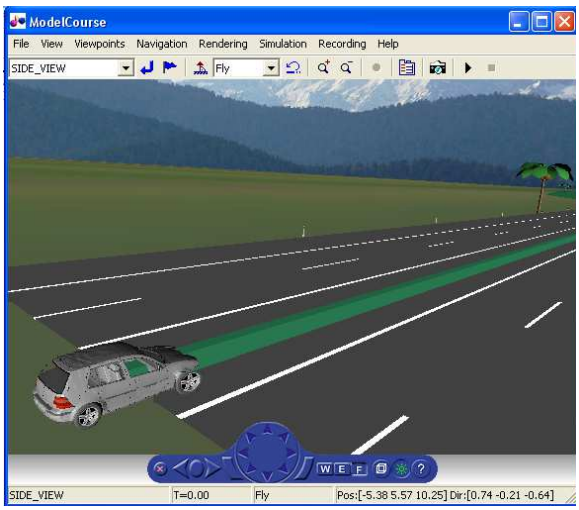

Figure 3.53: Virtual Reality Vehicle Simulations

The visualization of the vehicle is made by using a virtual reality model of a Golf IV. The vehicle is performing the simulated 3 DOF, while the cylinder strokes calculated and presented above were given as inputs to the model. The virtual models contain implemented properties of the real system and try to highlight the vehicles behaviour in certain situations.

The two-lane model

The vehicle models presented and implemented so far took in consideration only the vertical acceleration. In order to implement MCA for the 3 DOF EFDS, the longitudinal and lateral acceleration is also needed. The two-lane model is considered in this work. The vehicle model takes into consideration a simple vehicle suspension. The wheels are connected through spring and damper elements to the vehicle chassis. The wheel centres can only move perpendicularly on the road [Schramm et al., 2010]. This means that complex wheel suspension characteristics like camber and caster changes are neglected. However, this model is complex enough for spatial vehicle dynamic analysis and for being a basis model for a driving simulator.

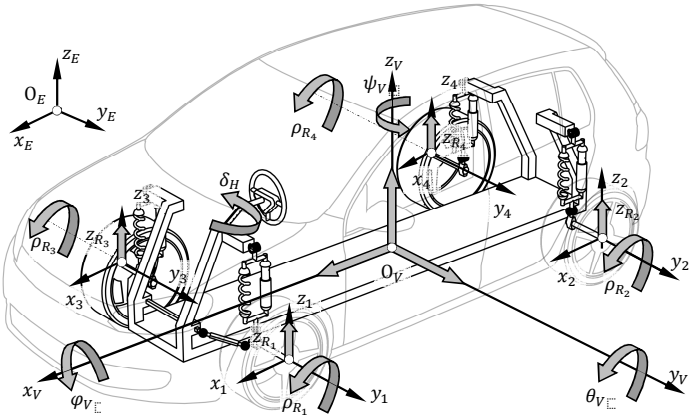

Figure 3.54: DOF of the spatial twin-track model [Schramm et al., 2010]

The mathematical model has 14 DOF: the coordinates of the vehicle's centre of gravity x_v, y_v, z_v, the Cardan shaft angle of the vehicle body $\psi_v, \theta_v, \varphi_v$, the rotation of the wheel about its roll axis $\rho_{R_i}, i = 1 \ldots 4$ and the vertical movement of the wheel $z_{R_i}, i = 1, \ldots, 4$ [Schramm et al., 2010]. The correlation between the vehicle's coordinate system to the inertial coordinate system is made with the help of the transformation matrix, presented before in the inverse kinematics subchapter. For the angular velocity of the vehicle body in coordinates of the fixed vehicle coordinate system and relative to the inertial coordinate system [Schramm et al., 2010]:

$$ {}^{V}_{E}\boldsymbol{\omega}_v = \begin{bmatrix} \omega_{V,x} \\ \omega_{V,y} \\ \omega_{V,z} \end{bmatrix} = \begin{bmatrix} \dot{\varphi}_v - \dot{\psi}_V \sin\theta_V \\ \dot{\theta}_V \cos\varphi_v + \dot{\psi}_V \cos\theta_V \sin\varphi_V \\ -\dot{\theta}_V \sin\varphi_v + \dot{\psi}_V \cos\theta_V \cos\varphi \end{bmatrix} = \boldsymbol{T}_\omega \begin{bmatrix} \dot{\psi}_V \\ \dot{\theta}_V \\ \dot{\varphi}_V \end{bmatrix}, \tag{3.71} $$

where:

$$ \boldsymbol{T}_\omega = \begin{bmatrix} -\sin\theta_V & 0 & 1 \\ \cos\theta_V \sin\varphi_V & \cos\varphi_V & 0 \\ \cos\theta_V \cos\varphi_V & -\sin\varphi_V & 0 \end{bmatrix}. \tag{3.72} $$

Accordingly, the movement of each wheel relative to the stationary coordinate system K_E

can be described. For the steered front wheels, the motion is described as follows [Schramm et al., 2010]:

$$ {}^{E}\boldsymbol{T}_{R_1} = {}^{E}\boldsymbol{T}_{R_3} = \boldsymbol{T}_z(\psi_V + \delta) = \begin{bmatrix} cos(\psi_V + \delta) & -sin(\psi_V + \delta) & 0 \\ sin(\psi_V + \delta) & cos(\psi_V + \delta) & 0 \\ 0 & 0 & 1 \end{bmatrix}. \tag{3.73} $$

It is assumed that the maximum angle of turn is the same both for the wheels and for linearly dependent on the steering wheel angle as a function of time:

$$ \delta_1 = \delta_3 = \delta = i_L \cdot \delta_H(t). \tag{3.74} $$

And for the rear wheels (no steering $\delta_2 = \delta_4 = 0$):

$$ {}^{E}\boldsymbol{T}_{R_2} = {}^{E}\boldsymbol{T}_{R_4} = \boldsymbol{T}_z(\psi_V) = \begin{bmatrix} cos\,\psi_V & -sin\,\psi_V & 0 \\ sin\,\psi_V & cos\,\psi_V & 0 \\ 0 & 0 & 1 \end{bmatrix}. \tag{3.75} $$

Furthermore, the rotation of the coordinate system of the wheel with respect to the fixed vehicle coordinate system for the front axle is defined [Schramm et al., 2010]:

$$ {}^{V}\boldsymbol{T}_{R_1} = {}^{V}\boldsymbol{T}_{R_3} = \boldsymbol{T}_x^T(\varphi_V) \cdot \boldsymbol{T}_y^T(\theta_V) \cdot \boldsymbol{T}_z(\delta) \tag{3.76} $$

$$ = \begin{bmatrix} cos\,\delta\,cos\,\theta_V & -sin\,\delta\,cos\,\theta_V & -sin\,\theta_V \\ sin\,\varphi_V\,sin\,\theta_V\,cos\,\delta + cos\,\varphi_V\,sin\,\delta & -sin\,\varphi_V\,sin\,\theta_V\,sin\,\delta + cos\,\varphi_V\,cos\,\delta & sin\,\varphi_V\,cos\,\theta_V \\ cos\,\varphi_V\,sin\,\theta_V\,cos\,\delta - sin\,\varphi_V\,sin\,\delta & -cos\,\varphi_V\,sin\,\theta_V\,sin\,\delta - sin\,\varphi_V\,cos\,\delta & cos\,\varphi_V\,cos\,\theta_V \end{bmatrix} $$

And for the rear axle:

$$ {}^{V}\boldsymbol{T}_{R_2} = {}^{V}\boldsymbol{T}_{R_4} = \boldsymbol{T}_x^T(\varphi_V) \cdot \boldsymbol{T}_y^T(\theta_V) = \begin{bmatrix} cos\,\theta_V & 0 & -sin\,\theta_V \\ sin\,\varphi_V\,sin\,\theta_V & cos\,\varphi_V & sin\,\varphi_V\,cos\,\theta_V \\ cos\,\varphi_V\,sin\,\theta_V & -sin\,\varphi_V & cos\,\varphi_V\,cos\,\theta_V \end{bmatrix} \tag{3.77} $$

The linear momentum of the vehicle body [Schramm et al., 2010]:

$$ m_v \ddot{\boldsymbol{r}}_v = \sum_{i=1}^{4} \boldsymbol{F}_i + \boldsymbol{G} + \boldsymbol{F}_w = \sum_{i=1}^{4} \boldsymbol{F}_i - m_v g \boldsymbol{e}_z + \boldsymbol{F}_w \tag{3.78} $$

The previously presented equations were implemented in Matlab/Simulink in order to obtain the 14 DOF vehicle model. This model was further coupled with the MCA. Their design is described in the following subchapter.

3.3.2 Design of Motion Cueing Filters in the Laplace Domain

Correct motion in a driving simulator can increase the degree of realism of the simulation [Colombet et al., 2008], but incorrect motion cues can distract the driver [Denne, 1996]. Thus, the simulator's control algorithms have to be carefully designed. It was presented in previous subchapters that the vehicle model calculates the displacements, velocities and accelerations of the vehicle the human is assumingly driving. Since the EFDS has limited DOF and workspace, it cannot reproduce 1:1 the outputs of the vehicle model. Hence, special algorithms that transform the vehicle's motion in achievable motion by the driving simulator are designed.

The literature available on MCA is vast. There are more types of strategies applied: classical, adaptive, optimal, nonlinear, etc. [Augusto and Loureiro, 2009]. The classical motion algorithm computes the acceleration of the motion platform along any DOF, by high pass filtering the corresponding vehicle acceleration, as presented in [Gutridge, 2004] (Fig. 3.55). The disadvantages of this kind of algorithms are reducing the rendered accelerations and not using the whole workspace of the platform, since they are designed for the worst case scenario [Augusto and Loureiro, 2009]. The advantage is increasing the driving fidelity when the simulator is near to its neutral position [Colombet et al., 2008].

Figure 3.55: The classical motion cueing strategy

The adaptive algorithms were first developed by Parrish et al. and their design is based on the classical strategy [Nehaoua et al., 2008]. The difference is that the filters integrate time varying gains, in this way adapting its response to all situations needed, as it can be observed in Fig. 3.56.

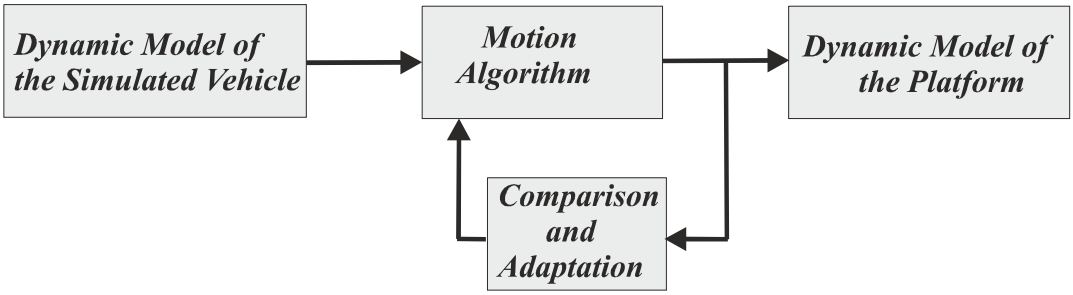

Figure 3.56: The adaptive motion cueing strategy

The optimal algorithms were first developed by Sivan in 1982, and then implemented by Reid and Nahon in 1985 and they solve a transfer function, which relates the simulated vehicle's motion with the driving simulator's motion, such that the difference between the felt signals in both is minimized [Nehaoua et al., 2008; Augusto and Loureiro, 2009]. In order to obtain the felt or perceived motion by the driver, these algorithms integrate a mathematical model of the human vestibular system, as it can be observed in Fig. 3.57.

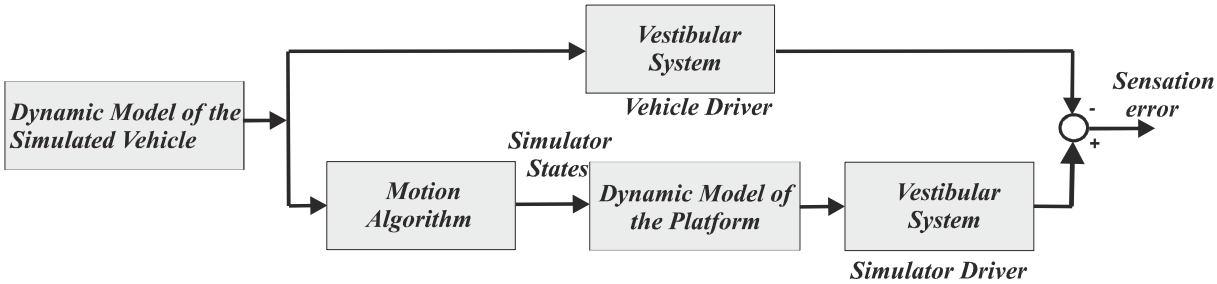

Figure 3.57: The optimal motion cueing strategy

The classical strategy is the most used strategy in the driving simulators [Gutridge, 2004]. This research deals with the classical approach, due to the manoeuvres to be tested, the limited workspace available and the simplicity of the design. This strategy was first used in the control of the flight simulators with 6 DOF. Different kind of motion cueing algorithms for driving simulators based on this type of strategy are discussed in the literature [Gutridge, 2004; Nehaoua et al., 2008; Krissada and Witaya, 2009]. The classical MCA consist of *high pass* and *low pass linear filters*. As already observed by Gutridge, the high pass filters attenuate all low frequency accelerations which tend to drive the motion platform to the

physical limits and it keeps the high frequency accelerations unchanged [Gutridge, 2004]. By high passing the longitudinal, lateral and vertical accelerations, the driving simulator will not reach its dynamical limitations. The returning of the platform to its neutral position is referred to as washout, in literature. Low pass filters are applied during tilt coordination, to attenuate high frequency accelerations and keep the low frequency accelerations unchanged. The algorithms studied in this work follow the same strategy; however the specific transfer functions are developed based on the studied EFDS, as a contribution to this research.

Two kinds of classical MCA were developed for the 3 DOF EFDS. The first motion cueing strategy implemented in this work is presented in Fig. 3.58. As it can be observed in the figure, the roll and pitch rate are scaled with respect to the available workspace and then high pass filtered, integrated and added to the resulting tilted angles in order to obtain the pitch, respectively roll angle. The vertical acceleration is high pass filtered; a rate limitation is applied, obtaining the vertical displacement of the platform.

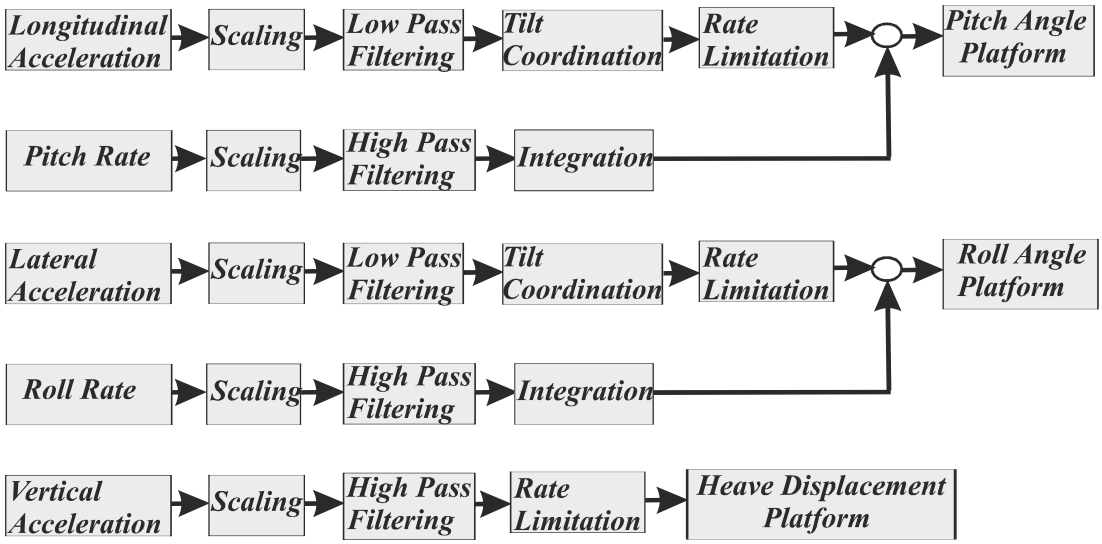

Figure 3.58: The first classical motion cueing strategy implemented

The parameters describing these linear filters were calculated with respect to the available workspace and human motion thresholds, following the approach proposed in [Nehaoua et al., 2006]. Considering a low pass filter between the longitudinal acceleration of the simulated vehicle, $a_{x_{model}}$ and the filtered acceleration, $a_{x_{LF}}$ [Nehaoua et al., 2006]:

$$\frac{a_{x_{LF}}}{a_{x_{model}}} = \frac{k_f}{s^2 + 2\zeta_f \omega_{n_f} s + \omega_{n_f}^2} \tag{3.79}$$

The constraint equations applied in order to calculate the damping coefficient, ζ_f the natural pulsation, ω_{nf} and the scaling factor k_f are [Nehaoua et al., 2006]:

$$\begin{aligned} k_f \xi_f \omega_{n_f} &< W_{max} \\ k_f \xi_f^2 \omega_{n_f}^2 &< v_t \\ k_f \xi_f^3 \omega_{n_f}^3 &< a_t \end{aligned} \tag{3.80}$$

Where W_{max} states for the maximum workspace of the EFDS, v_t and a_t stand for the human perception thresholds and ξ_f is calculated with respect to the damping coefficient of the filter, as proposed in [Nehaoua et al., 2006]:

$$\xi_f = exp\left[\frac{\zeta_f}{\sqrt{\zeta_f^2 - 1}} ln\left(\zeta_f - \sqrt{\zeta_f^2 - 1}\right)\right] \tag{3.81}$$

The MCA are designed with respect to the human perception and human's expectations of motion cues to be provided. Rendering only the angles of the simulated vehicle to the motion platform is not enough, due to the motion perception definition. The body feels the accelerations and judges the motion.

Defining r as the visually simulated horizontal acceleration and the platform tilt angles for the roll and pitch motion are defined as follows [Reymond et al., 2000]:

$$\alpha_{roll} = a\sin(\frac{\Gamma_{lateral}}{g}),$$
$$\alpha_{pitch} = a\sin(\frac{\Gamma_{longitudinal}}{g}). \tag{3.82}$$

As stated in [Augusto and Loureiro, 2009], using tilt angles creates a relationship between the accelerations felt in the vehicle and the rotational angles of the platform. This is possible because the vestibular system does not perceive any difference between the translational and the gravitational accelerations. However, the tilting of the platform has to be done with respect to the human motion thresholds, as it is shown here.

The velocity of the tilting cannot exceed the human motion thresholds. Otherwise, the human will perceive the rotation of the simulator. This, of course will lead to false motion cues, since the vehicle does not rotate in real life scenarios, while breaking, for example. Simulated acceleration through tilt coordination should also not exceed 0.5 g, in order to avoid the Auber Effect [Groberg et al., 1969]. In addition distortions of the subjective vertical were noted to appear when the tilt angle went past 30° [Hatada et al., 1980]. In [Luyat, 2005] the subjective vertical is described as the apparent gravitational vertical for each participant who is physically oblique in tilted posture. The considered thresholds applied here are given in Table 3.17 [Meiry, 1958].

Table 3.17: Motion thresholds used in simulations [Meiry, 1958]

Motion	**Value**	**Units**
Roll	3	$^\circ/s$
Pitch	3.6	$^\circ/s$
Heave	0.01g	m/s^2

The second strategy implemented in this work tried to couple in the pitch and roll motion, the high frequency longitudinal accelerations, respectively the high frequency lateral acceleration as shown in Fig. 3.59. A similar approach was used by Krissada and Wannasuphoprasit, for a driving simulator, but it was implemented on a scaled vehicle, so the paper does not discuss the impact of this algorithm on the driver or on the realism of the driving simulator [Krissada and Wannasuphoprasit, 2009]. However, these aspects are discussed here. The goal of designing and implementing such a MCA is to test the influence of the high frequency acceleration on the driver's perception through experimental testing; since the impact of motion cueing on the human behaviour is still not fully understood [Colombet et al., 2008].

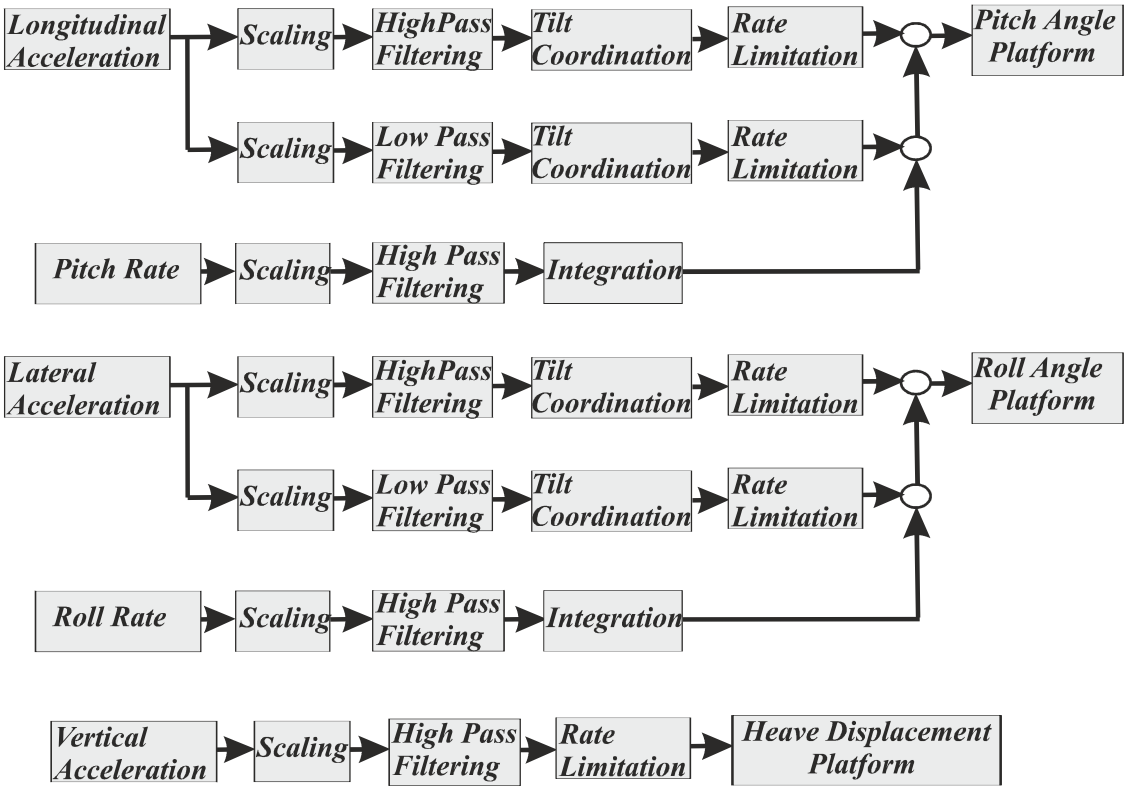

Figure 3.59: The second classical motion cueing strategy implemented

The control algorithms were developed with respect to the workspace and actuators limitations of the 3 DOF driving simulator with RPS topology, as presented in Fig. 3.60.

Figure 3.60: The 3 DOF EFDS

The design of the MCA was first made for the pitch motion as can be observed in Fig. 3.61. The inputs of this model are the longitudinal acceleration and the pitch rate (the pitch angular velocity).

These signals form together the pitch angle achievable by the motion platform. Since the pitch angle is discussed, the longitudinal acceleration is needed to give a feeling of breaking or accelerating but also introducing time delay in the system. This problem was solved by recalculating the parameters of the filters.

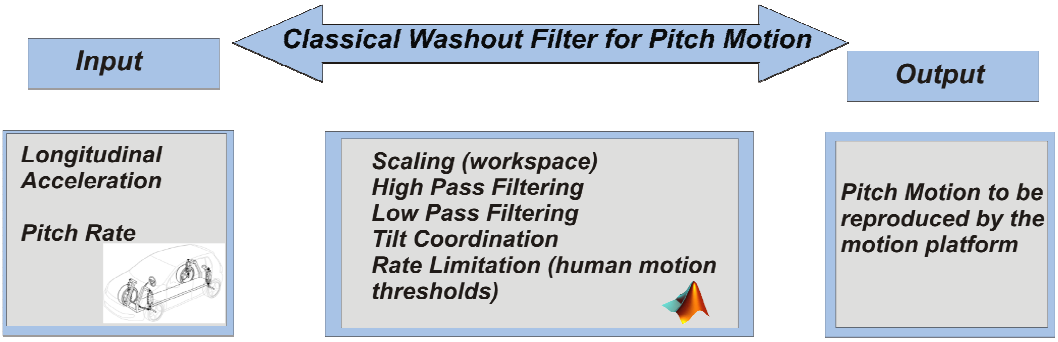

Figure 3.61: The classical motion cueing strategy for pitch motion implemented in Matlab/Simulink

Fig. 3.62 shows the output of the low pass second order filter designed for the longitudinal acceleration of the simulated vehicle, while inputting the longitudinal acceleration registered for a braking manoeuvre with the help of IPG Car Maker. It can be observed in the figure how the second order filter works by attenuating high frequency accelerations.

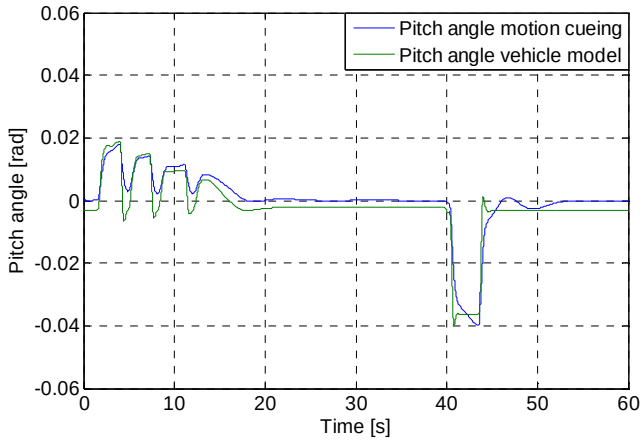

Figure 3.62: The output of the second order low pass filter (simulation results)

While designing these filters, the attention was directed also on the output signal in order to avoid introducing false motion cues. An example is given in Fig. 3.63. A high pass filter was designed for the longitudinal acceleration. Starting at time $t = 40$ s it can be observed a false cue given by the filter. The initial signal does not behave like the output signal. When introduced in the motion of the simulator, this signal will cause the platform to perform a double ride, which is not correct. This filter was redesigned in order to avoid this kind of mistakes, as it can be observed in the set of figures presenting data recorded from real time simulations (Fig. 3.67 and Fig. 3.68).

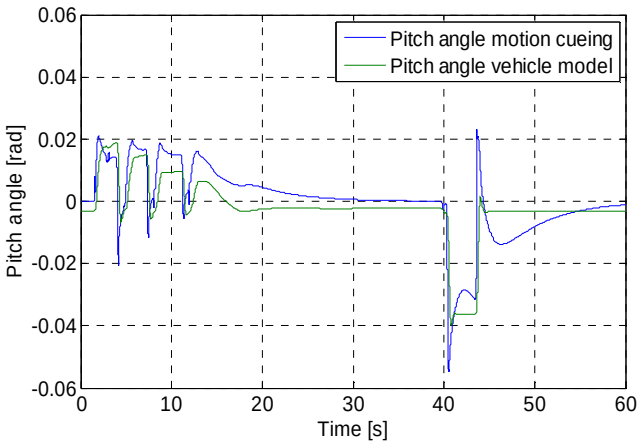

Figure 3.63: An incorrect second order high pass filtered studied

In Fig. 3.64 the step response of a stable low pass filter can be observed. A step function with amplitude 0.25 was given as input to the filter.

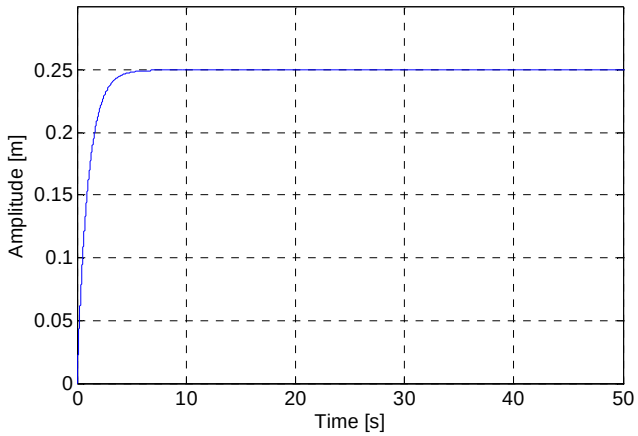

Figure 3.64: The step response of a low pass filter designed

After this analysis, the following parameters were chosen to be used in controlling the 3 DOF EFDS.

Table 3.18: The calculated parameters Laplace filters

Degree of freedom	$\mathbf{k_f}$	$\boldsymbol{\omega_{n_f}}$	ζ_f
Longitudinal acceleration	0.2	0.54	1
Roll angle	0.2	0.6	1
Pitch angle	0.2	1	1.91
Vertical acceleration	0.3	0.72	1.1
Lateral acceleration	0.25	0.63	1.5

The Bode diagrams for the low and pass filters were also created in order to obtain their frequency response. The magnitude and the phase shift diagram of a first order high pass filter, respectively a first order low pass filter designed, can be observed in Fig. 3.65, respectively in Fig. 3.66.

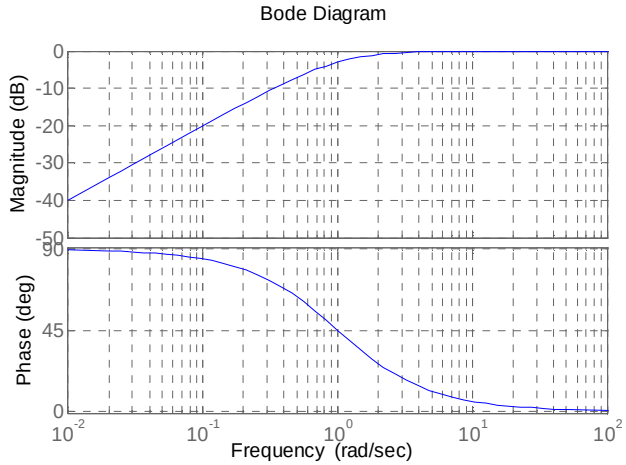

Figure 3.65: The Bode diagram of the first order high pass filter

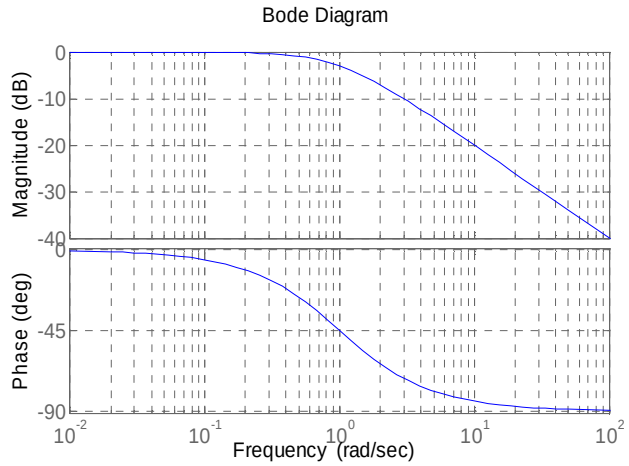

Figure 3.66: The Bode diagram of the first order low pass filter

Fig. 3.67 and 3.68 present results from simulations using the first and the second MCA considered here. It can be easily noticed the high frequency nature of the second roll angle obtained and presented in Fig. 3.67b.

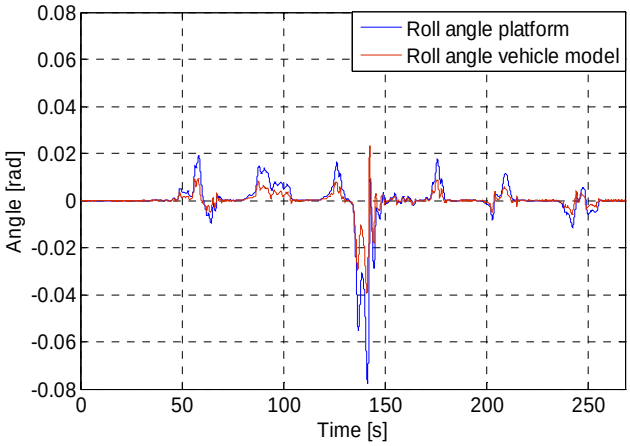

Figure 3.67a: Roll angle obtained from the first MCA (blue) and roll angle obtained from the vehicle model simulation (red)

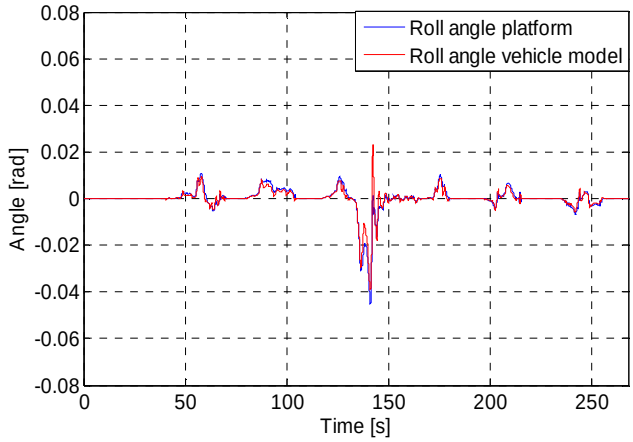

Figure 3.67b: Roll angle obtained from the second MCA (blue) and roll angle obtained from the vehicle model simulation (red)

Although the amplitude of the pitch angle is almost the same for both algorithms,for the considered manoeuvre, it is obvious in Fig. 3.68b that the pitch angle obtained in the second algorithm introduces almost no time delay in the system. Each filter used for cueing the

motion was designed with respect to the DOF, workspace of the simulator, human perception threshold and actuators limitations, as presented in [Capustiac et al., 2011b].

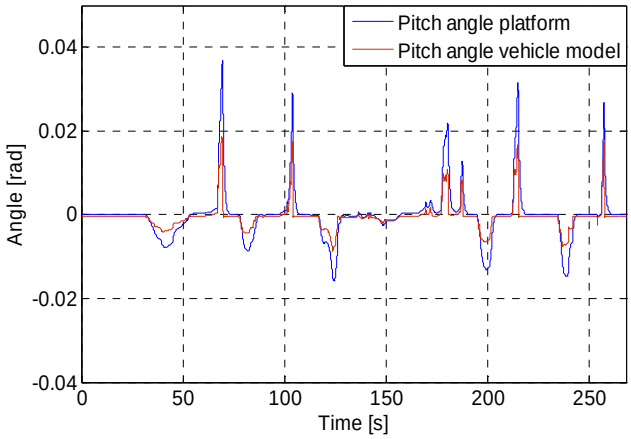

Figure 3.68a: Pitch angle obtained from the first MCA (blue) and roll angle obtained from the vehicle model simulation (red)

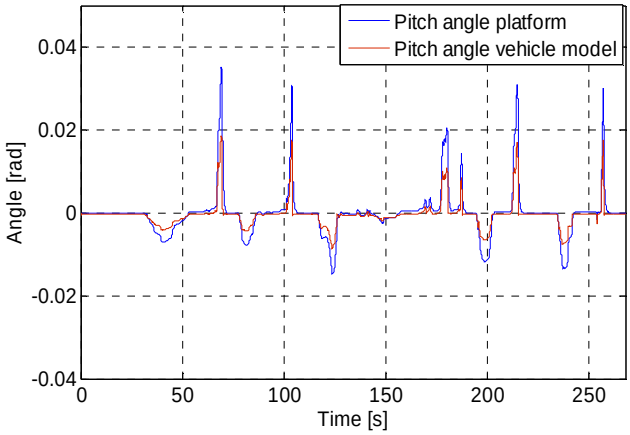

Figure 3.68b: Pitch angle obtained from the second MCA (blue) and roll angle obtained from the vehicle model simulation (green)

A number of offline tests were conducted in order to test how the motion algorithms are working with the whole driving simulator (vehicle model, pedals, steering wheel, etc.) conforming with the control strategy presented in Fig.3.69.

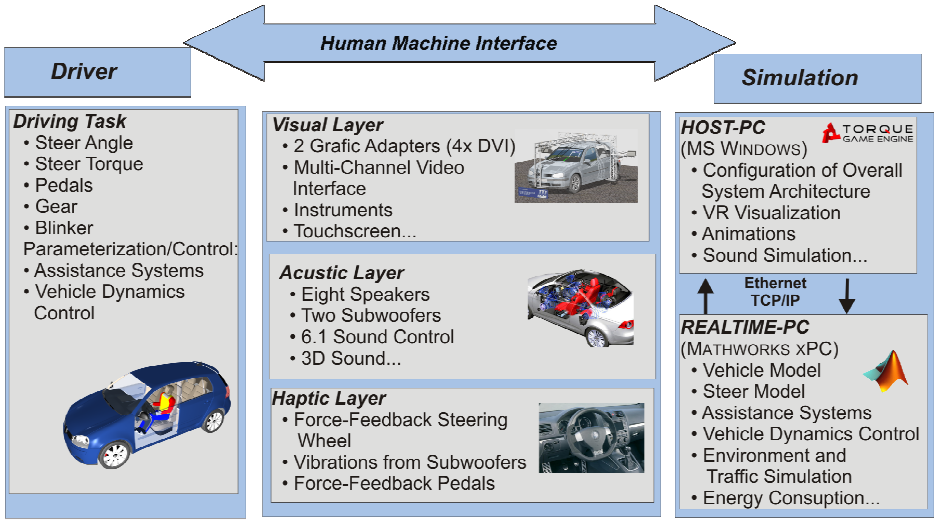

Figure 3.69a: The overall control strategy implemented – the HMI

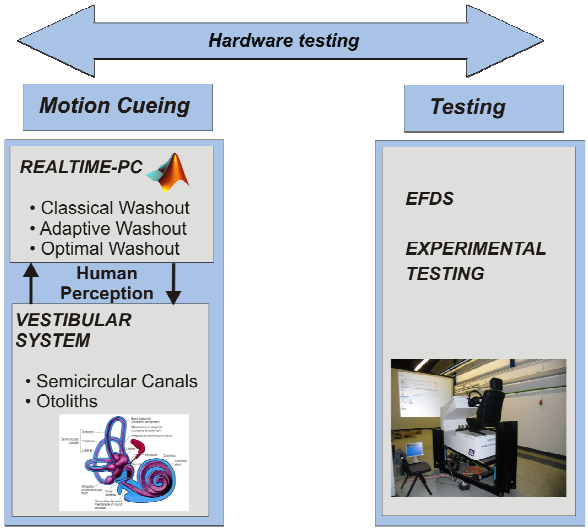

Figure 3.69b: The overall control strategy implemented – the Hardware testing

The driver interacts with the simulator with steering wheel and pedals. This data is transmitted in real time to the vehicle models implemented in Matlab/Simulink. The accelerations and velocities calculated by these models are used as inputs for the MCA. With the help of the inverse kinematics of the motion platform, the strokes of the actuators are obtained.

After being processed, the information is sent to the actuators, via UDP communication. The data was saved with special blocks provided by xPC Target, the Mathworks real time module. Details about the implementation of the models on the hardware are given in the Appendix A; the communication between the hardware, the simulation PC and the real time PC is discussed.

A number of tests were conducted in order to investigate the EFDS's behaviour and to analyse the correctness of the outputted signals. A city simulated scenario was drove and the first MCA was used. The following figures present results from these tests. The translational accelerations can be observed in Fig. 3.70 and 3.71. These accelerations are used further in the MCA in order to obtain the motion of the EFDs, presented in Fig. 3.74 and Fig. 3.75.

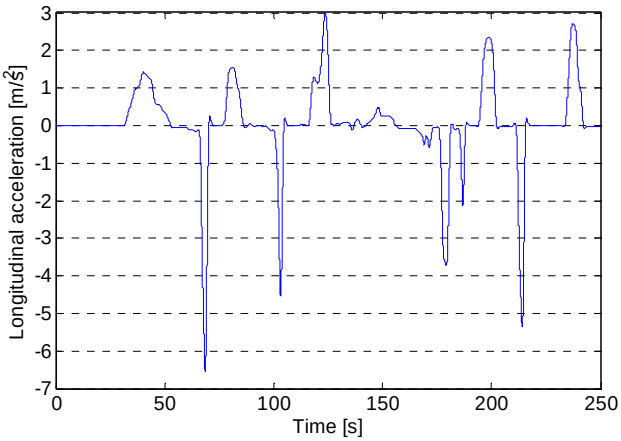

Figure 3.70: The longitudinal acceleration obtained from the 14 DOF vehicle model

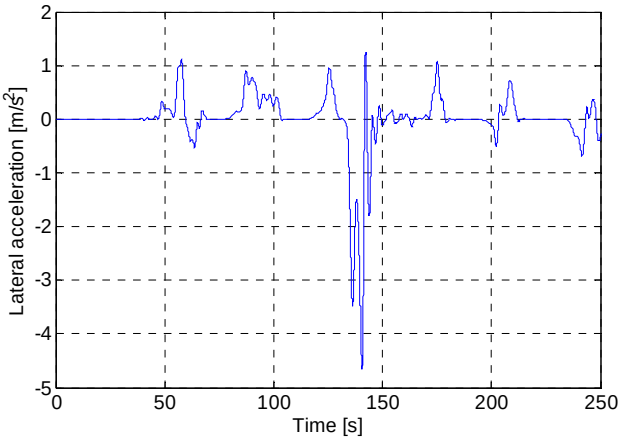

Figure 3.71: The lateral acceleration obtained from the 14 DOF vehicle model

Fig. 3.72 and 3.73 present the roll respectively pitch angular velocity of the vehicle's CG. The velocity of the simulated vehicle are further scaled and filtered in order to obtain the cued and achievable motion by the mobile platform.

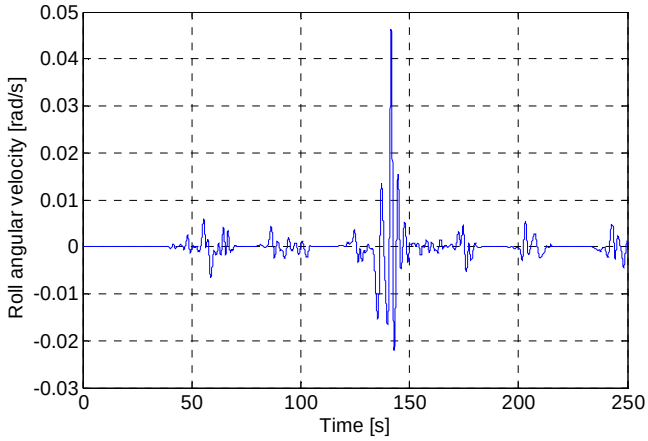

Figure 3.72: The roll angular velocity obtained from the 14 DOF vehicle model

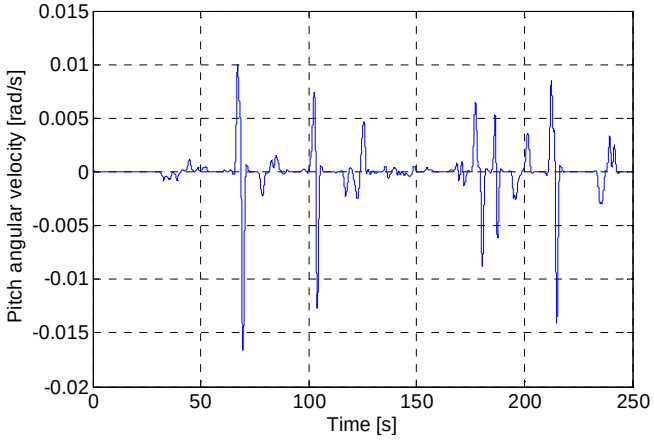

Figure 3.73: The pitch angular velocity obtained from the 14 DOF vehicle model

Fig. 3.74 and 3.75 present the output of the first MCA, the motion of the mobile platform. It can be observed how the EFDS behaves, while trying to reproduce and cue the motion received from the vehicle model.

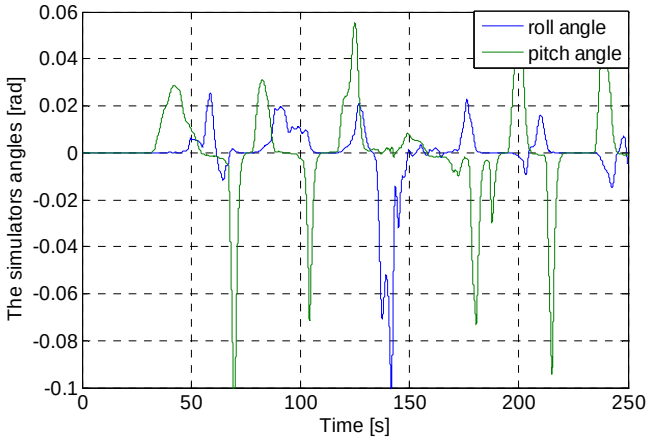

Figure 3.74: The platform's roll and pitch angle obtained from the MCA

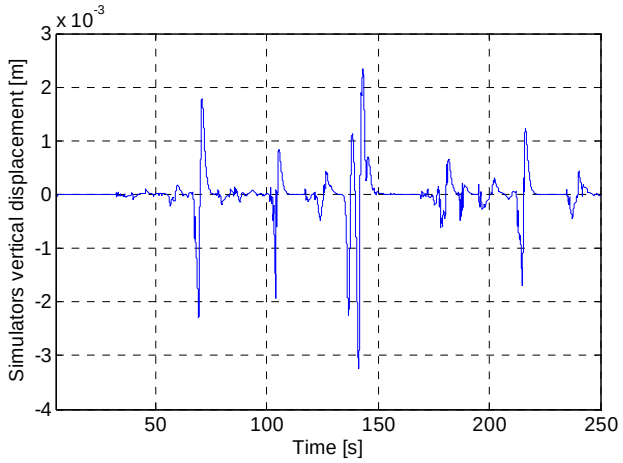

Figure 3.75: The platform's vertical displacement obtained from the MCA

The inverse kinematics implemented and discussed in the previous subchapter is calculating the displacements of the 3 actuators, as presented in Fig. 3.76.

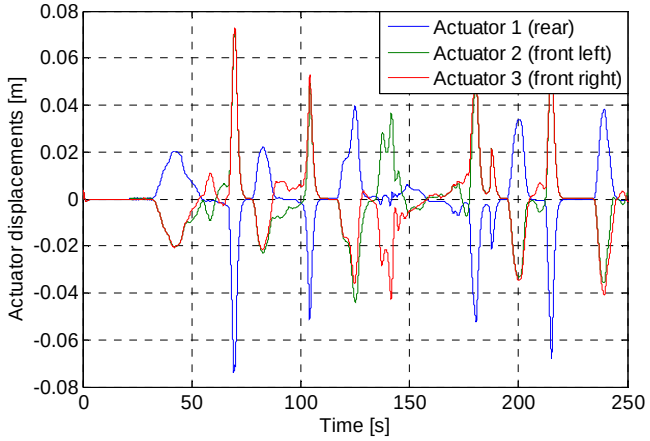

Figure 3.76: The actuators strokes obtained from the inverse kinematics

3.3.3 Discretization of the Motion Cueing Filters

The control in real-time is achieved by using xPC Target. This module developed by MathWorks provides a library of I/O device drivers, a real-time kernel, and an interface for real-time monitoring, parameter tuning, and data logging [MAT, 2011]. This module can only load discrete systems. After calculating all the parameters for the motion cueing filters, the Laplace transfer functions were discretized, with the function 'c2d' (continuous to discrete) provided by Matlab. The method used was the bilinear approximation. The z transformation is actually finding a pole/zero representation in the z plane for a discrete-time system. This method is based on integral approximation where the frequency response of the inputted original continuous system is the same with the frequency response of the obtained discrete system [Capustiac et al., 2011b]. The second order high pass longitudinal acceleration filter:

$$\frac{a_{xhf}}{a_x} = \frac{0.999z^2 - 1.998z + 0.999}{z^2 - 1.998z + 0.998} \quad (3.83)$$

The first order low pass longitudinal acceleration filter:

$$\frac{a_{xlf}}{a_x} = \frac{0.0007138z + 0.0007138}{z - 0.9986} \quad (3.84)$$

The first order high pass pitch rate filter:

$$\frac{p_h}{p} = \frac{0.9967z + 0.9967}{z - 0.9934} \quad (3.85)$$

The second order high pass longitudinal acceleration filter:

$$\frac{a_{yhf}}{a_y} = \frac{0.999z^2 - 1.998z + 0.999}{z^2 - 1.998z + 0.998} \quad (3.86)$$

The first order low pass longitudinal acceleration filter:

$$\frac{a_{ylf}}{a_y} = \frac{9.999e-005z + 9.999e-005}{z - 0.9998} \quad (3.87)$$

The second order high pass roll rate filter:

$$\frac{r_h}{r} = \frac{0.999z^2 - 1.998z + 0.999}{z - 0.9998} \quad (3.88)$$

The second order high pass vertical acceleration filter:

$$\frac{a_z}{a_{zhf}} = \frac{(0.9967z - 0.9967)(0.0007138z - 0.0007138)}{(z - 0.9934)(z - 0.9986)} \quad (3.89)$$

This subchapter presented the development of the MCA for the EFDS. Since these algorithms are one of the most important components of the simulator, the design was achieved with respect to the design and cost constraints and the human motion perception mechanism. Two kinds of algorithms were designed, in order to investigate whether using high frequency accelerations have any influence on the driver. To the best knowledge of the author, this particular aspect is not clearly stated in the literature though. In order to implement the algorithms in real time, the filters were transformed into 'z' domain.

4 Experimental Results

This chapter presents and discusses results from the experimental testing concerning the concepts studied in this doctoral work, the actuation of a mock-up driving simulator and the actuation of a vehicle.

As already presented in the previous chapter, the actuation of the entire vehicle is to be made with four hydraulic actuators. It was investigated whether the actuators can reproduce the amplitudes needed by simulating different road profiles. The frequency response of these systems was studied and it was found that above frequencies of 1 Hz, the response of the actuators is deteriorating. The phase angle decreases dramatically at this frequency as well, leading to a larger phase shift between the output and input signal. This introduces unacceptable time delays in the driving simulator. The results are discussed in detail below.

The MCA described in Chapter 3 were implemented on the hardware in order to perform real time simulation. The actuators used in the mock-up driving simulator concept are developed by SEW Company [SEW, 2011].

Once the real-time communication between the Matlab/Simulink models and the actuators was enabled, the tests that represent the purpose of this research were run. Consequently, six total days of experimental testing with participants were conducted. Since it is difficult to find extensive work dealing with the limitations of driving simulators, the conducted experiments are trying to explain some open problems found in the specialized literature: what level of reality can a driving simulator reach? What are the limitations of a driving simulator from both the physical point of view and the related human motion perception? The limitations of the driving simulator can refer to reduced workspace and DOF, but also to the poor OF, to the limited FOV, or to incorrect MCA. It was assumed in this research that these characteristics can be evaluated by human drivers.

Twenty-six participants took part in the first study, where the goal was to investigate the realism validity of the simulation from the point of view of the human perception. The obtained results will be discussed here. The second study involved again twenty-six participants and it focused on the determination of the influence of different parameters on the overall subjective degree of realism rated by the participants. The design of the experiments was made applying an optimization method in order to save time and cost.

Three parameters of the simulation were studied in detail:

- Motion;
- OF;
- Vibration in the steering wheel or the haptic response in the steering wheel as is being referred to in this chapter.

The testing methodology and the interpretations of the results are given here. The data registered during the experimental testing was used for estimation purposes for different transfer functions. These mathematical tools should be able to characterise the behaviour of the 3 DOF EFDS. Thus, any researcher should be able to refer to the capabilities and limitations of the system, both from a dynamical aspect and from the point of view of human perception. This is further possible through the transfer functions, which are discussed in Chapter 5.

4.1. Hydraulic Stand Experimental Results

The actuation of the vehicle driving simulator is to be made with 4 hydraulic cylinders developed by Integral Hydraulik [InH, 2011]. Understanding their behaviour was crucial before building the setup. For this purpose, a hydraulic stand was built with one of the 4 ZXH63/28-250 type cylinders. The hydraulic actuator has two chambers, separated by a piston. Hence, there are two different piston areas and two piston velocities, given in Table 4.1. For piston positioning, a position sensor is used. The control is made through a servo valve of the HVM057 OB-040-1200 type. The technical data of these actuators has already been given in Table 3.10.

Table 4.1: Hydraulic cylinder characteristics [InH, 2011]

Cylinder	**Piston Area**	**Piston Velocity**
$A_{cyl,1}$	$3.12 \cdot 10^{-3} m^2$	$0.21 m/s$
$A_{cyl,2}$	$2.5 \cdot 10^{-3} m^2$	$0.26 m/s$

The experimental testing was conducted according to Fig. 4.1. The mathematical model of the hydraulic cylinder, described by equations (3.35) – (3.51) together with the PI controller was run on the simulation PC, where Matlab/Simulink is installed. In order to control the hydraulic piston in real-time, the xPC Mathworks Module was used. xPC Target enables the user to execute Simulink models on a target computer (real time computer in Fig. 4.1) for different real time applications.

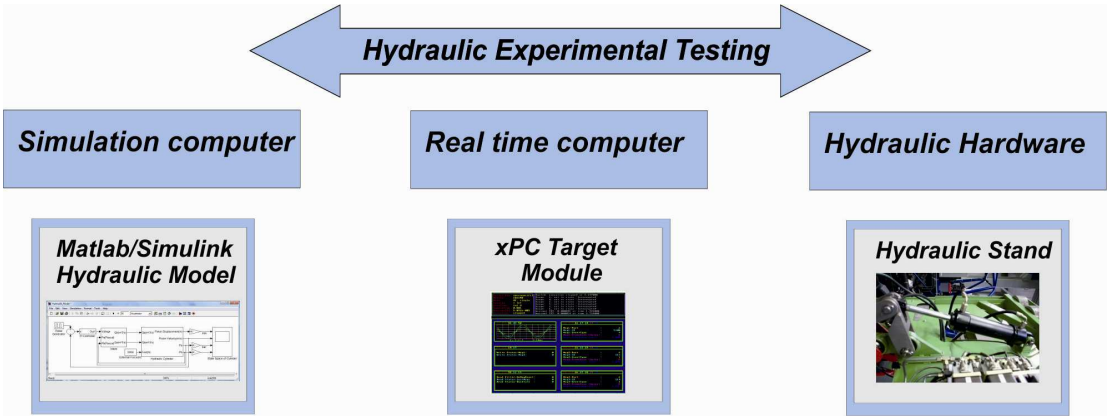

Figure 4.1: The components of the real-time testing experiment

The road profiles modelled and presented in Chapter 3.1.3 were tested on the hydraulic actuators. These road profiles were simulated with respect to the road condition (ISO classification) and the vehicle's velocity. The middle position for the actuator's stroke was set to be of 0.1 m and different categories of roads were tested as it can be observed in Table 4.2.

It was assumed in this research that the following road categories are representative for studying the response given by the considered actuator. The velocity of the vehicle was assumed to be constant and the considered values can be observed in the following table. Table 4.2 also shows the maximum tyre-road contact forces for different road categories and vehicle velocities. These values were calculated from the vehicle comfort dynamic model presented in Chapter 3.1.3 and described by equations (3.58) – (3.61). It was assumed that for studying the behaviour of the hydraulic cylinders the following simulated road categories are representative.

Table 4.2: Road categories tested on the hydraulic hardware

Road category [ISO8608]	**Maximal tyre - road contact forces kN**	**Vehicle velocity m/s**
A (very good)	3.9	10
C (average)	4.25	10
D (poor)	5.9	10
E (very poor)	6.2	10
A (very good)	4.6	30
B (good)	5.5	30
C (average)	8	30
A (very good)	4.8	50
B (good)	5.7	50

The next set of figures shows results from the experimental testing conducted based on the scheme proposed in Fig. 4.1. Since the velocity of the vehicle together with the road irregularities were assumed to be constant during this experimental testing, the following figures show the stationary response of the system.

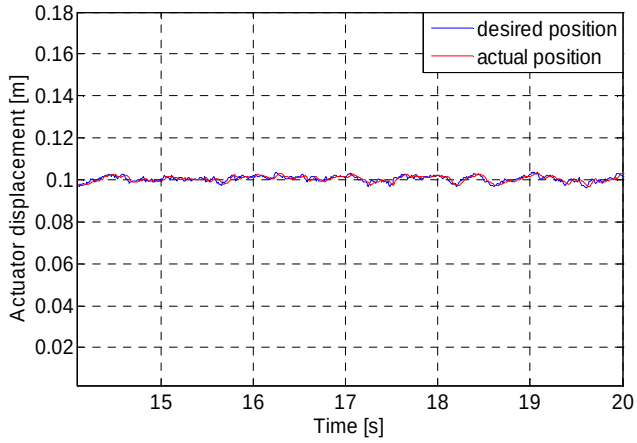

Figure 4.2a: Actuator displacements (red) versus the desired road roughness (blue) for road category A, 10 m/s velocity

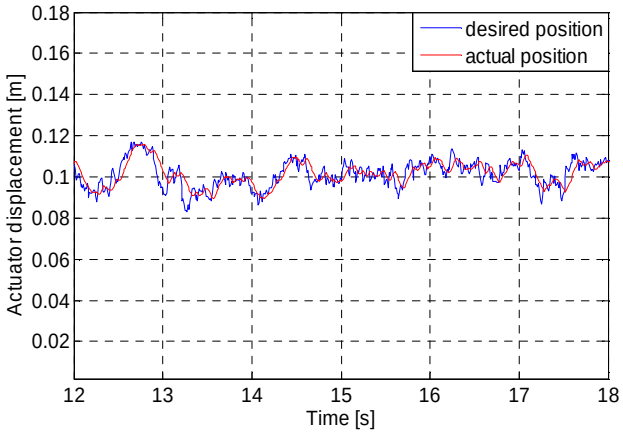

Figure 4.2b: Actuator displacements (red) versus the desired road roughness (blue) for road category C, 10 m/s velocity

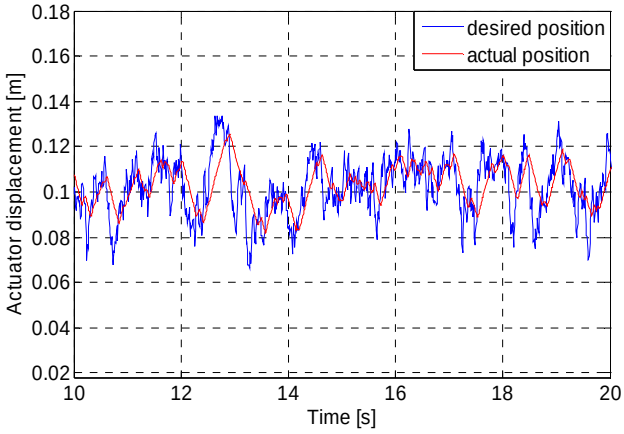

Figure 4.2c: Actuator displacements (red) versus the desired road roughness (blue) for road category D, 10 m/s velocity

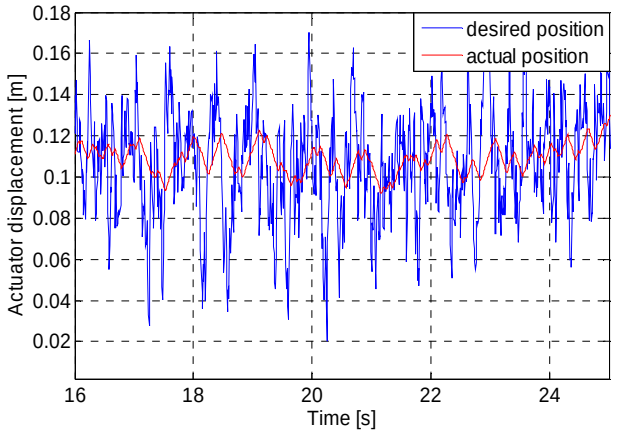

Figure 4.2d: Actuator displacements (red) versus the desired road roughness (blue) for road category E, 10 m/s velocity

Fig. 4.2 shows the desired position of the hydraulic piston (blue), and of the actual position (red), while introducing the road roughness corresponding to four road categories (very good, average, poor and very poor, according to ISO 8608) with constant velocity of 10 m/s. It can be clearly observed in the figures that the time delay of the actual position increases when the velocity of the vehicle increases too. Next, random road irregularities for three road categories (very good, good and average according to ISO 8608) were given as desired position for the hydraulic model and are presented in the following set of figures. It was assumed the vehicle is driving with a velocity of 30 m/s.

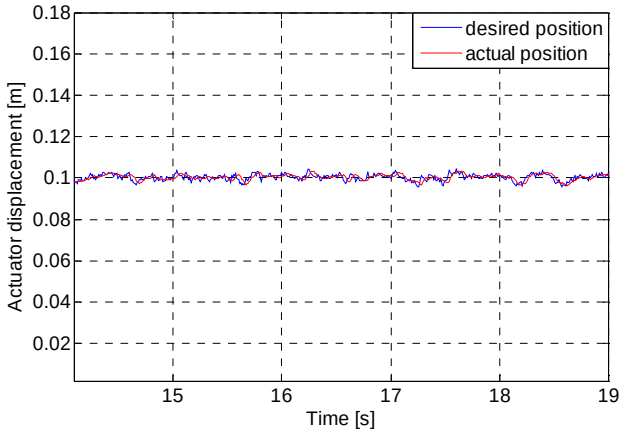

Figure 4.3a: Actuator displacements (red) versus the desired road roughness (blue) for road category A, 30 m/s velocity

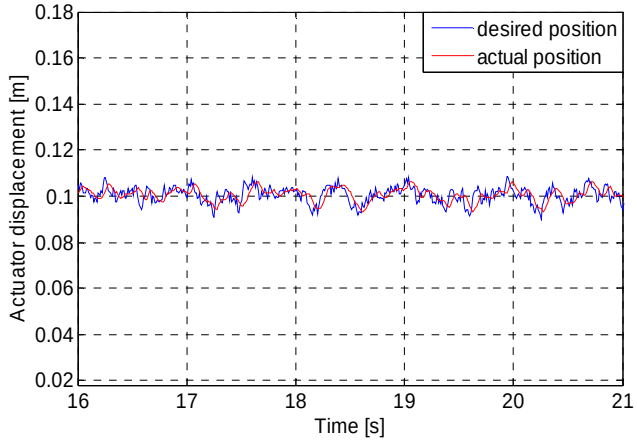

Figure 4.3b: Actuator displacements (red) versus the desired road roughness (blue) for road category B, 30 m/s velocity

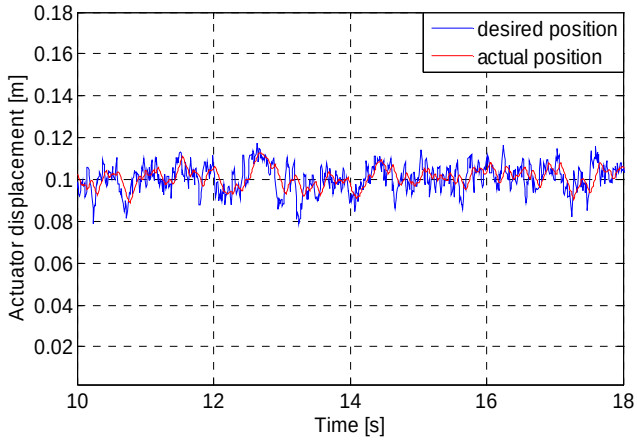

Figure 4.3c: Actuator displacements (red) versus the desired road roughness (blue) for road category C, 30 m/s velocity

The vehicle velocities considered are the same: 10 m/s (Fig. 4.2), 30 m/s (Fig. 4.3) and 50 m/s (Fig. 4.4). Once the amplitudes of the inputted signal are increasing, the time delay increases. It can also be observed that the amplitude response is deteriorating when the frequency and velocity of the vehicle is increasing too.

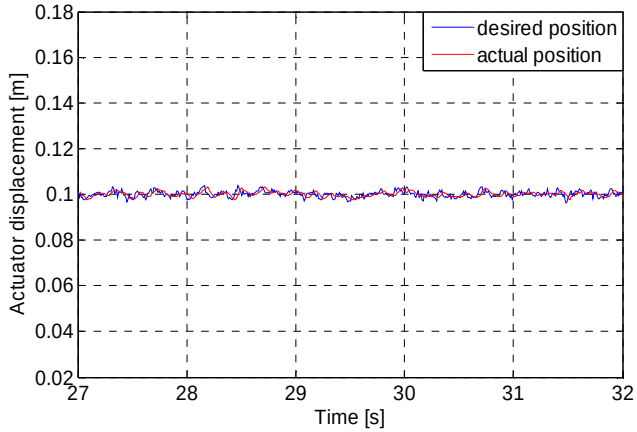

Figure 4.4a: Actuator displacements (red) versus the desired road roughness (blue) for road category A, 50 m/s velocity

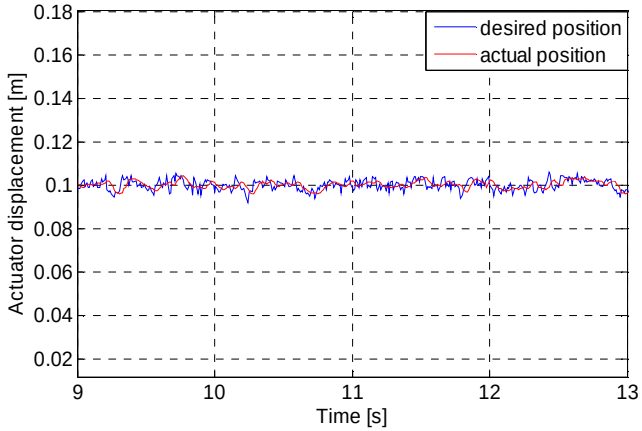

Figure 4.4b: Actuator displacements (red) versus the desired road roughness (blue) for road category B, 50 m/s velocity

It can be easily observed that regardless of the different velocities, 10 m/s (Fig. 4.2), 30 m/s (Fig. 4.3) and 50 m/s (Fig. 4.4) the actuator's piston cannot follow the input signal. The registered time delay approaches 1 s and the amplitudes cannot even follow 50% of the desired stroke, as already discussed in the bachelor thesis [Reiff, 2011].

The response of the actuators is deteriorating starting with the frequency of 1 Hz. The frequency range of the vehicle was already discussed in Chapter 3, and it was proven to dominate in the range 0.7-15 Hz. The Bode diagram of this system was drawn and presented in Fig. 4.5.

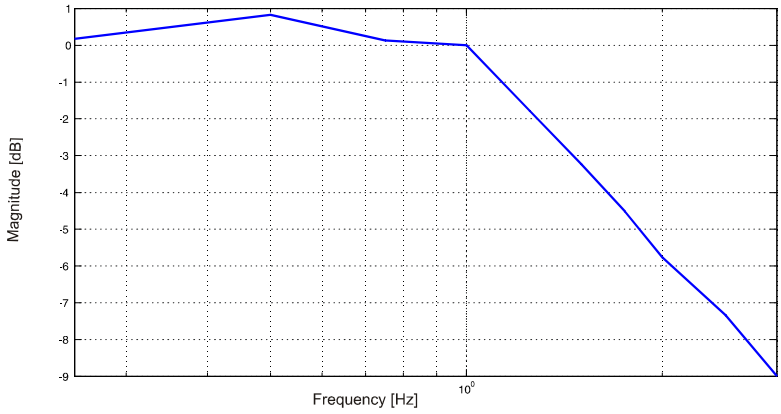

Figure 4.5a: Bode diagram: amplitude response [Reiff, 2011]

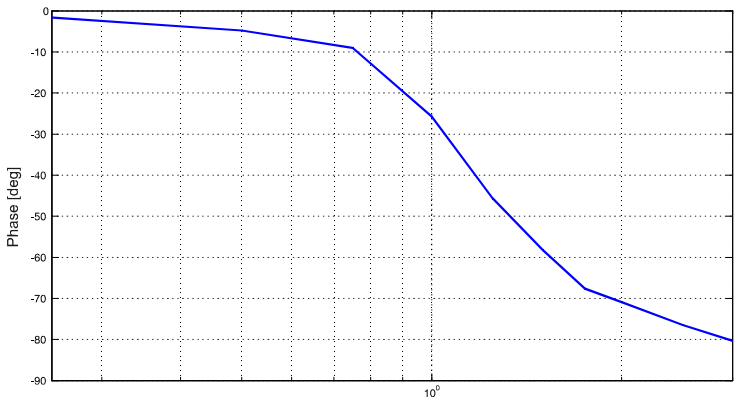

Figure 4.5b: Bode diagram: phase response [Reiff, 2011]

It can be observed on the Bode diagram that the phase angle also decreases dramatically at this frequency, leading to a larger phase shift between the output and input signal. It can be concluded that the output lags the input signal more and more, as discussed in [Reiff, 2011].

Reproducing the road excitation in a driving simulator is not a crucial problem, but reproducing a manoeuvre leads to false and incorrect motion cues provided to the driver. It was concluded that the actuators cannot be used for this application.

4.2. Experimental Testing with Participants

There were two sets of experimental testing with participants conducted, as a cooperation between the Technical University of Cluj-Napoca, the University of Duisburg-Essen and the University of Applied Sciences Gelsenkirchen, Department Bocholt. The main goals of this testing was to evaluate different control algorithms, to study the system limitations, and to determine the subjective degree of realism of the simulation environment.

Two sets of each three days of testing were conducted in Bocholt, where the 3 DOF EFDS was placed. During simulations the following data was registered: the simulated vehicle's positions, velocities and accelerations, the steering wheel's angle, the pedals positions and the actuators displacements and velocities. The required statistical data was obtained through questionnaires.

The questionnaires were originally written in German and can be found in the Appendix section of this doctoral thesis. For all the asked questions, the grading scale was used to rank the authenticity of motion, visual, haptical cues, the immersion of the driver in the simulation environment, etc. The scale was taken from 0 to 100%, where 100% represents the feeling experienced while driving in a real car. It was assumed that the calculated mean values over 50% represent satisfactory results.

4.2.1 The determination of the overall subjective involvement degree in the simulated environment

The goal of this first experiment was to study these limitations of the EFDS and find what is important to simulate in a driving simulator.

Figure 4.6: The experimental set-up used for the testing

Twenty six participants took part in this study, 22 of them men and 4 women. The experiments were conducted at three different days, in Bocholt. The drivers involved in the experiments were mostly students. They were aged between 21 and 46 years. The average age was 23.5 years. All participants had a driving license. The average driving – year experience was of 6 years. Having a driving licence was a precondition in participating in this study. Twelve drivers involved in the study had already interacted with a driving simulator, before the study took place.

Conducting the experiments

A three-day set of experimental testing was conducted between 13.04.2011 and 15.04.2011. The goal was to establish the overall subjective degree of realism of the simulation. Each participant proceeded with the experimental testing individually. A total time of 45 minutes was allocated to each of them. The goal of the testing was explained beforehand to each and every participant, and then they were asked to occupy the driver's seat. They were asked to handle the simulator as they would their own vehicle and to drive according to the road traffic regulations.

Each driver involved in the experiment was asked to drive first a 4-5 minute drive in order to get adjusted to the simulation environment. The participants were asked whether they could get acquainted with the simulator and once they were comfortable with the simulated environment, the actual experiment started. They were asked to drive three times an ISO lane change manoeuvre and a city scenario for each of the MCA. Every time the scenario needed to be changed or reloaded, the driver had to wait in the seat for maximum 20s. After completing the driving tasks, each of them answered 17 questions in order to obtain the needed statistical information.

Figure 4.7: Simulated scenario used in the experimental testing

Driving Simulator Experiment Questionnaire

The questionnaire was designed to have three main parts: the general questions (age, gender, driving experience, etc.), the realism and interaction questions, and the MCA evaluation questions.

The total number of 17 questions were discussed and certified by a member with psychological doctoral studies background from the Mechatronics Department at the University of Duisburg-Essen. The main part of the questionnaires concerned with the realism of the virtual environment and with the human simulator interaction and are presented in Table 4.3.

Table 4.3: Questionnaire Explanation

Question Number	Question
1	How would you grade the response of the simulated environment to your performed actions?
2	How would you grade your involvement in the simulated environment?
3	How fast was your adjustment to the simulation environment?
4	How easy was for you to perform the required tasks?
5	Did you experience simulation sickness in the driving simulator?
6	Did any aspect of the simulation distract you from performing the driving task?
7	How real (natural) seemed the haptic response to you?
8	How natural was the feeling while steering?
9	How natural was the feeling while using the gas and brake pedals?
10	How consistent was the experience in the simulated environment with that in the real world?

Experimental Testing Results

The statistical data was analysed with the help of Excel and Sigmaplot. None of the participants experienced simulation sickness. This represents a good result, since the appearance of such symptoms could be interpreted as an effect of introducing false motion or visual cues in the driving simulator. Simulation sickness can negatively interfere with the validity of the results obtained in experimental testing. As discussed in [Mollenhauer, 2004], these symptoms can be very unpleasant for the drivers.

When asked to rate the response of the simulator for their own performed actions, the mean value obtained from the questionnaires was of 60.8%. 50% percent of the drivers involved in the testing, rated the authenticity of the motion with 60%; 30% of the participants rated the motion with 70% and the rest rated the motion reproduced in the driving simulator with 80% or more, as it can be observed in the following diagram.

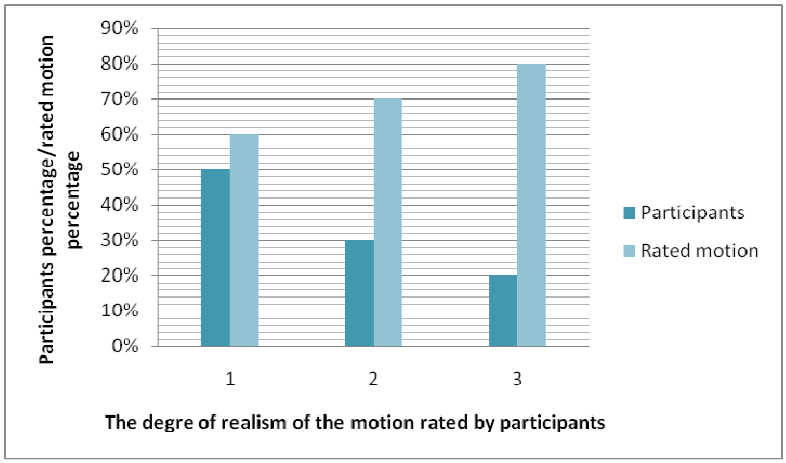

Figure 4.8: The EFDS motion rated by the drivers

The participants ranked the motion obtained while using the first algorithm with 68.84% and while using the second algorithm, with 64.2%.

Since from a statistical point of view this data does not represent a significant difference, it was decided to evaluate the MCA once more.

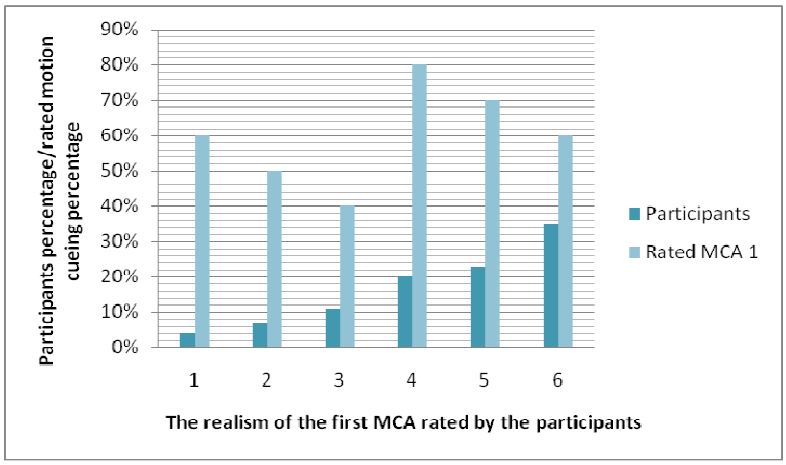

Figure 4.9: Participants rating the first MCA

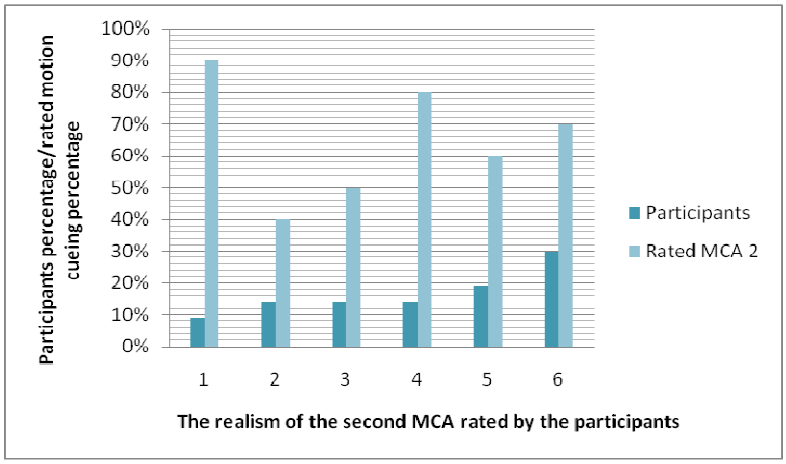

Figure 4.10: Participants rating the second MCA

When asked to rate their own involvement in the simulated environment, the mean value obtained from the data analyses was of 62.3 %. None of the participants stated that aspects of the simulation distracted them to perform the required actions. However, three of the drivers stated that they were bothered by a jerk in the graphic provided by the simulation.

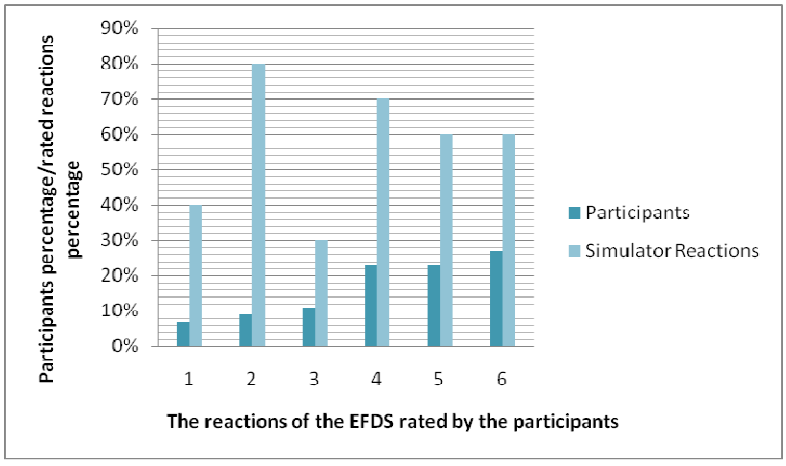

Figure 4.11: Participants rating the reactions of the driving simulator

85% of the participants rated their adjustment to the simulated environment as fast or very fast, and 15% stated that the adjustment was slow. The statistical data, between the participants who had driven a simulator before and the participants who had not experience a

simulator driving until then, was also analysed. 42 % of the drivers involved in the experiments, which had driven such a system before, rated their adjustment to the simulation environment as very fast, the same amount of participants rated their adjustment as fast, and 16 % of them rated their adjustment as slow. Only 28% of the drivers who experienced simulator driving for the first time rated their adjustment as very fast, 58% rated it as fast, and 14% as slow.

When asked about how easy was it to perform the driving tasks, 62% of the participants stated that it was easy for them to perform them. When analysing the grading of the drivers who had already driven such a machine and of the ones who did not, the results were very similar. 33% of those familiar with the simulation environment stated it was very easy for them to perform the tasks, 59% stated it was easy and 8% stated it was difficult to perform all the needed tasks. When asking the drivers who had not experienced this kind of driving before, 28% said it was very easy for them, 58% stated it was easy and 14% stated it was difficult to drive in such an environment. The only three participants who stated it was difficult to perform the driving tasks were women participants. However, the number of female participants is too small to generalize these results.

The realism of the steering wheel usage was rated with 59.2% by the participants.

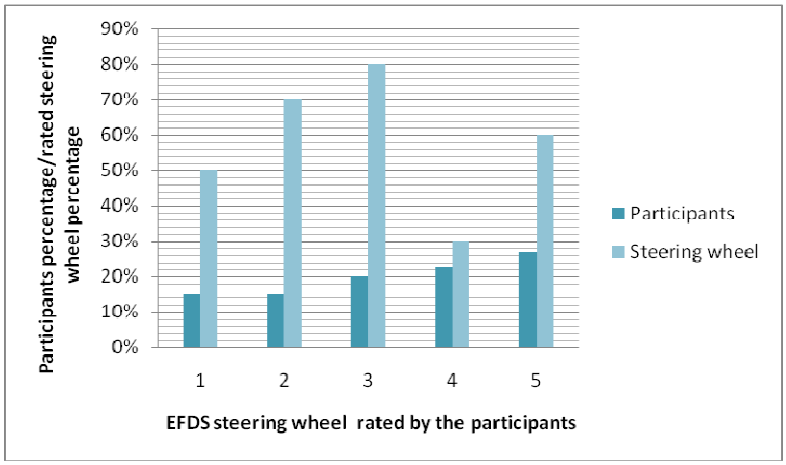

Figure 4.12: The participants rating the steering wheel feedback in the driving simulator

When asked to rate the immersions of their senses in the overall simulation, the mean value obtain was 62 % compared with a real life situation.

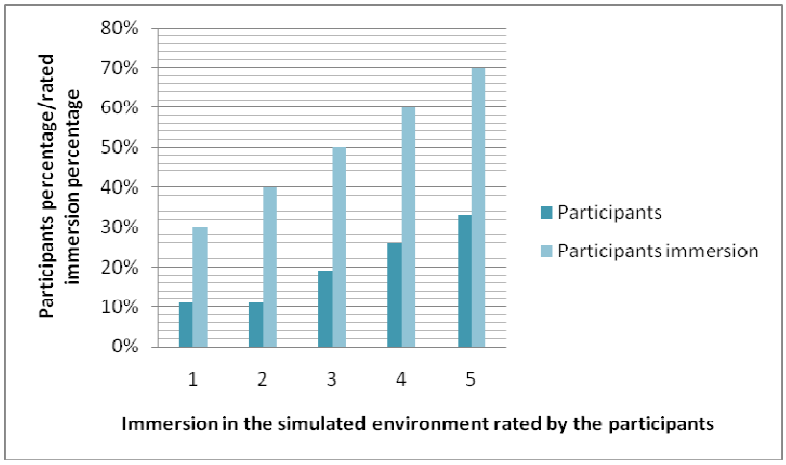

Figure 4.13: The participants rated immersion in the simulation

The feeling while breaking the simulator received the lowest rate with 45.3%.

While performing a 100% breaking manoeuvre, vibrations appeared in the simulator, reducing the degree of authenticity of the motion. After completing the tests, the source of the vibrations was investigated. The models were verified. The first solution was to remove all the assistance systems integrated in the overall model. Although the antilock braking system (ABS) was the first suspected source of these vibrations, it was shown the models in simulations behaved normally. The accelerations, velocities and positions of the vehicle while the participants drove the simulator were saved and then investigated to see if some indications could be found. The forward acceleration contained a very strong noise. The gas and brake pedals were suspected to introduce this noise in the system because of the data measured by the sensors.

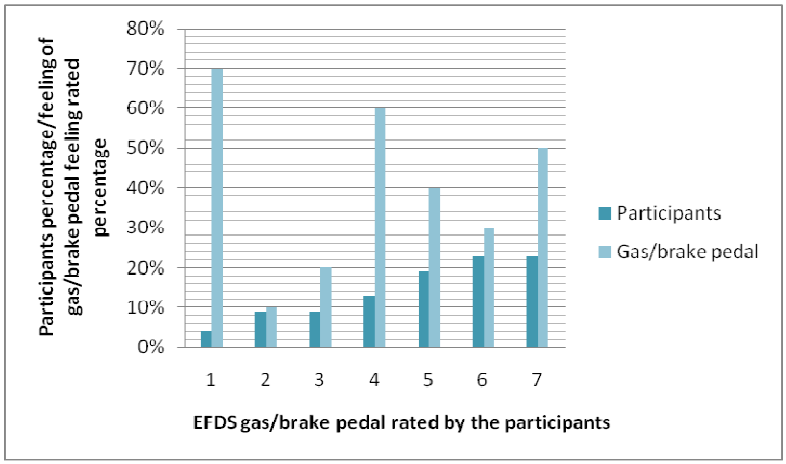

Figure 4.14: Participants rating the driving simulator gas/brake pedals reactions

A new set of tests was developed, and it was shown that this noise was introduced in the system by these sensors. These data were further transmitted to the vehicle model and then to the MCA. Although these algorithms contain filters, the noise was too strong to be completely removed. The solution was to recalculate the sample time of the system. The initial sample time used was of 1 ms, which was appropriate for the models designed in Matlab, but not for the Logitech pedals. The new sample time used for data acquisition was of 20 ms. When driving both of the motion algorithms with this new sample time, the vibrations were ceased, and the feeling of using the braking pedal became more realistic. Hence, it is recommended to use a real breaking system when designing a driving simulator. The following figures present data recorded during the experimental testing. While driving on the city simulated scenario, the data recorded on the third day of experimental testing for the fifth driver is presented below. Fig. 4.15 presents the velocity of the simulated vehicle driven through the driving simulator.

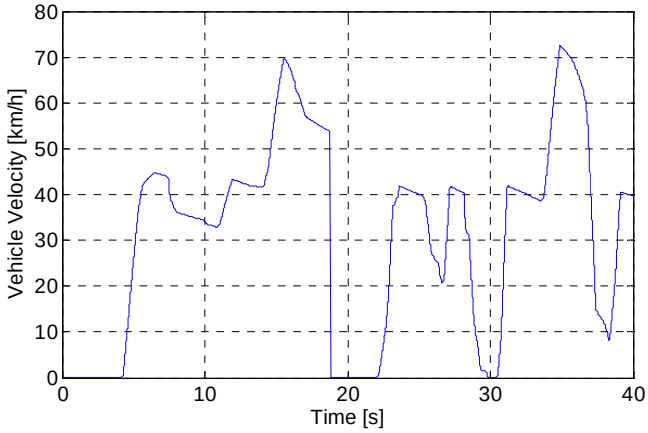

Figure 4.15: The velocity of the vehicle driven in the experimental testing

Fig. 4.16 shows the longitudinal, respectively, the lateral acceleration of the simulated vehicle, while driving in a simulated scenario with the velocity given in Fig. 4.15.

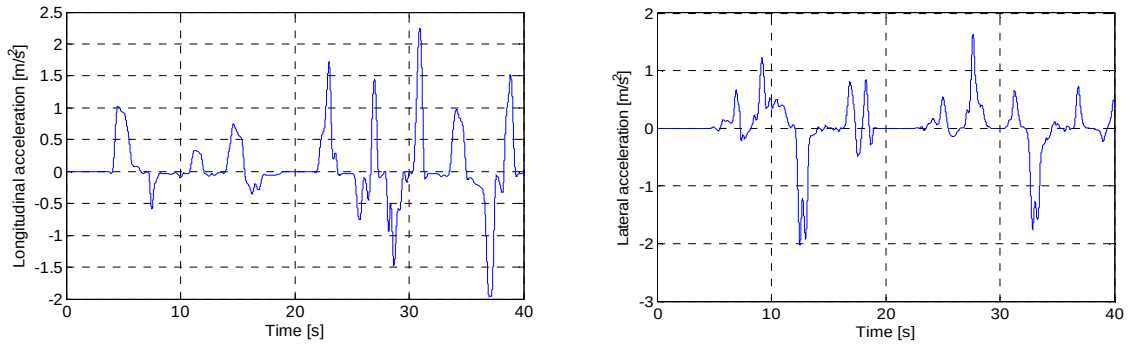

Figure 4.16: The longitudinal, respectively, lateral acceleration of the simulated vehicle

Fig. 4.17 presents the angular velocities of the simulated vehicle, while driving in a city scenario with the velocity presented in Fig. 4.15.

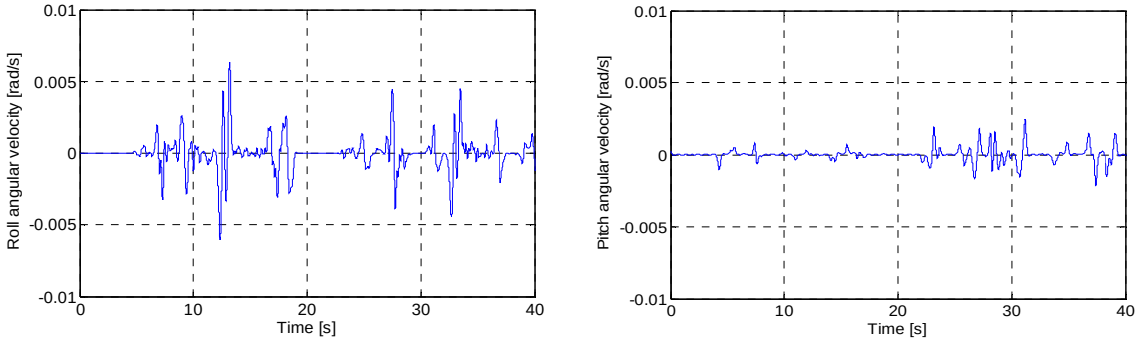

Figure 4.17: The roll, respectively, pitch angular velocity of the simulated vehicle

Fig. 4.18 presents the actuator displacements and velocities recorded while the participant was driving in the simulated city scenario.

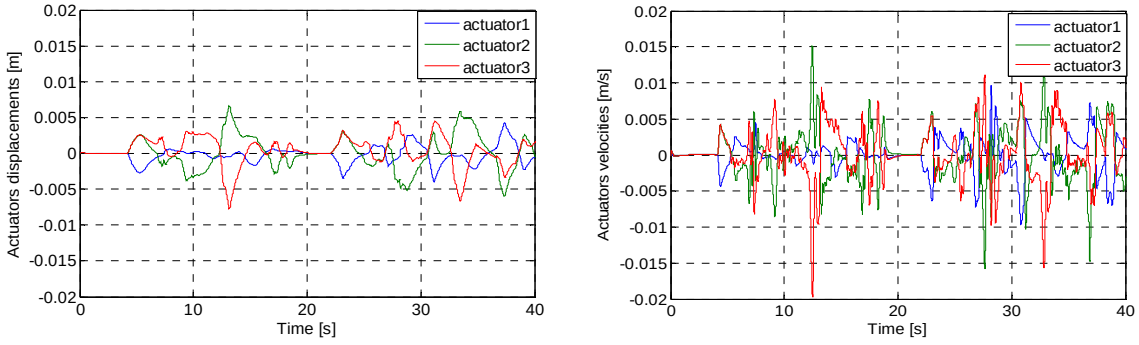

Figure 4.18: The driving simulator actuator displacements and velocities while reproducing the accelerations and velocities presented above

4.2.2 The determination of the influence of different parameters on the overall subjective degree of realism

The second set of experimental tests was conducted in order to establish the influence of different parameters on the subjective degree of realism of the simulation. The tests were conducted between 06.06.2011 and 10.06.2011.

The Design of the experiment using the Taguchi Method

The Taguchi method was used in order to identify the variables that influence the results, following the method proposed in [Paraianu et al., 2011]. Three parameters were studied, and for each parameter two levels were considered. Genuchi Taguchi developed this optimization technique in the 1950s [Macleod et al., 1999]. It is a simple analysing and optimization method for complex systems. The Taguchi design of experiments is described by the following steps:

- Defining the experiment goals;
- Defining the parameters that influence the studied process. These parameters have to be variable ones, which affect the performance of the defined process;
- Designing the corresponding orthogonal arrays for the defined parameters;
- Conducting the experiments indicated by the orthogonal array;
- Analysing the data from the experiments and conducting the needed calculation for the parameter influenced determination [Unal and Dean, 1991].

In this experiment, the three parameters investigated were: motion, OF and haptic response. In this way, as a contribution to this research, the influence of the motion of the driving simulator, the OF and the vibrations in the steering wheel on the subjective degree of realism are investigated. As stated before, the studied parameters have to be variable. This optimization method works with different levels for one parameter. Once the number of the parameters and levels is known, the orthogonal array can be selected. This doctoral work assumes three parameters with two levels, as presented in Table 4.4.

Table 4.4: Investigated parameters and their levels

Parameters	**First Level**	**Second Level**
Motion	0 DOF	3 DOF
OF	Low OF scenario	High OF scenario
Haptic	No vibrations in the steering wheel	Vibrations in the steering wheel

The two levels considered for the motion parameter are of 0 DOF and 3 DOF. The low level considered for the OF was a very poor object simulated scenario, which was only a street, as can be observed in Fig. 4.19 left. The second level was considered a high OF scenario. A city scenario, corresponding to Köln town was used as the second level for the OF, as it is presented in Fig. 4.19 right. The two levels for the third parameter were no vibrations for the first level and vibrations in the steering wheel for the second level. In the second level, the vibrations were activated while driving on the road lane. The name of the assistance system is *lane departure warning* (LDW) and it should give a feedback to the driver when leaving his lane. This mechanism was implemented in the vehicles for increasing the road safety. There are two types of such systems: the lane departure warning, when the system warns the driver by means of vibrations, visual or acoustical signals that he or she left the driving lane, and the lane keeping system, where the system warns the driver and when there is no immediate

action taken, it interferes and keeps the vehicle on the initial driving lane. The first automotive manufacturer to introduce such an assistance system was Nissan, which implemented lane keeping assistance in 2001 in their model, Cima [Nis, 2011].

Figure 4.19: First level of the OF (left); second level of the OF (right)

After choosing the parameters to be studied in the experiments and their levels, the experimental orthogonal array was written, as shown in Table 4.5. For 3 parameters, a number of 9 experiments would have been necessary. But such an array highlights the most significant tests to be conducted. This method was chosen with respect to its simplicity; and hence, one of the objectives of this research, was to determine how important the rendering of different cues in a driving simulator is.

Table 4.5: L4 Orthogonal Array

Experiment Number	Motion	OF	Haptic Response
T1	Level 1	Level 1	Level 1
T2	Level 1	Level 2	Level 2
T3	Level 2	Level 1	Level 2
T4	Level 2	Level 2	Level 1

This matrix enables the necessary data acquisition for parameter influence determination with an optimal number of experimental testing. The following table presents the orthogonal array that these experiments were based on.

Table 4.6: Driving Simulator Experiments

Experiment Number	Motion	OF	Haptic Response
T1	0 DOF	Highway scenario	No vibrations
T2	0 DOF	Köln scenario	LDW
T3	3 DOF	Highway scenario	LDW
T4	3 DOF	Köln scenario	No vibrations

Conducting the experiments

Which cues are important to be reproduced in a driving simulator or how many DOF should such a system have are still open questions in the literature [Kemeny, 2009]. The effect of the motion on the subjective degree of realism is investigated in this subchapter.

Twenty six participants took part in this study, 22 men and 4 women. The experiments were conducted in three different days, in Bocholt, between the 06.06.2011 – 10.06.2011. The drivers involved in the study were mostly students and they were aged between 21 and 48.

The average age was 25 years. All participants had a driving license and used to drive between 1,500 and 20,000 km per year. The average driving-year experience was of 5.5 years, with an average of 22,830 km driven per year. Having a driving licence was a precondition in participating in this study also. 70% of them had already interacted with a driving simulator before this second study took place.

Figure 4.20: A participant driving the driving simulator

The same setup discussed in chapter 4.2.1 was used here as well. Each participant proceeded with the experimental testing individually, as already highlighted in 4.2.1. A total of 30 minutes was allocated to each of them and they were asked to drive a city and a highway scenario. The tests were carried out following the methodology already described in 4.2.1.

Results

The same statistical analysis was performed as described in the previous subchapter. The participants drove the four scenarios as described in Table 4.6, and after each experiment they were asked to rate the realism of the simulator using the same scale from 0% to 100%, as presented in 4.2.1. The results are discussed in this subchapter.

As stated before, the number of levels assumed in the Taguchi analysis was assumed to be two. Twenty six observations were considered, since there were twenty six participants involved, each indicating a degree of realism for the correspondent scenario. The following table presents the mean values calculated for each experiment.

Table 4.7: The mean values for the overall subjective degree of realism obtained in experiments

Experiment Number	Motion	OF	Haptic Response	Mean Realism Degree
T1	0 DOF	Highway scenario	No vibrations	31.4%
T2	0 DOF	Kö ln scenario	LDW	42%
T3	3 DOF	Highway scenario	LDW	66%
T4	3 DOF	Kö ln scenario	No vibrations	56%

In order to perform the needed analysis, some new coefficients have to be introduced. The sum of results (the four percentages presented in the last column of Table 4.7) is defined [Unal and Dean, 1991]:

$$T = \sum_{i=1}^{N_{\exp}} R_{d_i} \,. \tag{4.1}$$

The correction factor, CF is:

$$CF = \frac{T^2}{i}, i = 1..4 \,. \tag{4.2}$$

The total sum of squares due to total variation, ST is:

$$ST = \sum_{i=1}^{N_{exp}} R_{d_i} - CF \,. \tag{4.3}$$

The sum of squares, S_h due to the h factor is considered:

$$S_h = \underbrace{\frac{(\sum_{j=1}^{l_1} R_{d_j})^2}{l_1}}_{level1} + \underbrace{\frac{(\sum_{j=1}^{l_2} R_{d_j})^2}{l_2}}_{level2} \,. \tag{4.4}$$

The variance of the h factor, V_h is calculated:

$$V_h = \frac{S_z}{DOF_{exp}}, \tag{4.5}$$

Where the DOF of the experiments are calculated:

$$DOF_{exp} = N_{levels} - N_{obs} \,. \tag{4.6}$$

The total error, e is calculated as:

$$e = N_{exp} \cdot N_{obs} - 1 - \sum_{i=1}^{N_{param}} DOF_{param_i} \,. \tag{4.7}$$

The pure sum of squares, $S_h^{'}$ is defined as:

$$S_h^{'} = V_h - (V_{h_e} \cdot DOF_{param_1}) \,. \tag{4.8}$$

And finally the percentage contribution of factor P_{h_i}, is calculated Paraianu et al., 2011]:

$$P_{h_i} = \frac{S_h^{'}}{ST \cdot 100} \cdot \tag{4.9}$$

These equations were solved for the data given in Table 4.7. The final equation reveals the percentage influence of each parameter on the participants overall subjective degree of realism. Table 4.8 presents the results obtained.

Table 4.8: Percentage contribution of the analysed parameters on the overall realism degree

Studied parameters	**Influence percentage on the overall realism degree of the simulation**
Motion	84.75%
OF	0.01%
Haptic	15.22%

It was shown in this research that the influence of actuating the platform was of 84.75% on the degree of realism perceived by the 26 drivers involved in the experiment.

The vibrations in the steering wheel, through the LDW system were calculated to have an influence of 15.22% on the participants. These are very interesting results in what concerns driver's acceptance. The drivers involved in these experiments could easily adapt to the assistance system provided and their immersion in the simulated environment was significantly influenced by the activation of the LDW option.

Although two different scenarios were used in order to stimulate the OF, this was found to have only a 0.01% influence. Durkee proved in [Durke, 2010], that while performing experiments with the Western Transportation Institute's high fidelity driving simulator, with low and high OF, the participants estimated the velocity of the vehicle better, when driving in a high OF simulated scenario. The purpose of the experiments conducted in the present research was not supposed to investigate the speed perception in a driving simulator. Still, the influence of the OF on the degree of realism found is very small. However, since Jamson proved that a driving simulator requires a 120º FOV in [Jamson, 2000], and since the EFDS used here had a smaller FOV, it could be possible that the OF is actually dependent on the FOV and has an influence on the realism of the virtual environment. Nevertheless, this is possible only when this condition is fulfilled.

It has also been demonstrated how much the driver of such a system is influenced by motion. One of the 17 questions that the participants had to answer concerns how realistic the motion of the driving simulator was.

It has been proved that with the studied EFDS, the drivers rated the motion and the accelerations felt with 70.41%, compared to the experience of driving a real vehicle. It has already been shown that the influence of this motion on the human perception of reality is very high. Once these results are understood, the importance of motion in a driving simulator is emphasized. But more obvious is the fact that with a low cost solution, a sufficient subjective degree of realism is obtained. These results are interpreted in this research as emphasizing the fact that irrespective of the DOF of the actuation mechanism, a motion driving simulator should provide correct motion cues. The development of the vehicle models and of the MCA should be approached, so that the system provides motion as similar as possible to the real vehicle, as already discussed in this doctoral work. Fig. 4.21 shows the influence of the three studied parameters on the subjective degree of realism. The variation of the parameters is shown from the first level to the second one. It can be noticed that the motion has the biggest variation, just like the parameters with the biggest influence and that the OF has a very small variation.

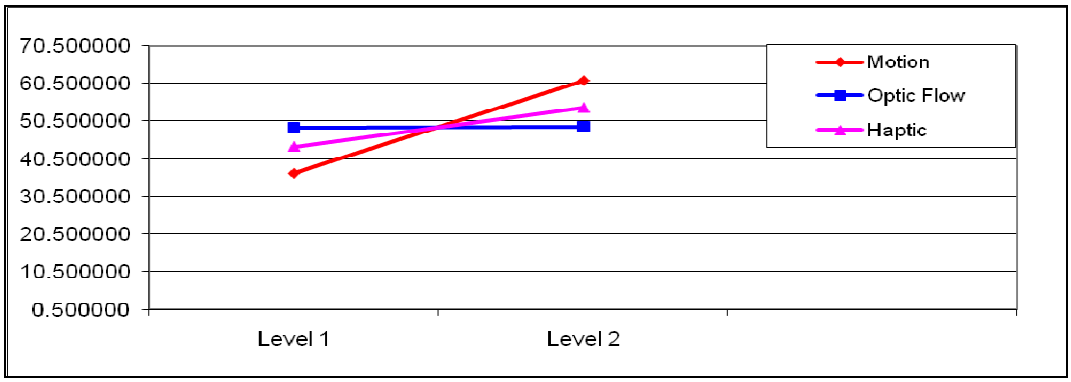

Figure 4.21: The influence of the three studied parameters on the overall degree of realism rated by the participants

None of the participants in this second testing experienced simulation sickness. As stated before, in the first set of experiments, some problems with the breaking manoeuvre were registered. The feeling of using the gas and brake pedal received then the lowest rate, of

45.3%. Since some modifications were made for these experiments, the feeling of using these pedals was again addressed in the questionnaires. The mean value calculated was found to be of 57.2%. The results obtained are better, but the recommendation for using real gas and brake pedals in such a machine remains.

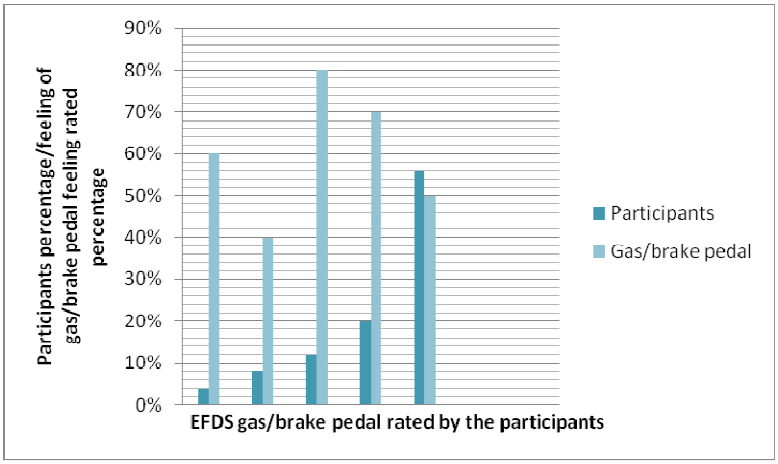

Figure 4.22: Participants rating the driving simulator's reactions

In the same experimental tests the participants were asked to drive the city scenario with the first MCA. The motion base was active on all three axes. The drivers involved in the testing were asked to rate the realism of the simulation. Then they were asked to drive the same scenario, but this time with the motion base completely turned off. So this time, the EFDS behaved like a static one. The participants were again asked to rate the realism of the simulation and the goal of this test was to verify the MCA and to investigate and prove that rendering motion cues in the EFDS brings advantages and increases the realism of the simulation. Indeed the mean value obtained for the realism degree while driving without motion is of 21%, while driving with motion cues, the realism degree registered is of 56%, as presented in Table 4.9.

Table 4.9: Mean value for the overall subjective degree of realism obtained in experiments concerning the motion

Experiment Number	Motion	OF	Haptic Response	Mean Realism Degree
M1	3 DOF	Köln scenario	No vibrations	56%
M2	0 DOF	Köln scenario	No vibrations	21%

4.2.3 Evaluation of the MCA

In the same time interval, when the second experimental testing was being performed, between 06.06.2011 and 10.06.2011, the two kinds of MCA designed and described in the previous chapter were evaluated once more. The participants were asked to drive the highway simulated scenario, once with the first MCA, and then with the second MCA. After each drive they were asked to rate the realism of the motion of the driving simulator and to briefly explain if there was any difference between them. As stated before, both algorithms approached the classical design, being based on linear filters. These algorithms incorporate transfer functions that filter the low or the high pass frequencies. The main difference between them is that the second algorithm introduces the high longitudinal, respectively, lateral frequency acceleration component in the motion of the mobile platform as well.

When investigating the data obtained while simulating offline these algorithms, it was observed that the amplitudes of the angles and displacements of the platform while using the

second MCA were smaller than when using the first algorithm. The mean value of the degree of motion realism while driving with the first algorithm was found to be of 60%, and while driving with the second algorithm, the mean value was found to be of 68%.

Table 4.10: The mean value for the overall subjective degree of realism obtained in experiments concerning the MCA

Experiment Number	Motion	OF	Haptic Response	Mean Realism Degree
MCA1	3DOF	Highway scenario	No vibrations	60.62%
MCA2	3DOF	Highway scenario	No vibrations	68.12%

All the participants, who drove the driving simulator in the first experimental testing (75% from the total number of participants or 19 participants) as well, stated that the breaking/acceleration pedals reacted better than in the first trial.

Again when consulting the mean values obtained for the degree of realism concerning the two MCA, it can be seen there is only an 8% difference. That represents only 2 participants who stated that the second algorithm reproduced the motion in a better way.

As said before, the second algorithm included the high frequency component of the signals too, so that the behaviour of the simulator was more aggressive compared to the first algorithm. The amplitudes of the motion were smaller and the motion was faster. 81% of the total participants in the experiment (21 drivers) appreciated this with respect to the braking manoeuvre. Since the motion was faster and its amplitudes were smaller, the feeling of accelerating/braking was stronger and it was appreciated to be more realistic.

All the drivers who chose the second algorithm to be better, stated that they appreciated the fact that the amplitudes of the motion were smaller, but only concerning the pitch motion. When asked about the response of the driving simulator to the roll motion, corresponding to driving in a curve, lane change, etc. 70% of the total number of participants (18 drivers) preferred the first MCA response.

When asked to explain their choice, the reasons named in the questionnaires where: the response of the driving simulator while driving in a curve was very precise, when using the first driving simulator, and while using the second, the motion was too short and too fast. It was then concluded that while accelerating and braking, the degree of realism increases while introducing fast motion, through the high frequency component of the acceleration, so the driver is experiencing the kind of motion he is expecting to sense, since this is what he or she is used to feel while driving his or hers own vehicle.

However, when introducing these high frequency signals in the driving simulator, while driving in a curve, the short/fast motion was not considered natural anymore. In this research, these results were interpreted as follows: while rolling, for a realistic driving experience, a very fast reaction of the simulator together with road inputs is sufficient.

Fig. 4.23 presents the roll angular velocity frequency response for both algorithms. The data recorded while the fourth participant was driving on the third day of experiments is presented and discussed. The roll angular velocity of the platform was recorded during simulations and then the FFT was used to get the frequency response of the signals. It can be easily observed the difference in the frequency nature of these signals.

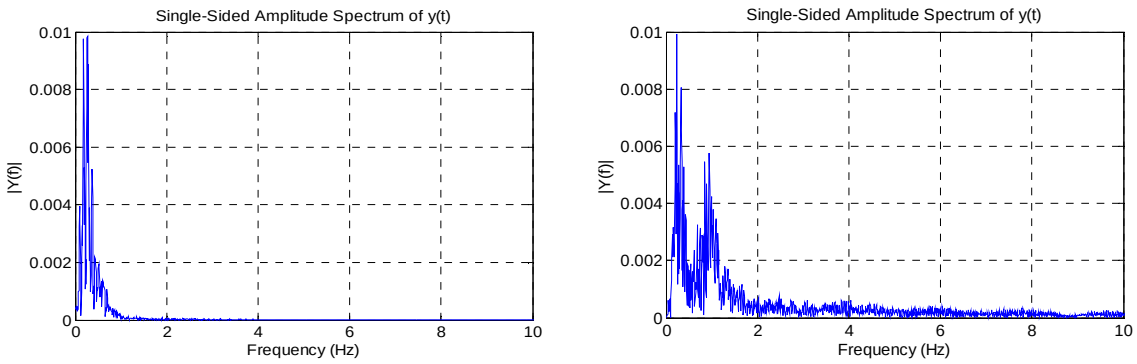

Figure 4.23: The frequency response of the roll angular velocity recorded in real time from the first MCA (left), respectively the second MCA (right)

The solution used in the experimental testing represents the 3 DOF driving simulator using sliding actuators. The whole vehicle simulator could not be used since the behaviour of the hydraulic actuators did not allow this. However, the capabilities of this system were studied. The limitations of these cylinders were investigated and are presented in this research. The phase angle decreased dramatically at 1 Hz, leading to a larger phase shift between output and input signal. It can be concluded that the output lags the input signal more and more.

In order to test the models developed, the mock-up driving simulator, was used in the experimental testing. Two sets of experiments were conducted in sic different days, in order to study the overall subjective involvement degree in the simulated environment and the influence of different parameters on the overall subjective degree of realism. The participants of these experiments could easily adapt to the assistance system provided and their immersion in the simulated environment was significantly influenced by the activation of LDW option.

It is proved in this chapter that with the studied 3 DOF EFDS, the drivers rated the motion and the accelerations felt with 70.41%, compared to the experience of driving a real vehicle. It was already shown that the influence of this motion on the human perception of reality is very high.

5 Model Validation

The goal of recording data in the experimental testing was to estimate transfer functions between the motion of the simulated vehicle, of the driving simulator and of the motion registered at the driving simulator's headrest. Such a transfer function gives the relation between the input and the output of a system, with respect to the spatial or temporal frequency. These transfer functions give us the limitations of the EFDS. Once the velocities/acceleration of the driver's head are known, the perceived motion can also be approximated by using the mathematical models of the vestibular system, already presented in Chapter 3.

During all experimental testing, an acceleration sensor was used to record the motion at the driving simulator's headrest. The Microstrain sensor can detect and measure the accelerations, velocities and angles on 3 axes (Fig. 5.1). For each manoeuvre driven by each participant, this data was measured and recorded. No connection to Matlab/Simulink was established, since the sensor's software enables data collection. A different computer was used for measurement and acquisition. The computer was running on a Windows XP system and could read the data from the serial output of the sensor. The sensor provides two serial operating modes, the RS 232 and the RS 485 one. All recorded data was saved on the hard drive of the considered computer.

The 3DM-GX1 sensor can output:

- the translational acceleration of all 3 axes;
- the angular velocities about all three axes;
- the transformation matrix of the current position of the sensor with respect to the fixed coordinate system;
- the quaternion or gimbal angles direct from the transformation matrix [MIC, 2011].

The sensor was mounted on the headrest of the driver's seat in order to record the needed data. The eleven vector outputted by the sensor represent the time, the roll, pitch respectively yaw angles, the roll pitch respectively yaw angular accelerations and the roll, pitch respectively yaw velocities and the timer ticks.

Figure 5.1: The acceleration sensor used for recording the accelerations, positions and angles of the headrest [MIC, 2011]

This sensor is designed to operate over the full 360º of angular motion on all three axes. It contains a 16 bit A/D converter and a microcontroller for outputting its orientation. It is being used in different applications from robotics, medical applications or mobile cameras. The

sensor's software combines the sensor outputs and eliminates the inertial influences on the accelerometers. These algorithms enable the sensor to have good results both in a static and dynamic environment. The sampling rate of this sensor is 75 Hz and the sample time used for data acquisitioning is 0.01s. That was the smallest value offered by the 3DM-GX1 sensor and it was used in the experimental testing. Considering a rotation matrix $\boldsymbol{M_s}$, the sensor will calculate the orientation:

$$\boldsymbol{M}_S = \begin{bmatrix} M_{11} & M_{12} & M_{13} \\ M_{21} & M_{22} & M_{23} \\ M_{31} & M_{32} & M_{33} \end{bmatrix}, \tag{5.1}$$

and this will satisfy the following relation:

$$\boldsymbol{VL} = \boldsymbol{M}_S \cdot \boldsymbol{VE} \tag{5.2}$$

between the sensor's vector expressed in the 3 DM-GX1 local coordinate system $\mathbf{VL}$, and the sensor's vector expressed in earth fixed coordinate system, $\boldsymbol{VE}$. The Euler angles are being calculated following the 'ZYX' formulation [MIC, 2011]:

$$\begin{aligned} \theta &= \arcsin(-M_{13}), \\ \phi &= \arctan\left(\frac{M_{23}}{M_{33}}\right), \\ \psi &= \arctan\left(\frac{M_{12}}{M_{11}}\right). \end{aligned} \tag{5.3}$$

The rotation matrix $\boldsymbol{M}_S$ has the following form:

$$\boldsymbol{M}_S = \begin{pmatrix} \cos\psi \cdot \cos\theta & \sin\psi \cdot \cos\theta & -\sin\theta \\ \cos\psi \cdot \sin\theta \cdot \sin\phi - \sin\psi \cdot \cos\phi & \sin\psi \cdot \sin\theta \cdot \sin\phi - \cos\psi \cdot \cos\phi & \cos\theta \cdot \sin\phi \\ \cos\psi \cdot \sin\theta \cdot \cos\phi + \sin\psi \cdot \sin\phi & \sin\psi \cdot \sin\theta \cdot \cos\phi - \cos\psi \cdot \sin\phi & \cos\theta \cdot \cos\phi \end{pmatrix}. \tag{5.4}$$

The orientation in quaternion form can be obtained by deriving the rotation matrix:

$$\boldsymbol{Q}_S = \begin{bmatrix} q_{s_0} \\ q_{s_1} \\ q_{s_2} \\ q_{s_3} \end{bmatrix}. \tag{5.5}$$

The measured signals were disturbed by noise, so this data needed to be filtered. This filter should be able to remove the noise, without losing the important information from the signal. The Kalman approach was used in this work.

A Kalman filter is an algorithm for state estimation of a time variant system. It gives an efficient recursive computing solution for estimating the minimum error variance [Welch and Bishop, 2006]. It was first proposed in 1960 by R. Kalman to solve a linear filtering problem by using a recursive solution [Welch and Bishop, 2006]. Such a filter estimates the state of a process by using a reverse reaction, represented by measurements. Thus, the filter equations are divided into two groups: time update equations and measurement update equations.

Given the linear stochastic differential equation as presented in [Welch and Bishop, 2006]:

$$\begin{aligned} \boldsymbol{x}_k &= \boldsymbol{A}_k \boldsymbol{x}_{k-1} + \boldsymbol{B}_k \boldsymbol{u}_k + \boldsymbol{w}_k, \\ \boldsymbol{z}_k &= \boldsymbol{C}_k \boldsymbol{x}_k + \boldsymbol{v}_k. \end{aligned} \tag{5.6}$$

where $\boldsymbol{A}_k$ is a matrix that relates the state at the previous step to the state at the current step, $\boldsymbol{B}_k$ is a matrix relating the optimal control input to the state $\boldsymbol{x}_k$, $\boldsymbol{C}_k$ is a matrix relating the state to the measurement $\boldsymbol{v}_k$. $\boldsymbol{w}_k$ is the process noise and $\boldsymbol{v}_k$ is defined as the measurement noise. The state space vector $\boldsymbol{x}_k$ contains all the needed information, but it cannot be directly measured. The vector $\boldsymbol{z}_k$, is a function of $\boldsymbol{x}_k$, and can be directly measured, but it contains the noise $\boldsymbol{v}_k$. The process noise covariance, $\boldsymbol{Q}_k$ is defined as [Naidu and Raol, 2008]:

$$\boldsymbol{Q}_k = E(\boldsymbol{w}_k \cdot \boldsymbol{w}_k^T), \tag{5.7}$$

where $E()$ stands for the expected value. The measurement noise covariance, $\boldsymbol{R}_k$ is defined as:

$$\boldsymbol{R}_k = E(\boldsymbol{v}_k \cdot \boldsymbol{v}_k^T). \tag{5.8}$$

The state prediction is defined [Naidu and Raol, 2008]:

$$\hat{\boldsymbol{x}}_{k-1 \mid k-1} = \boldsymbol{A}_k \hat{\boldsymbol{x}}_{k-1 \mid k-1}, \tag{5.9}$$

The prediction error covariance is defined [Naidu and Raol, 2008]:

$$\boldsymbol{P}_{k \mid k-1} = \boldsymbol{A}_k \boldsymbol{P}_{k-1 \mid k-1} \boldsymbol{A}_k^T + \boldsymbol{Q}_k, \tag{5.10}$$

The estimator should have the error variance as diminished as possible. The Kalman filter is described by the following equations [Naidu and Raol, 2008]:

$$\vartheta = \boldsymbol{z}_k - \boldsymbol{C}_k \hat{\boldsymbol{x}}_{k \mid k-1}, \tag{5.11}$$

$$\boldsymbol{S}_k = \boldsymbol{C}_k \boldsymbol{P}_{k \mid k-1} \boldsymbol{C}_k^T + \boldsymbol{R}_k \tag{5.12}$$

$$\boldsymbol{K}_k = \boldsymbol{P}_{k \mid k-1} \boldsymbol{C}_k^T \boldsymbol{S}_k^{-1} \tag{5.13}$$

$$\hat{\boldsymbol{x}}_{k \mid k} = \hat{\boldsymbol{x}}_{k \mid k-1} + \boldsymbol{K}_k \vartheta \tag{5.14}$$

$$\boldsymbol{P}_{k \mid k} = \left(\boldsymbol{I} - \boldsymbol{K}_k \boldsymbol{C}_k\right) \boldsymbol{P}_{k \mid k-1} \tag{5.15}$$

These equations are given with respect to the innovation ϑ, the innovation covariance $\boldsymbol{S}_k$, the gain matrix $\boldsymbol{K}_k$, the estimated state $\hat{\boldsymbol{x}}$ and the estimation error covariance $\boldsymbol{P}_k$.the estimation error covariance matrix $\boldsymbol{P}_k$ [Naidu and Raol, 2008]. The measurement noise was quantified before the experimental testing. In order to determine the cut-off frequency of the recorded signal with the Microstrain sensor, the signal was recorded without any motion of the simulator. The FFT was used again in this process. The process variance was chosen to be

very small, following the approach proposed in [Welch and Bishop, 2006] in order to allow flexibility in "tuning" the filter. The first value of the estimated vector was decided to be the first value of the studied filtered. The above presented equations were implemented in Matlab. The following figures present results obtained from the filters. With light blue are given the signals taken from the sensor, and with red, the filtered signal.

Figure 5.2: Roll angle signal obtained from the sensor (blue) and filter (red)

Figure 5.3: Pitch angle signal obtained from the sensor (blue) and filter (red)

All the signals recorded with the help of the sensor (angles, velocities and accelerations) were filtered. The data recorded in the simulations was analysed and used for transfer function estimation. Using the Matlab/Simulink System Identification Toolbox [MAT, 2011], a transfer function between the angular velocity of the vehicle model and the filtered angular velocity recorded with the help of the acceleration sensor was established with the following structure (using a second-order system with complex poles):

$$G(s) = \frac{k}{(1 + 2\xi T_\omega s + T_\omega^2 s^2)} e^{-T_d s} \quad (5.16)$$

The values obtained for these parameters from the System Identification Toolbox are fiven in Table 5.1 and Fig. 5.4 shows the step response of the estimated transfer function and Fig. 5.5 shows the output of the transfer function.

Table 5.1: Estimated Values for the Roll Motion

Identified parameter	**Value**
k	0.52
T_w	0.05
ξ	1.64
T_d	0.02

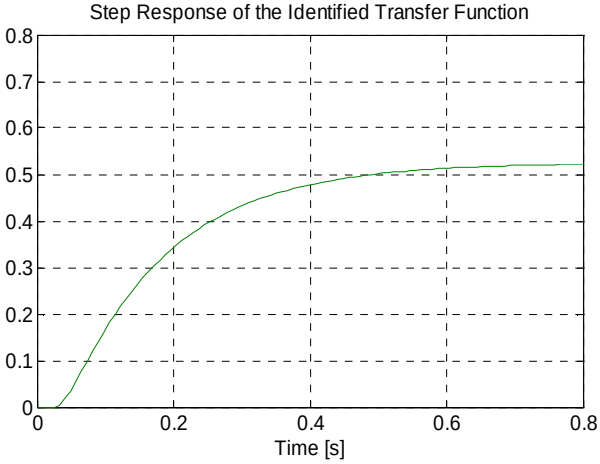

Figure 5.4: Step response of the identified transfer function

After obtaining the parameters values through estimation, the model was validated with the help of the same tool. With black it is shown the sensor measured signal, with green, the estimated signal with first order disturbance model, and with blue, the estimated signal with second order disturbance model. It can be observed that the best fit between the measured signal and the estimated one was obtained while estimating the transfer function using a second order disturbance model. In this work the estimated transfer function for the angular velocity is assumed to be valid for the pitch motion as well.

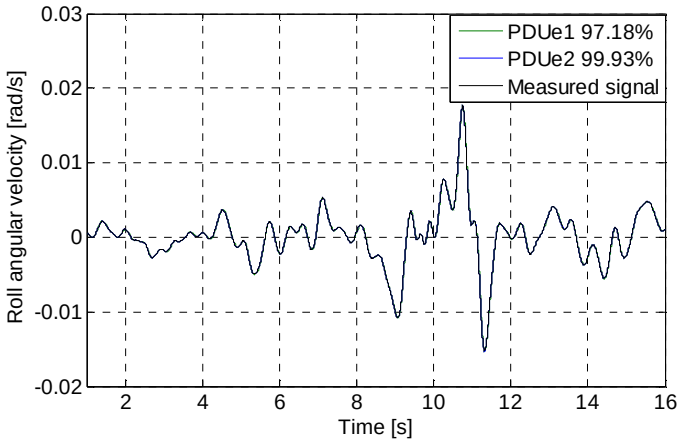

Figure 5.5: Different disturbance model noise comparisons angular motion estimation function

A transfer function between the angular velocity of the vehicle model and the filtered angular velocity recorded with the acceleration sensor was obtained based on real measurements made in driving simulator's experimental tests. This function can be used further in estimating the angular velocity felt by the driver in the 3 DOF simulator.

In order to estimate a transfer function between the vertical acceleration of the driving simulator and the filtered vertical acceleration, the same algorithm was implemented. Table 5.2 presents the estimated values.

Table 5.2: Estimated Values for the Heave Motion

Identified parameter	**Value**
k	0.29
T_w	1.11
ξ	0.32
T_d	0.3

Fig. 5.6 shows the output of the estimated transfer function. After obtaining the parameter values through estimation, the model was validated with the help of the same tool. With black it is shown the sensor measured signal, with green, the estimated signal with first order disturbance model, and with blue, the estimated signal with second order disturbance model. It can be observed that the best fit between the measured signal and the estimated one was obtained while estimating the transfer function using a second order disturbance model.

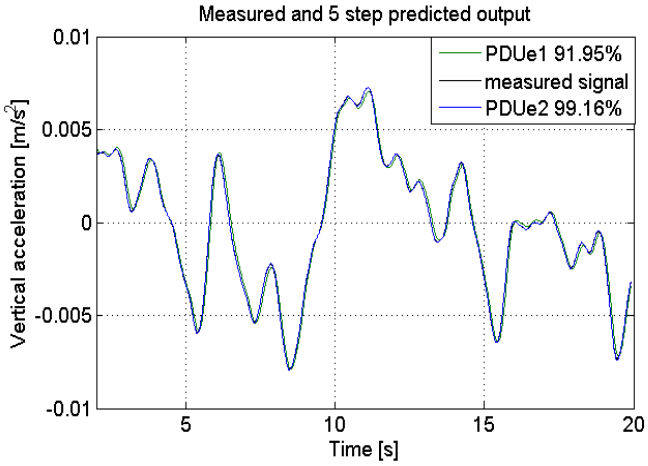

Figure 5.6: Different disturbance model noise comparisons heave estimation function

The present chapter completes the fourth chapter of this doctoral thesis. It has been previously shown how much the human driver is affected by the rendering of motion in the driving simulator. Also, it was experimentally proven that integrating the high frequency component of the longitudinal acceleration into the MCA improves the braking/acceleration feeling. Blaauw named four methods for behavioural validation of driving simulators [Blaauw, 1982]. Using subjective criteria was one of them and it was consequently approached here. Since the results were satisfactory, especially with respect to the motion of the driving simulator, where the author brought the most contribution, it is assumed the initial goal of the work has been achieved. Although the motion of the vehicle is very important in the EFDS discussed, this research focuses also on the human perception. Thus, an acceleration sensor placed on the headrest recorded the motion during the experimental testing. It has already been emphasized in this doctoral work that the vestibular system has a major role in perceiving the motion. The inputs of this system are the velocities and accelerations of the driver's head. The purpose of this research was not to model this human organ, since there is an impressive amount of studies and researches older than 70 years dealing with this subject. This work focused on what is important with respect to human perception and rendering in an EFDS.

6 Conclusions and Future Work

A driving simulator is a virtual reality device in which the drivers should be able to feel as if they were actually driving a real vehicle. These simulators are used in different areas and are found in universities, in the automotive or in entertainment industry.

Since the driving task is still not fully mathematically modelled, it is important to address the driver's behaviour problem. There are special running programs in order to decrease the number of accidents on the European roads [EUA, 2011]. There are still many unsolved problems concerning the driving task. Hence, the need of studying more the driver's behaviour is emphasized. Driving simulators are tools used very often for this purpose. An impressive number of articles were published based on studies conducted using driving simulators. These machines are actually perfect tools for this kind of studies. They can provide a safe study environment.

A driving simulator cannot identically reproduce real life situations or sensations, due to workspace and actuator limitations. Hence, the question which arises here is: what should a driving simulator reproduce? Having in mind the fact that in order to use a driving simulator for training and research purposes, this machine has to offer a realistic driving experience to its driver.

There is impressive research focusing on this theme. The driving simulators are getting more and more complex in order to be more realistic. Different game engines are used to simulate virtual environments as realistically as possible. Driving simulators addressed the rendering of hearing cues as well. Haptic feedback is also usually reproduced in a driving simulator. And of course, motion cueing strategies have been used since the 1950s. All this effort was made to create and reproduce a realistic driving experience. However, these systems are very expensive.

When building such a system, a compromise usually has to be made. The question that follows is: what should be necessarily included in such a machine? As a contribution of the author, it was proved in this research that the influence of the motion on the subjective degree of realism is of 84%. The vibrations in the steering wheel improved the realism of the simulation and had a 15% impact. Although the visualization of the environment in the DRIVASSIST simulators was done with the help of a commercial game engine, which ensures a high level of realism and an easy adaption of scenarios, the impact of a high OF was very small on the subjective degree of realism. It was concluded after analyzing the results obtained, that a driving simulator should include a motion platform and should approach a correct design of the motion cueing strategy.

Although there is a lot of available research dealing with the development and optimization of driving simulators, it is difficult to find extensive work focusing on the driving simulator limitations and failures. This thesis was written in order to prove that the limitations of the system can be understood. The last two chapters focus on the results obtained from experimental testing. It was assumed that addressing subjective criteria can be used in order to study the limitations. When rating different parts of the simulation, important knowledge was gained. Consequently, it has also been presented. This only refers to dynamical limitations. In order to have knowledge of the perceived motion as well, a set of mathematical identification was conducted. As a contribution of the author, transfer functions between the motion of the driving simulator and the motion recorded on the simulator's headrest were estimated. These functions contain important information. Once the head's motion is known with the help of the vestibular models available in literature, the perceive motion is determined. Since the data

used for estimation was recorded in real time simulation, the estimated transfer functions refer to the dynamical limitations of the system. These transfer functions can be used for validation and also for evaluation of the driving simulator purposes.

The main goal of this research is the development of a 3 degrees of freedom cost effective driving simulator, which integrates design and cost constraints, the human perception of motion, and real vehicle motion. The system was further used in experimental testing in order to determine the overall subjective involvement degree in the simulated environment and the influence of different parameters on the overall subjective degree of realism. The motivation of this research comes from the importance of the addressed problem and all the included factors.

In the *second chapter* of this thesis, the driving simulators are discussed with respect to their applicability, advantages and limitations. The results that were obtained and published before by researchers are discussed in this part of the thesis as well. The importance of the problem is once more emphasised. New systems are proved or validated with the help of these machines. New knowledge with respect to the vehicle or driver's behaviour is gained with each successful published study. As part of the cooperation between the Technical University of Cluj-Napoca and the University of Duisburg-Essen, this doctoral thesis is based on the previous researches conducted on the DRIVASSIST simulators. Significant work was already published concerning the static simulators. This research aims to improve the knowledge concerning the DRIVASSIST simulators.

The *third chapter* of the thesis further explains the development of the mathematical models used for the development of the cost effective driving simulator. The three degrees of freedom chosen to be simulated with the active driving simulator are roll, pitch, and heave and they were chosen with respect to the simplicity of the design, type of psycho-physic studies to be carried out and the global cost of such a system. The actuation solutions taken into account are discussed concerning kinematical and dynamical analyses, as trade-off solutions with respect to the available workspace, singularity configurations, the behaviour of the system, and the maximum forces needed in the frame of the overall cost constraints in order to define the driving simulator.

While concerned with real vehicle motion, the driving simulator addressed two main vehicle models: a seven degrees of freedom and a fourteen degrees of freedom model. These models were implemented in Matlab and different simulation results were presented. Since the chassis and body vibrations caused by road irregularities are high frequency vibrations and they have a differential action on the human body, depending on the parameters of the vibration, they were integrated together with a simple multi body human model and the seven degrees of freedom vehicle model. The goal was to investigate the effect of road vibrations on the vehicle, the human body and the driving simulator. A frequency analysis of the mathematical models representing the vestibular system was conducted in order to understand the behaviour of the system.

In order to study the interaction between the hydraulic cylinders and the vehicle, a seven degrees of freedom inverse vehicle model was developed, as a contribution to this research. The dynamic transfer path between the actuators and the vehicle body was understood. Together with a PI controller, a control strategy for the vehicle simulator was obtained.

For the driving simulator's design and for understanding the human motion perception, the models developed by J. Meiry were considered in this doctoral work. In the same chapter, the motion cueing strategy is also discussed. Since the accelerations, velocities and displacements obtained from the vehicle models cannot be exactly reproduced by the cost effective driving simulator, the classical motion cueing strategy was implemented. The goal of designing and

implementing such motion cueing algorithms was to test the influence of the high frequency acceleration on the driver's perception through experimental testing. The design of these filters represents a contribution to the doctoral work.

The *fourth* and the *fifth chapters* illustrate the results obtained in the experimental testing and the validation of the models. The Taguchi method was used in order to identify the variables that influence the results. Three parameters were studied, and for each parameter two levels were considered: the motion, the optical flow and haptics. It has also been shown that with the studied driving simulator the drivers rated the motion and the accelerations felt with 70.41%, compared to the experience of driving a real vehicle. The solution used in the experimental testing represents the three degrees of freedom driving simulator using sliding actuators. The whole vehicle simulator could not be used since the behaviour of the hydraulic actuators did not allow this. However, the capabilities of this system were also investigated. In addition, the limitations of these cylinders were investigated and are presented in this research.

The *future work* based on this research should focus on adding at least one more degree of freedom and thus, it will study the improvement with respect to the overall degree of realism. The recommendation is to use at least on translational degree of freedom more, for the actuation system. Also, a larger heave motion could improve the degree of realism. Thus, the actuators would not reach their limitations so fast, larger displacements would be possible, and the mobile platform will not need to come back so fast to its neutral position. On the other hand, in order to investigate the theory that a high optical flow enables a realistic experience in a driving simulator, a larger field of view needs to be used. Since Durkee concluded that a large field of view gas a greater impact on the simulation realism perceived by the drivers of a driving simulator than the motion [Durkee, 2010], the importance of this parameter is emphasized. The recommendation is to use a 360º field of view in order to prove the relation between the optical flow and field of view and also to introduce the differential motion parallax in the cost effective driving simulator. Since the motion parallax, is still not a usual component of driving simulators, its impact on the human perception in a driving simulator could be studied. A completely enclosed virtual environment should be also provided to the driver. This should immerse him or her in the simulation. Kemeny stated the need for any other motion cueing strategy except the classical one, but this has not been proved so far [Kemeny and Penerai, 2003]. However, interesting results can be obtained using an optimal strategy [Nehaoua et al., 2006]. These kinds of algorithms include also the vestibular system model. Since this research focused on modelling of the vestibular system, an optimal motion cueing algorithm should be tested on the cost effective driving simulator in order to investigate their influence on the degree of realism.

Appendix A: Implementation on the Hardware of the MCA

The actuators used in this application are developed by the SEW Company [SEW, 2011]. The first attempt to communicate with this system was made with using an S-function written in C language and implemented in Matlab. The S-function expected 3 arguments for each of the actuators' three axes. The implementation of this function failed, because, as required by the actuation system, it needed to load a dynamic library (TcAdsDll.DLL). This did not allow the simulation in real time, because xPC Target cannot load dynamic libraries. The use of a static library is allowed by xPC, but it is not supported by the control system provided.

For this reason, the data from the models developed and presented above are sent to the actuators via UDP communication (User Datagram Protocol). This kind of communication provides a connectionless host-to-host communication path. The addressing is made using the IP address and a port number. The communication uses datagram messages, which are sent one at a time. The IP is used to address the correct host in the network and the port number is used to route the datagram to the correct host process, as described in [Lay, 2011]. As defined by [EthC, 2011], a UDP datagram has the following format:

16 bit source port number	16-bit destination port number
16 bit UDP length	16-bit UDP checksum
Data	

Since the data transfer is enabled through the IP, the UDP has to identify only the destination and its ports. The PLC software used in this application is TwinCAT [Twi, 2011]. With its help and of an industrial PC, all common PLC systems can be replaced [Farkas et al., 2010]. This system incorporates a run time system, which runs the control algorithms in real time. The TwinCAT communication with Matlab is enabled through the OPC standard communication. The OPC Toolbox is available in order to make a connection to Simulink through the library standard blocks. The communication with Matlab is possible through a set of written commands [Farkas et al., 2010].

The data sent from the inverse kinematics block was processed in order to be recognized by the PEW system. As it was already presented, the outputs of the inverse kinematics of the 3 DOF motion system are values in m. The control system recognizes these values even if they are declared differently. The middle position expected is of 17500, which is equivalent to 0.175 m. In order to achieve this, a transformation was applied. The outputted data from the inverse kinematics block was transformed into mm and then a multiplying factor of 100 was used. Once the system receives this data, the communication is established. The platform can perform in this way a motion in the range 0-350 mm. First the platform was to be driven in the middle position (0.175m), and then the driving simulator can be used.

Several limitation and saturation blocks were added in the Simulink model in order not to exceed the maximum workspace by a more violent manoeuvre driven, as it can be observed in the following figure.

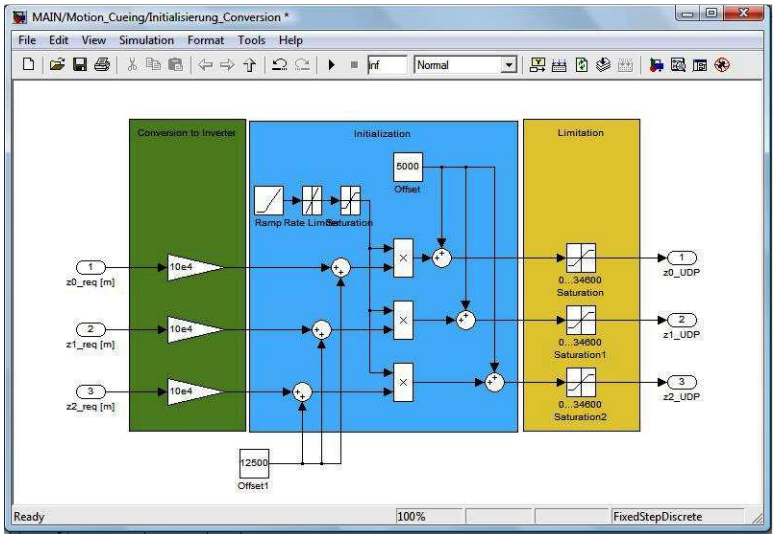

Matlab/Simulink limitations blocks

The three vertical displacements of the actuators were limited; the velocity of the actuators should not exceed 1 m/s. Since the tilting coordination block implemented uses trigonometrically functions, the accelerations that are introduced were limited so that the system does not have errors. The sample time used in all simulations was considered to be of 1 ms. All models were build accordingly.

Appendix B: Experimental Testing Questionnaire

Fragebogen-Nr.:
(nicht ausfüllen)

Fragebogen zur Ermittlung von Wirklichkeit in einen Fahrsimulator

Sehr geehrter Versuchsteilnehmer, sehr geehrter Versuchsteilnehmerinnen,

im Rahmen eine Kooperation zwischen die Fachhochschule Gelsenkirchen, der Universität Duisburg-Essen und der Technische Universität aus Cluj-Napoca und führen wir im Zeitraum 13.04.2011-15.04.2011 eine schriftliche Befragung der Versuchsteilnehmer bei der Erprobung eines dynamischen Fahrsimulators durch. Zweck dieser Befragung ist es, genauere Kenntnis darüber zu gewinnen, ein Vergleich Fahrerleben im Pkw und Fahrsimulator, damit zukünftige Fahrsimulatoren eine möglichst realistische Fahrsituation bei der Erforschung von verschiedenen Fragen der zum Beispiel Fahrsicherheit von Buschpiloten ermöglichen können. Die Antworten werden vertraulich behandelt und dienen ausschließlich der späteren statistischen Analyse. Die Befragung wird von Dipl.-Ing. Alina Capustiac, Universität Duisburg-Essen, Lehrstuhl für Mechatronik durchgeführt. Für Rückfragen schreiben Sie bitte eine Email an: capustiac@imech.de.

Fragebogen 1 – Generelles

		Date			
1.1	Geschlecht	Männlich		Weiblich	
1.2	Alter _____				
1.3	Haben Sie einen Führerschein?	Ja		Nein	
1.4	Jahre Fahrpraxis _____				
1.5	Durchschnittlich gefahrene Kilometer pro Jahr _____				
1.6	Sind Sie bereits einen Fahrsimulator gefahren?	Ja		Nein	

Fragebogen 2 – Wirklichkeit
Bitte beantworten Sie folgende Fragen in Bezug auf das Gefühl während der Fahrt ein echtes Auto.

2.1	Wie würden Sie die Reaktion des Fahrsimulators auf die von Ihnen durchgeführten Fahraktionen bewerten? 0% 10 20 30 40 50 60 70 80 90 100%
2.2	Wie authentisch empfanden Sie das Audio-Feedback? 0% 10 20 30 40 50 60 70 80 90 100%
2.3	Wie authentisch empfanden Sie das haptische Feedback? 0% 10 20 30 40 50 60 70 80 90 100%
2.4	Wie authentisch empfanden Sie die Lenkung des Fahrsimulators? 0% 10 20 30 40 50 60 70 80 90 100%
2.5	Wie authentisch empfanden Sie das Gefühl während der Benutzung von Brems- und Gaspedal? 0% 10 20 30 40 50 60 70 80 90 100%
2.6	In wie weit stimmen Ihre Erfahrungen in der simulierten Umgebung mit denen der realen Welt überein? 0% 10 20 30 40 50 60 70 80 90 100%
2.7	Wie schätzen Sie Ihre Immersion während der Simulation ein?

	0% 10 20 30 40 50 60 70 80 90 100%			
2.8	Wie schnell war Ihr Anpassung an die Simulationsumgebung? 0% 10 20 30 40 50 60 70 80 90 100%			
2.9	Wie einfach war es für Sie, die Fahraufgaben durchzuführen?			
	Sehr einfach	Einfach	Schwer	Sehr Schwer
2.10	Wie authentisch wirkten die während der Simulation bereitgestellten akustischen, visuellen und haptischen Informationen auf Sie? 0% 10 20 30 40 50 60 70 80 90 100%			
2.11	Empfanden Sie während der Simulation Übelkeitsgefühle?			
	Ja		Nein	
	Wenn ja, bitte wählen Sie:			
	Überanstrengung der Augen			
	Schwindelgefühl			
	Kopfschmerzen			
	Übelkeit			
	Andere:			
2.12	Haben Aspekte der Simulation Sie von der Durchführung der Fahraufgabe abgelenkt?			
	Ja		Nein	

Fragebogen 3 – Szenarien

3.1	Szenario 1 0% 10 20 30 40 50 60 70 80 90 100%
3.2	Szenario 2 0% 10 20 30 40 50 60 70 80 90 100%
3.3	Szenario 0% 10 20 30 40 50 60 70 80 90 100% 3
3.4	Szenario 4 0% 10 20 30 40 50 60 70 80 90 100%
3.5	Szenario 5 0% 10 20 30 40 50 60 70 80 90 100%

Vielen Dank für Ihre Mitarbeit!

Bibliography:

[ADR, 2011] A drive homepage: www.a-drive.de, August, 2011.

[Alidoost et al., 2010] Alidoost, M., Rezazadeh, G., and Hadad-Derafshi, M. (2010). On The Modelling of a MEMS Based Capacitive Accelerometer For Measurement of Tractor Seat Vibration. In *Sensors & Transdurcers*, Vol. 115, No. 4, pp 29-42.

[Arioui et al., 2009] Arioui, H., Hima, S., and Nehaoua, L. (2009). 2 DOF Low Cost Platform For Driving Simulator: Modeling And Control, In *Proceedings of the IEEE/ASME International Conference and Advanced Intelligent Mechatronics*, Singapore, pp 1206-1211.

[Augusto and Loureiro, 2009] Augusto, B., and Loureiro, R. (2009). Motion Cueing In The Chalmers Driving Simulator. A Model Predictive Approach. Master of Science Thesis, Chalmers University of Technology.

[Azad, 2006] Azad, N. (2006). Dynamic Modelling and Stability Controller Development For Articulated Steer Vehicles, Doctoral Thesis, University of Waterloo, Canada.

[Barbu et al., 2007] Barbu, D., Barbu, I., and Druga, C. (2007). Theoretical Considerations Concerning the Human Body Behaviour In A Vibrational Medium. In *Fascicle of Management and Technological Engineering*, Vol. 6, No. 16.

[Baron et al., 1980] Baron, S., Lancraft, R., and Zacharias, G. (1980). Pilot/Vehicle Model Analysis of Visual and Motion Cue Requirements in Flight Simulation. NASA Report 3312.

[Berger et al., 2010] Berger, D., Schukte-Pelkum, J., and Bülthoff, H. (2010). Simulating Believable Forward Accelerations On A Stewart Motion Platform. In *ACM Transactions on Applied Perception*, Vol. 7, No. 1, 2010.

[Beusmans, 1998] Beusmans, J. (1998). Optic Flow And The Metric Of The Visual Ground Plane. In *Vision Reearch.*, Vol. 38, No. 8, pp 1153-1170.

[Blaauw, 1982] Blaauw, G. (1982). Driving Experience And Task Demands In Simulator And Instrumented Car: A Validation Study. Progress Report II, Report No. IZF.

[Blana, 1996] Blana, E. (1996). A Survey Of Driving Research Simulators Around The World. University of Leeds, Working Paper 481.

[BMW, 2011] BMW homepage: http://www.bmw.com/, August, 2011.

[Borah et al., 1988] Borah J., Young L., and Curry R. (1988). Optimal Estimator Model for Human Spatial Orientation, Applied Science Laboratories, Waltham, Massachusetts 02154, Report 545:51-73.

[Bouma, 2011] Bouma, B., Overview and Control of DC and AC Motors: www.calvin.edu/~pribeiro/courses/engr315/DC-AC-Motors-Control.doc, August, 2011

[Bruenger-Koch, 2005] Bruenger-Koch, M. (2005). Motion Parameter Tuning And Evaluation For The DLR Automotive Simulator. In *Proceedings of the Conference DSC North America*, pp: 262-270.

[Buzdugan, 1980] Buzdugan, G. (1980). Izolarea Vibratorie A Masinilor. Editura Academiei Romane, Bucuresti (in Romanian)

[Capustiac and Brisan, 2008] Capustiac A., and Brisan, C. (2008). Aspects Concerning

Utilisation of Matlab In Calibration Simulation for Partner Robots. In *Proceedings of the 4th International Conference Robotics 08*, Brasov, Romania.

[Capustiac and Brisan, 2009] Capustiac A., and Brisan, C. (2009). Basic Aspects Concerning Development Of The Hybrid Road and Driving Simulator. In *Proceedings of the 10th IFToMM International Symposium on Science of Mechanisms and Machines – SYROM 09*, Brasov, Romania, pp 275-283.

[Capustiac and Brisan, 2010] Capustiac, A., and Brisan, C. (2010). Aspects Concerning VRML Simulation Of Calibration For Parallel Mechanisms. In *Mechanisms and Machine Science, 1, Volume 5, New Trends in Mechanism Science*, Part 1, edited by Springer, pp 73-81.

[Capustiac et al., 2010a] Capustiac, A., Unterreiner, M., and Schramm, D. (2010). Actuation Strategy For A New Driving Simulator Setup. In *The Journal of State Phenomena. Volumes: Robotics and Automation Subsystems, 166-167*, pp 109-114.

[Capustiac et al., 2010b] Capustiac, A., Hesse, B., Brandt, T., Schramm, D., and Brisan C. (2010). Design Of A Flexible Low Cost Driving Simulator. In *The 1st Joint International Conference on Multibody System Dynamics Book of Abstracts (IMSD 2010)*, Lappeenranta, pp 91-93.

[Capustiac et al., 2010c] Capustiac, A., Csiszar, A., and Brisan, C. (2010). Aspects Concerning Dynamic Modelling For A Class Of Reconfigurable Driving Simulators. In *Proceedings of the IEEE – International Conference on Automation, Quality and Testing, Robotics*, Cluj-Napoca, Romania, pp 1-6.

[Capustiac et al., 2011a] Capustiac, A., Hesse, B., Schramm D., and Banabic, D. (2011). A Human Centered Control Strategy For A Driving Simulator. In *The International Journal of Mechanical & Mechatronics Engineering IJMME-IJENS*, Vol. 11, No. 01, pp 45-52.

[Capustiac et al., 2011b] Capustiac, A., Banabic, D., Schramm, D., and Ossendoth, U. (2011). Motion Cueing: From Design Until Implementation, In *Proceedings of the Romanian Academy*, Vol. 12, No 3, pp 249-256.

[Capustiac et al., 2011c] Capustiac, A., Hesse, B., Schramm, D., and Banabic, D. (2011). Importance Of Introducing Motion Cues In A Driving Simulator. In *Proceedings Of The IASTED International Conference on Applied Simulation and Modelling (ASM 2011)* Crete, Greece, pp 278-283.

[Chapron and Colinot, 2007] Chapron, T.; and Colinot, J. (2007). The New PSA Peugeot-Citroën Advanced Driving Simulator Overall Design And Motion Cue Algorithm. In *Proceedings of DSC 2007*, Iowa, US.

[Chuang et al., 2008] Chuang, Y., Liao, C. and Chieng, W. (2008). Optimal Motion Cueing for 5-DOF Motion Simulations via a 3-DOF Motion Simulator. In *Control Engineering Practice*, Vol. 17, No. 1, pp 170-184.

[Colombet et al., 2008] Colombet, F., Dagdelen, M., Reymond, G., Pere, C., Merienne, F., and Kemeny, A. (2008). Motion Cueing: What Is The Impact On The Driver's Behaviour? In *Proceedings Of The DSC 2008 Europe*, Monaco, pp: 171-182.

[CzA, 2011] The Czech Airlines homepage: www.czechairlines.com, August, 2011.

[Dagdelen et al., 2002] Dagdelen, M., Reymond, G., and Kemeny, A. (2002). Analysis Of The Visual Compensation In The Renault Driving Simulator. In *Proceedings of the DSC2002 Conference*, Paris, France, pp 110-119.

[Dagdelen et al., 2009] Dagdelen, M., Reymond, G., Kemeny, A., Bordier, M., and Maizi, N. (2009), Model-Based Predictive Motion Cueing Strategy For Vehicle Driving Simulators. In *Control Engineering Practice* Vol. 17, Issue 9, pp 995-1003.

[DAI, 2011] Daimler AG website: http://www.daimler.com/, August 2011

[Denne, 1989] Denne, P. (1989). Extending The Human Experience. Lecture to the Conference on Leisure Opportunities, London.

[Denne, 1996] Denne, P. (1996). Simulators For Leisure – A New Industry. IEE Conference on Simulation, Warwick.

[Denne, 2004] Denne, P. (2004). Motion Platforms Or Motions Seats. Transforce Developments Ltd. No. 2004-09-01. 2004-09-01.

[DIN4150, 1999] DIN 4150-3:1999 Structural Vibration - Effects Of Vibration On Structures.

[DRV, 2011] DRIVASSIST homepage: www.drivassist.de, August, 2011.

[Durkee, 2010] Durkee, S. (2010). The Effect Of Simulation Attributes On Driver Perception And Behaviour. Master Of Science Thesis, Montana State University.

[Dursteler, 2004] Dursteler, J., Movement In Visualisation, In *The digital magazine of InfoVis.net*, 2004

[DYM, 2011] Dymola homepage: http://www.3ds.com/products/catia/portfolio/dymola, August, 2011.

[Ellis and Chalmers, 2006] Ellis, G., and Chalmers, A. (2006). The Effect Of Translational Ego-Motion On The Perception Of High Fidelity Animations, In *Proceedings of the Spring Conference on Computer Graphics*. ACM, New York.

[Eskandarian et al., 2008] Eskandarian A., Delaigue P., Sayed R., and Mortazavi A. (2008) Development And Verification Of A Truck Driving Simulator For Driver Drowsiness Studies. Report, available on: http://www.cisr.gwu.edu/truck_sim.pdf

[EthC, 2011] Ethernet Communication, Document Number: 350080-002, www.netburner.com/downloads/communication_over_ethernet.doc, August, 2011.

[EUA, 2011] European Union Accidents Database, July 2010 http://ec.europa.eu/transport/road_safety/pdf/observatory/historical_evol.pdf

[Evans, 1991] Evans, L. (1991). Traffic Safety And The Driver. New York: Van Nostrand Reinhold.

[Farkas et al., 2011] Farkas, L., Blaho, M., and Hnat, J. (2011). Industrial Communication Between Matlab And The Ethercat Fieldbus.

[Ford, 2011] Ford Company homepage: http://media.ford.com/images/10031/DSFL.pdf, August, 2011.

[Gaspar and Nadai, 2007] Gaspar, P., and Nadai, L. (2007). Estimation Of Dynamical Parameters Of Road Vehicles On Freeways. In *Proceeding of the 5th International Symposium on Intelligent Systems and Informatics*, Serbia, pp 107-112.

[Gibson et al., 1959] Gibson, E., Gibson, J., Smith, O., and Flock, H. (1959). Motion Parallax As A Determinant Of Perceived Depth. In *Journal of Experimental Psychology*, Vol. 58, No.1.

[Gillespie, 1992] Gillespie, T., Fundamentals Of Vehicle Dynamics, 1992, Edition: 1

[Godley et al., 2002] Godley, S., Triggs, T., and Fildes, B. (2002). Driving Simulator Validation For Speed Research. In Accident Analysis and Prevention, No. 34, pp 589–600.

[Gough, 1957] Gough V. (1957). Contribution To Discussion Of Papers On Research In Automobile Stability, Control And Tyre Performance, In *Proceedings of the Automobile Division Institution of Mechanical Engineering*, pp 392.

[Gregory, 1974] Gregory, R. (1974). Concepts And Mechanisms Of Perception, First edition, Simon & Schuster Adult Publishing Group.

[Griffiths and Gillespie, 2005] Griffiths, P., and Gillespie, R. (2005). A Driving Simulator For Teaching Embedded Automotive Control Applications. In *Proceedings of the 2005 American Control Conference*, Portland, US, pp 722–726.

[Groberg et al., 1969] Groberg, D., Dustmann, R., and Beck, E., (1969). The Effect Of Body And Head Tilt In The Perception Of Vertical: Comparison Of Body And Head Tilt With Left And Right Handed, Male And Female Subjects. In *Neuropsychologia*, Vol. 7, pp 89-100.

[Guglielmino et al., 2008] Guglielmino E., Sireteanu, T., Stammers, C., Chita, G., and Giuclea, M. (2008). Semi-Active Suspension Control. Improved Vehicle Ride And Road. Springer ISBN 978-1-84800-230-2, 2008, pp 29-40.

[Gutridge, 2004] Gutridge, J. (2004). Three degree of freedom simulator motion cueing using classical washout filters and acceleration feedback. Master of Science Thesis, Virginia Polytechnic Institute, US.

[GWU, 2011] George Washington University websitehttp://www.cisr.gwu.edu/simspec.pdf August, 20011

[Hac, 1987] Hac, A. (1987). Adaptive Control Of Vehicle Suspension. In *Vehicle System Dynamics*, Vol. 16, No. 2, pp 57-74.

[Harms, 1993] Harms, L. (1993). Driving Performance On A Real Road And In A Driving Simulator: Results Of A Validation Study. In *Proceedings of the 5th International Conference on Vision in Vehicles*, Glasgow, Scotland.

[Harrison et al., 2010] Harrison, G., Haruvy, E., and Rutstrom, E. (2010). Remarks On Virtual World And Virtual Reality Experiments. In *Southern Economic Journal*, December, pp 1-12.

[Hatada et al., 1980] Hatada, T., Sakata, H., and Kusaka, H. (1980). Psychophysical Analysis Of The Sensation Of Reality Induced By A Visual Wide Field Display. In *Society of Motion Picture and Television Engineers Journal*, Vol. 89, pp 117-126.

[He et al., 2008] He, L., Qin, G., Zhang, Y., and Chen, L. (2010). Non-Stationary Random Vibration Analysis Of Vehicle With Fractional Damping, In *Proceedings of the International Conference on Intelligent Computation Technology and Automation*, pp 150-157.

[Heckhoff et al., 2007] Heckhoff,, C., Albadawi, A., Germann, R., Brandt, T., Hiller, M., and Schramm, D. (2007). Motion Control Of A Large Scale Quadruped Walking Robot. In *Proceedings of Multibody Dynamics*, ECCOMAS Thematic Conference Italy.

[Hesse et al., 2009] Hesse, B., Hiesgen, G., Brandt, T., and Schramm, D. (2009). A Driving Simulator As A Tool For The Early Characteristics Validation Of Human-Centered

Mechatronic Systems. In *Proceedings of VDI Mechatronik*.

[Heydinger et al., 2002] Heydinger, G., Salaani, M., Garrot, W., and Grygier, P. (2002). Vehicle Dynamics Modelling For The National Advanced Driving Simulator. *In Proceedings of the Institution of Mechanical Engineers*, pp 307-318.

[Hirata, 2005] Hirata, T. (2005). Development Of Driving Simulation System: Movic-T4 And Its Application To Traffic Safety Analysis In Underground Urban Expressways. Doctoral Dissertation, Tokyo Institute of Technology.

[Horst and Hogema, 2011] Horst, A., and Hogema, J. (2011). Driving Simulator Research On Safe Highway Design And Operation. In *Transportation Research Board Annual Meeting*, Paper 11-1363.

[Hyder, 2010] Hyder, A. (2010). Design And Implementation Of Remotely Controlled Laboratory Experiments. Master of Science Thesis, Georgia Institute of Technology, US.

[InH, 2011] Integral Hydraulik homepage: http://integral-hydraulik.com/en/integral/nbsp.html, August, 2011

[InM, 2011] InMotion Simulation Homepage: http://www.inmotionsimulation.com/, August 2011.

[IPG, 2011] IPG Car Maker homepage: http://www.ipg.de/, August, 2011.

[ISO 8608, 1995] ISO 8608:1995 Mechanical Vibration-Road Surface Profiles-Reporting Of Measured Data.

[ISO 2631, 2003] ISO 2631:2003, Mechanical Vibration And Shock-Evaluation Of Human Exposure To Whole-Body Vibration.

[ISO 3888, 1999] ISO 3888-1:1999, Passenger Cars-Test Track For A Severe Lane-Change Manoeuvre.

[ISO 5982, 2001] ISO 5982:2001. Mechanical Vibration And Shock-Range Of Idealized Values To Characterize Seated-Body Biodynamic Response Under Vertical Vibration.

[Jamson, 2000] Jamson, H. (2000). Driving Simulation Validity: Issues Of Field Of View And Resolution. In *Proceedings of Driving Simulators Conference*, Paris, France, pp 57-64.

[Jamson, 2001] Jamson, H. (2001). Image Characteristics And Their Effect On Driving Simulator Validity, In *Proceedings of the First International Driving Symposium on Human Factors in Driver Assessment, Training and Vehicle Design*, pp 190-195.

[Jones et al., 2007] Jones, R., Jones, J., Trick, L., and Vallis, L. (2007). Can Galvanic Vestibular Stimulation Reduce Simulator Adaptation Syndrome? In *Proceedings of the 4th International Driving Symposium on Human Factors in Driver Assessment, Training and Vehicle Design*, pp 534-540.

[Karimi and Nategh, 2011] Karimi D., and Nategh M. (2011). A Statistical Approach To The Forward Kinematics Nonlinearity Analysis Of Gough-Stewart Mechanism. In *Journal of Applied Mathematics*, vol. 2011, Article ID 393072, 17 pages, 2011. doi:10.1155/2011/393072

[Kamada et al., 2008] Kamada, T., Miyoshi, N., and Nagai, M. (2008). Experimental Study On Forward Collision Warning System Adapted For Driver Characteristics. In *Journal of Mechanical Systems for Transportation and Logistics*, Vol. 1, No. 2, pp 223-230.

[Kapur et al., 2007] Kapur P., Ranganath R., and Nataraju B. (2007). Analysis Of Stewart

Platform With Flexural Joints At Singular Configurations. iN *Proceedings of the 12th IFToMM World Congress*, Besancon, France.

[Kemeny and Penerai, 2003] Kemeny, A., and Penerai, F. (2003) Evaluation Perception In Driving Simulation Experiments. In *Trends in Cognitive Sciences*, Vol. 7, No.1, pp 31-37.

[Kemeny, 1993] Kemeny, A. (1993). A Cooperative Driving Simulator. In *Proceedings of the 1993 ITEC Conference*, London, UK, pp 67-71.

[Kemeny, 2009] Kemeny, A. (2009). Driving Simulation for virtual testing and perception studies. In *Proceedings of DSC Europe*, Monaco, 4-6 February.

[Koutsopoulos et al., 1994] Koutsopoulos, H., Lotan, T., and Yang, Q. (1994). A Driving Simulator And Its Application For Modelling Route Choice In The Presence Of Information. In *Transportation Research Review*, Vol. 2, No. 2, pp 91-107.

[Krissada and Wannasuphoprasit, 2009] Krissada, C., and Wannasuphoprasit, W. (2009). Washout Filter For A 3 DOF Simulator. In *Proceedings of the 5th International Conference on Automotive Engineering*, pp 1-6.

[Kruczek and Stribrsky, 2007] Kruczek, A., and Stribrsky, A. (2007). A Full Car Model For Active Suspension-Some Practical Aspects, In *Proceedings of IEEE International Conference on Mechatronics*, Istanbul, Turkey.

[Lappe et al., 1999] Lappe, M., Bremmer, F., and Van Den Berg, A. (1999). Perception Of Self-Motion From Visual Flow. In *Trends in Cognitive Sciences*, Vol. 3. No. 9, pp 329-336.

[Lay, 2011] UDP Communication http://www.laynetworks.com/Comparative%20analysis_TCP%20Vs%20UDP.htm, August 2011

[Lee, 1976] Lee, D. (1976). A Theory Of Visual Control Of Braking Based On Information About Time To Collision. In *Perception*, Vol. 5, pp 473-459.

[Lee et al., 1998] Lee, W., Kim, J., and Cho, J. (1998). A Driving Simulator As A Virtual Reality Tool. In *Proceedings of the 1998 IEEE International conference on Robotics and Automation*, Leuven, Belgium, pp 71-76.

[Lee et al., 2007] Lee, W., Sung, D., Lee, Y., Kim, Y., and Cho, J. (2007). Driving Simulation For Evaluation Of Driver Assistance Systems And Driving Management Systems. Report in the frame of the project: Development of National Traffic Core Technology.

[Lewis and Griffin, 1997] Lewis, C., and Griffin, M. (1997). Human Factors Consideration In Clinical Applications Of Virtual Reality, In *Virtual Reality in Neuro-Psycho-Physiology*.

[Liang and Li, 2005] Liang Y. and Li, J. (2005). A Study Of Active Suspension Based On Full DOF Vehicle Model, In *Journal Univ. Eng.* Vol. 4 No. 2.

[Luyat, 2005] Luyat, M., Mobarek, S., Leconte, C., and Gentaz, E. (2005). The Plasticity Of Gravitational Reference Frame And The Subjective Vertical: Peripheral Visual Information Affects The Oblique Effect. In *Neuroscience Letters*, No. 385, pp 215–219.

[Macaulay, 1963] Macaulay, M. (1963). Measurement of Road Surfaces. In *Advances in Automobile Engineering - Part 1*. Oxford: Pergamon Press.

[Macleod et al., 1999] Macleod, C., Dror, G., and Maxwell, G. (1999). Training Artificial

Neural Networks Using Taguchi Methods. In Journal Artificial Intelligence Review, Vol. 13, No. 3.

[Maeda et al., 2005] Maeda, C., Kawamura, A., Shirakawa, T., Nakatsuji, T., and Kumada, K. (2005). Reproducibility Of The Vehicle Vertical Motion By KIT Driving Simulator Using The Actual Measurement Data. In *Journal of the Eastern Asia Society for Transportation Studies*, Vol. 6, pp 2734-2746.

[MAT, 2011] Matlab/Simulink homepage: http://www.mathworks.com/products/matlab/, August, 2011.

[MAZ, 2011] Mazda homepage: http://www.mazda.com/.

[McCann, and Nguye, 2007] McCann, R., and Nguye, S., (2007). System Identification For A Model-Based Observer Of A Road Roughness Profiler. In *Proceedings of the IEEE Technical Conference*, Fayetteville, pp 336-343.

[Meiry, 1958] Meiry, J. (1958). The Vestibular System And Human Dynamic Space Orientation, Doctoral Dissertation, Massachusetts Institute of Technology, US.

[Meiry and Young, 1968] Meiry, J., and Young, L. (1968). Biophysical Evaluation Of The Human Vestibular System. Semi-annual status report.

[Mellor, 2002] Mellor, C. (2002). Quick-Change Artists: Why Techs Must Get Ready For Reconfigurable Manufacturing. In *The Ontario Technologist*, Jan/Feb, pp 12-15

[Merlet, 2006] Merlet, J.P. (2006). Parallel Robots. Springer, ISBN-10 1-4020-4132-2.

[MIC, 2011] Microstrain homepage: http://www.microstrain.com/, August, 2011.

[Milosevic and Milic, 1990] Milosevic, S., and Milic, J. (1990). Speed Perception In Road Curves. In *Journal of Safety Research*, Vol. 21, pp 19-23.

[Mitschke, 1995] Mitschke, M. (1995) Dynamik Der Kraftfahrzeuge. Springer, ISBN: 3-5405-6164-1.

[Mollenhauer, 2004] Mollenhauer, A. (2004). Simulator Adaptation Syndrome Literature Review – Report.

[MTS, 2011] MTS Company homepage:http://www.mts.com/en/products/producttype/test-systems /simulation-systems/road-simulation/index.htm, August, 2011.

[Muksian and Nash, 1974] Muksian, R., and Nash, C. (1974). A Model For The Response Of Seated Humans To Sinusoidal Displacements Of The Seat. In *Journal of Biomechanics*, Vol. 7, pp 209-15.

[NADS, 2011] The National Advanced Driving Simulator: http://www.nads-sc.uiowa.edu/, August 2011

[Naidu and Raol, 2008] Naidu, V., and Raol, J. (2008). Object Tracking using Image Registration and Kalman Filter. In*: International Conference on Avionics Systems*, 22-23 Feb. 2008, RCI, Hyderabad.

[Nehaoua et al., 2006] Nehaoua, L., Arioui, H., Espie, S., and Mohellebi, H. (2006). Motion Cueing Algorithms For Small Driving Simulator. In *Proceedings of the IEEE International Conference on Robotics and Automation*, Orlando, US, pp 3189-3194.

[Nehaoua et al., 2008] Nehaoua, L., Mohellebi, H., Amouri, A., Arioui, H., Espie, S., and Kheddar, A. (2008) Design and Control of a Small-Clearance Driving Simulator. In IEEE Transactions on Vehicular Technology. Vol. 57, No. 2, pp 736-746.

[Nilsson, 1993] Nilsson, L. (1993). Simulator Studies And Driver Behaviour Research. In

Driving future vehicles, pp 401–407.

[Nis, 2011] Nissan Company homepage: http://www.nissanusa.com/, August 2011.

[Olstam, 2007] Olstam, J. (2007). Combining Autonomous Vehicles And Controlled Events In Driving Simulator Experiments. Young Researchers Seminar, Brno, Czech Republic.

[Ormsby and Young, 1977] Ormsby, C., and Young, L. (1977). Integration Of Semicircular Canal And Otolith Information For Multisensory Orientation Stimuli, In *Elsevier,* 1977.

[Paraianu et al., 2011] Paraianu, L., Comsa, S., Bichis, I., and Banabic, D. (2011). Influence Of The Mechanical Parameters On The Forming Limit Curve, In *Steel Research International, Special Edition: 10th International Conference on Technology of Plasticity, Aachen, Germany 2011*, pp 744-749.

[Peli et al., 2005] Peli, E., Bowers, A., Mandel, A., Higgins, K., Goldstein, R., and Bobrow, L. (2005). Design For Simulator Performance Evaluations Of Driving With Vision Impairments And Visual Aids. In *Transportation Research Record,* No. 1937, pp 128-135.

[Planque et al., 1991] Planque S., Petit C., and Chapeau D. (1991). A System For Identifying Lapses Of Alertness When Driving, Renault Paper.

[Prothero, 1998] Prothero, J. (1998). Physological Presence Measures, Human Interface Lab. http://www.hitl.washington.edu/publications/r-98-11/node15.html, August 2011

[Reich et al., 1996] Reich, F., Bernasch, J., and Löwenau, J. (1996). Online Steering Dynamics in the BMW Driving Simulator. In *Proceedings of the IMAGE Conference*, Arizona, US.

[Reiff, 2011] Reiff, M. (2011). Entwicklung eines Mechatronischen Systems zur Vertikalen Anregung eines Fahrsimulators. Bachelor Thesis. University of Duisburg-Essen, Germany. (In German)

[Reymond and Kemeny, 2000] Reymond, G., and Kemeny, A. (2000). Motion Cueing In The Renault Driving Simulator. In *Vehicle Systems Dynamics*, Vol. 34, pp 249–259.

[Reymond et al., 2000] Reymond, G., Heidet, A., Canry, M., and Kemeny, A. (2000). Validation Of Renault's Dynamic Simulator For Adaptive Cruise Control Experiments. In *Proceedings Of The DSC'00 Conference*, Paris, France.

[Reymond et al., 2001] Reymond, G., Kemeny, A., Droulez, J., and Berthoz, A. (2001). Role Of Lateral Acceleration In Curve Driving: Driver Model And Experiments On A Real Vehicle And A Driving Simulator. In *Human Factors*, Vol. 43, pp 483–495.

[Riccio and Stoffgregen, 1991] Riccio, G., and Stoffgregen, T. (1991). An Ecological Theory Of Motion Sickness And Postural Instability. In *Ecological Psychology*, Vol. 3, No. 3.

[Rill, 2008] Rill, G. (2008). Vehicle Dynamics-Lecture Notes, Regensburg University of Applied Science.

[Rode, 2007] Rode, J. (2007). Entwicklung Eines Hochdynamischen Fahrsimulators Mit Linearantrieben Mit Realitätsnahmen Fahrwerksverhalten Für Wissenschaftliche Und Industrielle Anwendungsmöglichkeiten. Bachelor Thesis. University of Applied Sciences Gelsenkirchen, Department Bocholt (In German).

[Roza et al., 2007] Roza, M., Wentink, M., and Feenstra, P. (2007). Performance Testing Of The Desdemona Motion System. In *Proceedings Of AIAA Modeling And Simulation*

Technologies Conference And Exhibit, South Carolina, US.

[Rydstrom, 2009] Rydstrom, A. (2009). The Use Of Haptics When Interacting With In-Car Interfaces, Doctoral Thesis, Lulea Universtiy Of Technology, Sweden.

[Schramm et al., 2010] Schramm, D., Hiller, M., and Bardini, R. (2010). Modellbildung Und Simulation der Dynamik Von Kraftfahrzeugen. Edited by Springer. (In German)

[SEW, 2011] SEW Company: http://www.sew-eurodrive.com/ August, 2011

[Shiraishi, 2001] Shiraishi, S. (2001). Development Of A Compact Driving Simulator For The Training Beginners At Schools. In *Journal of Society of Automotive Engineers of Japan*, Vol. 57, pp 72-77.

[SIM, 2003] Simusys Report. (2003) Innovative High Performance Motion Simulation System For Entertainment, Research And Training Applications, Contract nr: CRAFT-IST - 1999 – 56418.

[Sivak, 1996] Sivak, M. (1996). The Information That Drivers Use: Is It Indeed 90% Visual? In *Perception*, Vol. 25, No. 9, pp 1081-1089.

[Slob, 2008] Slob, J. (2008). State-Of-The-Art Driving Simulators, A Literature Survey. DCT Report, Eindhoven.

[Snowden et al., 1998] Snowden, R., Stimpson, N., and Ruddle, R. (1998). Speed Perception Fogs Up As Visibility Drops. In *Nature*, Vol. 392, Nr. 450.

[Sottek et al., 2005] Sottek R., Krebber W., and Stanley, G. (2005). Tools And Methods For Product Sound Design Of Vehicles. Report 2005-01-2513, SAE International.

[Spangler, 1966] Spangler, E. (1966). GMR Road Profilometer A Method For Measuring Road Profile. In *Highway Research Record*, Vol. 121, Washington.

[Stein and Mucka, 2003] Stein, G., and Mucka, P., (2003). Theoretical Investigations Of A Linear Planar Model Of A Passenger Car With Seated People. In *Proceedings Of The Institution Of Mechanical Engineers*, Vol. 217, No. 4.

[Straus, 2005] Straus, S. (2005). New, Improved, Comprehensive and Automated Driver's License Test and Vision Screening System, Project 559(1) Research notes, Arizona Department of Transportation.

[SW, 2011] Solid Works homepage: http://www.solidworks.com/, August, 2011.

[Tchermychouk, 1999] Tchermychouk, V. (1999). Objective Assessment Of Static And Dynamic Seats Under Vehicular Vibrations. Master Thesis, Concordia University, Montreal, Canada.

[Telban and Cardullo, 2005] Telban, R.m and Cardullo, F. (2005). Motion Cueing Algorithm Development: Human Centred Linear And Nonlinear Approaches. NASA 2005-213747 Report.

[TOY, 2011] Toyota Company homepage: http://www.toyota.com/, August, 2011.

[Treisman, 1977] Treisman, M., 1977. Motion Sickness: An Evolutionary Hypothesis. In *Science*, No. 197.

[TRQ, 2011] Torque Game Engine: http://www.garagegames.com/products/torque-3d, August, 2011.

[Tsimhoni and Liu, 2003] Tsimhoni, O., and Liu, Y. (2003). Steering A Driving Simulator Using The Queueing Network Model Human Processor. In *Proceedings of the Second International Driving Symposium on Human Factors in Driver Assessment, Training and*

Vehicle Design, Utah, USA, pp 81-85.

[Twi, 2011] TwinCat homepage: www.beckhoff.si/english/twincat/default.htm , August, 2011.

[Unal and Dean, 1991] Unal, R., and Dean, E. (1991). Taguchi Approach To Design Optimization For Quality And Cost: An Overview. Annual Conference Of The International Society Of Parametric Analysts.

[Untaru et al., 1981] Untaru M., Stoicescu A., Potincu G., G.Peres, and Tabacu, I. (1981). Dinamica Autovehiculelor Pe Roti. Editura Didsctica si Pedagogica. (In Romanian)

[Van Egmond et al., 1949] Van Egmond, A., Groen, J., and Jongkees, L. (1949). The Mechanics Of The Semicircular Canal. In Journal Of Physiology. No. 110, pp 1-17.

[VDI 2057, 2002] VDI 2057:2002. Human Exposure To Mechanical Vibrations. Whole Body Vibrations. Düsseldorf: Verein Deutscher Inginieure.

[Von der Heyde and Riecke, 2001] Von Der Heyde, M., and Riecke, B. (2001). How To Cheat In Motion Simulation – Comparing The Engineering And Fun Ride Approach To Motion Cueing. Technical Report, 089, Max Planck Institute, Germany.

[VTI, 2011] The Swedish National Road And The Transport Research Institute Homepage:

http://www.vti.se/templates/Page11866.aspx, August, 2011.

[Wang et al., 2005] Wang, H., Kearney, J., Cremer, J., and Willemsen, P. (2005). Steering Behaviours For Autonomous Vehicles In Virtual Environments. In *Proceedings Of The IEEE Virtual Reality (VR'0*5) Bonn, Germany, pp 155-162.

[Welch and Bishop, 2006] Welch, G., and Bishop, G. (2006) An Introduction To The Kalman Filter. TR 95-041.

[Wentink et al., 2005] Wentink, M., Bles, W., and Hosman, R. (2005). Design & Evaluation Of Spherical Washout Algorithm For Desdemona Simulator. In *Proceedings Of The AIAA Modeling And Simulation Technologies Conference And Exhibit*, San Francisco, California

[Young, 1982] Young, L. (1982). Perception Of The Body In Space: Mechanisms, In Handbook Of Physiology - The Nervous System III, pp. 1023-1066.

[Yoshimoto and Suetomi, 2008] Yoshimoto, K., and Suetomi T. (2008). The History Of Research And Development Of Driving Simulators In Japan. In *Journal Of Mechanical Systems For Transportation And Logistics*, Vol. 1, No. 2, pp 159-169.

[Yu and Jun, 2005] Yu, L. and Jun, L. (2005). A Study Of Active Suspension Based On Full DOF Vehicle Model. In *Mechanical & Electrical Engineering*, Vol. 4, No. 2.

[Zeller, 1932] Zeller, W. (1932). Ein Beitrag zur Untersuchung der Mechanischen Erschütterungen in ihrer Auswirkung auf Den Menschlichen Organismus. Schalltechnik, 5, pp 24-34. (In German)

Scientific Papers published:

1. Capustiac A. and Brisan, C. (2008). Aspects Concerning Utilisation Of Matlab In Calibration Simulation For Partner Robots. In *Proceedings of the 4th International Conference Robotics 08*, Brasov, Romania, ISBN 978-973-598-387-1.
2. Capustiac A. and Brisan, C. (2009). Basic Aspects Concerning Development Of The Hybrid Road And Driving Simulator. In *Proceedings Of The 10th Iftomm International Symposium On Science Of Mechanisms And Machines – SYROM 09*, Brasov, Romania, pp 275-283, ISBN 978-90-481-3521-9.
3. Capustiac, A. and Brisan, C. (2009). Aspects Concerning Application Of Virtual Reality Toolbox In Development Of Virtual Models For Parallel Robots. In *Proceedings Of The Conference On Technological Education And Educational Technologies (CNETTE 2009*), 4-5 June, 2009, ISSN 2066 -446X, Cluj-Napoca, Romania. (In Romanian)
4. Capustiac, A. and Brisan, C. (2010). Aspects Concerning VRML Simulation Of Calibration For Parallel Mechanisms. In *Mechanisms And Machine Science, 1, Volume 5, New Trends In Mechanism Science,* Part 1, Edited By Springer, pp 73-81, ISBN 9789048196890.
5. Capustiac, A., Unterreiner, M., and Schramm, D. (2010). Actuation Strategy For A New Driving Simulator Setup. In *The Journal Of State Phenomena. Volumes: Robotics And Automation Subsystems, 166-167*, pp 109-114, ISSN: 1662-9779.
6. Capustiac, A., Hesse, B., Brandt, T., Schramm, D., and Brisan C. (2010). Design Of A Flexible Low Cost Driving Simulator. In *The 1st Joint International Conference On Multibody System Dynamics Book Of Abstracts (IMSD 2010)*, Lappeenranta, pp 91-93, ISBN: 978-952-214-778-3.
7. Capustiac, A., Csiszar, A., and Brisan, C. (2010). Aspects Concerning Dynamic Modelling For A Class Of Reconfigurable Driving Simulators. In *Proceedings Of The IEEE – International Conference On Automation, Quality And Testing, Robotics*, Cluj-Napoca, Romania, pp 1-6, ISBN: 978-1-4244-6724-2.
8. Capustiac, A., Hesse, B., Schramm D., and Banabic, D. (2011). A Human Centered Control Strategy For A Driving Simulator. In *The International Journal Of Mechanical & Mechatronics Engineering IJMME-IJENS*, Vol. 11, No. 01, pp 45-52, ISSN: 2077-124X.
9. Capustiac, A., Banabic, D., Schramm, D., and Ossendoth, U. (2011). Motion Cueing: From Design Until Implementation, In *Proceedings Of The Romanian Academy*, Vol. 12, No 3, pp. 249-256.
10. Capustiac, A., Hesse, B., Schramm, D., and Banabic, D. (2011). Importance Of Introducing Motion Cues In A Driving Simulator. In *Proceedings Of The IASTED International Conference On Applied Simulation And Modelling (ASM 2011)* Crete, Greece, pp 278-283, ISBN: 978-0-88986-884-7.
11. Capustiac, A., and Banabic, D. (2011). Efficiency Of Using A Low Cost Driving Simulator In Studies Concerning Driver's Perception. In *Proceedings Of PRODOC Conference,* 24 June 2011, Cluj-Napoca, Romania.